FINITE ELEMENT MODELING OF PIEZOELECTRIC BIMORPHS WITH CONDUCTIVE POLYMER ELECTRODES

by

Laura Marie Lediaev

A dissertation submitted in partial fulfillment
of the requirements for the degree

of

Doctor of Philosophy

in

Physics

MONTANA STATE UNIVERSITY
Bozeman, Montana

May 2010

APPROVAL

of a dissertation submitted by

Laura Marie Lediaev

This dissertation has been read by each member of the dissertation committee and has been found to be satisfactory regarding content, English usage, format, citations, bibliographic style, and consistency, and is ready for submission to the Division of Graduate Education.

V. Hugo Schmidt, Ph.D.

Approved for the Department of Physics

Richard J. Smith, Ph.D.

Approved for the Division of Graduate Education

Carl A. Fox, Ph.D.

STATEMENT OF PERMISSION TO USE

In presenting this dissertation in partial fulfillment of the requirements for a doctoral degree at Montana State University, I agree that the Library shall make it available to borrowers under rules of the Library. I further agree that copying of this dissertation is allowable only for scholarly purposes, consistent with "fair use" as prescribed in the U.S. Copyright Law. Requests for extensive copying or reproduction of this dissertation should be referred to ProQuest Information and Learning, 300 North Zeeb Road, Ann Arbor, Michigan 48106, to whom I have granted "the exclusive right to reproduce and distribute my dissertation in and from microform along with the non-exclusive right to reproduce and distribute my abstract in any format in whole or in part."

Laura Marie Lediaev

May 2010

TABLE OF CONTENTS

LIST OF FIGURES

LIST OF FIGURES - CONTINUED

LIST OF FIGURES - CONTINUED

LIST OF FIGURES - CONTINUED

LIST OF FIGURES - CONTINUED

LIST OF FIGURES - CONTINUED

ABSTRACT

The purpose of my research has been to find a good way to solve for the mechanical and electrical behavior of piezoelectric polymer bimorphs which are electroded with a low to medium conductivity material. Traditionally, metal with very high conductivity has been used as the electrode material. Any applied voltage to an electrode will be distributed nearly instantaneously and uniformly throughout the electrode. Because of this quality, the voltage was assumed to be known and uniform for any applied voltage signal, including high frequency signals. The disadvantage of metal is that it is stiffer than polymers, and thus impedes the bending of the bimorph to a greater extent than for comparable polymer electrodes. With the modern invention of conductive polymers with acceptably high conductivities, it is now possible to manufacture piezoelectric devices with finite conductivity electrodes. For all but the very lowest frequencies of applied voltage signals, the voltage distribution cannot be assumed to be uniform throughout the electrode, nor can it be assumed to be exactly in phase. With finite conductivity electrodes there will be a loss in voltage amplitude due to resistivity, and there will also be a phase lag. The piezoelectric problem involves solving a coupled set of differential equations which involve mechanical displacement and electric potential. The electrical behavior of the electrodes is also included in the formulation, so that the voltage distribution in the electrodes is solved for simultaneously with the mechanical displacement and electric potential in the piezoelectric sheets. In this dissertation the coupled set of differential equations was solved using the Finite Element Method with quadratic Lagrange finite elements. The piezoelectric polymer which was modeled was polyvinylidene fluoride (PVDF). The conductive polymer of interest was PEDOT-PSS, although the model is valid for any type of isotropic finite conductivity material. The results of the work show that for moderate conductivity, the mechanical response of the bimorph is very good. There will not be a large phase lag within the first frequency mode. The bimorph resonates at low frequencies, and so any large effect from finite conductivity would only occur at higher modes.

CHAPTER 1

INTRODUCTION

The problem that is solved in this dissertation is the bending of a piezoelectric polymer bimorph with lossy electrodes. Previous work has modeled actuators with the assumption of perfectly conducting electrodes, since before recently only metal electrodes (usually silver) have been commercially available for piezoelectric polymer sheets. These metal electrodes substantially stiffen the sheets and significantly reduce the displacement attainable for a given applied voltage. With the advent of highly conducting polymers that can be applied as electrodes, much more displacement can be attained for a given voltage. However, the much lower conductivity of these polymers compared to metals makes it necessary to take into account the voltage distribution across the electrodes when a time-varying voltage is applied to the electrode contacts. In this work, the effect of this spatial voltage distribution on the actuator performance is taken into account for the first time. The finite element analysis in this work is based on sinusoidal voltage applied to a rectangular bimorph actuator made of two polyvinylidene fluoride (PVDF) sheets with PEDOT-PSS electrodes. The electrodes were included in the model, and all the variables involved (electric potential and mechanical displacement) were solved simultaneously. The model involved a set of coupled linear second-order differential equations. The equations were converted into a finite element formulation, and solved using quadratic Lagrange finite elements. The z-deflection was found to be too small when using linear elements. This phenomenon is called locking [11].

PVDF History and Applications

Piezoelectricity is a linear coupling between electrical and mechanical processes [1]. In the direct piezoelectric effect, when a piezoelectric material is compressed, an electric polarization is formed across the material. In fact, the prefix piezo is derived from the Greek word for press [1]. The converse piezoelectric effect is when an applied electric field causes the piezoelectric to mechanically deform.

Piezoelectricity is made possible due to certain kinds of crystal structures which lack a center of symmetry. Materials which are piezoelectric come in several forms. There are single crystals, ceramics, and polymers (semi-crystalline) [20].

Polyvinylidene-fluoride (PVDF) is a piezoelectric polymer, which for actuator applications often comes in the form of a thin sheet (30 microns thick). It is stretched along the x direction to align the long chain molecules, and is poled in the z direction to align the electro-negative and electro-positive parts of the molecular units (the hydrogen and fluorine atoms) to create a strong piezoelectric constant, as shown in figure 1.2.

Because of the aligned dipoles, there is a charge polarization. When an electric field is applied across the PVDF sheet, the molecules will either stretch or contract, depending on the direction of the field, as shown in figures 1.3 and 1.4. The other dimensions of the PVDF sheet will also change. The thickness of the sheet is very small, but the length is substantial and even an elongation of only a small percent will be noticeable. When an electric field is applied across two sheets that are glued together with opposite polarization, the sheets will bend out of the plane. This is a bimorph, and the deflection is much larger than the elongation of an individual sheet. This conversion from electric field to mechanical deformation and vice versa is very useful.

A transducer is a device, or material, which converts one type of energy into another. In the case of piezoelectricity, the conversion is between mechanical and electrical energy. Piezoelectricity is a coupling between mechanical and electrical processes [1]. It is a fundamental process, and couples mechanical and electrical energy in a linear fashion. The piezoelectric effect was first discovered in 1880 by Pierre Curie. This effect is now an established branch of crystal physics. Piezoelectricity also finds wide application in the electrical engineering field. Piezoelectric materials have been widely used as electromechanical transducers, such as ultrasonic generators, filters, sensors, and actuators. They have also been used for other purposes, such as Braille keyboards, hi-fi tweeters, and sonar receivers.

The direct piezoelectric effect is that electric polarization is produced by mechanical stress (deformation). Closely related to it is the converse effect, where a crystal becomes strained when an electric field is applied. Both effects are manifestations of the same fundamental property of the crystal. Many of the theoretical concepts of electronics are based on linear systems response. The piezoelectric effect is basically understood to be a result of the linear interaction between mechanical and electrical systems.

The piezoelectric effect is present in many biopolymers, such as wood, bone, tendon, and even DNA. Eiichi Fukada, at the Kobayashi Institute of Physical Research in Japan, extended the field of research from natural biopolymers to synthetic polypeptides. In 1969 was the first report of piezoelectricity in a synthetic commercial polymer (PVDF), by Heiji Kawai [1], also at the Kobayashi Institute. PVDF became commercially available in 1961 for its use as a thermoplastic. It has good resistance to chemical erosion, and it is a good electric insulator, suitable for electrical insulation of wires. Of the piezoelectric polymer films, those which are based on PVDF have the highest piezoelectric and pyroelectric activity [2].

Polyvinylidene fluoride film, with chemical structure $(CH_2 - CF_2)_n$, is manufactured by melting PVDF pellets and then putting it through rollers and exposing it to a high electric field in order to align the dipoles. There are several ways to create and pole the film. The method which produces the strongest piezoelectric constants seems to be stretching and poling simultaneously, instead of stretching, and then poling at a lower temperature for a longer time. For applications which require high quality, the PVDF samples must be produced in smaller amounts with precisely defined properties by way of a process which controls the amplitude, duration, and the history of the electric field [4]. If the material is not poled, then the PVDF will predominantly be in the α phase. The crystal packing is such that the dipoles alternate and cancel. In the β phase the hydrogen-fluorine dipoles are all on the same side of the carbon backbone, and poling causes individual chains to align in the same direction, and the dipoles reinforce. The overall film is 50% amorphous, so half does not contribute to the piezoelectricity of the material, while the rest has crystal structure. Figure 1.1 shows a graphic of a PVDF molecule. The carbon backbone is shown by the black spheres. The hydrogen is on top colored white, and the fluorine is on the bottom in green.

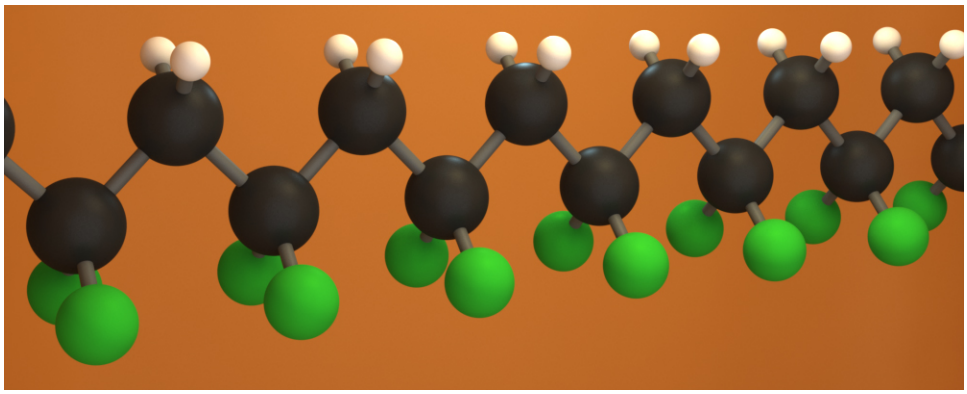

Figure 1.1: The PVDF Molecule. Black = C, white = H, green = F.

The PVDF molecule has a permanent electric dipole. The fluorine side of the molecule is electro-negative, while the hydrogen side is electro-positive. This is shown schematically in figure 1.2. In the converse piezoelectric effect, when an electric field is applied antiparallel to the polarization direction, the molecule stretches (figure 1.3). When the electric field is parallel to the polarization direction, the molecule shrinks (figure 1.4).

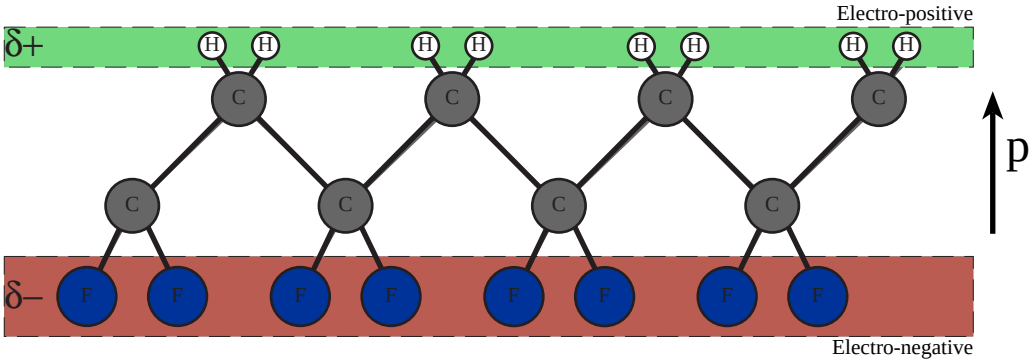

Figure 1.2: PVDF schematic.

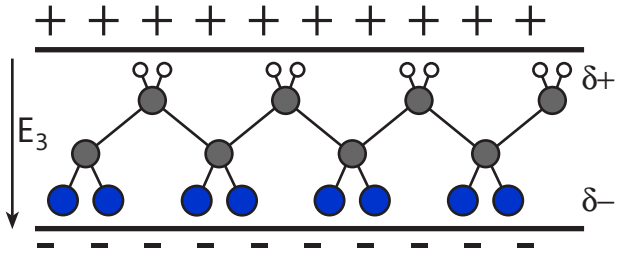

Figure 1.3: PVDF stretch.

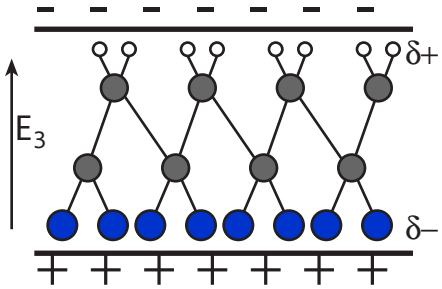

Figure 1.4: PVDF shrink.

The Conductive Polymer PEDOT-PSS

Poly(3,4-ethylenedioxythiophene) poly(styrenesulfonate) is a polymer mixture of two ionomers. The PEDOT part is a conjugated organic polymer, also called an intrinsically conducting polymer or a synthetic metal [5]. This class of polymer is different from conducting polymers which are a mixture of a nonconductive polymer and a conducting material such as metal or carbon powder. PEDOT does not have an intrinsically high conductivity. Conjugated organic polymers are either electrical insulators or semiconductors to start with. Their conductivity can be increased by several order of magnitude by doping with small amounts of dopants. The conjugated polymers which are capable of drastically increasing their conductivity with doping are called electronic polymers. Since 1990 these types of polymers have become of great scientific and technological importance because of their use in light emitting diodes. The native conductivity is in the range 10^{-10} to 10^{-5} S/cm, while the doped conductivity can be in the range of about 1 to 10^4 S/cm, or higher. At ultra-low temperature, one doped polymer, poly(3-hexylthiophene) actually attained superconductivity. The conductivity of a good metal such as gold is 4.9×10^5 S/cm at 0° C [7], and 4.3×10^5 S/cm at 20° C [8]. Silver has conductivity 6.67×10^5 S/cm at 0° C [7].

Chapter Outline

Chapter 1 contains the introduction, which discusses the history and uses of piezoelectric actuators, PVDF, and the conductive polymer PEDOT-PSS.

Chapter 2 describes the constitutive equations which describe the mechanical and electrical response of the bimorph. The material constants are also described in detail.

Chapters 3 and 4 solve the static deflection of the bimorph. An analytical model is also developed for the x and z deflections based on the Bernoulli-Euler beam model.

Chapters 5 and 6 solve the case of harmonic time dependence. The applied voltage is sinusoidal, and the response of the bimorph is also sinusoidal. The resonance frequencies and the mode shapes are found. An analytical model was developed for this case, which was an extension of the analytical model used for the static case.

Chapter 7 presents the conclusions, including a summary of the results and recommendations for future work.

Appendix A has an introduction to the Finite Element Method, including an extensive section on using the higher-order Hermite finite elements for solving a second order problem.

Appendix B and C list computer code used for solving the problems. Appendix B contains some of the C programs used for generating the results in this Dissertation. The C programs are fast, and use the C-Lapack package for solving linear systems. Appendix C contains an example Mathematica program. The advantage with using Mathematica is that the numerical precision can be specified to be any value. I used Mathematica for testing the effects of numerical roundoff, to ensure that no errors were caused by roundoff. The reason that Mathematica was not used to generate all the results is because it is very slow. Also, using more precision causes the problem to require the use of more computer memory, which is in short supply.

CHAPTER 2

CONSTITUTIVE EQUATIONS

Constitutive equations relate the various types of fields. In the case of piezoelectricity the variables of interest are mechanical displacement $\boldsymbol{u}$, and the electric field $\boldsymbol{E}$. In the dynamic case, the electric field is changing so there is also a magnetic field, but in most cases this is neglected, and the quasi-static approximation for the electric field is used. A quantity that is sometimes taken into account is the temperature, since material constants can be affected by the temperature, but that will also be disregarded here. For a basic electro-mechanical (piezoelectric) problem, the constitutive equations are as follows:

$$\boldsymbol{T} = \boldsymbol{c}^E \cdot \boldsymbol{S} - \boldsymbol{e} \cdot \boldsymbol{E} \quad \text{or} \quad T_{ij} = c^E_{ijkl} S_{kl} - e_{mij} E_m, \tag{2.1}$$

$$\boldsymbol{D} = \boldsymbol{e} \cdot \boldsymbol{S} + \boldsymbol{\varepsilon}^S \cdot \boldsymbol{E} \quad \text{or} \quad D_n = e_{nkl} S_{kl} + \varepsilon^S_{nm} E_m. \tag{2.2}$$

The coefficients on the right-hand sides are material constants, where $\boldsymbol{c}$ is the elasticity, $\boldsymbol{\varepsilon}$ is the dielectric constant, and $\boldsymbol{e}$ is a piezoelectric constant. These are all tensor quantities. The electric quantities are the electric field $\boldsymbol{E}$, and the electric displacement $\boldsymbol{D}$. The mechanical quantities are the stress $\boldsymbol{T}$ (force per area), and strain $\boldsymbol{S}$, which are second rank tensors. The expression for strain is given below in terms of the mechanical displacement.

$$S_{kl} = \frac{1}{2}\left(\frac{\partial u_k}{\partial x_l} + \frac{\partial u_l}{\partial x_k}\right), \quad \text{where } \boldsymbol{u} = \{u, v, w\} \text{ and } \boldsymbol{x} = \{x, y, z\}. \tag{2.3}$$

In addition to the constitutive equations, we also have the electric charge condition in the piezoelectric sheets (which are a dielectric material with no electric conductivity), and the charge continuity equation in the electrodes.

Zero-charge condition in the piezoelectric sheets:

$$\boldsymbol{\nabla} \cdot \boldsymbol{D} = 0. \tag{2.4}$$

In the electrode, where ρ_q is the volume charge density:

$$\boldsymbol{\nabla} \cdot \boldsymbol{D} = \rho_q \qquad \text{Gauss's law.} \tag{2.5}$$

Gauss's law always applies, but in a dielectric with no initial net charge the charge will remain neutral at all times and there will not be a non-zero charge volume density.

The charge conservation (continuity) equation for the electrodes, where $\boldsymbol{J}$ is the current density (current per area):

$$\boldsymbol{\nabla} \cdot \boldsymbol{J} + \frac{\partial \rho_q}{\partial t} = 0 \qquad \text{Equation of Continuity.} \tag{2.6}$$

Another way of writing this is

$$\boldsymbol{\nabla} \cdot \left(\boldsymbol{J} + \frac{\partial \boldsymbol{D}}{\partial t} \right) = 0. \tag{2.7}$$

$$\boldsymbol{J} + \frac{\partial \boldsymbol{D}}{\partial t} = \boldsymbol{\nabla} \times \boldsymbol{H} \qquad \text{Maxwell-Ampère law.} \tag{2.8}$$

$\boldsymbol{H}$ is the magnetic field, which is neglected in the quasi-static approximation.

At the interface between two different materials (mediums), where the normal vector for material one is $\hat{\boldsymbol{n}}_1$ and points into material two (and $\hat{\boldsymbol{n}}_2$=-$\hat{\boldsymbol{n}}_1$), the field continuity conditions are as follows:

$$\hat{\boldsymbol{n}}_1 \cdot \boldsymbol{D}_1 + \hat{\boldsymbol{n}}_2 \cdot \boldsymbol{D}_2 = \rho_s, \tag{2.9}$$

$$\hat{\boldsymbol{n}}_1 \times \boldsymbol{H}_1 + \hat{\boldsymbol{n}}_2 \times \boldsymbol{H}_2 = \boldsymbol{J}_s, \tag{2.10}$$

where ρ_s is the surface charge density (charge per area), and $\boldsymbol{J}_s$ is the surface (tangential) current density (current per meter).

The constitutive equation for the electric current density in the electrode:

$$\boldsymbol{J} = \sigma \boldsymbol{E}. \tag{2.11}$$

For a simple material, the conductivity σ does not depend on direction. More generally, σ is a tensor, and

$$J_i = \sigma_{ij} E_j. \tag{2.12}$$

In a material such as PEDOT-PSS, which is made of long polymers, it is possible that if the strands were all stretched out in the same direction, the conductivity would be highest in the stretch direction, and smaller in transverse directions. The conductivity tensor would most likely be symmetric, since charge could just as easily flow backwards as forwards, so $\sigma_{ij} = \sigma_{ji}$.

In the quasi-static approximation for the electric field,

$$\boldsymbol{E} = -\boldsymbol{\nabla}\phi, \tag{2.13}$$

where ϕ is the electric potential.

The equations which govern the time dependent behavior of the variables are called the equations of motion. For the elastic variables, we have a Newton's second law ($\boldsymbol{F} = m\boldsymbol{a}$) type equation. There is no equation of motion for the electric potential, so the equation of continuity is used to determine ϕ. In the absence of body forces (gravity), the force equations for $\boldsymbol{u}$ are:

$$\rho \frac{\partial^2 \boldsymbol{u}}{\partial t^2} = \boldsymbol{\nabla} \cdot \boldsymbol{T} \quad \text{or} \quad \rho \frac{\partial^2 u_i}{\partial t^2} = \frac{\partial T_{ij}}{\partial x_j}. \tag{2.14}$$

$$\rho\frac{\partial^2 u}{\partial t^2} = \frac{\partial T_{11}}{\partial x} + \frac{\partial T_{12}}{\partial y} + \frac{\partial T_{13}}{\partial z} \tag{2.15}$$

$$\rho\frac{\partial^2 v}{\partial t^2} = \frac{\partial T_{21}}{\partial x} + \frac{\partial T_{22}}{\partial y} + \frac{\partial T_{23}}{\partial z} \tag{2.16}$$

$$\rho\frac{\partial^2 w}{\partial t^2} = \frac{\partial T_{31}}{\partial x} + \frac{\partial T_{32}}{\partial y} + \frac{\partial T_{33}}{\partial z} \tag{2.17}$$

The notation used for the various quantities and material constants will be clarified in this section. The matrices $\boldsymbol{T}$ and $\boldsymbol{S}$ are symmetric, and the tensor $\boldsymbol{e}$ is symmetric in its last two indices. The tensor $\boldsymbol{c}$ is symmetric in the first and second pair of indices, and also the two pairs can be interchanged.

$$c_{ijkl} = c_{(ij)(kl)} = c_{(kl)(ij)} \tag{2.18}$$

Because of the symmetries, the constitutive equations can be written in an abbreviated form, which is called matrix notation. Each symmetric pair of indices is condensed into a single index that runs from 1 to 6. The convention is to condense the two indices as follows:

$$11 \to 1, \quad 22 \to 2, \quad 33 \to 3, \quad 23 \to 4, \quad 13 \to 5, \quad 12 \to 6 \tag{2.19}$$

With the index notation, the equations for stress become

$$T_\lambda = c^E_{\lambda\mu} S_\mu - e_{m\lambda} E_m, \tag{2.20}$$

where

$$T_{ij} \to T_\lambda \text{ for all } i, j,$$

$$S_{ij} \to S_\lambda \text{ for } i = j,$$

and

$$2S_{ij} \to S_\lambda \text{ for } i \neq j.$$

With this condensed notation, we get the following set of equations for $\boldsymbol{T}$ and $\boldsymbol{D}$.

$$T_1 = c_{11}S_1 + c_{12}S_2 + c_{13}S_3 + c_{16}S_6 + c_{15}S_5 + c_{14}S_4 - e_{11}E_1 - e_{21}E_2 - e_{31}E_3 \tag{2.21}$$

$$T_2 = c_{21}S_1 + c_{22}S_2 + c_{23}S_3 + c_{26}S_6 + c_{25}S_5 + c_{24}S_4 - e_{12}E_1 - e_{22}E_2 - e_{32}E_3 \tag{2.22}$$

$$T_3 = c_{31}S_1 + c_{32}S_2 + c_{33}S_3 + c_{36}S_6 + c_{35}S_5 + c_{34}S_4 - e_{13}E_1 - e_{23}E_2 - e_{33}E_3 \tag{2.23}$$

$$T_6 = c_{61}S_1 + c_{62}S_2 + c_{63}S_3 + c_{66}S_6 + c_{65}S_5 + c_{64}S_4 - e_{16}E_1 - e_{26}E_2 - e_{36}E_3 \tag{2.24}$$

$$T_5 = c_{51}S_1 + c_{52}S_2 + c_{53}S_3 + c_{56}S_6 + c_{55}S_5 + c_{54}S_4 - e_{15}E_1 - e_{25}E_2 - e_{35}E_3 \tag{2.25}$$

$$T_4 = c_{41}S_1 + c_{42}S_2 + c_{43}S_3 + c_{46}S_6 + c_{45}S_5 + c_{44}S_4 - e_{14}E_1 - e_{24}E_2 - e_{34}E_3 \tag{2.26}$$

$$D_n = e_{n\lambda}S_\lambda + \varepsilon^S_{nm}E_m \tag{2.27}$$

$$D_1 = e_{11}S_1 + e_{12}S_2 + e_{13}S_3 + e_{14}S_4 + e_{15}S_5 + e_{16}S_6 + \varepsilon_{11}E_1 + \varepsilon_{12}E_2 + \varepsilon_{13}E_3 \tag{2.28}$$

$$D_2 = e_{21}S_1 + e_{22}S_2 + e_{23}S_3 + e_{24}S_4 + e_{25}S_5 + e_{26}S_6 + \varepsilon_{21}E_1 + \varepsilon_{22}E_2 + \varepsilon_{23}E_3 \tag{2.29}$$

$$D_3 = e_{31}S_1 + e_{32}S_2 + e_{33}S_3 + e_{34}S_4 + e_{35}S_5 + e_{36}S_6 + \varepsilon_{31}E_1 + \varepsilon_{32}E_2 + \varepsilon_{33}E_3 \tag{2.30}$$

The material for the piezoelectric sheets is PVDF, which has crystal symmetry $mm2$ and allows the following forms for the material constants:

$$c_{\lambda\mu} = \begin{bmatrix} c_{11} & c_{12} & c_{13} & \cdot & \cdot & \cdot \\ c_{12} & c_{22} & c_{23} & \cdot & \cdot & \cdot \\ c_{13} & c_{23} & c_{33} & \cdot & \cdot & \cdot \\ \cdot & \cdot & \cdot & c_{44} & \cdot & \cdot \\ \cdot & \cdot & \cdot & \cdot & c_{55} & \cdot \\ \cdot & \cdot & \cdot & \cdot & \cdot & c_{66} \end{bmatrix} \tag{2.31}$$

$$e_{i\lambda} = \begin{bmatrix} \cdot & \cdot & \cdot & \cdot & e_{15} & \cdot \\ \cdot & \cdot & \cdot & e_{24} & \cdot & \cdot \\ e_{31} & e_{32} & e_{33} & \cdot & \cdot & \cdot \end{bmatrix} \tag{2.32}$$

$$\varepsilon_{mn} = \begin{bmatrix} \varepsilon_1 & \cdot & \cdot \\ \cdot & \varepsilon_2 & \cdot \\ \cdot & \cdot & \varepsilon_3 \end{bmatrix} \tag{2.33}$$

These constants are for PVDF that is oriented so that the sheet is in the x-y plane. Also, during the manufacturing process the sheet is stretched in the x direction and is poled in the z direction. Poling is when a high electric field is applied in order to align the dipoles in the PVDF molecules so that there is an overall strong piezoelectric constant.

With the allowed non-zero material constants, we get the following set of equations for PVDF.

$$T_1 = c_{11}S_1 + c_{12}S_2 + c_{13}S_3 - e_{31}E_3 \tag{2.34}$$

$$T_2 = c_{12}S_1 + c_{22}S_2 + c_{23}S_3 - e_{32}E_3 \tag{2.35}$$

$$T_3 = c_{13}S_1 + c_{23}S_2 + c_{33}S_3 - e_{33}E_3 \tag{2.36}$$

$$T_4 = c_{44}S_4 - e_{24}E_2 \tag{2.37}$$

$$T_5 = c_{55}S_5 - e_{15}E_1 \tag{2.38}$$

$$T_6 = c_{66}S_6 \tag{2.39}$$

$$D_1 = e_{15}S_5 + \varepsilon_1 E_1 \tag{2.40}$$

$$D_2 = e_{24}S_4 + \varepsilon_2 E_2 \tag{2.41}$$

$$D_3 = e_{31}S_1 + e_{32}S_2 + e_{33}S_3 + \varepsilon_3 E_3 \tag{2.42}$$

To help clarify the definition of each of the variables, they are listed here.

$$\begin{aligned} &S_1 = \frac{\partial u}{\partial x}, \quad S_2 = \frac{\partial v}{\partial y}, \quad S_3 = \frac{\partial w}{\partial z}, \\ &S_4 = \frac{\partial v}{\partial z} + \frac{\partial w}{\partial y}, \quad S_5 = \frac{\partial u}{\partial z} + \frac{\partial w}{\partial x}, \quad S_6 = \frac{\partial u}{\partial y} + \frac{\partial v}{\partial x} \end{aligned} \tag{2.43}$$

$$E_1 = -\frac{\partial \phi}{\partial x}, \quad E_2 = -\frac{\partial \phi}{\partial y}, \quad E_3 = -\frac{\partial \phi}{\partial z} \tag{2.44}$$

The equations of motion for PVDF:

$$\begin{aligned}\rho\frac{\partial^2 u}{\partial t^2} &= \frac{\partial T_1}{\partial x}+\frac{\partial T_6}{\partial y}+\frac{\partial T_5}{\partial z} = \frac{\partial}{\partial x}\left(c_{11}S_1+c_{12}S_2+c_{13}S_3-e_{31}E_3\right)\\ &\quad+\frac{\partial}{\partial y}\left(c_{66}S_6\right)+\frac{\partial}{\partial z}\left(c_{55}S_5-e_{15}E_1\right)\\ &= c_{11}\frac{\partial^2 u}{\partial x^2}+c_{66}\frac{\partial^2 u}{\partial y^2}+c_{55}\frac{\partial^2 u}{\partial z^2}+\left(c_{12}+c_{66}\right)\frac{\partial^2 v}{\partial x\partial y}\\ &\quad+\left(c_{13}+c_{55}\right)\frac{\partial^2 w}{\partial x\partial z}+\left(e_{31}+e_{15}\right)\frac{\partial^2\phi}{\partial x\partial z}\end{aligned} \tag{2.45}$$

$$\begin{aligned}\rho\frac{\partial^2 v}{\partial t^2} &= \frac{\partial T_6}{\partial x}+\frac{\partial T_2}{\partial y}+\frac{\partial T_4}{\partial z} = \frac{\partial}{\partial x}\left(c_{66}S_6\right)\\ &\quad+\frac{\partial}{\partial y}\left(c_{12}S_1+c_{22}S_2+c_{23}S_3-e_{32}E_3\right)+\frac{\partial}{\partial z}\left(c_{44}S_4-e_{24}E_2\right)\\ &= \left(c_{12}+c_{66}\right)\frac{\partial^2 u}{\partial x\partial y}+c_{66}\frac{\partial^2 v}{\partial x^2}+c_{22}\frac{\partial^2 v}{\partial y^2}+c_{44}\frac{\partial^2 v}{\partial z^2}\\ &\quad+\left(c_{23}+c_{44}\right)\frac{\partial^2 w}{\partial y\partial z}+\left(e_{32}+e_{24}\right)\frac{\partial^2\phi}{\partial y\partial z}\end{aligned} \tag{2.46}$$

$$\begin{aligned}\rho\frac{\partial^2 w}{\partial t^2} &= \frac{\partial T_5}{\partial x}+\frac{\partial T_4}{\partial y}+\frac{\partial T_3}{\partial z} = \frac{\partial}{\partial x}\left(c_{55}S_5-e_{15}E_1\right)+\frac{\partial}{\partial y}\left(c_{44}S_4-e_{24}E_2\right)\\ &\quad+\frac{\partial}{\partial z}\left(c_{13}S_1+c_{23}S_2+c_{33}S_3-e_{33}E_3\right)\\ &= \left(c_{13}+c_{55}\right)\frac{\partial^2 u}{\partial x\partial z}+\left(c_{23}+c_{44}\right)\frac{\partial^2 v}{\partial y\partial z}+c_{55}\frac{\partial^2 w}{\partial x^2}\\ &\quad+c_{44}\frac{\partial^2 w}{\partial y^2}+c_{33}\frac{\partial^2 w}{\partial z^2}+e_{15}\frac{\partial^2\phi}{\partial x^2}+e_{24}\frac{\partial^2\phi}{\partial y^2}+e_{33}\frac{\partial^2\phi}{\partial z^2}\end{aligned} \tag{2.47}$$

$$\begin{aligned}\boldsymbol{\nabla}\cdot\boldsymbol{D} &= \frac{\partial D_1}{\partial x}+\frac{\partial D_2}{\partial y}+\frac{\partial D_3}{\partial z} = \frac{\partial}{\partial x}\left(e_{15}S_5+\varepsilon_1 E_1\right)+\frac{\partial}{\partial y}\left(e_{24}S_4+\varepsilon_2 E_2\right)\\ &\quad+\frac{\partial}{\partial z}\left(e_{31}S_1+e_{32}S_2+e_{33}S_3+\varepsilon_3 E_3\right)\\ &= \left(e_{15}+e_{31}\right)\frac{\partial^2 u}{\partial x\partial z}+\left(e_{24}+e_{32}\right)\frac{\partial^2 v}{\partial y\partial z}+e_{15}\frac{\partial^2 w}{\partial x^2}+e_{24}\frac{\partial^2 w}{\partial y^2}\\ &\quad+e_{33}\frac{\partial^2 w}{\partial z^2}-\varepsilon_1\frac{\partial^2\phi}{\partial x^2}-\varepsilon_2\frac{\partial^2\phi}{\partial y^2}-\varepsilon_3\frac{\partial^2\phi}{\partial z^2} = 0\end{aligned} \tag{2.48}$$

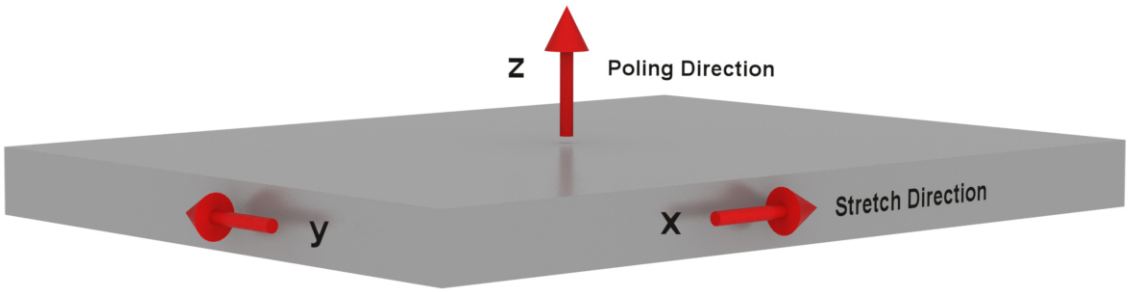

Figure 2.1: PVDF material directions.

In looking for references of the piezoelectric constants, I have found literature which lists a different form than $\boldsymbol{e}$, namely $\boldsymbol{g}$ [9]. To convert from the g_{ij} piezoelectric constants to e_{ij}, the following two sums are used, which make use of the elasticity and dielectric constants:

$$d_{nkl} = \varepsilon^{T}_{nm} g_{mkl}, \tag{2.49}$$

$$e_{nij} = d_{nkl} c^{E}_{klij} = \varepsilon^{T}_{nm} g_{mkl} c^{E}_{klij}. \tag{2.50}$$

Given that ε_{ij} has only diagonal terms that are non-zero:

$$e_{nij} = \sum_{kl} \varepsilon_{nn} g_{nkl} c_{klij} \tag{2.51}$$

$$e_{n\lambda} = \sum_{\mu} \varepsilon_{nn} g_{n\mu} c_{\mu\lambda} \tag{2.52}$$

The g_{ij} have the same non-zero entries as e_{ij}.

$$e_{31} = \varepsilon_3 \left(g_{31} c_{11} + g_{32} c_{12} + g_{33} c_{13} \right) \tag{2.53}$$

$$e_{32} = \varepsilon_3 \left(g_{31} c_{12} + g_{32} c_{22} + g_{33} c_{23} \right) \tag{2.54}$$

$$e_{33} = \varepsilon_3 \left(g_{31} c_{13} + g_{32} c_{23} + g_{33} c_{33} \right) \tag{2.55}$$

$$e_{24} = \varepsilon_2 g_{24} c_{44} \tag{2.56}$$

$$e_{15} = \varepsilon_1 g_{15} c_{55} \tag{2.57}$$

The following values were given for $\boldsymbol{g}$ [9].

$$g_{i\lambda} = \begin{bmatrix} \cdot & \cdot & \cdot & \cdot & -0.32 & \cdot \\ \cdot & \cdot & \cdot & -0.27 & \cdot & \cdot \\ 0.21 & 0.03 & -0.46 & \cdot & \cdot & \cdot \end{bmatrix} \text{V}\cdot\text{m/N} \tag{2.58}$$

For PVDF we have the following set of material constants.

$$c_{\lambda\mu} = \begin{bmatrix} 3.70 & 1.47 & 1.23 & \cdot & \cdot & \cdot \\ 1.47 & 3.20 & 1.00 & \cdot & \cdot & \cdot \\ 1.23 & 1.00 & 1.51 & \cdot & \cdot & \cdot \\ \cdot & \cdot & \cdot & 0.55 & \cdot & \cdot \\ \cdot & \cdot & \cdot & \cdot & 0.59 & \cdot \\ \cdot & \cdot & \cdot & \cdot & \cdot & 0.70 \end{bmatrix} \times 10^9 \text{ N/m}^2 \tag{2.59}$$

$$e_{i\lambda} = \begin{bmatrix} \cdot & \cdot & \cdot & \cdot & -1.34 & \cdot \\ \cdot & \cdot & \cdot & -1.05 & \cdot & \cdot \\ 1.81 & -0.392 & -2.88 & \cdot & \cdot & \cdot \end{bmatrix} \times 10^{-2} \text{ N/V}\cdot\text{m} \tag{2.60}$$

$$\varepsilon_{mn} = \begin{bmatrix} 7.35 & \cdot & \cdot \\ \cdot & 9.27 & \cdot \\ \cdot & \cdot & 8.05 \end{bmatrix} \times \varepsilon_0 \left(= 8.85 \times 10^{-12} \text{ C}^2/\text{N}\cdot\text{m}^2\right) \tag{2.61}$$

CHAPTER 3

BIMORPH: STATIC 3D CASE

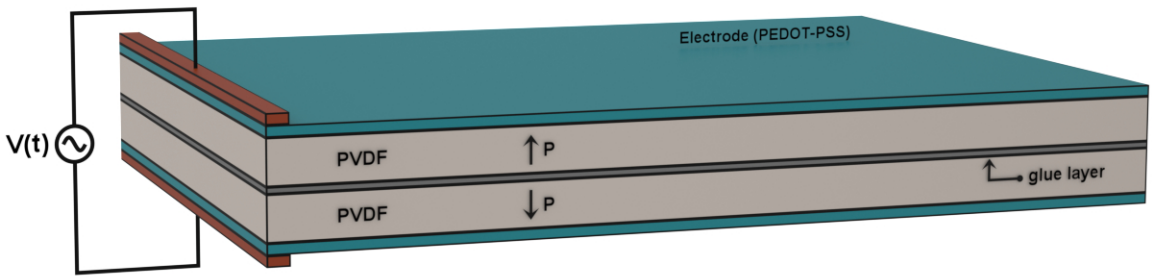

Figure 3.1: Schematic of a bimorph (series configuration).

A piezoelectric bimorph consists of two thin piezoelectric sheets which have been glued together, and two electrodes which are on the outside of the sheets, as shown in figure 3.1. The piezoelectric sheets are made of poly(vinylidene fluoride), abbreviated PVDF, and the electrodes are made of the commercially available conducting polymer PEDOT-PSS. The bottom electrode is usually grounded, and an alternating voltage is applied to the top electrode. This creates a nearly uniform electric field across the PVDF. The mechanical response of the bimorph is only dependent on the resulting electric field, so it is possible to shift the applied voltage by a constant with identical results. If the total applied voltage is $V_0 \sin \omega t$, then a common scenario is to have $(V_0/2)\sin \omega t$ applied to the top electrode, and $-(V_0/2)\sin \omega t$ applied to the bottom electrode.

The piezoelectric sheets are manufactured so as to have a permanent electric dipole, and an applied electric field will either cause a sheet to lengthen or shorten, depending on the alignment of the dipole to the field. For an actuator, the polarization directions of the two sheets are opposite each other so that one sheet will lengthen while the other

shortens, causing the whole actuator to bend. This configuration is called a series bimorph. The parallel configuration is where there are three electrodes. There is a middle electrode between the piezoelectric sheets, which is grounded. The same voltage is then applied to the outer electrodes, and in this case the polarization direction would be the same in the two sheets.

Figure 3.1 above shows a schematic of a bimorph, with exaggerated thickness. The thickness of each PVDF sheet is 30 microns, since that is the common thickness for commercially available PVDF sheets. The glue layer exists, but is neglected in modeling the actuator. In order to apply a voltage to the electrodes, metal strips are glued on to one end using highly conductive metallic glue. A wire is then glued to the strips, which connects the strips to the voltage source. The electrodes, made of PEDOT-PSS, are applied to the piezoelectric sheets by using an inkjet printer to print on multiple layers until the desired thickness is achieved. The electrodes are printed onto the PVDF before the bimorph is assembled. The thickness of the electrode affects its conductivity, but thicker electrodes are also stiffer and adversely affect the bimorph's ability to bend.

In the static case, where a constant (non-time-changing) voltage is applied, the set of coupled equations describing mechanical displacement and electrical potential are as follows.

$$\frac{\partial T_1}{\partial x} + \frac{\partial T_6}{\partial y} + \frac{\partial T_5}{\partial z} = 0 \tag{3.1}$$

$$\frac{\partial T_6}{\partial x} + \frac{\partial T_2}{\partial y} + \frac{\partial T_4}{\partial z} = 0 \tag{3.2}$$

$$\frac{\partial T_5}{\partial x} + \frac{\partial T_4}{\partial y} + \frac{\partial T_3}{\partial z} = 0 \tag{3.3}$$

$$\frac{\partial D_1}{\partial x} + \frac{\partial D_2}{\partial y} + \frac{\partial D_3}{\partial z} = 0 \tag{3.4}$$

The following definitions can be made in order to simplify notation.

$$\boldsymbol{t}_u = T_1\hat{\boldsymbol{x}} + T_6\hat{\boldsymbol{y}} + T_5\hat{\boldsymbol{z}} \tag{3.5}$$

$$\boldsymbol{t}_v = T_6\hat{\boldsymbol{x}} + T_2\hat{\boldsymbol{y}} + T_4\hat{\boldsymbol{z}} \tag{3.6}$$

$$\boldsymbol{t}_w = T_5\hat{\boldsymbol{x}} + T_4\hat{\boldsymbol{y}} + T_3\hat{\boldsymbol{z}} \tag{3.7}$$

With this notation, the governing equations are simple and only involve the divergence.

$$\boldsymbol{\nabla} \cdot \boldsymbol{t}_u = 0 \tag{3.8}$$

$$\boldsymbol{\nabla} \cdot \boldsymbol{t}_v = 0 \tag{3.9}$$

$$\boldsymbol{\nabla} \cdot \boldsymbol{t}_w = 0 \tag{3.10}$$

$$\boldsymbol{\nabla} \cdot \boldsymbol{D} = 0 \tag{3.11}$$

The weak form of the governing equations are shown below. For each differential equation, we first multiply by the appropriate variation, and integrate over the entire domain of the problem (the volume of the bimorph). The divergence operator is then transferred to the variation variable, and we get a boundary integral. The volume (or domain) integral is represented by Ω. The boundary of Ω is represented by Γ. The normal vector, which points out of the volume along Γ, is $\hat{\boldsymbol{n}}$. A schematic of a domain and boundary is shown in figure A.1, in appendix A.

$$\int_\Omega \boldsymbol{\nabla}\delta u \cdot \boldsymbol{t}_u \, \mathrm{d}\Omega - \oint_\Gamma \delta u \, \boldsymbol{t}_u \cdot \hat{\boldsymbol{n}} \, \mathrm{d}\Gamma = 0 \tag{3.12}$$

$$\int_\Omega \boldsymbol{\nabla}\delta v \cdot \boldsymbol{t}_v \, \mathrm{d}\Omega - \oint_\Gamma \delta v \, \boldsymbol{t}_v \cdot \hat{\boldsymbol{n}} \, \mathrm{d}\Gamma = 0 \tag{3.13}$$

$$\int_\Omega \boldsymbol{\nabla}\delta w \cdot \boldsymbol{t}_w \, \mathrm{d}\Omega - \oint_\Gamma \delta w \, \boldsymbol{t}_w \cdot \hat{\boldsymbol{n}} \, \mathrm{d}\Gamma = 0 \tag{3.14}$$

$$\int_\Omega \boldsymbol{\nabla}\delta \phi \cdot \boldsymbol{D} \, \mathrm{d}\Omega - \oint_\Gamma \delta \phi \, \boldsymbol{D} \cdot \hat{\boldsymbol{n}} \, \mathrm{d}\Gamma = 0 \tag{3.15}$$

The procedure for converting a differential equation into its weak form is illustrated here. The differential equation is multiplied by the variation of the primary variable (u in this example), and integrated over the entire domain.

$$\begin{aligned}
&\int_\Omega \delta u \left(\frac{\partial T_1}{\partial x} + \frac{\partial T_6}{\partial y} + \frac{\partial T_5}{\partial z} \right) \mathrm{d}\Omega = 0 \\
&= -\int_\Omega \left(\frac{\partial \delta u}{\partial x} T_1 + \frac{\partial \delta u}{\partial y} T_6 + \frac{\partial \delta u}{\partial z} T_5 \right) \mathrm{d}\Omega \\
&\qquad + \underbrace{\int_\Omega \left(\frac{\partial}{\partial x}(\delta u T_1) + \frac{\partial}{\partial y}(\delta u T_6) + \frac{\partial}{\partial z}(\delta u T_5) \right) \mathrm{d}\Omega}_{\displaystyle\int_\Omega \boldsymbol{\nabla} \cdot \left[\delta u \left(T_1 \hat{\boldsymbol{x}} + T_6 \hat{\boldsymbol{y}} + T_5 \hat{\boldsymbol{z}} \right) \right] \mathrm{d}\Omega} \\
&\qquad\qquad \longrightarrow \oint_\Gamma \left[\delta u \left(T_1 \hat{\boldsymbol{x}} + T_6 \hat{\boldsymbol{y}} + T_5 \hat{\boldsymbol{z}} \right) \right] \cdot \hat{\boldsymbol{n}} \, \mathrm{d}\Gamma \\
&\qquad\qquad \longrightarrow \oint_\Gamma \delta u \, \boldsymbol{t}_u \cdot \hat{\boldsymbol{n}} \, \mathrm{d}\Gamma
\end{aligned} \tag{3.16}$$

The quantities in the boundary integrals tell us what are good boundary conditions. If we specify the value of the variable along the boundary, then the variation will be precisely zero. On the other hand, we could specify the surface tractions ($\boldsymbol{t}_u \cdot \hat{\boldsymbol{n}}$), or the surface charge density $\boldsymbol{D} \cdot \hat{\boldsymbol{n}}$ for the electrical condition. The simplest case is to specify these values to equal zero whenever the variable itself is not being specified on the boundary. If either one value or the other is specified on Γ, then the entire boundary integral is zero. This will be the case here for all the variables.

The explicit forms of the governing equations in the weak form are shown here, where the boundary integrals are equal to zero.

$$\begin{aligned}
\int_\Omega \Bigg[&\frac{\partial \delta u}{\partial x} \left(c_{11} \frac{\partial u}{\partial x} + c_{12} \frac{\partial v}{\partial y} + c_{13} \frac{\partial w}{\partial z} + e_{31} \frac{\partial \phi}{\partial z} \right) + c_{66} \frac{\partial \delta u}{\partial y} \left(\frac{\partial u}{\partial y} + \frac{\partial v}{\partial x} \right) \\
&+ \frac{\partial \delta u}{\partial z} \left(c_{55} \left(\frac{\partial u}{\partial z} + \frac{\partial w}{\partial x} \right) + e_{15} \frac{\partial \phi}{\partial x} \right) \Bigg] \mathrm{d}\Omega = 0
\end{aligned} \tag{3.17}$$

$$\begin{aligned}
\int_\Omega \Bigg[&c_{66} \frac{\partial \delta v}{\partial x} \left(\frac{\partial u}{\partial y} + \frac{\partial v}{\partial x} \right) + \frac{\partial \delta v}{\partial y} \left(c_{12} \frac{\partial u}{\partial x} + c_{22} \frac{\partial v}{\partial y} + c_{23} \frac{\partial w}{\partial z} + e_{32} \frac{\partial \phi}{\partial z} \right) \\
&+ \frac{\partial \delta v}{\partial z} \left(c_{44} \left(\frac{\partial v}{\partial z} + \frac{\partial w}{\partial y} \right) + e_{24} \frac{\partial \phi}{\partial y} \right) \Bigg] \mathrm{d}\Omega = 0
\end{aligned} \tag{3.18}$$

$$\int_\Omega \left[\frac{\partial \delta w}{\partial x}\left(c_{55}\left(\frac{\partial u}{\partial z}+\frac{\partial w}{\partial x}\right)+e_{15}\frac{\partial \phi}{\partial x}\right)+\frac{\partial \delta w}{\partial y}\left(c_{44}\left(\frac{\partial v}{\partial z}+\frac{\partial w}{\partial y}\right)+e_{24}\frac{\partial \phi}{\partial y}\right) + \frac{\partial \delta w}{\partial z}\left(c_{13}\frac{\partial u}{\partial x}+c_{23}\frac{\partial v}{\partial y}+c_{33}\frac{\partial w}{\partial z}+e_{33}\frac{\partial \phi}{\partial z}\right)\right] \mathrm{d}\Omega = 0 \tag{3.19}$$

$$\int_\Omega \left[\frac{\partial \delta \phi}{\partial x}\left(e_{15}\left(\frac{\partial u}{\partial z}+\frac{\partial w}{\partial x}\right)-\varepsilon_1\frac{\partial \phi}{\partial x}\right)+\frac{\partial \delta \phi}{\partial y}\left(e_{24}\left(\frac{\partial v}{\partial z}+\frac{\partial w}{\partial y}\right)-\varepsilon_2\frac{\partial \phi}{\partial y}\right) + \frac{\partial \delta \phi}{\partial z}\left(e_{31}\frac{\partial u}{\partial x}+e_{32}\frac{\partial v}{\partial y}+e_{33}\frac{\partial w}{\partial z}-\varepsilon_3\frac{\partial \phi}{\partial z}\right)\right] \mathrm{d}\Omega = 0 \tag{3.20}$$

The solutions of the variables, which we are trying to find, are functions and can thus can be considered to have an infinite number of degrees of freedom. In the finite element method, we reduce the problem from having infinite degrees of freedom, to one of finite degrees of freedom. The problem is transformed so we are solving for a finite set of unknown coefficients. The functions for u, v, w and ϕ are approximated by a finite set of basis functions of our choosing, where the i^{th} basis function is denoted by ψ_i.

$$u(\boldsymbol{x}) \approx \sum_{i=1}^{N} u_i \psi_i(\boldsymbol{x}), \qquad \delta u(\boldsymbol{x}) \approx \sum_{i=1}^{N} \delta u_i \psi_i(\boldsymbol{x}) \tag{3.21}$$

$$v(\boldsymbol{x}) \approx \sum_{i=1}^{N} v_i \psi_i(\boldsymbol{x}), \qquad \delta v(\boldsymbol{x}) \approx \sum_{i=1}^{N} \delta v_i \psi_i(\boldsymbol{x}) \tag{3.22}$$

$$w(\boldsymbol{x}) \approx \sum_{i=1}^{N} w_i \psi_i(\boldsymbol{x}), \qquad \delta w(\boldsymbol{x}) \approx \sum_{i=1}^{N} \delta w_i \psi_i(\boldsymbol{x}) \tag{3.23}$$

$$\phi(\boldsymbol{x}) \approx \sum_{i=1}^{N} \phi_i \psi_i(\boldsymbol{x}), \qquad \delta \phi(\boldsymbol{x}) \approx \sum_{i=1}^{N} \delta \phi_i \psi_i(\boldsymbol{x}) \tag{3.24}$$

The only necessary condition on the basis functions is that they form a complete set, meaning the sum of all the functions equals one, $\sum_{i=1}^{N} \psi_i(\boldsymbol{x}) = 1$. In the Finite Element Method (FEM), the basis functions are usually polynomials. If the polynomials go up to a certain order (cubic, for example), then all the lower order polynomials are also represented by the basis functions. For example, we would not have a basis that included first and third order polynomials, but didn't include second order polynomials.

In an elasticity problem such as the bimorph, there are drastically different dimensions involved. The thickness is very small compared to the length, and the z deflection

is also large. Because of this, the order of the basis functions has to be sufficient in order the prevent what is called locking, where the deflection solution is much smaller than it should be. It appears that using a second order basis is sufficient, while a linear basis causes locking.

In the Finite Element Method, the series approximations for each variable are substituted into the governing differential equations. For each i^{th} variation, such as δu_i, we get an independent equation which is equal to zero, since all variations are independent from each other. Each term involving a variation is individually equal to zero. If we have N total unknown coefficients for each variable, then the problem involves solving for a total of $4N$ unknowns. From the 4 differential equations, we get a $4N \times 4N$ linear system. The coefficients are then found by inverting the resulting matrix, which will be symmetric, but not positive-definite. The matrix is indefinite because of the inclusion of the electrical continuity equation, which has the opposite sign of the potential, relative to the elasticity equations.

$$\begin{bmatrix} \boldsymbol{K}^{11} & \boldsymbol{K}^{12} & \boldsymbol{K}^{13} & \boldsymbol{K}^{14} \\ \left(\boldsymbol{K}^{12}\right)^T & \boldsymbol{K}^{22} & \boldsymbol{K}^{23} & \boldsymbol{K}^{24} \\ \left(\boldsymbol{K}^{13}\right)^T & \left(\boldsymbol{K}^{23}\right)^T & \boldsymbol{K}^{33} & \boldsymbol{K}^{34} \\ \left(\boldsymbol{K}^{14}\right)^T & \left(\boldsymbol{K}^{24}\right)^T & \left(\boldsymbol{K}^{34}\right)^T & \boldsymbol{K}^{44} \end{bmatrix} \cdot \begin{bmatrix} \boldsymbol{u} \\ \boldsymbol{v} \\ \boldsymbol{w} \\ \boldsymbol{\phi} \end{bmatrix} = \begin{bmatrix} \boldsymbol{F}^1 \\ \boldsymbol{F}^2 \\ \boldsymbol{F}^3 \\ \boldsymbol{F}^4 \end{bmatrix} \tag{3.25}$$

The bold vectors such as $\boldsymbol{u}$ are the collection of all the (N) nodal values for that variable. The matrix is called the stiffness matrix, and the right-hand side is called the load vector. Since we don't have any force terms, the only non-zero contributions to $\boldsymbol{F}^i$ are from the non-zero boundary node entries in the $\boldsymbol{K}^{mn}$ sub-matrices. In the simple case where the bimorph is glued to the wall, the only non-zero entries are from the boundary potential nodes. On the top face we have a non-zero applied potential. These few nodes give the only non-zero contributions to the load vector, since the mechanical boundary conditions are all equal to zero. Either the displacements are equal to zero on the boundary, or the surface tractions are specified to be zero.

Each of the sub-matrices have $N \times N$ entries, which are listed here.

$$K_{ij}^{11} = \int_\Omega \left[c_{11} \frac{\partial \psi_i}{\partial x} \frac{\partial \psi_j}{\partial x} + c_{66} \frac{\partial \psi_i}{\partial y} \frac{\partial \psi_j}{\partial y} + c_{55} \frac{\partial \psi_i}{\partial z} \frac{\partial \psi_j}{\partial z} \right] \mathrm{d}\Omega \tag{3.26}$$

$$K_{ij}^{12} = \int_\Omega \left[c_{12} \frac{\partial \psi_i}{\partial x} \frac{\partial \psi_j}{\partial y} + c_{66} \frac{\partial \psi_i}{\partial y} \frac{\partial \psi_j}{\partial x} \right] \mathrm{d}\Omega \tag{3.27}$$

$$K_{ij}^{13} = \int_\Omega \left[c_{13} \frac{\partial \psi_i}{\partial x} \frac{\partial \psi_j}{\partial z} + c_{55} \frac{\partial \psi_i}{\partial z} \frac{\partial \psi_j}{\partial x} \right] \mathrm{d}\Omega \tag{3.28}$$

$$K_{ij}^{14} = \int_\Omega \left[e_{31} \frac{\partial \psi_i}{\partial x} \frac{\partial \psi_j}{\partial z} + e_{15} \frac{\partial \psi_i}{\partial z} \frac{\partial \psi_j}{\partial x} \right] \mathrm{d}\Omega \tag{3.29}$$

$$K_{ij}^{22} = \int_\Omega \left[c_{66} \frac{\partial \psi_i}{\partial x} \frac{\partial \psi_j}{\partial x} + c_{22} \frac{\partial \psi_i}{\partial y} \frac{\partial \psi_j}{\partial y} + c_{44} \frac{\partial \psi_i}{\partial z} \frac{\partial \psi_j}{\partial z} \right] \mathrm{d}\Omega \tag{3.30}$$

$$K_{ij}^{23} = \int_\Omega \left[c_{23} \frac{\partial \psi_i}{\partial y} \frac{\partial \psi_j}{\partial z} + c_{44} \frac{\partial \psi_i}{\partial z} \frac{\partial \psi_j}{\partial y} \right] \mathrm{d}\Omega \tag{3.31}$$

$$K_{ij}^{24} = \int_\Omega \left[e_{32} \frac{\partial \psi_i}{\partial y} \frac{\partial \psi_j}{\partial z} + e_{24} \frac{\partial \psi_i}{\partial z} \frac{\partial \psi_j}{\partial y} \right] \mathrm{d}\Omega \tag{3.32}$$

$$K_{ij}^{33} = \int_\Omega \left[c_{55} \frac{\partial \psi_i}{\partial x} \frac{\partial \psi_j}{\partial x} + c_{44} \frac{\partial \psi_i}{\partial y} \frac{\partial \psi_j}{\partial y} + c_{33} \frac{\partial \psi_i}{\partial z} \frac{\partial \psi_j}{\partial z} \right] \mathrm{d}\Omega \tag{3.33}$$

$$K_{ij}^{34} = \int_\Omega \left[e_{15} \frac{\partial \psi_i}{\partial x} \frac{\partial \psi_j}{\partial x} + e_{24} \frac{\partial \psi_i}{\partial y} \frac{\partial \psi_j}{\partial y} + e_{33} \frac{\partial \psi_i}{\partial z} \frac{\partial \psi_j}{\partial z} \right] \mathrm{d}\Omega \tag{3.34}$$

$$K_{ij}^{44} = -\int_\Omega \left[\varepsilon_1 \frac{\partial \psi_i}{\partial x} \frac{\partial \psi_j}{\partial x} + \varepsilon_2 \frac{\partial \psi_i}{\partial y} \frac{\partial \psi_j}{\partial y} + \varepsilon_3 \frac{\partial \psi_i}{\partial z} \frac{\partial \psi_j}{\partial z} \right] \mathrm{d}\Omega \tag{3.35}$$

Assuming the material constants are uniform, we can take those out of the integrals. This is valid everywhere except at the transition from the lower to the upper piezoelectric sheet. There some care must be made for the electric terms since the $e_{i\lambda}$ change sign. The $\boldsymbol{M}^{\mu\nu}$ matrices are just the integrals of the derivatives of the basis functions, so that $\boldsymbol{M}_{ij}^{\mu\nu} = \int_\Omega \frac{\partial \psi_i}{\partial \mu} \frac{\partial \psi_j}{\partial \nu} \, \mathrm{d}\Omega$.

$$\boldsymbol{K}^{11} = c_{11} \boldsymbol{M}^{xx} + c_{66} \boldsymbol{M}^{yy} + c_{55} \boldsymbol{M}^{zz} \tag{3.36}$$

$$\boldsymbol{K}^{12} = c_{12} \boldsymbol{M}^{xy} + c_{66} \left(\boldsymbol{M}^{xy} \right)^T \tag{3.37}$$

$$\boldsymbol{K}^{13} = c_{13} \boldsymbol{M}^{xz} + c_{55} \left(\boldsymbol{M}^{xz} \right)^T \tag{3.38}$$

$$\boldsymbol{K}^{14} = e_{31}\boldsymbol{M}^{xz} + e_{15}\left(\boldsymbol{M}^{xz}\right)^T \tag{3.39}$$

$$\boldsymbol{K}^{22} = c_{66}\boldsymbol{M}^{xx} + c_{22}\boldsymbol{M}^{yy} + c_{44}\boldsymbol{M}^{zz} \tag{3.40}$$

$$\boldsymbol{K}^{23} = c_{23}\boldsymbol{M}^{yz} + c_{44}\left(\boldsymbol{M}^{yz}\right)^T \tag{3.41}$$

$$\boldsymbol{K}^{24} = e_{32}\boldsymbol{M}^{yz} + e_{24}\left(\boldsymbol{M}^{yz}\right)^T \tag{3.42}$$

$$\boldsymbol{K}^{33} = c_{55}\boldsymbol{M}^{xx} + c_{44}\boldsymbol{M}^{yy} + c_{33}\boldsymbol{M}^{zz} \tag{3.43}$$

$$\boldsymbol{K}^{34} = e_{15}\boldsymbol{M}^{xx} + e_{24}\boldsymbol{M}^{yy} + e_{33}\boldsymbol{M}^{zz} \tag{3.44}$$

$$\boldsymbol{K}^{44} = -\varepsilon_1\boldsymbol{M}^{xx} - \varepsilon_2\boldsymbol{M}^{yy} - \varepsilon_3\boldsymbol{M}^{zz} \tag{3.45}$$

As a test problem, we have the following specifications for a bimorph. There are two PVDF sheets, each 30 microns thick. The bimorph is 2.5 centimeters long and 1.25 centimeters wide. The bottom face is grounded $(\phi = 0)$, and the top face has an applied voltage of 600 volts. The bimorph is clamped at the left end ($u = 0$ at $x = 0$), but the y and z displacements are nearly free. v is specified to be zero along the vertical line $(x = 0, y = 0)$ for symmetry reasons, and w is only specified to be zero at the point $(x = 0, y = 0, z = 0)$. This puts less constraint on the overall deformation of the bimorph. Wherever the boundary displacements are not specified, the surface tractions are zero. The shape of the bimorph after deformation is shown in figure 3.2.

The problem was solved using the Finite Element Method using quadratic Lagrange elements, so that each element contains 3 nodes in each direction, for a total of 27 nodes per element. Because the only way that I know which solves the system of linear equations accurately is using a direct solver, the problem size is limited by the amount of my computer's memory. For a bimorph which is broken into $8 \times 6 \times 6$ quadratic elements, there are a total of 2535 nodes with 4 degrees of freedom (DOFs) per node, for a total of 10,140 DOFs. The matrix size needed for this system is $N \times N \approx 10^8$. Double floating point precision was used, and the total amount of memory required was 950 MB.

Increasing the number of divisions along any axis would very quickly overrun the computer memory, which was 4 GB on a 64-bit system. The results at this level of mesh refinement were still good. The results are consistent with results from the 2D model, which allows a much higher mesh refinement.

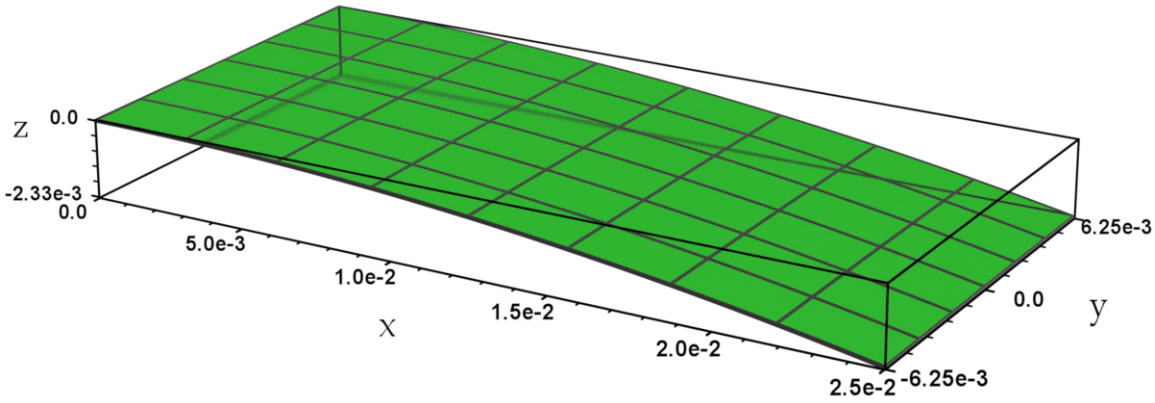

Figure 3.2: The deformed shape with 600 V applied voltage. Dimensions in meters.

Figure 3.3 shows v at $x = L$. It is anti-symmetric, and proportional to $y \cdot z$. Its magnitude is an order of magnitude smaller than u, which is already three orders of magnitude smaller than w. Figure 3.4 shows u at $x = L$. It appears that u is independent of y, at least at the end of the bimorph. We can see from figure 3.5, where w is plotted at $x = 0$, that there is some curvature in the y direction. Figure 3.6 shows $\partial w/\partial y$ at $x = 0$, which is exactly linear, and thus w has constant curvature in the y direction, and w is proportional to y^2. This dependence on y is so small that it is not noticeable in figure 3.2.

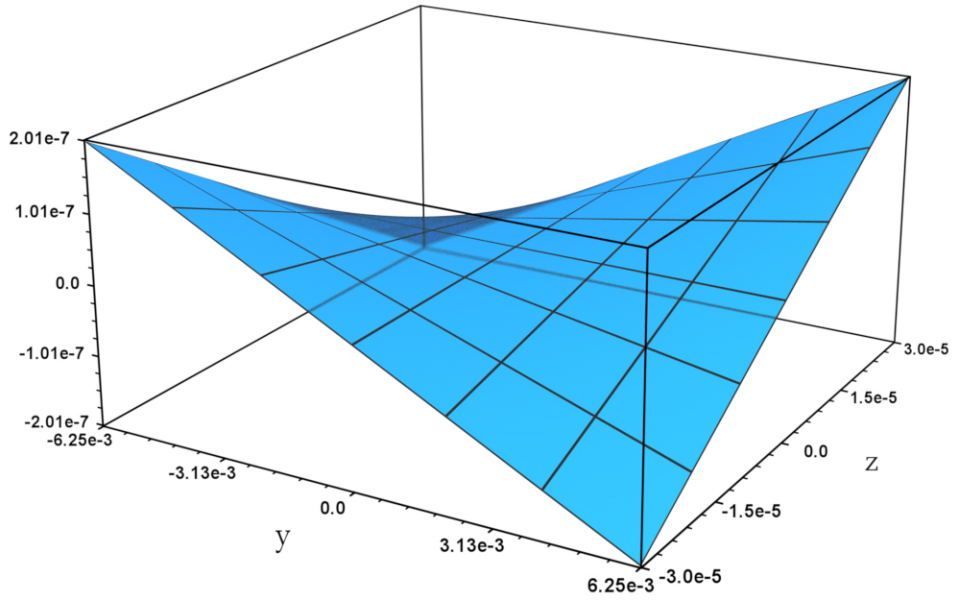

Figure 3.3: v at $x = L$.

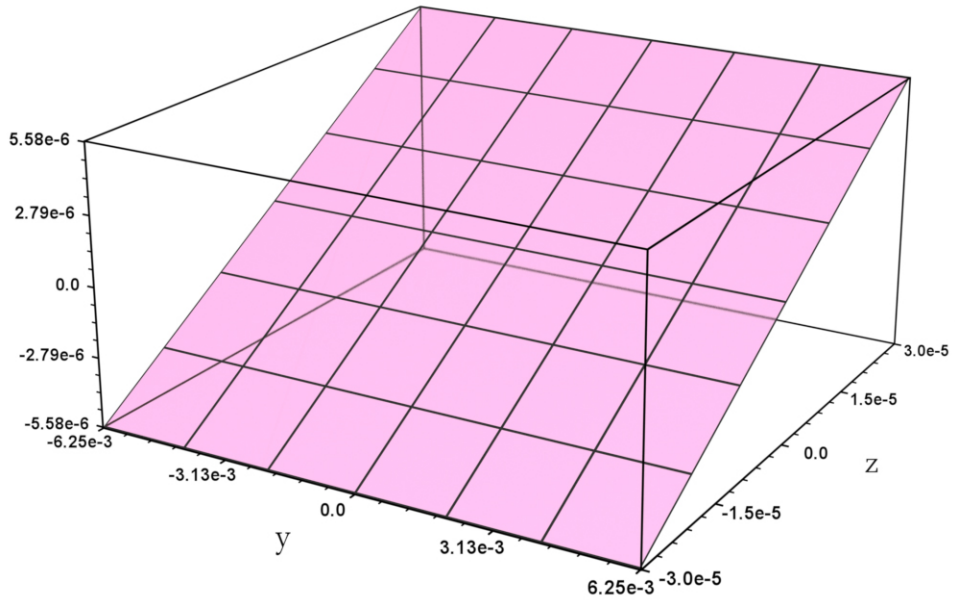

Figure 3.4: u at $x = L$.

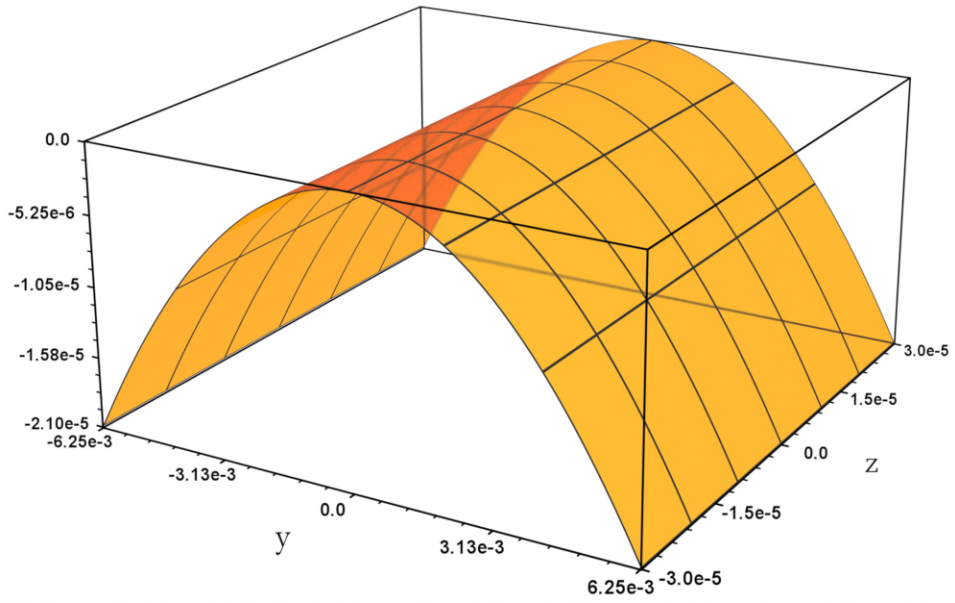

Figure 3.5: w at $x = 0$.

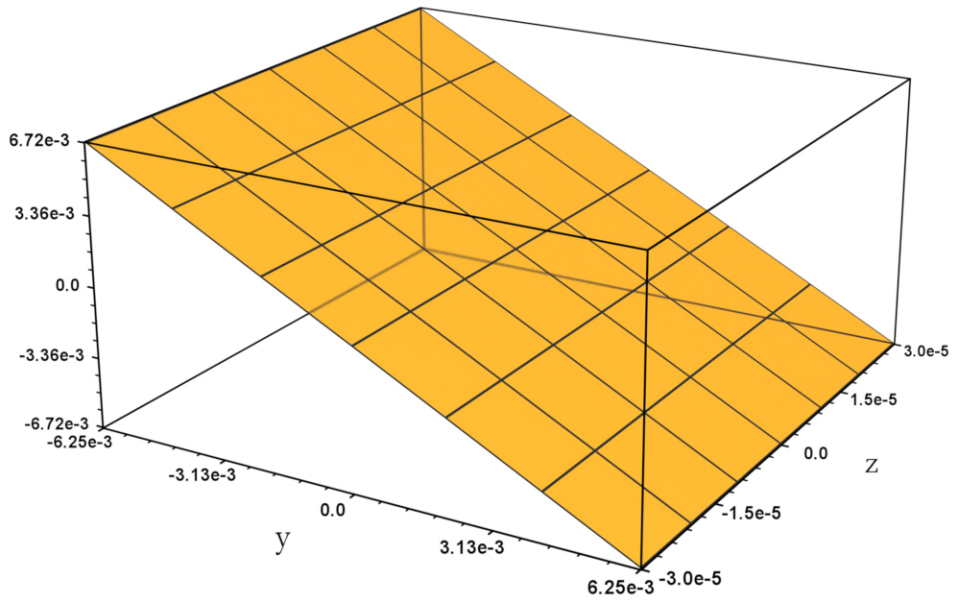

Figure 3.6: $\partial w/\partial y$ at $x = 0$.

CHAPTER 4

BIMORPH: STATIC 2D CASE

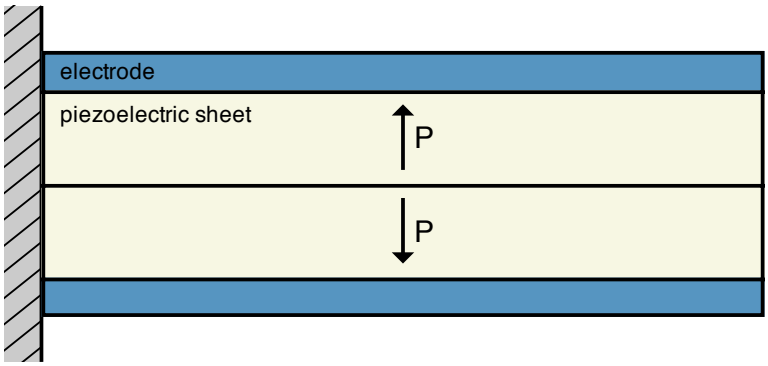

Figure 4.1: Schematic of a bimorph.

In the two-dimensional case, the bimorph is thin in the y direction, as shown schematically in figure 4.1. There are several types of beam approximations, commonly ranging from second order to fourth order. Different methods make different assumptions about the type of bending that occurs. The simplest thin beam approximation is to set $T_2 = 0$. There is only bending in the x-z plane, so $T_4 = T_6 = 0$, but T_5 is not zero. Also, $D_2 = 0$ since there is no applied electric field component in the y direction and $S_4 = 0$.

$$T_2 = c_{12}S_1 + c_{22}S_2 + c_{23}S_3 - e_{32}E_3 = 0 \tag{4.1}$$

We solve for S_2, and substitute it into the other equations.

$$S_2 = \frac{1}{c_{22}}\left(e_{32}E_3 - c_{12}S_1 - c_{23}S_3\right) \tag{4.2}$$

$$\begin{aligned} T_1 =& c_{11}S_1 + c_{12}S_2 + c_{13}S_3 - e_{31}E_3 \\ =& c_{11}S_1 + c_{12}\left(\frac{e_{32}E_3 - c_{12}S_1 - c_{23}S_3}{c_{22}}\right) + c_{13}S_3 - e_{31}E_3 \\ =& \left(c_{11} - \frac{c_{12}^2}{c_{22}}\right)S_1 + \left(c_{13} - \frac{c_{12}c_{23}}{c_{22}}\right)S_3 - \left(e_{31} - \frac{c_{12}}{c_{22}}e_{32}\right)E_3 \end{aligned} \tag{4.3}$$

$$\begin{aligned} T_3 =& c_{13}S_1 + c_{23}S_2 + c_{33}S_3 - e_{33}E_3 \\ =& c_{13}S_1 + c_{23}\left(\frac{e_{32}E_3 - c_{12}S_1 - c_{23}S_3}{c_{22}}\right) + c_{33}S_3 - e_{33}E_3 \\ =& \left(c_{13} - \frac{c_{23}c_{12}}{c_{22}}\right)S_1 + \left(c_{33} - \frac{c_{23}^2}{c_{22}}\right)S_3 - \left(e_{33} - \frac{c_{23}}{c_{22}}e_{32}\right)E_3 \end{aligned} \tag{4.4}$$

$$\begin{aligned} D_3 =& e_{31}S_1 + e_{32}S_2 + e_{33}S_3 + \varepsilon_3 E_3 \\ =& e_{31}S_1 + e_{32}\left(\frac{e_{32}E_3 - c_{12}S_1 - c_{23}S_3}{c_{22}}\right) + e_{33}S_3 + \varepsilon_3 E_3 \\ =& \left(e_{31} - \frac{c_{12}}{c_{22}}e_{32}\right)S_1 + \left(e_{33} - \frac{c_{23}}{c_{22}}e_{32}\right)S_3 + \left(\varepsilon_3 - \frac{e_{32}^2}{c_{22}}\right)E_3 \end{aligned} \tag{4.5}$$

We can define new material constants.

$$c_{11}^* = c_{11} - \frac{c_{12}^2}{c_{22}}, \quad c_{13}^* = c_{13} - \frac{c_{12}c_{23}}{c_{22}}, \quad c_{33}^* = c_{33} - \frac{c_{23}^2}{c_{22}} \tag{4.6}$$

$$e_{31}^* = e_{31} - \frac{c_{12}}{c_{22}}e_{32}, \quad e_{33}^* = e_{33} - \frac{c_{23}}{c_{22}}e_{32}, \quad \varepsilon_3^* = \varepsilon_3 - \frac{e_{32}^2}{c_{22}} \tag{4.7}$$

With these new constants, we can define a new set of governing differential equations.

$$T_1 = c_{11}^* S_1 + c_{13}^* S_3 - e_{31}^* E_3 \tag{4.8}$$

$$T_3 = c_{13}^* S_1 + c_{33}^* S_3 - e_{33}^* E_3 \tag{4.9}$$

$$T_5 = c_{55}S_5 - e_{15}E_1 \tag{4.10}$$

$$D_1 = e_{15}S_5 + \varepsilon_1 E_1 \tag{4.11}$$

$$D_3 = e_{31}^* S_1 + e_{33}^* S_3 + \varepsilon_3^* E_3 \tag{4.12}$$

Static condition:

$$\frac{\partial T_1}{\partial x} + \frac{\partial T_5}{\partial z} = 0 \tag{4.13}$$

$$\frac{\partial T_5}{\partial x} + \frac{\partial T_3}{\partial z} = 0 \tag{4.14}$$

$$\frac{\partial D_1}{\partial x} + \frac{\partial D_3}{\partial z} = 0 \tag{4.15}$$

Weak form:

$$\int_\Omega \left[\frac{\partial \delta u}{\partial x} T_1 + \frac{\partial \delta u}{\partial z} T_5 \right] \mathrm{d}\Omega = 0 \tag{4.16}$$

$$\int_\Omega \left[\frac{\partial \delta w}{\partial x} T_5 + \frac{\partial \delta w}{\partial z} T_3 \right] \mathrm{d}\Omega = 0 \tag{4.17}$$

$$\int_\Omega \left[\frac{\partial \delta \phi}{\partial x} D_1 + \frac{\partial \delta \phi}{\partial z} D_3 \right] \mathrm{d}\Omega = 0 \tag{4.18}$$

$$\int_\Omega \left[\frac{\partial \delta u}{\partial x} \left(c_{11}^* S_1 + c_{13}^* S_3 - e_{31}^* E_3 \right) + \frac{\partial \delta u}{\partial z} \left(c_{55} S_5 - e_{15} E_1 \right) \right] \mathrm{d}\Omega = 0 \tag{4.19}$$

$$\int_\Omega \left[\frac{\partial \delta w}{\partial x} \left(c_{55} S_5 - e_{15} E_1 \right) + \frac{\partial \delta w}{\partial z} \left(c_{13}^* S_1 + c_{33}^* S_3 - e_{33}^* E_3 \right) \right] \mathrm{d}\Omega = 0 \tag{4.20}$$

$$\int_\Omega \left[\frac{\partial \delta \phi}{\partial x} \left(e_{15} S_5 + \varepsilon_1 E_1 \right) + \frac{\partial \delta \phi}{\partial z} \left(e_{31}^* S_1 + e_{33}^* S_3 + \varepsilon_3^* E_3 \right) \right] \mathrm{d}\Omega = 0 \tag{4.21}$$

$$\int_\Omega \left[\frac{\partial \delta u}{\partial x} \left(c_{11}^* \frac{\partial u}{\partial x} + c_{13}^* \frac{\partial w}{\partial z} + e_{31}^* \frac{\partial \phi}{\partial z} \right) + \frac{\partial \delta u}{\partial z} \left(c_{55} \left(\frac{\partial u}{\partial z} + \frac{\partial w}{\partial x} \right) + e_{15} \frac{\partial \phi}{\partial x} \right) \right] \mathrm{d}\Omega = 0 \tag{4.22}$$

$$\int_\Omega \left[\frac{\partial \delta w}{\partial x} \left(c_{55} \left(\frac{\partial u}{\partial z} + \frac{\partial w}{\partial x} \right) + e_{15} \frac{\partial \phi}{\partial x} \right) + \frac{\partial \delta w}{\partial z} \left(c_{13}^* \frac{\partial u}{\partial x} + c_{33}^* \frac{\partial w}{\partial z} + e_{33}^* \frac{\partial \phi}{\partial z} \right) \right] \mathrm{d}\Omega = 0 \tag{4.23}$$

$$\int_\Omega \left[\frac{\partial \delta \phi}{\partial x} \left(e_{15} \left(\frac{\partial u}{\partial z} + \frac{\partial w}{\partial x} \right) - \varepsilon_1 \frac{\partial \phi}{\partial x} \right) + \frac{\partial \delta \phi}{\partial z} \left(e_{31}^* \frac{\partial u}{\partial x} + e_{33}^* \frac{\partial w}{\partial z} - \varepsilon_3^* \frac{\partial \phi}{\partial z} \right) \right] \mathrm{d}\Omega = 0 \tag{4.24}$$

The form of the sub-matrices:

$$\boldsymbol{K}^{11} = c_{11}^* \boldsymbol{M}^{xx} + c_{55} \boldsymbol{M}^{zz} \tag{4.25}$$

$$\boldsymbol{K}^{12} = c_{13}^* \boldsymbol{M}^{xz} + c_{55} \left(\boldsymbol{M}^{xz} \right)^T \tag{4.26}$$

$$\boldsymbol{K}^{13} = e_{31}^* \boldsymbol{M}^{xz} + e_{15} \left(\boldsymbol{M}^{xz} \right)^T \tag{4.27}$$

$$\boldsymbol{K}^{22} = c_{55} \boldsymbol{M}^{xx} + c_{33}^* \boldsymbol{M}^{zz} \tag{4.28}$$

$$\boldsymbol{K}^{23} = e_{15} \boldsymbol{M}^{xx} + e_{33}^* \boldsymbol{M}^{zz} \tag{4.29}$$

$$\boldsymbol{K}^{33} = -\varepsilon_1 \boldsymbol{M}^{xx} - \varepsilon_3^* \boldsymbol{M}^{zz} \tag{4.30}$$

The test case that was chosen is a bimorph with length $L = 2.5 \times 10^{-2}$ meters, height $H = 6 \times 10^{-5}$ meters, and applied voltage $V_0 = 600$ volts. In the static case, each electrode

will have a uniform voltage. The voltage is applied (specified) everywhere on the lower and upper surfaces of the bimorph ($z = \pm H/2$). The dielectric breakdown electric field for PVDF is 3×10^8 V/m [19], and 600 V over 60 microns gives a field strength of 1×10^7 V/m which is well below the breakdown point. The solutions for the variables, along with their derivatives, are shown in figures 4.2-4.11. Figure 4.9 shows the difference between the linear solution for the potential and the FEM solution. The electric field differs from constant because of the direct piezoelectric effect. If there was no piezoelectricity, then the PVDF would be a plain dielectric, and the electric field would be constant with the value $E_3 = -V_0/H$.

Figure 4.2 shows the solution for the z-deflection w, which has a maximum value at the tip of $w(L) = -2.334$ mm. The amplitude of w is very large compared to the x-deflection. The overall shape of the deformed bimorph is thus dominated by w. The shape of w is parabolic in the x direction, and nearly constant in the z direction (the z dependence is very small). This is evident from the x derivative of w, shown in figure 4.3, which shows that $\partial w/\partial x$ is linear. Since the value of w and $\partial w/\partial x$ are both zero at $x = 0$, w is equal to a constant times x^2. Thus, the curvature of the bimorph is constant.

The z-derivative of w is shown in figure 4.4. The z-dependence is quite small, but not zero. The derivative is linear, except there is a jump at $z = 0$. This is because there is a jump in the ferroelectric polarization, and thus in the piezoelectric constants, between the two piezoelectric sheets. All of the e_{ijk} piezoelectric constants in one sheet have the opposite sign relative to the other sheet. If a transition layer is created between the two sheets so that the piezoelectric constants vary continuously, then $\partial w/\partial z$ will be continuous. This type of bimorph was solved numerically with the Finite Element Method. The total thickness was kept the same, and a very thin transition layer was created at $z = 0$ from $z = -w_t$ to $z = w_t$, where w_t is the transition layer thickness which

is much smaller than the thickness of a PVDF sheet. The tip deflection was found to decrease very slightly due to this assumed transition layer. The transition layer would be very difficult, if not impossible, to actually manufacture, since the poling method of simply applying a very strong electric field causes the dipoles all to align in the same direction. The transition layer requires the dipoles all to vary continuously over a distance. Mathematically speaking, it would remove the discontinuity in several of the derivatives of interest, and allow the use of some advanced FEM techniques which require continuous derivatives.

When the bimorph bends downward, the top surface will stretch, so u is positive, while the bottom surface will shrink and have a negative u. As can be seen in figure 4.5, u is proportional to xz. Both $\partial u/\partial x$ and $\partial u/\partial z$ are linear, as can be seen in figures 4.6 and 4.7. At a particular value of x, u will vary linearly and symmetrically about $z = 0$. The volume of a sheet will tend to be conserved, so that as u increases, w will tend to decrease. In this way, we can see how the z derivative on the top sheet is negative, and positive on the bottom sheet, since the top sheet will get thinner in response to it lengthening, and the bottom sheet will get thicker in response to the sheet getting shorter. From this description, it would seem that the derivative should be a continuous plane symmetric about $z = 0$. This is the effect from bending alone. In addition to the bending effect on w, we also have an effect from the converse piezoelectric effect. When an electric field is applied across a piezoelectric sheet which is free, it will get shorter and thicker when the electric field is aligned with the polarization, or longer and thinner when the field is antiparallel to the polarization. Since the field will be parallel in the bottom sheet, it will get thicker by a certain amount from the converse piezoelectric effect. The top sheet will get thinner by the same amount. Since the two sheets are glued together at $z = 0$, the contribution to w from the converse effect will be zero there, and

vary linearly toward the $\pm h$ surfaces. Thus, the contribution to $\partial w/\partial z$ from the converse effect will be constant. Thus, we add a positive constant to $\partial w/\partial z$ in the bottom layer, and subtract the same constant from $\partial w/\partial z$ in the top layer, which accounts for the gap in $\partial w/\partial z$ at $z = 0$.

The electric potential is shown in figure 4.8. The electric field component in the z direction is nearly constant, and so the potential varies linearly with only a very small deviation. $\partial\phi/\partial z = -E_3$ is shown in figure 4.10. The direct piezoelectric effect will cause a slight variation from linearity in the potential, which is shown in figure 4.9. The difference is piece-wise quadratic. The magnitude of the difference is only 0.44/600, which is less than 0.1%. This indicates that it is accurate to assume a constant electric field when using simplified models.

The numerical results for the x derivative of ϕ are shown in figure 4.11. This plot shows erroneous behavior in the derivative. The FEM solution only provides the functions for the variables, not their derivatives. To find the derivatives, we simply take the derivative of the series solution $u' = \sum u_i \psi_i'$. There is always the possibility of not having enough numerical precision, and thus the derivatives will be inaccurate compared with the solution. That does not seem to be what has happened here. The same problem was solved using 30 decimal places of precision in Mathematica, which is nearly twice the 16 digits of precision found in double floating point numbers in C programs. The same behavior was seen, which indicates something else is going on. The derivative should be zero everywhere since the potential is a constant in x in this example.

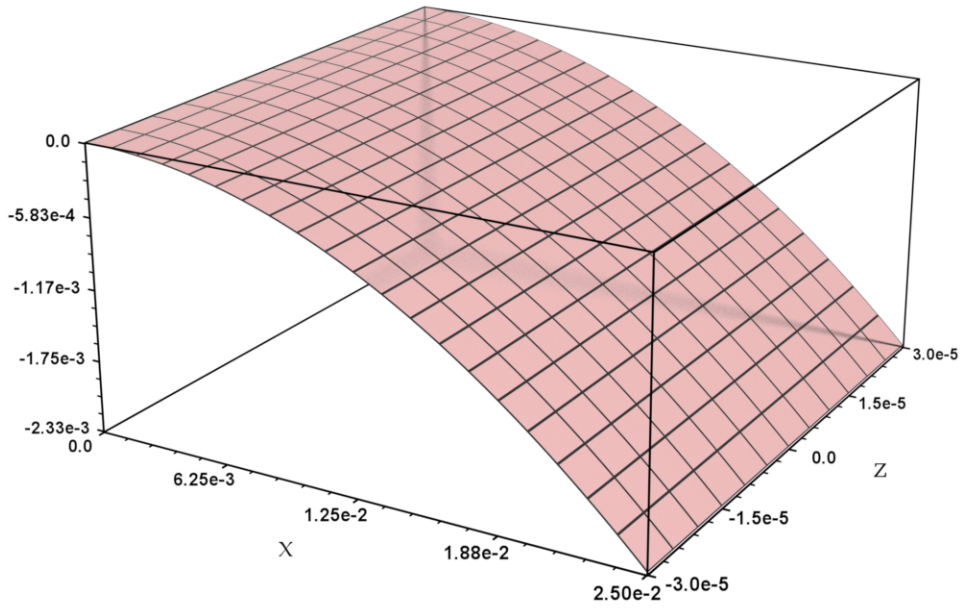

Figure 4.2: w

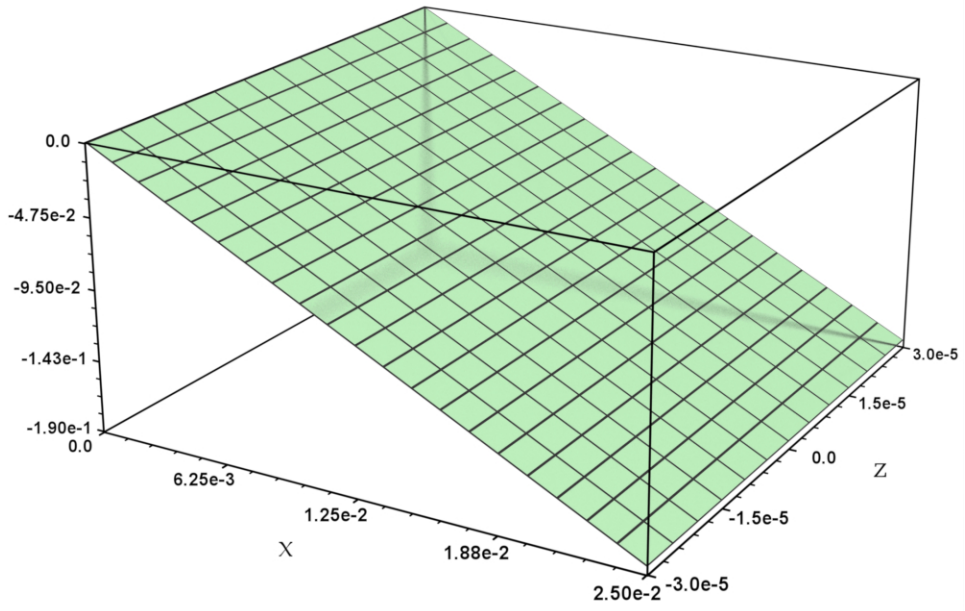

Figure 4.3: $\partial w/\partial x$

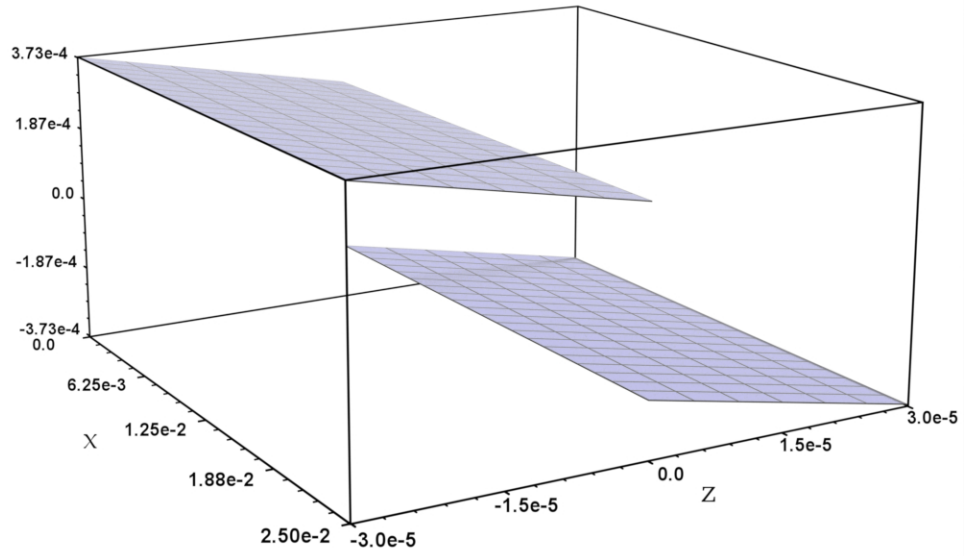

Figure 4.4: $\partial w/\partial z$

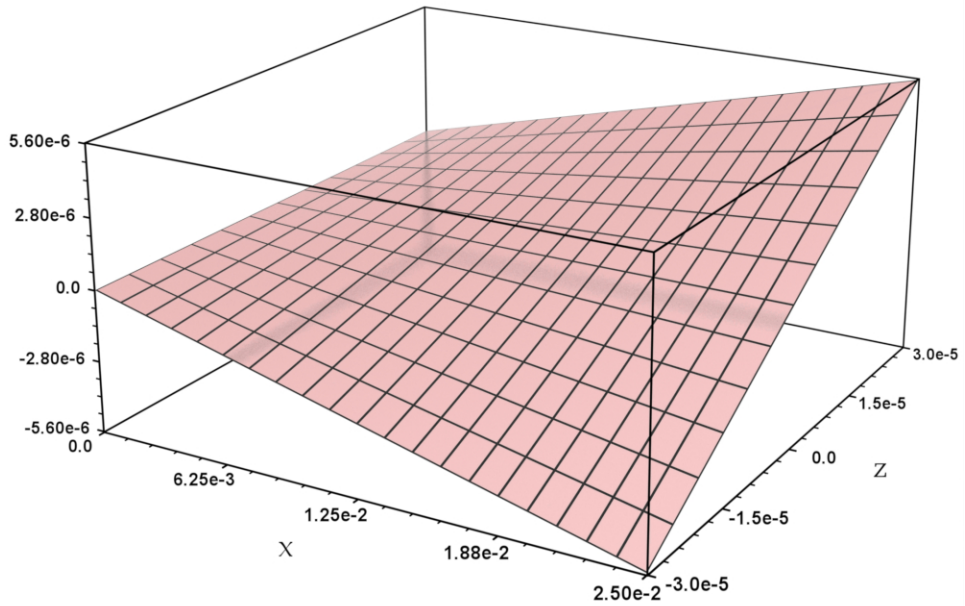

Figure 4.5: u

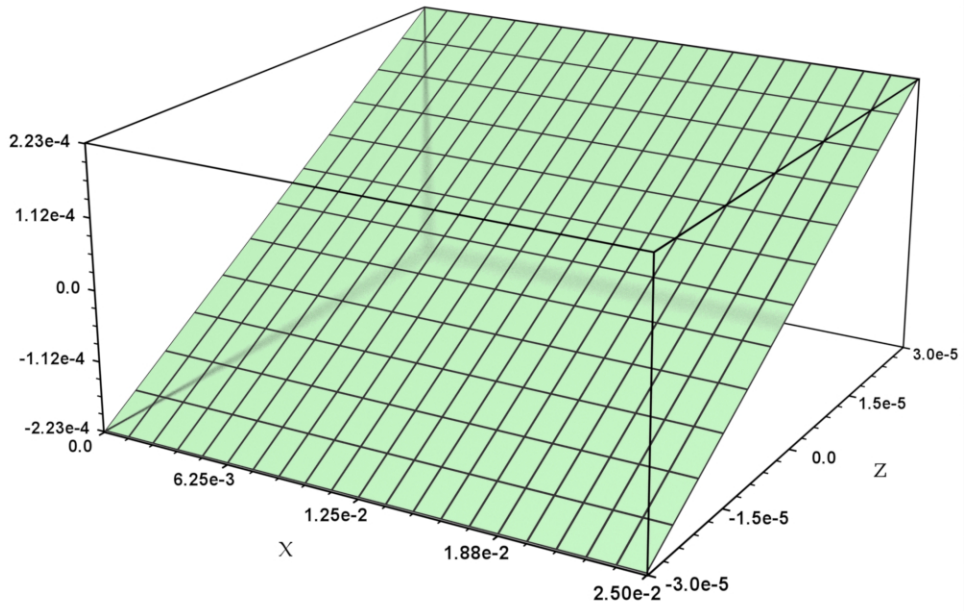

Figure 4.6: $\partial u/\partial x$

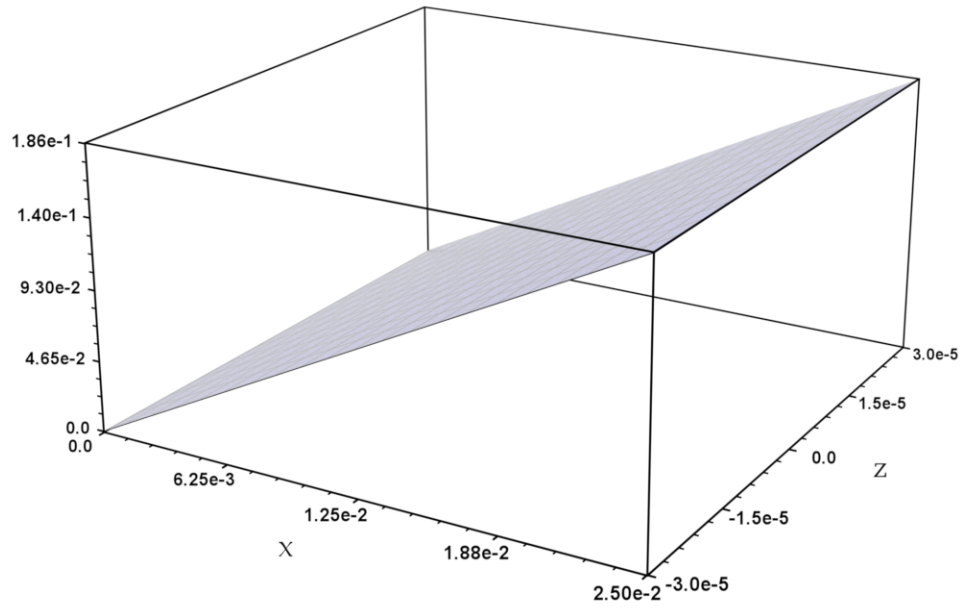

Figure 4.7: $\partial u/\partial z$

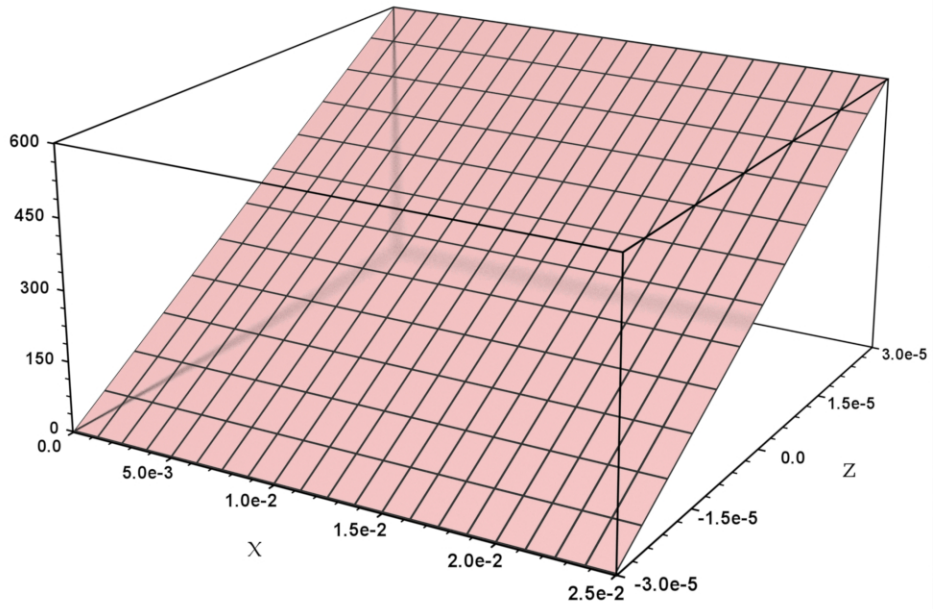

Figure 4.8: ϕ

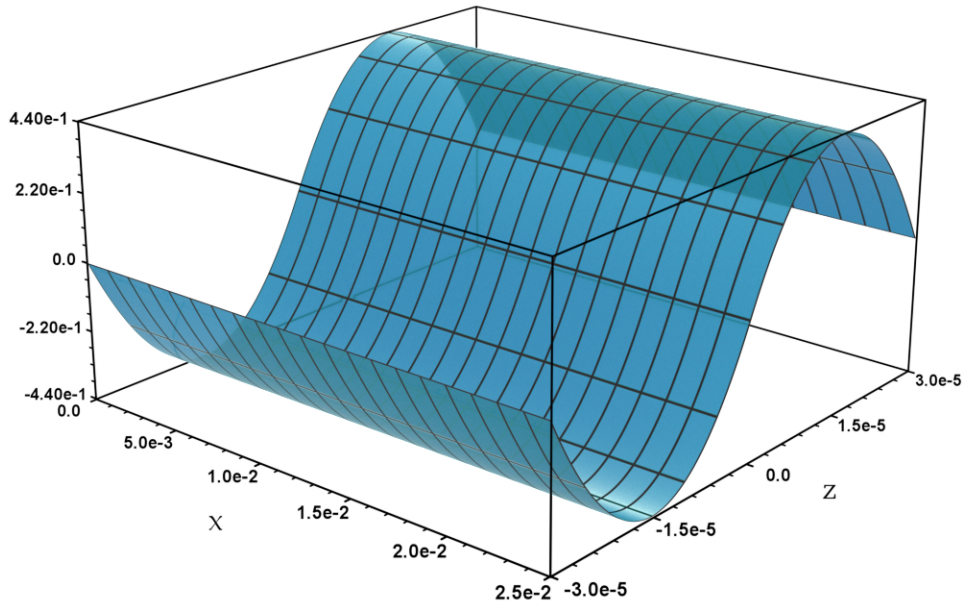

Figure 4.9: $\phi - \phi_{\text{linear}}$. How ϕ differs from linear, in volts. x and z in meters.

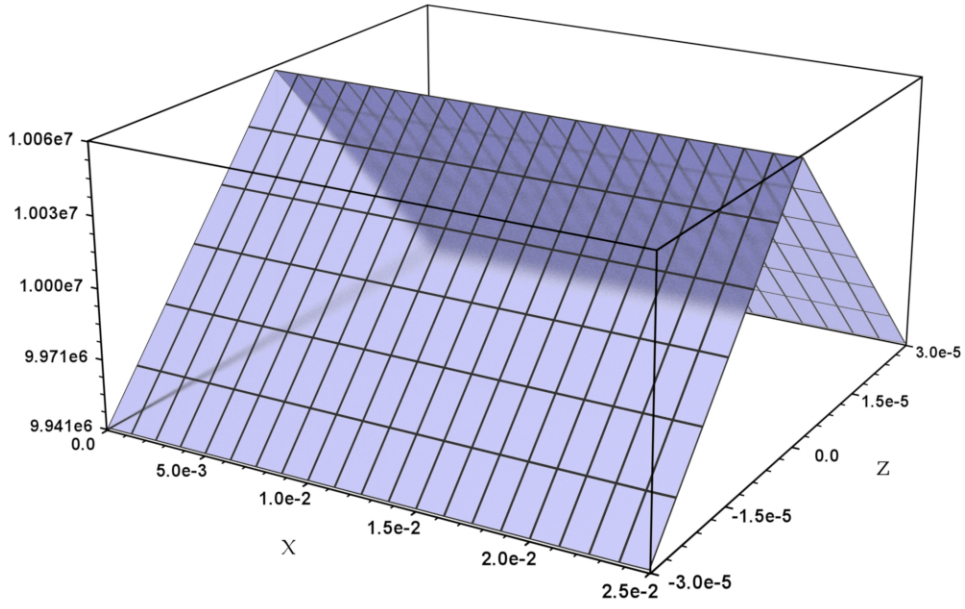

Figure 4.10: $\partial\phi/\partial z$

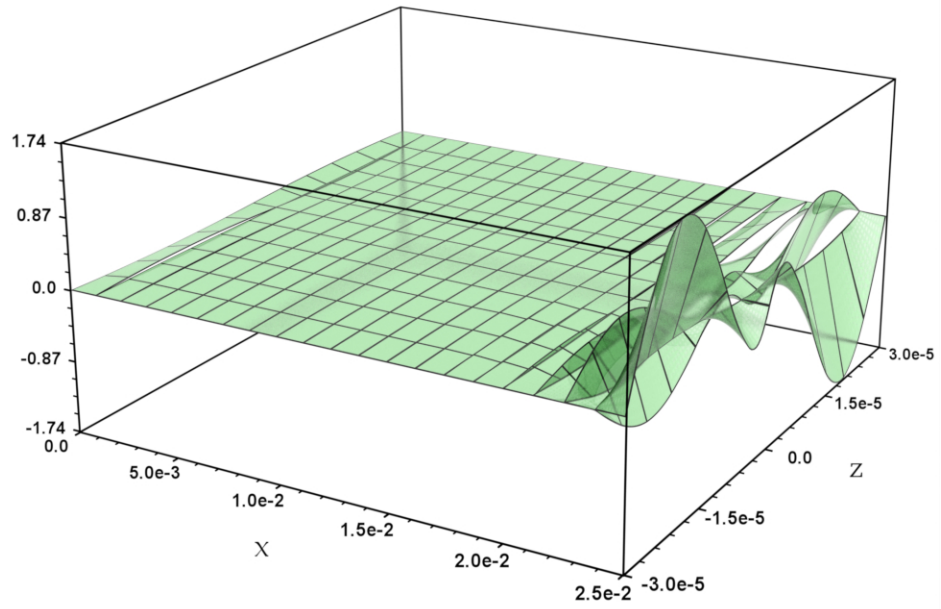

Figure 4.11: $\partial\phi/\partial x$, erroneous behavior.

Analytical Solutions

In trying to find in the literature analytical solutions for the deflection of the bimorph, a common model that is used is the Bernoulli-Euler beam model [11, 15, 16]. The three-dimensional bimorph is assumed to bend in a specific manner, which reduces the governing equation of the z-deflection to a 4^{th}-order differential equation in x only.

The more general 2D theory is given by the Mindlin-Reissner plate theory [11]. A plate is very thin in the z direction, but has comparable dimensions in the x and y directions. The assumptions governing this model are given as follows [11]:

1. Planar cross-sections which are perpendicular to the middle ($z = 0$) surface deform linearly and remain planar after bending. Thus straight lines lying on normals remain straight lines, but might not remain normal to the middle surface. This is the linearity hypothesis.
2. The z-deflection (w) does not depend on z, so $w = w\left(x, y\right)$.
3. The middle ($z = 0$) layer only deflects in the z direction (u and v are zero).
4. T_3 vanishes (=0).

From these constraints, we have the following forms for the displacements:

$$u = -z\,\theta_1\left(x, y\right), \tag{4.31}$$

$$v = -z\,\theta_2\left(x, y\right), \tag{4.32}$$

$$w = w\left(x, y\right), \tag{4.33}$$

where θ_1 and θ_2 are rotations in radians. If the bimorph has a non-deformed upward normal pointing in the $+z$ direction, then θ_1 is the rotation of the normal in the $x - z$ plane, while θ_2 is the rotation of the normal in the $y - z$ plane. The rotations are not known and must be solved for just like the deflections.

In order to eliminate the rotations as unknowns, we can further assume that:

5. A vector which starts out normal to the middle surface will remain normal to the middle surface after bending. This is the normal hypothesis.

With the normal hypothesis, the rotations will have the form

$$\theta_i = \frac{\partial w}{\partial x_i}, \tag{4.34}$$

so that

$$u = -z\frac{\partial w}{\partial x}, \tag{4.35}$$

and

$$v = -z\frac{\partial w}{\partial y}. \tag{4.36}$$

In the Bernoulli-Euler beam theory, the y deflection is small and is neglected. Now the z deflection will be a function of x only. The only strain that is non-zero is S_1.

$$S_1 = \frac{\partial u}{\partial x} = -z\frac{\partial^2 w}{\partial x^2} \tag{4.37}$$

For the piezoelectric bimorph,

$$T_1 = c_{11}S_1 - e_{31}E_3 = -c_{11}z\frac{\partial^2 w}{\partial x^2} - e_{31}E_3. \tag{4.38}$$

The piezoelectric constant e_{31} is constant within a PVDF sheet, but the top sheet has a negative sign relative to the bottom sheet. The torque, τ, is related to T_1 by the integral over the cross-section

$$\begin{aligned}\tau =& \int_{-h}^{h}\int_{y} z\,T_1\,\mathrm{d}y\,\mathrm{d}z \\ =& b\left[\int_{-h}^{0}\left(-c_{11}z^2\frac{\partial^2 w}{\partial x^2} - e_{31}E_3\,z\right)\mathrm{d}z + \int_{0}^{h}\left(-c_{11}z^2\frac{\partial^2 w}{\partial x^2} + e_{31}E_3\,z\right)\mathrm{d}z\right] \\ =& 2b\left(-c_{11}\frac{\partial^2 w}{\partial x^2}\frac{h^3}{3} + e_{31}E_3\frac{h^2}{2}\right),\end{aligned} \tag{4.39}$$

where $h = H/2$ is the thickness of one PVDF sheet, and b is the width of the bimorph. Here it is assumed that E_3 is constant through the thickness. The direct piezoelectric effect will cause a deviation in the electric field, but the difference is small. This expression allows E_3 to be x-dependent.

If we set the torque equal to zero, then we get the equation

$$\frac{\partial^2 w}{\partial x^2} = \frac{3e_{31}E_3}{2c_{11}h}. \tag{4.40}$$

We have the boundary conditions that at the left end $w = 0$, and also the slope is zero.

$$w(0) = 0 \tag{4.41}$$

$$\frac{\partial w}{\partial x}(0) = 0 \tag{4.42}$$

This gives the solution, for a uniform electric field

$$w(x) = \frac{3e_{31}E_3}{4c_{11}h}x^2, \tag{4.43}$$

$$u(x,z) = -\frac{3e_{31}E_3}{2c_{11}h}xz. \tag{4.44}$$

The tip deflection for $E_3 = -V_0/H$, applied voltage $V_0 = 600V$, total thickness $H = 6\times10^{-5}$ m, and length $L = 2.5$ cm is

$$w(L) = -\frac{3\left(1.819\times10^{-2}\right)\left(600\right)\left(2.5\times10^{-2}\right)^2}{2\left(3.70\times10^{9}\right)\left(6\times10^{-5}\right)^2} = -7.681\times10^{-4}\text{ m}. \tag{4.45}$$

The tip deflection value of -7.681×10^{-4} m is only one-third of the expected value of -2.334×10^{-3} m. There is definitely something not right about this solution. The problem may be in the assumption that w does not depend on z. If we drop that assumption, and instead use the thin beam assumption as before that $T_2 = 0$, and extend it so that $T_3 = 0$, then we get a much better result, which will be derived next. There is

a paper written by Jan Smits and Susan Dalke [13] titled "The Constituent Equations of Piezoelectric Bimorphs" which gives the following formula for the z-deflection:

$$w(x) = \frac{3 d_{31} E_3}{4h} x^2, \tag{4.46}$$

which gives a tip deflection of

$$w(L) = \frac{3\left(1.496 \times 10^{-11}\right)\left(600\right)\left(2.5 \times 10^{-2}\right)^2}{2\left(6 \times 10^{-5}\right)^2} = 2.338 \times 10^{-3} \text{ m}, \tag{4.47}$$

which is practically identical to the numerical solution of -2.334×10^{-3} meters. This formula was derived starting from a different form of the constituent equations. Now I will re-derive the previous expression using the $T_2 = 0$ and $T_3 = 0$ conditions.

$$T_1 = c_{11} S_1 + c_{12} S_2 + c_{13} S_3 - e_{31} E_3 \tag{4.48}$$

$$T_2 = c_{12} S_1 + c_{22} S_2 + c_{23} S_3 - e_{32} E_3 = 0 \tag{4.49}$$

$$T_3 = c_{13} S_1 + c_{23} S_2 + c_{33} S_3 - e_{33} E_3 = 0 \tag{4.50}$$

The values of S_2 and S_3 can be found.

$$\begin{pmatrix} c_{22} & c_{23} \\ c_{23} & c_{33} \end{pmatrix} \begin{pmatrix} S_2 \\ S_3 \end{pmatrix} = \begin{pmatrix} -c_{12} & e_{32} \\ -c_{13} & e_{33} \end{pmatrix} \begin{pmatrix} S_1 \\ E_3 \end{pmatrix} \tag{4.51}$$

$$\begin{pmatrix} S_2 \\ S_3 \end{pmatrix} = \frac{1}{c_{22} c_{33} - c_{23}^2} \begin{pmatrix} c_{33} & -c_{23} \\ -c_{23} & c_{22} \end{pmatrix} \begin{pmatrix} -c_{12} & e_{32} \\ -c_{13} & e_{33} \end{pmatrix} \begin{pmatrix} S_1 \\ E_3 \end{pmatrix} \tag{4.52}$$

Substituting the expression for S_2 and S_3 into T_1, we get an expression for T_1 with new material coefficients.

$$T_1 = c_{11}^{\bigstar} S_1 - e_{31}^{\bigstar} E_3 \tag{4.53}$$

$$c_{11}^{\bigstar} = c_{11} + \frac{c_{12}\left(-c_{33} c_{12} + c_{23} c_{13}\right) + c_{13}\left(c_{23} c_{12} - c_{22} c_{13}\right)}{c_{22} c_{33} - c_{23}^2} \tag{4.54}$$

$$e_{31}^{\bigstar} = e_{31} + \frac{c_{12}\left(-c_{33} e_{32} + c_{23} e_{33}\right) + c_{13}\left(c_{23} e_{32} - c_{22} e_{33}\right)}{c_{22} c_{33} - c_{23}^2} \tag{4.55}$$

When we substitute the expressions $e_{3j} = \sum_k d_{3k} c_{kj}$ into the expression above, we find that

$$e_{31}^{\bigstar} = d_{31} c_{11}^{\bigstar}. \tag{4.56}$$

It also turns out that

$$c_{11}^{\bigstar} = 1/s_{11}. \tag{4.57}$$

The inverse of the elasticity tensor is called the compliance tensor. Since the two tensors are inverses of each other, we have the relation

$$\sum_{p,q} c_{ijpq} s_{pqkl} = \delta_{(ij)(kl)}. \tag{4.58}$$

This also works in the reduced notation.

$$\sum_j c_{ij} s_{jk} = \delta_{ik}. \tag{4.59}$$

Here it is in matrix form. We also have $c_{44} = 1/s_{44}$, $c_{55} = 1/s_{55}$, and $c_{66} = 1/s_{66}$.

$$\begin{pmatrix} c_{11} & c_{12} & c_{13} \\ c_{12} & c_{22} & c_{23} \\ c_{13} & c_{23} & c_{33} \end{pmatrix} \begin{pmatrix} s_{11} & s_{12} & s_{13} \\ s_{12} & s_{22} & s_{23} \\ s_{13} & s_{23} & s_{33} \end{pmatrix} = \begin{pmatrix} 1 & 0 & 0 \\ 0 & 1 & 0 \\ 0 & 0 & 1 \end{pmatrix} \tag{4.60}$$

$$\boldsymbol{s} = \frac{1}{\mathrm{Det}\,(\boldsymbol{c})} \begin{pmatrix} c_{22}c_{23} - c_{23}^2 & c_{13}c_{23} - c_{12}c_{33} & c_{12}c_{23} - c_{13}c_{22} \\ c_{13}c_{23} - c_{12}c_{33} & c_{11}c_{33} - c_{13}^2 & c_{12}c_{13} - c_{11}c_{23} \\ c_{12}c_{23} - c_{13}c_{22} & c_{12}c_{13} - c_{11}c_{23} & c_{11}c_{22} - c_{12}^2 \end{pmatrix} \tag{4.61}$$

$$\mathrm{Det}\,(\boldsymbol{c}) = c_{11}\left(c_{22}c_{33} - c_{23}^2\right) - c_{12}\left(c_{12}c_{33} - c_{13}c_{23}\right) + c_{13}\left(c_{12}c_{23} - c_{13}c_{22}\right) \tag{4.62}$$

From here was can see that $s_{11} = 1/c_{11}^{\bigstar}$.

The rest of the analysis continues as before. When we do the torque integral, we assume that $\frac{\partial^2 w}{\partial x^2}$ is a constant, which means the bimorph has a constant curvature. We

now get the same expression for w as Smits and Dalke, and we also get an expression for u.

$$w(x) = \frac{3d_{31}E_3}{4h}x^2, \tag{4.63}$$

$$u(x,z) = -\frac{3d_{31}E_3}{2h}xz. \tag{4.64}$$

Now we can see what the maximum x deflection is according to this analysis. The maximum seen from the 2D static FEM was 5.60×10^{-5} m. This is in excellent agreement with the analytical result. It is good that both w and x have good agreement with the analytical result, which shows that the analytical model is consistent, and also that the numerical results are most likely accurate in more complicated cases.

$$u(L,h) = \frac{3\left(1.496\times10^{-11}\right)\left(600\right)}{2\left(6\times10^{-5}\right)}\left(2.5\times10^{-2}\right) = 5.61\times10^{-5}\text{m}. \tag{4.65}$$

We know that w has a small dependence on z, but we would need some extra conditions to determine the coefficients. From numerical results, we might guess that w has the form

$$w(x,z) = x^2 \times \begin{cases} w_0 + w_1 z + w_2 z^2 & \text{for } z > 0 \\ w_0 - w_1 z + w_2 z^2 & \text{for } z < 0 \end{cases} \tag{4.66}$$

where

$$w_0 = \frac{3d_{31}E_3}{4h}. \tag{4.67}$$

From numerical results, we can estimate the other coefficients, for the example problem of $V_0 = 600$ V and $h = 3\times10^{-5}$ m.

$$w_0 = -3.735 \tag{4.68}$$

$$w_1 = -2.328\times10^{-4} \tag{4.69}$$

$$w_2 = -4.715 \tag{4.70}$$

We thus have the empirical formula $w(x,z) = -x^2\left(3.735 + 2.328|z| + 4.715z^2\right)$. When $z = h$ we have the terms 3.7, 7.0×10^{-5}, and 4.2×10^{-9}, thus the second term is on the order of 10^{-5} times less than the leading term, and can be neglected.

Next we can look at the result from a slightly more involved problem. From [14] we have equations 4.71 to 4.74 which take into account the non-uniform electric field. This formula is for what is called a parallel bimorph, in which there is a third electrode between the two piezoelectric sheets. This middle electrode is grounded, and $V_0/2$ is applied to both the top and bottom electrodes. The polarizations of the two sheets point in the same direction, but the electric fields are opposite. The behavior should be identical to the series bimorph, for which the potential is only applied on the outside of the bimorph.

$$w(L) = \frac{3b_{11}b_{44}d_{31}L^2V_0/2}{\left(4b_{11}b_{44} - 3b_{14}^2\right)h^2} \tag{4.71}$$

$$b_{11} = \frac{c_{11}e_{33}^2 + c_{11}c_{33}\varepsilon_3 - c_{13}^2\varepsilon_3 - 2c_{13}e_{31}e_{33} + c_{33}e_{31}^2}{e_{33}^2 + c_{33}\varepsilon_3} \tag{4.72}$$

$$b_{14} = \frac{c_{13}e_{33} - c_{33}e_{31}}{e_{33}^2 + c_{33}\varepsilon_3} \tag{4.73}$$

$$b_{44} = \frac{c_{33}}{e_{33}^2 + c_{33}\varepsilon_3} \tag{4.74}$$

From this formula we get a tip deflection of -2.353×10^{-3} meters, which is also in good agreement with the FEM solution.

CHAPTER 5

BIMORPH: HARMONIC 3D CASE

When the electrode material does not have a very high conductivity, it cannot be assumed that the voltage distribution within the electrode will be uniform and instantaneously equal to the applied voltage when the applied voltage is changing with time. Within a conductive material, we have the following electrical continuity equation:

$$\boldsymbol{\nabla} \cdot \left(\boldsymbol{J} + \frac{\partial \boldsymbol{D}}{\partial t} \right) = 0. \tag{5.1}$$

The constitutive relation giving the electric current in terms of the electric field is

$$\boldsymbol{J} = \sigma \boldsymbol{E}, \tag{5.2}$$

where σ is the electric conductivity.

Since the electrode material is made of a polymer which is not piezoelectric, the constitutive relation for the electric displacement is

$$\boldsymbol{D} = \varepsilon \boldsymbol{E}, \tag{5.3}$$

where ε is the dielectric constant within the electrode. It is assumed that the electrode material is isotropic, so σ and ε are being treated as scalars.

The continuity equation for the electrode, written out in component form, is

$$\frac{\partial}{\partial x}\left(\sigma E_1 + \varepsilon \frac{\partial E_1}{\partial t} \right) + \frac{\partial}{\partial y}\left(\sigma E_2 + \varepsilon \frac{\partial E_2}{\partial t} \right) + \frac{\partial}{\partial z}\left(\sigma E_3 + \varepsilon \frac{\partial E_3}{\partial t} \right) = 0. \tag{5.4}$$

Within the piezoelectric sheets the conductivity is zero, and so there is no current.

$$\frac{\partial}{\partial t}\left(\frac{\partial D_1}{\partial x} + \frac{\partial D_2}{\partial y} + \frac{\partial D_3}{\partial z} \right) = 0 \tag{5.5}$$

Since the electric behavior of the electrodes is of more interest than the mechanical behavior, in the cases where the electrodes are not too thick and don't impede the bending motion, a convenient simplification is to only solve for the electric potential in the electrodes, and not include the mechanical displacement.

For the piezoelectric sheets, we have the equations of motion.

$$-\rho\frac{\partial^2 u}{\partial t^2}+\frac{\partial T_1}{\partial x}+\frac{\partial T_6}{\partial y}+\frac{\partial T_5}{\partial z}=0 \tag{5.6}$$

$$-\rho\frac{\partial^2 v}{\partial t^2}+\frac{\partial T_6}{\partial x}+\frac{\partial T_2}{\partial y}+\frac{\partial T_4}{\partial z}=0 \tag{5.7}$$

$$-\rho\frac{\partial^2 w}{\partial t^2}+\frac{\partial T_5}{\partial x}+\frac{\partial T_4}{\partial y}+\frac{\partial T_3}{\partial z}=0 \tag{5.8}$$

In a harmonic analysis, it is assumed that the response of the bimorph matches the frequency spectrum of the input voltage, without any non-linear effects. In the case where we have only a single input frequency, which is the case with a sinusoidal applied voltage, then the bimorph will respond at that same frequency. Using complex notation, we have the following forms for the variables.

$$u(\boldsymbol{x},t)=u_0(\boldsymbol{x})+\left(\alpha_u(\boldsymbol{x})+\mathrm{i}\beta_u(\boldsymbol{x})\right)\mathrm{e}^{\mathrm{i}\omega t} \tag{5.9}$$

$$v(\boldsymbol{x},t)=v_0(\boldsymbol{x})+\left(\alpha_v(\boldsymbol{x})+\mathrm{i}\beta_v(\boldsymbol{x})\right)\mathrm{e}^{\mathrm{i}\omega t} \tag{5.10}$$

$$w(\boldsymbol{x},t)=w_0(\boldsymbol{x})+\left(\alpha_w(\boldsymbol{x})+\mathrm{i}\beta_w(\boldsymbol{x})\right)\mathrm{e}^{\mathrm{i}\omega t} \tag{5.11}$$

$$\phi(\boldsymbol{x},t)=\phi_0(\boldsymbol{x})+\left(\alpha_\phi(\boldsymbol{x})+\mathrm{i}\beta_\phi(\boldsymbol{x})\right)\mathrm{e}^{\mathrm{i}\omega t} \tag{5.12}$$

where $\mathrm{e}^{\mathrm{i}\omega t}=\cos\omega t+\mathrm{i}\sin\omega t$, and $\mathrm{i}=\sqrt{-1}$.

These forms are substituted into the differential equations. After solving for the α's and β's, the final solution is the real part.

$$\begin{aligned} u(\boldsymbol{x}) &= \mathrm{Re}\left[u_0(\boldsymbol{x})+\left(\alpha_u(\boldsymbol{x})+\mathrm{i}\beta_u(\boldsymbol{x})\right)(\cos\omega t+\mathrm{i}\sin\omega t)\right] \\ &= u_0(\boldsymbol{x})+\alpha_u(\boldsymbol{x})\cos\omega t-\beta_u(\boldsymbol{x})\sin\omega t \end{aligned} \tag{5.13}$$

$$v(\boldsymbol{x}) = v_0(\boldsymbol{x}) + \alpha_v(\boldsymbol{x})\cos\omega t - \beta_v(\boldsymbol{x})\sin\omega t \tag{5.14}$$

$$w(\boldsymbol{x}) = w_0(\boldsymbol{x}) + \alpha_w(\boldsymbol{x})\cos\omega t - \beta_w(\boldsymbol{x})\sin\omega t \tag{5.15}$$

$$\phi(\boldsymbol{x}) = \phi_0(\boldsymbol{x}) + \alpha_\phi(\boldsymbol{x})\cos\omega t - \beta_\phi(\boldsymbol{x})\sin\omega t \tag{5.16}$$

The equations of motion for PVDF:

$$\begin{aligned}\int_\Omega \Bigg[&\frac{\partial}{\partial x}\left(c_{11}\frac{\partial u}{\partial x} + c_{12}\frac{\partial v}{\partial y} + c_{13}\frac{\partial w}{\partial z} + e_{31}\frac{\partial \phi}{\partial z}\right) + \frac{\partial}{\partial y}\left(c_{66}\left(\frac{\partial u}{\partial y} + \frac{\partial v}{\partial x}\right)\right) \\ &+ \frac{\partial}{\partial z}\left(c_{55}\left(\frac{\partial u}{\partial z} + \frac{\partial w}{\partial x}\right) + e_{15}\frac{\partial \phi}{\partial x}\right) - \rho\frac{\partial^2 u}{\partial t^2}\Bigg]\,\mathrm{d}\Omega = 0\end{aligned} \tag{5.17}$$

$$\begin{aligned}\int_\Omega \Bigg[&\frac{\partial}{\partial x}\left(c_{66}\left(\frac{\partial u}{\partial y} + \frac{\partial v}{\partial x}\right)\right) + \frac{\partial}{\partial y}\left(c_{12}\frac{\partial u}{\partial x} + c_{22}\frac{\partial v}{\partial y} + c_{23}\frac{\partial w}{\partial z} + e_{32}\frac{\partial \phi}{\partial z}\right) \\ &+ \frac{\partial}{\partial z}\left(c_{44}\left(\frac{\partial v}{\partial z} + \frac{\partial w}{\partial y}\right) + e_{24}\frac{\partial \phi}{\partial y}\right) - \rho\frac{\partial^2 v}{\partial t^2}\Bigg]\,\mathrm{d}\Omega = 0\end{aligned} \tag{5.18}$$

$$\begin{aligned}\int_\Omega \Bigg[&\frac{\partial}{\partial x}\left(c_{55}\left(\frac{\partial u}{\partial z} + \frac{\partial w}{\partial x}\right) + e_{15}\frac{\partial \phi}{\partial x}\right) + \frac{\partial}{\partial y}\left(c_{44}\left(\frac{\partial v}{\partial z} + \frac{\partial w}{\partial y}\right) + e_{24}\frac{\partial \phi}{\partial y}\right) \\ &+ \frac{\partial}{\partial z}\left(c_{13}\frac{\partial u}{\partial x} + c_{23}\frac{\partial v}{\partial y} + c_{33}\frac{\partial w}{\partial z} + e_{33}\frac{\partial \phi}{\partial z}\right) - \rho\frac{\partial^2 w}{\partial t^2}\Bigg]\,\mathrm{d}\Omega = 0\end{aligned} \tag{5.19}$$

$$\begin{aligned}\frac{\partial}{\partial t}\int_\Omega \Bigg[&\frac{\partial}{\partial x}\left(e_{15}\left(\frac{\partial u}{\partial z} + \frac{\partial w}{\partial x}\right) - \varepsilon_1\frac{\partial \phi}{\partial x}\right) + \frac{\partial}{\partial y}\left(e_{24}\left(\frac{\partial v}{\partial z} + \frac{\partial w}{\partial y}\right) - \varepsilon_2\frac{\partial \phi}{\partial y}\right) \\ &+ \frac{\partial}{\partial z}\left(e_{31}\frac{\partial u}{\partial x} + e_{32}\frac{\partial v}{\partial y} + e_{33}\frac{\partial w}{\partial z} - \varepsilon_3\frac{\partial \phi}{\partial z}\right)\Bigg]\,\mathrm{d}\Omega = 0\end{aligned} \tag{5.20}$$

In the electrode:

$$-\frac{\partial}{\partial x}\left(\sigma\frac{\partial \phi}{\partial x} + \varepsilon\frac{\partial}{\partial t}\frac{\partial \phi}{\partial x}\right) - \frac{\partial}{\partial y}\left(\sigma\frac{\partial \phi}{\partial y} + \varepsilon\frac{\partial}{\partial t}\frac{\partial \phi}{\partial y}\right) - \frac{\partial}{\partial z}\left(\sigma\frac{\partial \phi}{\partial z} + \varepsilon\frac{\partial}{\partial t}\frac{\partial \phi}{\partial z}\right) = 0. \tag{5.21}$$

The time-constant part of the solution is called the bias. For example, it is possible to have an applied voltage which has a non-zero average, or there could be a load applied to the bimorph so that its starting deformation is non-zero. In this case, the applied boundary conditions will have a constant part, and the biases can be solved exactly as in the static case. In fact, if the applied conditions are comprised of a sequence

of orthogonal frequencies (such as with a Fourier series), then the solution can be solved independently at each frequency, and we would have a final solution of the form

$$u(\boldsymbol{x}, t) = u_0(\boldsymbol{x}) + \sum_k \left(\alpha_u^k(\boldsymbol{x}) + \mathrm{i}\beta_u^k(\boldsymbol{x})\right) \mathrm{e}^{\mathrm{i}\omega_k t}. \tag{5.22}$$

For an applied voltage with a particular frequency ω, we have the following harmonic equations for PVDF.

$$\begin{aligned} 0 = &\left[\rho\omega^2\alpha_u + \frac{\partial}{\partial x}\left(c_{11}\frac{\partial \alpha_u}{\partial x} + c_{12}\frac{\partial \alpha_v}{\partial y} + c_{13}\frac{\partial \alpha_w}{\partial z} + e_{31}\frac{\partial \alpha_\phi}{\partial z}\right)\right. \\ &\quad \left. + \frac{\partial}{\partial y}\left(c_{66}\left(\frac{\partial \alpha_u}{\partial y} + \frac{\partial \alpha_v}{\partial x}\right)\right) + \frac{\partial}{\partial z}\left(c_{55}\left(\frac{\partial \alpha_u}{\partial z} + \frac{\partial \alpha_w}{\partial x}\right) + e_{15}\frac{\partial \alpha_\phi}{\partial x}\right)\right] \\ &+ \mathrm{i}\left[\rho\omega^2\beta_u + \frac{\partial}{\partial x}\left(c_{11}\frac{\partial \beta_u}{\partial x} + c_{12}\frac{\partial \beta_v}{\partial y} + c_{13}\frac{\partial \beta_w}{\partial z} + e_{31}\frac{\partial \beta_\phi}{\partial z}\right)\right. \\ &\quad \left. + \frac{\partial}{\partial y}\left(c_{66}\left(\frac{\partial \beta_u}{\partial y} + \frac{\partial \beta_v}{\partial x}\right)\right) + \frac{\partial}{\partial z}\left(c_{55}\left(\frac{\partial \beta_u}{\partial z} + \frac{\partial \beta_w}{\partial x}\right) + e_{15}\frac{\partial \beta_\phi}{\partial x}\right)\right] \end{aligned} \tag{5.23}$$

$$\begin{aligned} 0 = &\left[\rho\omega^2\alpha_v + \frac{\partial}{\partial y}\left(c_{12}\frac{\partial \alpha_u}{\partial x} + c_{22}\frac{\partial \alpha_v}{\partial y} + c_{23}\frac{\partial \alpha_w}{\partial z} + e_{32}\frac{\partial \alpha_\phi}{\partial z}\right)\right. \\ &\quad \left. + \frac{\partial}{\partial x}\left(c_{66}\left(\frac{\partial \alpha_u}{\partial y} + \frac{\partial \alpha_v}{\partial x}\right)\right) + \frac{\partial}{\partial z}\left(c_{44}\left(\frac{\partial \alpha_v}{\partial z} + \frac{\partial \alpha_w}{\partial y}\right) + e_{24}\frac{\partial \alpha_\phi}{\partial y}\right)\right] \\ &+ \mathrm{i}\left[\rho\omega^2\beta_v + \frac{\partial}{\partial y}\left(c_{12}\frac{\partial \beta_u}{\partial x} + c_{22}\frac{\partial \beta_v}{\partial y} + c_{23}\frac{\partial \beta_w}{\partial z} + e_{32}\frac{\partial \beta_\phi}{\partial z}\right)\right. \\ &\quad \left. + \frac{\partial}{\partial x}\left(c_{66}\left(\frac{\partial \beta_u}{\partial y} + \frac{\partial \beta_v}{\partial x}\right)\right) + \frac{\partial}{\partial z}\left(c_{44}\left(\frac{\partial \beta_v}{\partial z} + \frac{\partial \beta_w}{\partial y}\right) + e_{24}\frac{\partial \beta_\phi}{\partial y}\right)\right] \end{aligned} \tag{5.24}$$

$$\begin{aligned} 0 = &\left[\rho\omega^2\alpha_w + \frac{\partial}{\partial x}\left(c_{55}\left(\frac{\partial \alpha_u}{\partial z} + \frac{\partial \alpha_w}{\partial x}\right) + e_{15}\frac{\partial \alpha_\phi}{\partial x}\right)\right. \\ &\quad + \frac{\partial}{\partial y}\left(c_{44}\left(\frac{\partial \alpha_v}{\partial z} + \frac{\partial \alpha_w}{\partial y}\right) + e_{24}\frac{\partial \alpha_\phi}{\partial y}\right) \\ &\quad \left. + \frac{\partial}{\partial z}\left(c_{13}\frac{\partial \alpha_u}{\partial x} + c_{23}\frac{\partial \alpha_v}{\partial y} + c_{33}\frac{\partial \alpha_w}{\partial z} + e_{33}\frac{\partial \alpha_\phi}{\partial z}\right)\right] \\ &+ \mathrm{i}\left[\rho\omega^2\beta_w + \frac{\partial}{\partial x}\left(c_{55}\left(\frac{\partial \beta_u}{\partial z} + \frac{\partial \beta_w}{\partial x}\right) + e_{15}\frac{\partial \beta_\phi}{\partial x}\right)\right. \\ &\quad + \frac{\partial}{\partial y}\left(c_{44}\left(\frac{\partial \beta_v}{\partial z} + \frac{\partial \beta_w}{\partial y}\right) + e_{24}\frac{\partial \beta_\phi}{\partial y}\right) \\ &\quad \left. + \frac{\partial}{\partial z}\left(c_{13}\frac{\partial \beta_u}{\partial x} + c_{23}\frac{\partial \beta_v}{\partial y} + c_{33}\frac{\partial \beta_w}{\partial z} + e_{33}\frac{\partial \beta_\phi}{\partial z}\right)\right] \end{aligned} \tag{5.25}$$

$$
\begin{aligned}
0 = &-\omega\left[\frac{\partial}{\partial x}\left(e_{15}\left(\frac{\partial \beta_u}{\partial z}+\frac{\partial \beta_w}{\partial x}\right)-\varepsilon_1\frac{\partial \beta_\phi}{\partial x}\right)+\frac{\partial}{\partial y}\left(e_{24}\left(\frac{\partial \beta_v}{\partial z}+\frac{\partial \beta_w}{\partial y}\right)-\varepsilon_2\frac{\partial \beta_\phi}{\partial y}\right)\right.\\
&\left.+\frac{\partial}{\partial z}\left(e_{31}\frac{\partial \beta_u}{\partial x}+e_{32}\frac{\partial \beta_v}{\partial y}+e_{33}\frac{\partial \beta_w}{\partial z}-\varepsilon_3\frac{\partial \beta_\phi}{\partial z}\right)\right]\\
&+\mathrm{i}\omega\left[\frac{\partial}{\partial x}\left(e_{15}\left(\frac{\partial \alpha_u}{\partial z}+\frac{\partial \alpha_w}{\partial x}\right)-\varepsilon_1\frac{\partial \alpha_\phi}{\partial x}\right)+\frac{\partial}{\partial y}\left(e_{24}\left(\frac{\partial \alpha_v}{\partial z}+\frac{\partial \alpha_w}{\partial y}\right)-\varepsilon_2\frac{\partial \alpha_\phi}{\partial y}\right)\right.\\
&\left.+\frac{\partial}{\partial z}\left(e_{31}\frac{\partial \alpha_u}{\partial x}+e_{32}\frac{\partial \alpha_v}{\partial y}+e_{33}\frac{\partial \alpha_w}{\partial z}-\varepsilon_3\frac{\partial \alpha_\phi}{\partial z}\right)\right]
\end{aligned}
\tag{5.26}
$$

In the electrode:

$$
\begin{aligned}
0 = &\left[\frac{\partial}{\partial x}\left(-\sigma\frac{\partial \alpha_\phi}{\partial x}+\omega\varepsilon\frac{\partial \beta_\phi}{\partial x}\right)+\frac{\partial}{\partial y}\left(-\sigma\frac{\partial \alpha_\phi}{\partial y}+\omega\varepsilon\frac{\partial \beta_\phi}{\partial y}\right)+\frac{\partial}{\partial z}\left(-\sigma\frac{\partial \alpha_\phi}{\partial z}+\omega\varepsilon\frac{\partial \beta_\phi}{\partial z}\right)\right]\\
&+\mathrm{i}\left[-\frac{\partial}{\partial x}\left(\sigma\frac{\partial \beta_\phi}{\partial x}+\omega\varepsilon\frac{\partial \alpha_\phi}{\partial x}\right)-\frac{\partial}{\partial y}\left(\sigma\frac{\partial \beta_\phi}{\partial y}+\omega\varepsilon\frac{\partial \alpha_\phi}{\partial y}\right)-\frac{\partial}{\partial z}\left(\sigma\frac{\partial \beta_\phi}{\partial z}+\omega\varepsilon\frac{\partial \alpha_\phi}{\partial z}\right)\right]
\end{aligned}
\tag{5.27}
$$

Since these equations must be satisfied for both the real and imaginary parts, the two parts can be separated. We now have twice the number of unknowns that we had in the static case, since we need to solve for the cosine coefficients, and the sine coefficients.

$$
\begin{aligned}
0 = &\rho\omega^2\alpha_u+\frac{\partial}{\partial x}\left(c_{11}\frac{\partial \alpha_u}{\partial x}+c_{12}\frac{\partial \alpha_v}{\partial y}+c_{13}\frac{\partial \alpha_w}{\partial z}+e_{31}\frac{\partial \alpha_\phi}{\partial z}\right)\\
&+\frac{\partial}{\partial y}\left(c_{66}\left(\frac{\partial \alpha_u}{\partial y}+\frac{\partial \alpha_v}{\partial x}\right)\right)+\frac{\partial}{\partial z}\left(c_{55}\left(\frac{\partial \alpha_u}{\partial z}+\frac{\partial \alpha_w}{\partial x}\right)+e_{15}\frac{\partial \alpha_\phi}{\partial x}\right)
\end{aligned}
\tag{5.28}
$$

$$
\begin{aligned}
0 = &\rho\omega^2\beta_u+\frac{\partial}{\partial x}\left(c_{11}\frac{\partial \beta_u}{\partial x}+c_{12}\frac{\partial \beta_v}{\partial y}+c_{13}\frac{\partial \beta_w}{\partial z}+e_{31}\frac{\partial \beta_\phi}{\partial z}\right)\\
&+\frac{\partial}{\partial y}\left(c_{66}\left(\frac{\partial \beta_u}{\partial y}+\frac{\partial \beta_v}{\partial x}\right)\right)+\frac{\partial}{\partial z}\left(c_{55}\left(\frac{\partial \beta_u}{\partial z}+\frac{\partial \beta_w}{\partial x}\right)+e_{15}\frac{\partial \beta_\phi}{\partial x}\right)
\end{aligned}
\tag{5.29}
$$

$$
\begin{aligned}
0 = &\rho\omega^2\alpha_v+\frac{\partial}{\partial y}\left(c_{12}\frac{\partial \alpha_u}{\partial x}+c_{22}\frac{\partial \alpha_v}{\partial y}+c_{23}\frac{\partial \alpha_w}{\partial z}+e_{32}\frac{\partial \alpha_\phi}{\partial z}\right)\\
&+\frac{\partial}{\partial x}\left(c_{66}\left(\frac{\partial \alpha_u}{\partial y}+\frac{\partial \alpha_v}{\partial x}\right)\right)+\frac{\partial}{\partial z}\left(c_{44}\left(\frac{\partial \alpha_v}{\partial z}+\frac{\partial \alpha_w}{\partial y}\right)+e_{24}\frac{\partial \alpha_\phi}{\partial y}\right)
\end{aligned}
\tag{5.30}
$$

$$
\begin{aligned}
0 = &\rho\omega^2\beta_v+\frac{\partial}{\partial y}\left(c_{12}\frac{\partial \beta_u}{\partial x}+c_{22}\frac{\partial \beta_v}{\partial y}+c_{23}\frac{\partial \beta_w}{\partial z}+e_{32}\frac{\partial \beta_\phi}{\partial z}\right)\\
&+\frac{\partial}{\partial x}\left(c_{66}\left(\frac{\partial \beta_u}{\partial y}+\frac{\partial \beta_v}{\partial x}\right)\right)+\frac{\partial}{\partial z}\left(c_{44}\left(\frac{\partial \beta_v}{\partial z}+\frac{\partial \beta_w}{\partial y}\right)+e_{24}\frac{\partial \beta_\phi}{\partial y}\right)
\end{aligned}
\tag{5.31}
$$

$$\begin{aligned}0 =&\rho\omega^2\alpha_w + \frac{\partial}{\partial x}\left(c_{55}\left(\frac{\partial\alpha_u}{\partial z}+\frac{\partial\alpha_w}{\partial x}\right)+e_{15}\frac{\partial\alpha_\phi}{\partial x}\right)\\ &+\frac{\partial}{\partial y}\left(c_{44}\left(\frac{\partial\alpha_v}{\partial z}+\frac{\partial\alpha_w}{\partial y}\right)+e_{24}\frac{\partial\alpha_\phi}{\partial y}\right)\\ &+\frac{\partial}{\partial z}\left(c_{13}\frac{\partial\alpha_u}{\partial x}+c_{23}\frac{\partial\alpha_v}{\partial y}+c_{33}\frac{\partial\alpha_w}{\partial z}+e_{33}\frac{\partial\alpha_\phi}{\partial z}\right)\end{aligned} \tag{5.32}$$

$$\begin{aligned}0 =&\rho\omega^2\beta_w + \frac{\partial}{\partial x}\left(c_{55}\left(\frac{\partial\beta_u}{\partial z}+\frac{\partial\beta_w}{\partial x}\right)+e_{15}\frac{\partial\beta_\phi}{\partial x}\right)\\ &+\frac{\partial}{\partial y}\left(c_{44}\left(\frac{\partial\beta_v}{\partial z}+\frac{\partial\beta_w}{\partial y}\right)+e_{24}\frac{\partial\beta_\phi}{\partial y}\right)\\ &+\frac{\partial}{\partial z}\left(c_{13}\frac{\partial\beta_u}{\partial x}+c_{23}\frac{\partial\beta_v}{\partial y}+c_{33}\frac{\partial\beta_w}{\partial z}+e_{33}\frac{\partial\beta_\phi}{\partial z}\right)\end{aligned} \tag{5.33}$$

$$\begin{aligned}0 =&-\omega\left[\frac{\partial}{\partial x}\left(e_{15}\left(\frac{\partial\beta_u}{\partial z}+\frac{\partial\beta_w}{\partial x}\right)-\varepsilon_1\frac{\partial\beta_\phi}{\partial x}\right)+\frac{\partial}{\partial y}\left(e_{24}\left(\frac{\partial\beta_v}{\partial z}+\frac{\partial\beta_w}{\partial y}\right)-\varepsilon_2\frac{\partial\beta_\phi}{\partial y}\right)\right.\\ &\left.+\frac{\partial}{\partial z}\left(e_{31}\frac{\partial\beta_u}{\partial x}+e_{32}\frac{\partial\beta_v}{\partial y}+e_{33}\frac{\partial\beta_w}{\partial z}-\varepsilon_3\frac{\partial\beta_\phi}{\partial z}\right)\right]\end{aligned} \tag{5.34}$$

$$\begin{aligned}0 =&\omega\left[\frac{\partial}{\partial x}\left(e_{15}\left(\frac{\partial\alpha_u}{\partial z}+\frac{\partial\alpha_w}{\partial x}\right)-\varepsilon_1\frac{\partial\alpha_\phi}{\partial x}\right)+\frac{\partial}{\partial y}\left(e_{24}\left(\frac{\partial\alpha_v}{\partial z}+\frac{\partial\alpha_w}{\partial y}\right)-\varepsilon_2\frac{\partial\alpha_\phi}{\partial y}\right)\right.\\ &\left.+\frac{\partial}{\partial z}\left(e_{31}\frac{\partial\alpha_u}{\partial x}+e_{32}\frac{\partial\alpha_v}{\partial y}+e_{33}\frac{\partial\alpha_w}{\partial z}-\varepsilon_3\frac{\partial\alpha_\phi}{\partial z}\right)\right]\end{aligned} \tag{5.35}$$

In the electrode:

$$0 =\frac{\partial}{\partial x}\left(-\sigma\frac{\partial\alpha_\phi}{\partial x}+\omega\varepsilon\frac{\partial\beta_\phi}{\partial x}\right)+\frac{\partial}{\partial y}\left(-\sigma\frac{\partial\alpha_\phi}{\partial y}+\omega\varepsilon\frac{\partial\beta_\phi}{\partial y}\right)+\frac{\partial}{\partial z}\left(-\sigma\frac{\partial\alpha_\phi}{\partial z}+\omega\varepsilon\frac{\partial\beta_\phi}{\partial z}\right) \tag{5.36}$$

$$0 =-\frac{\partial}{\partial x}\left(\sigma\frac{\partial\beta_\phi}{\partial x}+\omega\varepsilon\frac{\partial\alpha_\phi}{\partial x}\right)-\frac{\partial}{\partial y}\left(\sigma\frac{\partial\beta_\phi}{\partial y}+\omega\varepsilon\frac{\partial\alpha_\phi}{\partial y}\right)-\frac{\partial}{\partial z}\left(\sigma\frac{\partial\beta_\phi}{\partial z}+\omega\varepsilon\frac{\partial\alpha_\phi}{\partial z}\right) \tag{5.37}$$

To convert to the weak form, the appropriate variation must be used in each case. For the equation which corresponds to the real part, we use the variation of the cosine

coefficient. The sine coefficient is used for the imaginary part.

$$0 = \int_\Omega \left[-\rho\omega^2 \delta\alpha_u \alpha_u + \frac{\partial \delta\alpha_u}{\partial x}\left(c_{11}\frac{\partial \alpha_u}{\partial x} + c_{12}\frac{\partial \alpha_v}{\partial y} + c_{13}\frac{\partial \alpha_w}{\partial z} + e_{31}\frac{\partial \alpha_\phi}{\partial z}\right) + \frac{\partial \delta\alpha_u}{\partial y}\left(c_{66}\left(\frac{\partial \alpha_u}{\partial y} + \frac{\partial \alpha_v}{\partial x}\right)\right) + \frac{\partial \delta\alpha_u}{\partial z}\left(c_{55}\left(\frac{\partial \alpha_u}{\partial z} + \frac{\partial \alpha_w}{\partial x}\right) + e_{15}\frac{\partial \alpha_\phi}{\partial x}\right)\right] \mathrm{d}\Omega \tag{5.38}$$

$$0 = \int_\Omega \left[-\rho\omega^2 \delta\beta_u \beta_u + \frac{\partial \delta\beta_u}{\partial x}\left(c_{11}\frac{\partial \beta_u}{\partial x} + c_{12}\frac{\partial \beta_v}{\partial y} + c_{13}\frac{\partial \beta_w}{\partial z} + e_{31}\frac{\partial \beta_\phi}{\partial z}\right) + \frac{\partial \delta\beta_u}{\partial y}\left(c_{66}\left(\frac{\partial \beta_u}{\partial y} + \frac{\partial \beta_v}{\partial x}\right)\right) + \frac{\partial \delta\beta_u}{\partial z}\left(c_{55}\left(\frac{\partial \beta_u}{\partial z} + \frac{\partial \beta_w}{\partial x}\right) + e_{15}\frac{\partial \beta_\phi}{\partial x}\right)\right] \mathrm{d}\Omega \tag{5.39}$$

$$0 = \int_\Omega \left[-\rho\omega^2 \delta\alpha_v \alpha_v + \frac{\partial \delta\alpha_v}{\partial y}\left(c_{12}\frac{\partial \alpha_u}{\partial x} + c_{22}\frac{\partial \alpha_v}{\partial y} + c_{23}\frac{\partial \alpha_w}{\partial z} + e_{32}\frac{\partial \alpha_\phi}{\partial z}\right) + \frac{\partial \delta\alpha_v}{\partial x}\left(c_{66}\left(\frac{\partial \alpha_u}{\partial y} + \frac{\partial \alpha_v}{\partial x}\right)\right) + \frac{\partial \delta\alpha_v}{\partial z}\left(c_{44}\left(\frac{\partial \alpha_v}{\partial z} + \frac{\partial \alpha_w}{\partial y}\right) + e_{24}\frac{\partial \alpha_\phi}{\partial y}\right)\right] \mathrm{d}\Omega \tag{5.40}$$

$$0 = \int_\Omega \left[-\rho\omega^2 \delta\beta_v \beta_v + \frac{\partial \delta\beta_v}{\partial y}\left(c_{12}\frac{\partial \beta_u}{\partial x} + c_{22}\frac{\partial \beta_v}{\partial y} + c_{23}\frac{\partial \beta_w}{\partial z} + e_{32}\frac{\partial \beta_\phi}{\partial z}\right) + \frac{\partial \delta\beta_v}{\partial x}\left(c_{66}\left(\frac{\partial \beta_u}{\partial y} + \frac{\partial \beta_v}{\partial x}\right)\right) + \frac{\partial \delta\beta_v}{\partial z}\left(c_{44}\left(\frac{\partial \beta_v}{\partial z} + \frac{\partial \beta_w}{\partial y}\right) + e_{24}\frac{\partial \beta_\phi}{\partial y}\right)\right] \mathrm{d}\Omega \tag{5.41}$$

$$0 = \int_\Omega \left[-\rho\omega^2 \delta\alpha_w \alpha_w + \frac{\partial \delta\alpha_w}{\partial x}\left(c_{55}\left(\frac{\partial \alpha_u}{\partial z} + \frac{\partial \alpha_w}{\partial x}\right) + e_{15}\frac{\partial \alpha_\phi}{\partial x}\right) + \frac{\partial \delta\alpha_w}{\partial y}\left(c_{44}\left(\frac{\partial \alpha_v}{\partial z} + \frac{\partial \alpha_w}{\partial y}\right) + e_{24}\frac{\partial \alpha_\phi}{\partial y}\right) + \frac{\partial \delta\alpha_w}{\partial z}\left(c_{13}\frac{\partial \alpha_u}{\partial x} + c_{23}\frac{\partial \alpha_v}{\partial y} + c_{33}\frac{\partial \alpha_w}{\partial z} + e_{33}\frac{\partial \alpha_\phi}{\partial z}\right)\right] \mathrm{d}\Omega \tag{5.42}$$

$$0 = \int_\Omega \left[-\rho\omega^2 \delta\beta_w \beta_w + \frac{\partial \delta\beta_w}{\partial x}\left(c_{55}\left(\frac{\partial \beta_u}{\partial z} + \frac{\partial \beta_w}{\partial x}\right) + e_{15}\frac{\partial \beta_\phi}{\partial x}\right) + \frac{\partial \delta\beta_w}{\partial y}\left(c_{44}\left(\frac{\partial \beta_v}{\partial z} + \frac{\partial \beta_w}{\partial y}\right) + e_{24}\frac{\partial \beta_\phi}{\partial y}\right) + \frac{\partial \delta\beta_w}{\partial z}\left(c_{13}\frac{\partial \beta_u}{\partial x} + c_{23}\frac{\partial \beta_v}{\partial y} + c_{33}\frac{\partial \beta_w}{\partial z} + e_{33}\frac{\partial \beta_\phi}{\partial z}\right)\right] \mathrm{d}\Omega \tag{5.43}$$

$$0 = -\int_\Omega \omega \left[\frac{\partial \delta\alpha_\phi}{\partial x}\left(e_{15}\left(\frac{\partial \beta_u}{\partial z} + \frac{\partial \beta_w}{\partial x}\right) - \varepsilon_1\frac{\partial \beta_\phi}{\partial x}\right) + \frac{\partial \delta\alpha_\phi}{\partial y}\left(e_{24}\left(\frac{\partial \beta_v}{\partial z} + \frac{\partial \beta_w}{\partial y}\right) - \varepsilon_2\frac{\partial \beta_\phi}{\partial y}\right) + \frac{\partial \delta\alpha_\phi}{\partial z}\left(e_{31}\frac{\partial \beta_u}{\partial x} + e_{32}\frac{\partial \beta_v}{\partial y} + e_{33}\frac{\partial \beta_w}{\partial z} - \varepsilon_3\frac{\partial \beta_\phi}{\partial z}\right)\right] \mathrm{d}\Omega \tag{5.44}$$

$$
\begin{aligned}
0 = \int_\Omega \omega \Bigg[& \frac{\partial \delta\beta_\phi}{\partial x}\left(e_{15}\left(\frac{\partial \alpha_u}{\partial z}+\frac{\partial \alpha_w}{\partial x}\right)-\varepsilon_1\frac{\partial \alpha_\phi}{\partial x}\right) \\
& + \frac{\partial \delta\beta_\phi}{\partial y}\left(e_{24}\left(\frac{\partial \alpha_v}{\partial z}+\frac{\partial \alpha_w}{\partial y}\right)-\varepsilon_2\frac{\partial \alpha_\phi}{\partial y}\right) \\
& + \frac{\partial \delta\beta_\phi}{\partial z}\left(e_{31}\frac{\partial \alpha_u}{\partial x}+e_{32}\frac{\partial \alpha_v}{\partial y}+e_{33}\frac{\partial \alpha_w}{\partial z}-\varepsilon_3\frac{\partial \alpha_\phi}{\partial z}\right)\Bigg] \mathrm{d}\Omega
\end{aligned}
\tag{5.45}
$$

In the electrode:

$$
\begin{aligned}
0 = \int_\Omega \Bigg[& \frac{\partial \delta\alpha_\phi}{\partial x}\left(-\sigma\frac{\partial \alpha_\phi}{\partial x}+\omega\varepsilon\frac{\partial \beta_\phi}{\partial x}\right)+\frac{\partial \delta\alpha_\phi}{\partial y}\left(-\sigma\frac{\partial \alpha_\phi}{\partial y}+\omega\varepsilon\frac{\partial \beta_\phi}{\partial y}\right) \\
& + \frac{\partial \delta\alpha_\phi}{\partial z}\left(-\sigma\frac{\partial \alpha_\phi}{\partial z}+\omega\varepsilon\frac{\partial \beta_\phi}{\partial z}\right)\Bigg] \mathrm{d}\Omega
\end{aligned}
\tag{5.46}
$$

$$
\begin{aligned}
0 = -\int_\Omega \Bigg[& \frac{\partial \delta\beta_\phi}{\partial x}\left(\sigma\frac{\partial \beta_\phi}{\partial x}+\omega\varepsilon\frac{\partial \alpha_\phi}{\partial x}\right)+\frac{\partial \delta\beta_\phi}{\partial y}\left(\sigma\frac{\partial \beta_\phi}{\partial y}+\omega\varepsilon\frac{\partial \alpha_\phi}{\partial y}\right) \\
& + \frac{\partial \delta\beta_\phi}{\partial z}\left(\sigma\frac{\partial \beta_\phi}{\partial z}+\omega\varepsilon\frac{\partial \alpha_\phi}{\partial z}\right)\Bigg] \mathrm{d}\Omega
\end{aligned}
\tag{5.47}
$$

Since the cosine and sine coefficients are coupled, a purely sinusoidal input voltage will generate cosine contributions, and there will be phase differences in the solution relative to the input. The “phase lag” is very important in understanding the response of the bimorph.

The harmonic linear system:

$$
\begin{bmatrix}
\boldsymbol{K}^{11} & \boldsymbol{K}^{12} & \boldsymbol{K}^{13} & \boldsymbol{K}^{14} & 0 & 0 & 0 & 0 \\
\left(\boldsymbol{K}^{12}\right)^T & \boldsymbol{K}^{22} & \boldsymbol{K}^{23} & \boldsymbol{K}^{24} & 0 & 0 & 0 & 0 \\
\left(\boldsymbol{K}^{13}\right)^T & \left(\boldsymbol{K}^{23}\right)^T & \boldsymbol{K}^{33} & \boldsymbol{K}^{34} & 0 & 0 & 0 & 0 \\
0 & 0 & 0 & \boldsymbol{K}^{88} & -\boldsymbol{K}^{81} & -\boldsymbol{K}^{82} & -\boldsymbol{K}^{83} & -\boldsymbol{K}^{84} \\
0 & 0 & 0 & 0 & \boldsymbol{K}^{11} & \boldsymbol{K}^{12} & \boldsymbol{K}^{13} & \boldsymbol{K}^{14} \\
0 & 0 & 0 & 0 & \left(\boldsymbol{K}^{12}\right)^T & \boldsymbol{K}^{22} & \boldsymbol{K}^{23} & \boldsymbol{K}^{24} \\
0 & 0 & 0 & 0 & \left(\boldsymbol{K}^{13}\right)^T & \left(\boldsymbol{K}^{23}\right)^T & \boldsymbol{K}^{33} & \boldsymbol{K}^{34} \\
\boldsymbol{K}^{81} & \boldsymbol{K}^{82} & \boldsymbol{K}^{83} & \boldsymbol{K}^{84} & 0 & 0 & 0 & \boldsymbol{K}^{88}
\end{bmatrix}
\cdot
\begin{bmatrix}
\boldsymbol{\alpha}_u \\ \boldsymbol{\alpha}_v \\ \boldsymbol{\alpha}_w \\ \boldsymbol{\alpha}_\phi \\ \boldsymbol{\beta}_u \\ \boldsymbol{\beta}_v \\ \boldsymbol{\beta}_w \\ \boldsymbol{\beta}_\phi
\end{bmatrix}
=
\begin{bmatrix}
\boldsymbol{F}^1 \\ \boldsymbol{F}^2 \\ \boldsymbol{F}^3 \\ \boldsymbol{F}^4 \\ \boldsymbol{F}^5 \\ \boldsymbol{F}^6 \\ \boldsymbol{F}^7 \\ \boldsymbol{F}^8
\end{bmatrix}
\tag{5.48}
$$

In PVDF:

$$
K_{ij}^{11} = \int_\Omega \left[c_{11}\frac{\partial \psi_i}{\partial x}\frac{\partial \psi_j}{\partial x}+c_{66}\frac{\partial \psi_i}{\partial y}\frac{\partial \psi_j}{\partial y}+c_{55}\frac{\partial \psi_i}{\partial z}\frac{\partial \psi_j}{\partial z}-\rho\omega^2\psi_i\psi_j \right] \mathrm{d}\Omega \tag{5.49}
$$

$$K_{ij}^{12} = \int_{\Omega} \left[c_{12} \frac{\partial \psi_i}{\partial x} \frac{\partial \psi_j}{\partial y} + c_{66} \frac{\partial \psi_i}{\partial y} \frac{\partial \psi_j}{\partial x} \right] \mathrm{d}\Omega \tag{5.50}$$

$$K_{ij}^{13} = \int_{\Omega} \left[c_{13} \frac{\partial \psi_i}{\partial x} \frac{\partial \psi_j}{\partial z} + c_{55} \frac{\partial \psi_i}{\partial z} \frac{\partial \psi_j}{\partial x} \right] \mathrm{d}\Omega \tag{5.51}$$

$$K_{ij}^{14} = \int_{\Omega} \left[e_{31} \frac{\partial \psi_i}{\partial x} \frac{\partial \psi_j}{\partial z} + e_{15} \frac{\partial \psi_i}{\partial z} \frac{\partial \psi_j}{\partial x} \right] \mathrm{d}\Omega \tag{5.52}$$

$$K_{ij}^{22} = \int_{\Omega} \left[c_{66} \frac{\partial \psi_i}{\partial x} \frac{\partial \psi_j}{\partial x} + c_{22} \frac{\partial \psi_i}{\partial y} \frac{\partial \psi_j}{\partial y} + c_{44} \frac{\partial \psi_i}{\partial z} \frac{\partial \psi_j}{\partial z} - \rho \omega^2 \psi_i \psi_j \right] \mathrm{d}\Omega \tag{5.53}$$

$$K_{ij}^{23} = \int_{\Omega} \left[c_{23} \frac{\partial \psi_i}{\partial y} \frac{\partial \psi_j}{\partial z} + c_{44} \frac{\partial \psi_i}{\partial z} \frac{\partial \psi_j}{\partial y} \right] \mathrm{d}\Omega \tag{5.54}$$

$$K_{ij}^{24} = \int_{\Omega} \left[e_{32} \frac{\partial \psi_i}{\partial y} \frac{\partial \psi_j}{\partial z} + e_{24} \frac{\partial \psi_i}{\partial z} \frac{\partial \psi_j}{\partial y} \right] \mathrm{d}\Omega \tag{5.55}$$

$$K_{ij}^{33} = \int_{\Omega} \left[c_{55} \frac{\partial \psi_i}{\partial x} \frac{\partial \psi_j}{\partial x} + c_{44} \frac{\partial \psi_i}{\partial y} \frac{\partial \psi_j}{\partial y} + c_{33} \frac{\partial \psi_i}{\partial z} \frac{\partial \psi_j}{\partial z} - \rho \omega^2 \psi_i \psi_j \right] \mathrm{d}\Omega \tag{5.56}$$

$$K_{ij}^{34} = \int_{\Omega} \left[e_{15} \frac{\partial \psi_i}{\partial x} \frac{\partial \psi_j}{\partial x} + e_{24} \frac{\partial \psi_i}{\partial y} \frac{\partial \psi_j}{\partial y} + e_{33} \frac{\partial \psi_i}{\partial z} \frac{\partial \psi_j}{\partial z} \right] \mathrm{d}\Omega \tag{5.57}$$

$$K_{ij}^{81} = \int_{\Omega} \omega \left[e_{31} \frac{\partial \psi_i}{\partial z} \frac{\partial \psi_j}{\partial x} + e_{15} \frac{\partial \psi_i}{\partial x} \frac{\partial \psi_j}{\partial z} \right] \mathrm{d}\Omega \tag{5.58}$$

$$K_{ij}^{82} = \int_{\Omega} \omega \left[e_{32} \frac{\partial \psi_i}{\partial z} \frac{\partial \psi_j}{\partial y} + e_{24} \frac{\partial \psi_i}{\partial y} \frac{\partial \psi_j}{\partial z} \right] \mathrm{d}\Omega \tag{5.59}$$

$$K_{ij}^{83} = \int_{\Omega} \omega \left[e_{15} \frac{\partial \psi_i}{\partial x} \frac{\partial \psi_j}{\partial x} + e_{24} \frac{\partial \psi_i}{\partial y} \frac{\partial \psi_j}{\partial y} + e_{33} \frac{\partial \psi_i}{\partial z} \frac{\partial \psi_j}{\partial z} \right] \mathrm{d}\Omega \tag{5.60}$$

$$K_{ij}^{84} = -\int_{\Omega} \omega \left[\varepsilon_1 \frac{\partial \psi_i}{\partial x} \frac{\partial \psi_j}{\partial x} + \varepsilon_2 \frac{\partial \psi_i}{\partial y} \frac{\partial \psi_j}{\partial y} \varepsilon_3 + \frac{\partial \psi_i}{\partial z} \frac{\partial \psi_j}{\partial z} \right] \mathrm{d}\Omega \tag{5.61}$$

In the electrode:

$$K_{ij}^{84} = -\int_{\Omega} \omega \varepsilon \left[\frac{\partial \psi_i}{\partial x} \frac{\partial \psi_j}{\partial x} + \frac{\partial \psi_i}{\partial y} \frac{\partial \psi_j}{\partial y} + \frac{\partial \psi_i}{\partial z} \frac{\partial \psi_j}{\partial z} \right] \mathrm{d}\Omega \tag{5.62}$$

$$K_{ij}^{88} = -\int_{\Omega} \sigma \left[\frac{\partial \psi_i}{\partial x} \frac{\partial \psi_j}{\partial x} + \frac{\partial \psi_i}{\partial y} \frac{\partial \psi_j}{\partial y} + \frac{\partial \psi_i}{\partial z} \frac{\partial \psi_j}{\partial z} \right] \mathrm{d}\Omega \tag{5.63}$$

Damping

It is possible for the elasticity to be complex, in which case we get mechanical damping. When looking at the response of the bimorph as a function of frequency, the amplitude of the deflection will blow up at the resonance frequencies. Having damping will cause those peaks to broaden, and the amplitude will not go to infinity. There can also be electrical damping and air resistance. There will already be some electrical damping because of the resistivity of the electrodes, and so we do not use any imaginary components of the piezoelectric constants or the dielectric permittivity. Air resistance is a non-linear function of the velocity of the air surrounding the bimorph. It requires solving the Navier-Stokes equations, which requires using a very different approach than simple Lagrange FEM. The Navier-Stokes equations can be converted to a finite element formulation, but the variables in the air resistance problem are air pressure and air velocity, while the variables for the bimorph problem are electric potential and mechanical displacement along with velocity. This system involves mixing different types of variable, which would be very difficult to solve for simultaneously. The problem is advanced enough that it would require a separate study.

$$c_{ij} = c'_{ij} + \mathrm{i}c''_{ij} \tag{5.64}$$

The elasticity constant splits into real and imaginary parts. This will strengthen the coupling between the cosine and sine coefficients. The modified differential equations are shown below.

$$
\begin{aligned}
0 = \Bigg[& \rho\omega^2\alpha_u + \frac{\partial}{\partial x}\left(c'_{11}\frac{\partial \alpha_u}{\partial x} - c''_{11}\frac{\partial \beta_u}{\partial x} + c'_{12}\frac{\partial \alpha_v}{\partial y} - c''_{12}\frac{\partial \beta_v}{\partial y} + c'_{13}\frac{\partial \alpha_w}{\partial z}\right. \\
& \left. - c''_{13}\frac{\partial \beta_w}{\partial z} + e_{31}\frac{\partial \alpha_\phi}{\partial z}\right) + \frac{\partial}{\partial y}\left(c'_{66}\left(\frac{\partial \alpha_u}{\partial y} + \frac{\partial \alpha_v}{\partial x}\right) - c''_{66}\left(\frac{\partial \beta_u}{\partial y} + \frac{\partial \beta_v}{\partial x}\right)\right) \\
& + \frac{\partial}{\partial z}\left(c'_{55}\left(\frac{\partial \alpha_u}{\partial z} + \frac{\partial \alpha_w}{\partial x}\right) - c''_{55}\left(\frac{\partial \beta_u}{\partial z} + \frac{\partial \beta_w}{\partial x}\right) + e_{15}\frac{\partial \alpha_\phi}{\partial x}\right)\Bigg] \\
& + \mathrm{i}\Bigg[\rho\omega^2\beta_u + \frac{\partial}{\partial x}\left(c'_{11}\frac{\partial \beta_u}{\partial x} + c''_{11}\frac{\partial \alpha_u}{\partial x} + c'_{12}\frac{\partial \beta_v}{\partial y} + c''_{12}\frac{\partial \alpha_v}{\partial y} + c'_{13}\frac{\partial \beta_w}{\partial z}\right. \\
& \left. + c''_{13}\frac{\partial \alpha_w}{\partial z} + e_{31}\frac{\partial \beta_\phi}{\partial z}\right) + \frac{\partial}{\partial y}\left(c'_{66}\left(\frac{\partial \beta_u}{\partial y} + \frac{\partial \beta_v}{\partial x}\right) + c''_{66}\left(\frac{\partial \alpha_u}{\partial y} + \frac{\partial \alpha_v}{\partial x}\right)\right) \\
& + \frac{\partial}{\partial z}\left(c'_{55}\left(\frac{\partial \beta_u}{\partial z} + \frac{\partial \beta_w}{\partial x}\right) + c''_{55}\left(\frac{\partial \alpha_u}{\partial z} + \frac{\partial \alpha_w}{\partial x}\right) + e_{15}\frac{\partial \beta_\phi}{\partial x}\right)\Bigg]
\end{aligned}
\tag{5.65}
$$

$$
\begin{aligned}
0 = \Bigg[& \rho\omega^2\alpha_v + \frac{\partial}{\partial y}\left(c'_{12}\frac{\partial \alpha_u}{\partial x} - c''_{12}\frac{\partial \beta_u}{\partial x} + c'_{22}\frac{\partial \alpha_v}{\partial y} - c''_{22}\frac{\partial \beta_v}{\partial y} + c'_{23}\frac{\partial \alpha_w}{\partial z}\right. \\
& \left. - c''_{23}\frac{\partial \beta_w}{\partial z} + e_{32}\frac{\partial \alpha_\phi}{\partial z}\right) + \frac{\partial}{\partial x}\left(c'_{66}\left(\frac{\partial \alpha_u}{\partial y} + \frac{\partial \alpha_v}{\partial x}\right) - c''_{66}\left(\frac{\partial \beta_u}{\partial y} + \frac{\partial \beta_v}{\partial x}\right)\right) \\
& + \frac{\partial}{\partial z}\left(c'_{44}\left(\frac{\partial \alpha_v}{\partial z} + \frac{\partial \alpha_w}{\partial y}\right) - c''_{44}\left(\frac{\partial \beta_v}{\partial z} + \frac{\partial \beta_w}{\partial y}\right) + e_{24}\frac{\partial \alpha_\phi}{\partial y}\right)\Bigg] \\
& + \mathrm{i}\Bigg[\rho\omega^2\beta_v + \frac{\partial}{\partial y}\left(c'_{12}\frac{\partial \beta_u}{\partial x} + c''_{12}\frac{\partial \alpha_u}{\partial x} + c'_{22}\frac{\partial \beta_v}{\partial y} + c''_{22}\frac{\partial \alpha_v}{\partial y} + c'_{23}\frac{\partial \beta_w}{\partial z}\right. \\
& \left. + c''_{23}\frac{\partial \alpha_w}{\partial z} + e_{32}\frac{\partial \beta_\phi}{\partial z}\right) + \frac{\partial}{\partial x}\left(c'_{66}\left(\frac{\partial \beta_u}{\partial y} + \frac{\partial \beta_v}{\partial x}\right) + c''_{66}\left(\frac{\partial \alpha_u}{\partial y} + \frac{\partial \alpha_v}{\partial x}\right)\right) \\
& + \frac{\partial}{\partial z}\left(c'_{44}\left(\frac{\partial \beta_v}{\partial z} + \frac{\partial \beta_w}{\partial y}\right) + c''_{44}\left(\frac{\partial \alpha_v}{\partial z} + \frac{\partial \alpha_w}{\partial y}\right) + e_{24}\frac{\partial \beta_\phi}{\partial y}\right)\Bigg]
\end{aligned}
\tag{5.66}
$$

$$
\begin{aligned}
0 = \Bigg[& \rho\omega^2\alpha_w + \frac{\partial}{\partial z}\left(c'_{13}\frac{\partial \alpha_u}{\partial x} - c''_{13}\frac{\partial \beta_u}{\partial x} + c'_{23}\frac{\partial \alpha_v}{\partial y} - c''_{23}\frac{\partial \beta_v}{\partial y} + c'_{33}\frac{\partial \alpha_w}{\partial z}\right. \\
& \left. - c''_{33}\frac{\partial \beta_w}{\partial z} + e_{33}\frac{\partial \alpha_\phi}{\partial z}\right) + \frac{\partial}{\partial x}\left(c'_{55}\left(\frac{\partial \alpha_u}{\partial z} + \frac{\partial \alpha_w}{\partial x}\right) - c''_{55}\left(\frac{\partial \beta_u}{\partial z} + \frac{\partial \beta_w}{\partial x}\right) + e_{15}\frac{\partial \alpha_\phi}{\partial x}\right) \\
& + \frac{\partial}{\partial y}\left(c'_{44}\left(\frac{\partial \alpha_v}{\partial z} + \frac{\partial \alpha_w}{\partial y}\right) - c''_{44}\left(\frac{\partial \beta_v}{\partial z} + \frac{\partial \beta_w}{\partial y}\right) + e_{24}\frac{\partial \alpha_\phi}{\partial y}\right)\Bigg] \\
& + \mathrm{i}\Bigg[\rho\omega^2\beta_w + \frac{\partial}{\partial z}\left(c'_{13}\frac{\partial \beta_u}{\partial x} + c''_{13}\frac{\partial \alpha_u}{\partial x} + c'_{23}\frac{\partial \beta_v}{\partial y} + c''_{23}\frac{\partial \alpha_v}{\partial y} + c'_{33}\frac{\partial \beta_w}{\partial z}\right. \\
& \left. + c''_{33}\frac{\partial \alpha_w}{\partial z} + e_{33}\frac{\partial \beta_\phi}{\partial z}\right) + \frac{\partial}{\partial x}\left(c'_{55}\left(\frac{\partial \beta_u}{\partial z} + \frac{\partial \beta_w}{\partial x}\right) + c''_{55}\left(\frac{\partial \alpha_u}{\partial z} + \frac{\partial \alpha_w}{\partial x}\right) + e_{15}\frac{\partial \beta_\phi}{\partial x}\right) \\
& + \frac{\partial}{\partial y}\left(c'_{44}\left(\frac{\partial \beta_v}{\partial z} + \frac{\partial \beta_w}{\partial y}\right) + c''_{44}\left(\frac{\partial \alpha_v}{\partial z} + \frac{\partial \alpha_w}{\partial y}\right) + e_{24}\frac{\partial \beta_\phi}{\partial y}\right)\Bigg]
\end{aligned}
\tag{5.67}
$$

The harmonic linear system with damping:

$$\begin{bmatrix} \boldsymbol{K}^{11} & \boldsymbol{K}^{12} & \boldsymbol{K}^{13} & \boldsymbol{K}^{14} & -\boldsymbol{K}^{51} & -\boldsymbol{K}^{52} & -\boldsymbol{K}^{53} & 0 \\ \left(\boldsymbol{K}^{12}\right)^T & \boldsymbol{K}^{22} & \boldsymbol{K}^{23} & \boldsymbol{K}^{24} & -\left(\boldsymbol{K}^{52}\right)^T & -\boldsymbol{K}^{62} & -\boldsymbol{K}^{63} & 0 \\ \left(\boldsymbol{K}^{13}\right)^T & \left(\boldsymbol{K}^{23}\right)^T & \boldsymbol{K}^{33} & \boldsymbol{K}^{34} & -\left(\boldsymbol{K}^{53}\right)^T & -\left(\boldsymbol{K}^{63}\right)^T & -\boldsymbol{K}^{73} & 0 \\ 0 & 0 & 0 & \boldsymbol{K}^{88} & -\boldsymbol{K}^{81} & -\boldsymbol{K}^{82} & -\boldsymbol{K}^{83} & -\boldsymbol{K}^{84} \\ \boldsymbol{K}^{51} & \boldsymbol{K}^{52} & \boldsymbol{K}^{53} & 0 & \boldsymbol{K}^{11} & \boldsymbol{K}^{12} & \boldsymbol{K}^{13} & \boldsymbol{K}^{14} \\ \left(\boldsymbol{K}^{52}\right)^T & \boldsymbol{K}^{62} & \boldsymbol{K}^{63} & 0 & \left(\boldsymbol{K}^{12}\right)^T & \boldsymbol{K}^{22} & \boldsymbol{K}^{23} & \boldsymbol{K}^{24} \\ \left(\boldsymbol{K}^{53}\right)^T & \left(\boldsymbol{K}^{63}\right)^T & \boldsymbol{K}^{73} & 0 & \left(\boldsymbol{K}^{13}\right)^T & \left(\boldsymbol{K}^{23}\right)^T & \boldsymbol{K}^{33} & \boldsymbol{K}^{34} \\ \boldsymbol{K}^{81} & \boldsymbol{K}^{82} & \boldsymbol{K}^{83} & \boldsymbol{K}^{84} & 0 & 0 & 0 & \boldsymbol{K}^{88} \end{bmatrix} \cdot \begin{bmatrix} \boldsymbol{\alpha}_u \\ \boldsymbol{\alpha}_v \\ \boldsymbol{\alpha}_w \\ \boldsymbol{\alpha}_\phi \\ \boldsymbol{\beta}_u \\ \boldsymbol{\beta}_v \\ \boldsymbol{\beta}_w \\ \boldsymbol{\beta}_\phi \end{bmatrix} = \begin{bmatrix} \boldsymbol{F}^1 \\ \boldsymbol{F}^2 \\ \boldsymbol{F}^3 \\ \boldsymbol{F}^4 \\ \boldsymbol{F}^5 \\ \boldsymbol{F}^6 \\ \boldsymbol{F}^7 \\ \boldsymbol{F}^8 \end{bmatrix} \tag{5.68}$$

$$K_{ij}^{51} = \int_\Omega \left[c_{11}'' \frac{\partial \psi_i}{\partial x} \frac{\partial \psi_j}{\partial x} + c_{66}'' \frac{\partial \psi_i}{\partial y} \frac{\partial \psi_j}{\partial y} + c_{55}'' \frac{\partial \psi_i}{\partial z} \frac{\partial \psi_j}{\partial z} \right] \mathrm{d}\Omega \tag{5.69}$$

$$K_{ij}^{52} = \int_\Omega \left[c_{12}'' \frac{\partial \psi_i}{\partial x} \frac{\partial \psi_j}{\partial y} + c_{66}'' \frac{\partial \psi_i}{\partial y} \frac{\partial \psi_j}{\partial x} \right] \mathrm{d}\Omega \tag{5.70}$$

$$K_{ij}^{53} = \int_\Omega \left[c_{13}'' \frac{\partial \psi_i}{\partial x} \frac{\partial \psi_j}{\partial z} + c_{55}'' \frac{\partial \psi_i}{\partial z} \frac{\partial \psi_j}{\partial x} \right] \mathrm{d}\Omega \tag{5.71}$$

$$K_{ij}^{62} = \int_\Omega \left[c_{66}'' \frac{\partial \psi_i}{\partial x} \frac{\partial \psi_j}{\partial x} + c_{22}'' \frac{\partial \psi_i}{\partial y} \frac{\partial \psi_j}{\partial y} + c_{44}'' \frac{\partial \psi_i}{\partial z} \frac{\partial \psi_j}{\partial z} \right] \mathrm{d}\Omega \tag{5.72}$$

$$K_{ij}^{63} = \int_\Omega \left[c_{23}'' \frac{\partial \psi_i}{\partial y} \frac{\partial \psi_j}{\partial z} + c_{44}'' \frac{\partial \psi_i}{\partial z} \frac{\partial \psi_j}{\partial y} \right] \mathrm{d}\Omega \tag{5.73}$$

$$K_{ij}^{73} = \int_\Omega \left[c_{55}'' \frac{\partial \psi_i}{\partial x} \frac{\partial \psi_j}{\partial x} + c_{44}'' \frac{\partial \psi_i}{\partial y} \frac{\partial \psi_j}{\partial y} + c_{33}'' \frac{\partial \psi_i}{\partial z} \frac{\partial \psi_j}{\partial z} \right] \mathrm{d}\Omega \tag{5.74}$$

CHAPTER 6

BIMORPH: HARMONIC 2D CASE

In the two-dimensional approximation, the bimorph is thin in the y direction (small width), and it can be approximated as a beam. The simplest approximation is to set $T_2 = 0$, and eliminate v as an unknown from the differential equations. This approximation can be made because the bending is only in the $x-z$ plane. There is no shear bending, so T_4 and T_6 are also zero. There would be no reason for an electric field component to develop in the y direction, so D_2 is zero. Since there is no asymmetry in the applied voltage about the $y = 0$ plane, there is no force which would induce the bimorph to twist. The bending is almost entirely in the $x-z$ plane, with a very small symmetric curvature in the $x-y$ plane which can be neglected.

The equations of motion for PVDF are similar to the 3D case, with the y quantities eliminated:

$$\rho \frac{\partial^2 u}{\partial t^2} = \frac{\partial T_1}{\partial x} + \frac{\partial T_5}{\partial z} \tag{6.1}$$

$$\rho \frac{\partial^2 w}{\partial t^2} = \frac{\partial T_5}{\partial x} + \frac{\partial T_3}{\partial z} \tag{6.2}$$

$$\frac{\partial}{\partial t}\left(\frac{\partial D_1}{\partial x} + \frac{\partial D_3}{\partial z}\right) = 0 \tag{6.3}$$

The continuity equation for the electrode, where σ is the electric conductivity and ε is the dielectric constant for the electrode:

$$\frac{\partial}{\partial x}\left(\sigma E_1 + \varepsilon \frac{\partial E_1}{\partial t}\right) + \frac{\partial}{\partial z}\left(\sigma E_3 + \varepsilon \frac{\partial E_3}{\partial t}\right) = 0. \tag{6.4}$$

Just as with the 2D static case, we find the value of S_2 by setting T_2 equal to zero, and then substituting the expression for S_2 into the remaining equations. We get new effective material constants, designated with a "*". The definitions for the two-dimensional

constitutive relations are as follows.

$$T_1 = c_{11}^* \frac{\partial u}{\partial x} + c_{13}^* \frac{\partial w}{\partial z} + e_{31}^* \frac{\partial \phi}{\partial z} \tag{6.5}$$

$$T_3 = c_{13}^* \frac{\partial u}{\partial x} + c_{33}^* \frac{\partial w}{\partial z} + e_{33}^* \frac{\partial \phi}{\partial z} \tag{6.6}$$

$$T_5 = c_{55} \left(\frac{\partial u}{\partial z} + \frac{\partial w}{\partial x} \right) + e_{15} \frac{\partial \phi}{\partial x} \tag{6.7}$$

$$D_1 = e_{15} \left(\frac{\partial u}{\partial z} + \frac{\partial w}{\partial x} \right) - \varepsilon_1 \frac{\partial \phi}{\partial x} \tag{6.8}$$

$$D_3 = e_{31}^* \frac{\partial u}{\partial x} + e_{33}^* \frac{\partial w}{\partial z} - \varepsilon_3^* \frac{\partial \phi}{\partial z} \tag{6.9}$$

In the harmonic analysis, the variables oscillate at the same frequency as the applied voltage.

$$u(\boldsymbol{x}, t) = u_0(\boldsymbol{x}) + \left(\alpha_u(\boldsymbol{x}) + \mathrm{i}\beta_u(\boldsymbol{x}) \right) \mathrm{e}^{\mathrm{i}\omega t} \tag{6.10}$$

$$w(\boldsymbol{x}, t) = w_0(\boldsymbol{x}) + \left(\alpha_w(\boldsymbol{x}) + \mathrm{i}\beta_w(\boldsymbol{x}) \right) \mathrm{e}^{\mathrm{i}\omega t} \tag{6.11}$$

$$\phi(\boldsymbol{x}, t) = \phi_0(\boldsymbol{x}) + \left(\alpha_\phi(\boldsymbol{x}) + \mathrm{i}\beta_\phi(\boldsymbol{x}) \right) \mathrm{e}^{\mathrm{i}\omega t} \tag{6.12}$$

If the applied voltage oscillates around a non-zero values (has a bias), then there will be a non-zero constant part to the solutions. The constant solution is found in the same way as the static problem.

The time-harmonic weak form for a given applied frequency ω is shown here. The integrals are performed only in the appropriate regions, so the integrals for PVDF are only performed over the PVDF sheets, while the continuity condition for the electrodes integral is only performed in the electrodes.

$$\begin{aligned} 0 = \int_\Omega \Bigg[& -\omega^2 \rho \delta\alpha_u \alpha_u + \frac{\partial \delta\alpha_u}{\partial x} \left(c_{11}^* \frac{\partial \alpha_u}{\partial x} + c_{13}^* \frac{\partial \alpha_w}{\partial z} + e_{31}^* \frac{\partial \alpha_\phi}{\partial z} \right) \\ & + \frac{\partial \delta\alpha_u}{\partial z} \left(c_{55} \left(\frac{\partial \alpha_u}{\partial z} + \frac{\partial \alpha_w}{\partial x} \right) + e_{15} \frac{\partial \alpha_\phi}{\partial x} \right) \Bigg] \mathrm{d}\Omega \end{aligned} \tag{6.13}$$

$$0 = \int_\Omega \left[-\omega^2 \rho \delta\beta_u \beta_u + \frac{\partial \delta\beta_u}{\partial x}\left(c_{11}^* \frac{\partial \beta_u}{\partial x} + c_{13}^* \frac{\partial \beta_w}{\partial z} + e_{31}^* \frac{\partial \beta_\phi}{\partial z} \right) + \frac{\partial \delta\beta_u}{\partial z}\left(c_{55}\left(\frac{\partial \beta_u}{\partial z} + \frac{\partial \beta_w}{\partial x} \right) + e_{15} \frac{\partial \beta_\phi}{\partial x} \right) \right] \mathrm{d}\Omega \tag{6.14}$$

$$0 = \int_\Omega \left[-\omega^2 \rho \delta\alpha_w \alpha_w + \frac{\partial \delta\alpha_w}{\partial x}\left(c_{55}\left(\frac{\partial \alpha_u}{\partial z} + \frac{\partial \alpha_w}{\partial x} \right) + e_{15} \frac{\partial \alpha_\phi}{\partial x} \right) + \frac{\partial \delta\alpha_w}{\partial z}\left(c_{13}^* \frac{\partial \alpha_u}{\partial x} + c_{33}^* \frac{\partial \alpha_w}{\partial z} + e_{33}^* \frac{\partial \alpha_\phi}{\partial z} \right) \right] \mathrm{d}\Omega \tag{6.15}$$

$$0 = \int_\Omega \left[-\omega^2 \rho \delta\beta_w \beta_w + \frac{\partial \delta\beta_w}{\partial x}\left(c_{55}\left(\frac{\partial \beta_u}{\partial z} + \frac{\partial \beta_w}{\partial x} \right) + e_{15} \frac{\partial \beta_\phi}{\partial x} \right) + \frac{\partial \delta\beta_w}{\partial z}\left(c_{13}^* \frac{\partial \beta_u}{\partial x} + c_{33}^* \frac{\partial \beta_w}{\partial z} + e_{33}^* \frac{\partial \beta_\phi}{\partial z} \right) \right] \mathrm{d}\Omega \tag{6.16}$$

$$0 = \int_\Omega -\omega \left[\frac{\partial \delta\alpha_\phi}{\partial x}\left(e_{15}\left(\frac{\partial \beta_u}{\partial z} + \frac{\partial \beta_w}{\partial x} \right) - \varepsilon_1 \frac{\partial \beta_\phi}{\partial x} \right) + \frac{\partial \delta\alpha_\phi}{\partial z}\left(e_{31}^* \frac{\partial \beta_u}{\partial x} + e_{33}^* \frac{\partial \beta_w}{\partial z} - \varepsilon_3^* \frac{\partial \beta_\phi}{\partial z} \right) \right] \mathrm{d}\Omega \tag{6.17}$$

$$0 = \int_\Omega \omega \left[\frac{\partial \delta\beta_\phi}{\partial x}\left(e_{15}\left(\frac{\partial \alpha_u}{\partial z} + \frac{\partial \alpha_w}{\partial x} \right) - \varepsilon_1 \frac{\partial \alpha_\phi}{\partial x} \right) + \frac{\partial \delta\beta_\phi}{\partial z}\left(e_{31}^* \frac{\partial \alpha_u}{\partial x} + e_{33}^* \frac{\partial \alpha_w}{\partial z} - \varepsilon_3^* \frac{\partial \alpha_\phi}{\partial z} \right) \right] \mathrm{d}\Omega \tag{6.18}$$

$$0 = \int_\Omega \left[\frac{\partial \delta\alpha_\phi}{\partial x}\left(-\sigma \frac{\partial \alpha_\phi}{\partial x} + \omega\varepsilon \frac{\partial \beta_\phi}{\partial x} \right) + \frac{\partial \delta\alpha_\phi}{\partial z}\left(-\sigma \frac{\partial \alpha_\phi}{\partial z} + \omega\varepsilon \frac{\partial \beta_\phi}{\partial z} \right) \right] \mathrm{d}\Omega \tag{6.19}$$

$$0 = -\int_\Omega \left[\frac{\partial \delta\beta_\phi}{\partial x}\left(\sigma \frac{\partial \beta_\phi}{\partial x} + \omega\varepsilon \frac{\partial \alpha_\phi}{\partial x} \right) + \frac{\partial \delta\beta_\phi}{\partial z}\left(\sigma \frac{\partial \beta_\phi}{\partial z} + \omega\varepsilon \frac{\partial \alpha_\phi}{\partial z} \right) \right] \mathrm{d}\Omega \tag{6.20}$$

If the elasticity constants have an imaginary part, then there will be mechanical damping. We can express each component of the elasticity tensor as having a real and imaginary part, where the real part is c'_{ij}, and the imaginary part is c''_{ij}.

$$c_{ij} = c'_{ij} + \mathrm{i} c''_{ij} \tag{6.21}$$

Now the real and imaginary parts of the solution will be further coupled because of the complex elasticity.

$$0 = \int_\Omega \left[-\omega^2 \rho \delta\alpha_u \alpha_u + \frac{\partial \delta\alpha_u}{\partial x}\left(c_{11}^{*\prime} \frac{\partial \alpha_u}{\partial x} + c_{13}^{*\prime} \frac{\partial \alpha_w}{\partial z} + e_{31}^* \frac{\partial \alpha_\phi}{\partial z} - c_{11}^{*\prime\prime} \frac{\partial \beta_u}{\partial x} - c_{13}^{*\prime\prime} \frac{\partial \beta_w}{\partial z} \right) + \frac{\partial \delta\alpha_u}{\partial z}\left(c'_{55}\left(\frac{\partial \alpha_u}{\partial z} + \frac{\partial \alpha_w}{\partial x} \right) + e_{15} \frac{\partial \alpha_\phi}{\partial x} - c''_{55}\left(\frac{\partial \beta_u}{\partial z} + \frac{\partial \beta_w}{\partial x} \right) \right) \right] \mathrm{d}\Omega \tag{6.22}$$

$$0 = \int_\Omega \left[-\omega^2 \rho \delta\beta_u \beta_u + \frac{\partial \delta\beta_u}{\partial x}\left(c_{11}^{*\prime} \frac{\partial \beta_u}{\partial x} + c_{13}^{*\prime} \frac{\partial \beta_w}{\partial z} + e_{31}^{*} \frac{\partial \beta_\phi}{\partial z} + c_{11}^{*\prime\prime} \frac{\partial \alpha_u}{\partial x} + c_{13}^{*\prime\prime} \frac{\partial \alpha_w}{\partial z} \right) + \frac{\partial \delta\beta_u}{\partial z}\left(c_{55}^{\prime} \left(\frac{\partial \beta_u}{\partial z} + \frac{\partial \beta_w}{\partial x} \right) + e_{15} \frac{\partial \beta_\phi}{\partial x} + c_{55}^{\prime\prime} \left(\frac{\partial \alpha_u}{\partial z} + \frac{\partial \alpha_w}{\partial x} \right) \right) \right] \mathrm{d}\Omega \tag{6.23}$$

$$0 = \int_\Omega \left[-\omega^2 \rho \delta\alpha_w \alpha_w + \frac{\partial \delta\alpha_w}{\partial x}\left(c_{55}^{\prime} \left(\frac{\partial \alpha_u}{\partial z} + \frac{\partial \alpha_w}{\partial x} \right) + e_{15} \frac{\partial \alpha_\phi}{\partial x} - c_{55}^{\prime\prime} \left(\frac{\partial \beta_u}{\partial z} + \frac{\partial \beta_w}{\partial x} \right) \right) + \frac{\partial \delta\alpha_w}{\partial z}\left(c_{13}^{*\prime} \frac{\partial \alpha_u}{\partial x} + c_{33}^{*\prime} \frac{\partial \alpha_w}{\partial z} + e_{33}^{*} \frac{\partial \alpha_\phi}{\partial z} - c_{13}^{*\prime\prime} \frac{\partial \beta_u}{\partial x} - c_{33}^{*\prime\prime} \frac{\partial \beta_w}{\partial z} \right) \right] \mathrm{d}\Omega \tag{6.24}$$

$$0 = \int_\Omega \left[-\omega^2 \rho \delta\beta_w \beta_w + \frac{\partial \delta\beta_w}{\partial x}\left(c_{55}^{\prime} \left(\frac{\partial \beta_u}{\partial z} + \frac{\partial \beta_w}{\partial x} \right) + e_{15} \frac{\partial \beta_\phi}{\partial x} + c_{55}^{\prime\prime} \left(\frac{\partial \alpha_u}{\partial z} + \frac{\partial \alpha_w}{\partial x} \right) \right) + \frac{\partial \delta\beta_w}{\partial z}\left(c_{13}^{*\prime} \frac{\partial \beta_u}{\partial x} + c_{33}^{*\prime} \frac{\partial \beta_w}{\partial z} + e_{33}^{*} \frac{\partial \beta_\phi}{\partial z} + c_{13}^{*\prime\prime} \frac{\partial \alpha_u}{\partial x} + c_{33}^{*\prime\prime} \frac{\partial \alpha_w}{\partial z} \right) \right] \mathrm{d}\Omega \tag{6.25}$$

$$0 = \int_\Omega -\omega \left[\frac{\partial \delta\alpha_\phi}{\partial x}\left(e_{15} \left(\frac{\partial \beta_u}{\partial z} + \frac{\partial \beta_w}{\partial x} \right) - \varepsilon_1 \frac{\partial \beta_\phi}{\partial x} \right) + \frac{\partial \delta\alpha_\phi}{\partial z}\left(e_{31}^{*} \frac{\partial \beta_u}{\partial x} + e_{33}^{*} \frac{\partial \beta_w}{\partial z} - \varepsilon_3^{*} \frac{\partial \beta_\phi}{\partial z} \right) \right] \mathrm{d}\Omega \tag{6.26}$$

$$0 = \int_\Omega \omega \left[\frac{\partial \delta\beta_\phi}{\partial x}\left(e_{15} \left(\frac{\partial \alpha_u}{\partial z} + \frac{\partial \alpha_w}{\partial x} \right) - \varepsilon_1 \frac{\partial \alpha_\phi}{\partial x} \right) + \frac{\partial \delta\beta_\phi}{\partial z}\left(e_{31}^{*} \frac{\partial \alpha_u}{\partial x} + e_{33}^{*} \frac{\partial \alpha_w}{\partial z} - \varepsilon_3^{*} \frac{\partial \alpha_\phi}{\partial z} \right) \right] \mathrm{d}\Omega \tag{6.27}$$

$$0 = \int_\Omega \left[\frac{\partial \delta\alpha_\phi}{\partial x}\left(-\sigma \frac{\partial \alpha_\phi}{\partial x} + \omega\varepsilon \frac{\partial \beta_\phi}{\partial x} \right) + \frac{\partial \delta\alpha_\phi}{\partial z}\left(-\sigma \frac{\partial \alpha_\phi}{\partial z} + \omega\varepsilon \frac{\partial \beta_\phi}{\partial z} \right) \right] \mathrm{d}\Omega \tag{6.28}$$

$$0 = -\int_\Omega \left[\frac{\partial \delta\beta_\phi}{\partial x}\left(\sigma \frac{\partial \beta_\phi}{\partial x} + \omega\varepsilon \frac{\partial \alpha_\phi}{\partial x} \right) + \frac{\partial \delta\beta_\phi}{\partial z}\left(\sigma \frac{\partial \beta_\phi}{\partial z} + \omega\varepsilon \frac{\partial \alpha_\phi}{\partial z} \right) \right] \mathrm{d}\Omega \tag{6.29}$$

The behavior of interest in solving the bimorph problem is how the bimorph responds to a given input voltage. When the desired effect is to have the greatest tip deflection, then we want to know what the deformations are, and what are the phase lags. It is usually not desirable to have the tip of the bimorph bending out of phase with the input voltage, although there may be some applications. There is some work being done in creating piezoelectric fins for underwater devices that can swim through the water in a similar manner to fish [18].

After we have solved for the cosine and sine components of the mechanical displacements and the electric potential, we can determine the amplitude and phase of

the solutions. First, instead of representing a solution as a cosine plus a sine solution, we can instead represent it as an amplitude and phase. The formula below shows how we can convert the solution into this form.

$$\begin{aligned}\phi &= \alpha\cos\omega t - \beta\sin\omega t = A\sin(\omega t+\delta)\\ &= A\sin\delta\cos\omega t + A\cos\delta\sin\omega t\end{aligned} \tag{6.30}$$

From here we see that

$$A\sin\delta = \alpha, \tag{6.31}$$

and

$$A\cos\delta = -\beta. \tag{6.32}$$

The phase can be found by taking any of the trigonometric inverses.

$$\delta = \sin^{-1}(\alpha/A) = \cos^{-1}\left(-\beta/A\right) = \tan^{-1}\left(-\alpha/\beta\right) \tag{6.33}$$

The problem was solved for a bimorph with length $L = 2.5$ cm, and an applied voltage of $V_0 = 600$ V. The voltage was applied symmetrically, so -300 V was applied to the bottom electrode, and 300 V was applied to the top electrode. The piezoelectric sheets each have a thickness of $h = 3\times10^{-5}$ m, which is a typical value available for commercial PVDF. The density of the PVDF is $\rho = 1.78\times10^{3}$ kg/m^3. Various values of electric conductivity were used so the effects of conductivity could be seen. For the results shown below, high conductivity refers to a conductivity $\sigma = 1$ S/m. Medium conductivity is 0.004 S/m, low conductivity is 0.001 S/m, and very low conductivity is 0.0001 S/m. The medium conductivity value was chosen because it resulted in a phase lag of approximately 45 degrees.

At high conductivity ($\sigma = 1$ S/m), the results are very nearly the same as with a uniform applied voltage, where the voltage is applied over the entire electrode. In these

cases where we are trying to find the electrical response of the electrodes themselves, the applied voltage is only applied along the small edge of the electrode at $x = 0$. Each electrode is given a height of $h_e = 1 \times 10^{-5}$ m. Since only the electric response of the electrode is being modeled, and not the mechanical response, the height doesn't matter much. Because of the way the voltage is applied (along the left edge), the current in the electrode will flow back and forth in the x direction, and have no detectable variation in the z direction. Practically speaking, then, the current is a function of x only. For the finite element formulation, the piezoelectric part of the bimorph was broken into 25×12 elements, which means there are 25 divisions along the x direction, and 12 divisions along the z direction. The electrodes each have 2 divisions in the z direction, and the same number of divisions in the x direction as the PVDF. Each element is quadratic, so each rectangle contains a total of 9 nodes (3×3). In this section, only the conductivity was varied, and all the results are for an angular frequency of $\omega = 50$ rad/s, which is well below the first resonance frequency of 116 rad/s.

Figures 6.1 to 6.16 show the results for the electric potential ϕ. The first four plots (figures 6.1 to 6.4) show the sine components of the potential. Since the applied voltage has a sine component only, the cosine components of the solutions will be zero for infinite conductivity and will increase in amplitude while the sine components decrease as the conductivity decreases. This will result in a phase lag. For high conductivity, the sine component looks just like the static solution, where the potential is uniform throughout each electrode. The only difference would be a greater contribution from the direct piezoelectric effect because of the increased deformation due to inertia. As the conductivity decreases, the amplitude decreases more and more dramatically at the end of the bimorph ($x = L$), until the amplitude is zero, and there is no potential difference across

the bimorph at the end. The plotting scale is equal in these four plots, since for any conductivity, the voltage at $x = 0$ will always be ± 300 V.

The second set of plots (figures 6.5 to 6.8) show the cosine components of the potential. Because of the boundary condition at $x = 0$ where the voltage is specified, the cosine component will always be zero at $x = 0$, and the sine component will alway be equal to ± 300 V. The cosine solutions are anti-symmetric about $z = 0$. As the conductivity decreases from high conductivity to very low conductivity, the cosine component starts out having a maximum value which is very small. For infinite conductivity, the value would be zero. At medium conductivity, the cosine component is quite large, reaching over half the value of the applied voltage. Then as the conductivity decreases further, the maximum value for the cosine component begins to decrease because of the amplitude loss due to the resistivity. Although the cosine component is comparable to the sine component near the end of the bimorph, both values are very small. The wave-like nature of the potential begins to become apparent in figures 6.7 and 6.8, with the wavelength of the attenuated wave decreasing with decreasing conductivity.

Figures 6.9 to 6.12 show the total amplitude of the potential, which decreases to nearly zero at low conductivity. Here the lossy nature of the electrodes is evident. The slope of the potential (the x derivative) is always zero at $x = L$ in the electrode, since the boundary condition is that the current is zero at the end.

Figures 6.13 to 6.16 show the phase lag. It ever increases with decreasing conductivity. The phase lag at $x = 0$ is always zero, since the voltage there is equal to the input voltage.

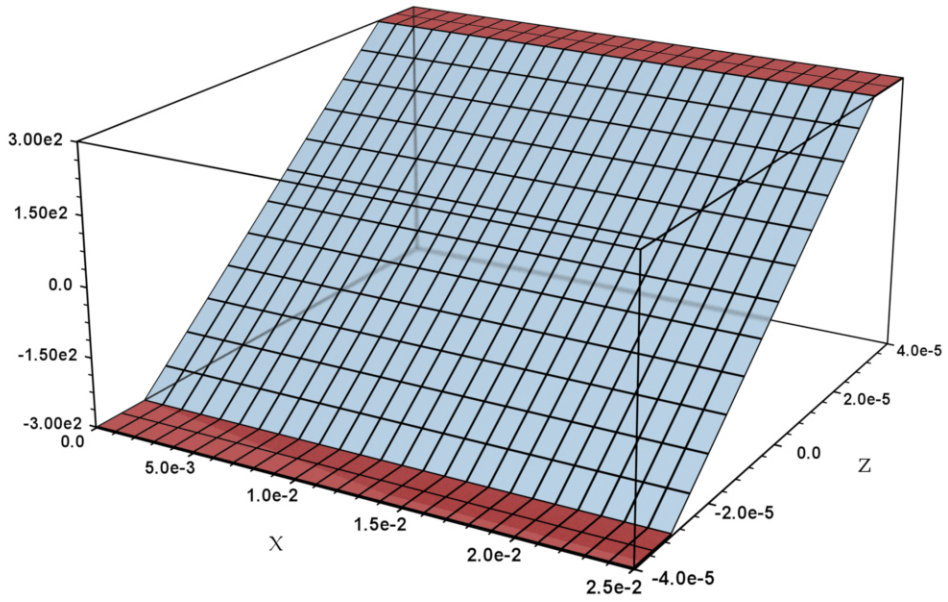

Figure 6.1: The sine component, $-\beta_\phi(x,z)$. High conductivity.

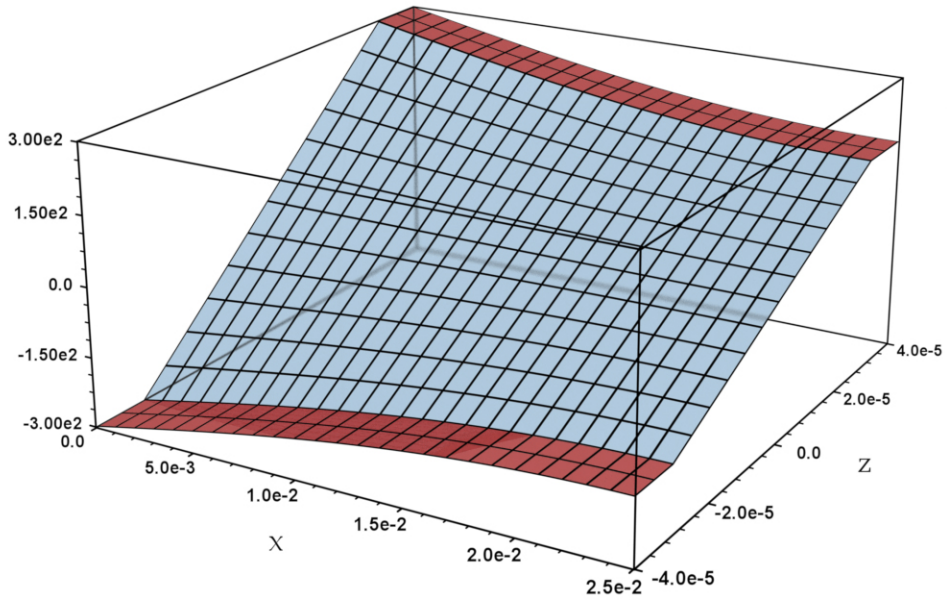

Figure 6.2: The sine component, $-\beta_\phi(x,z)$. Medium conductivity.

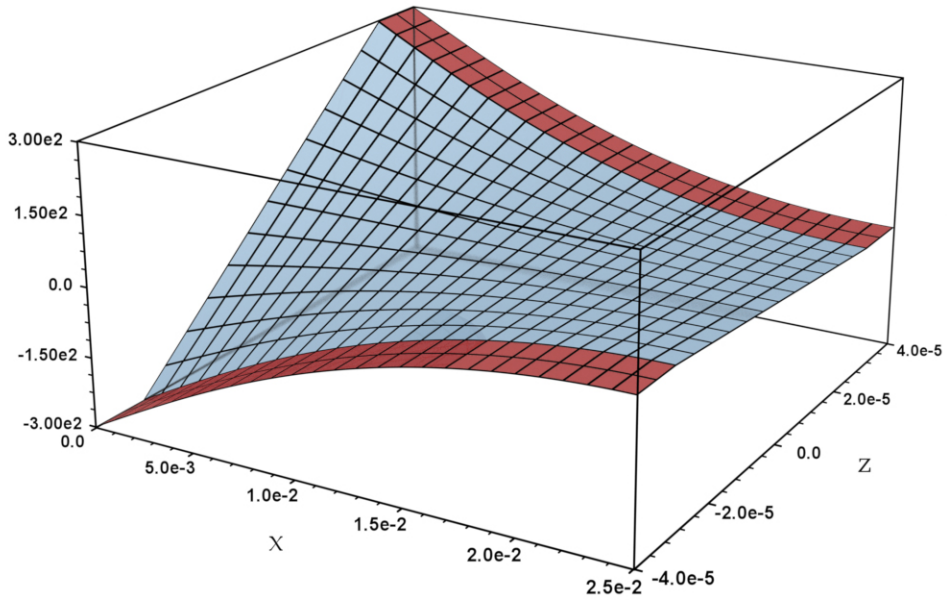

Figure 6.3: The sine component, $-\beta_\phi(x,z)$. Low conductivity.

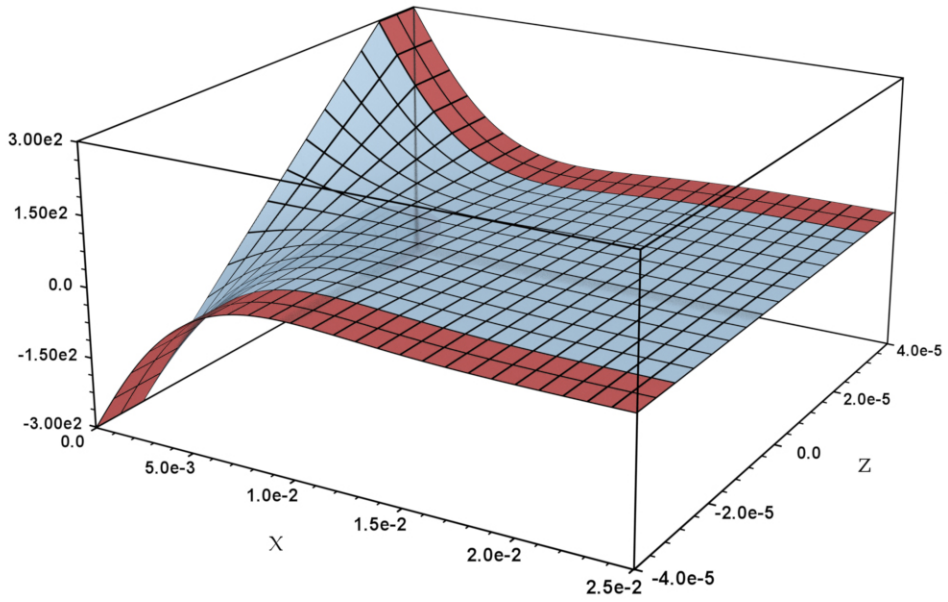

Figure 6.4: The sine component, $-\beta_\phi(x,z)$. Very low conductivity.

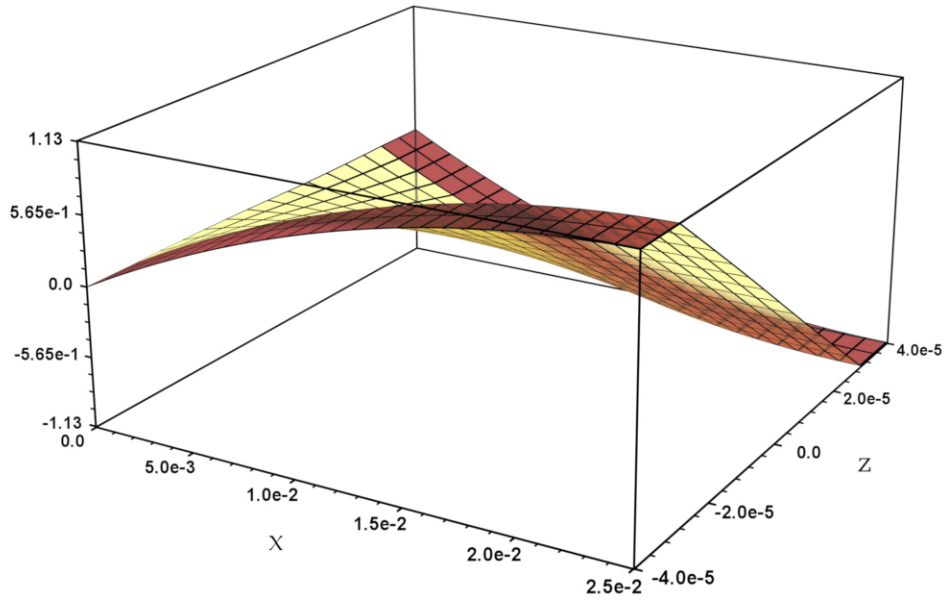

Figure 6.5: The cosine component, $\alpha_\phi(x,z)$. High conductivity.

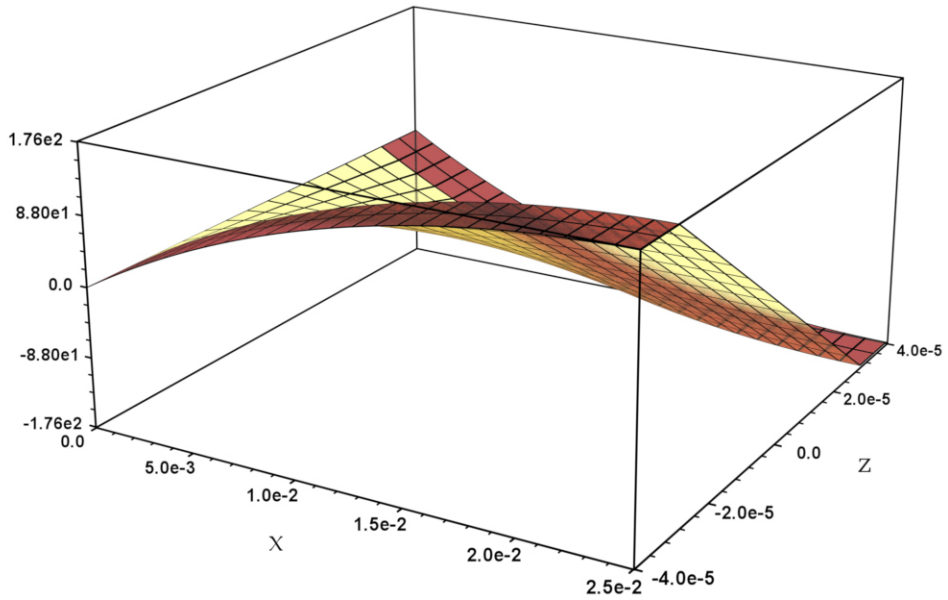

Figure 6.6: The cosine component, $\alpha_\phi(x,z)$. Medium conductivity.

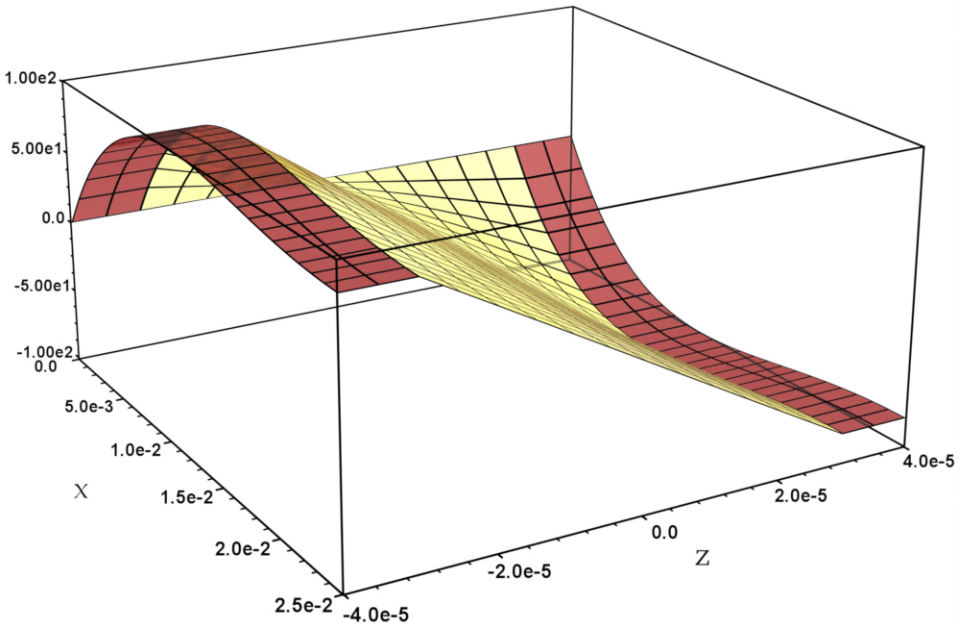

Figure 6.7: The cosine component, $\alpha_\phi(x,z)$. Low conductivity.

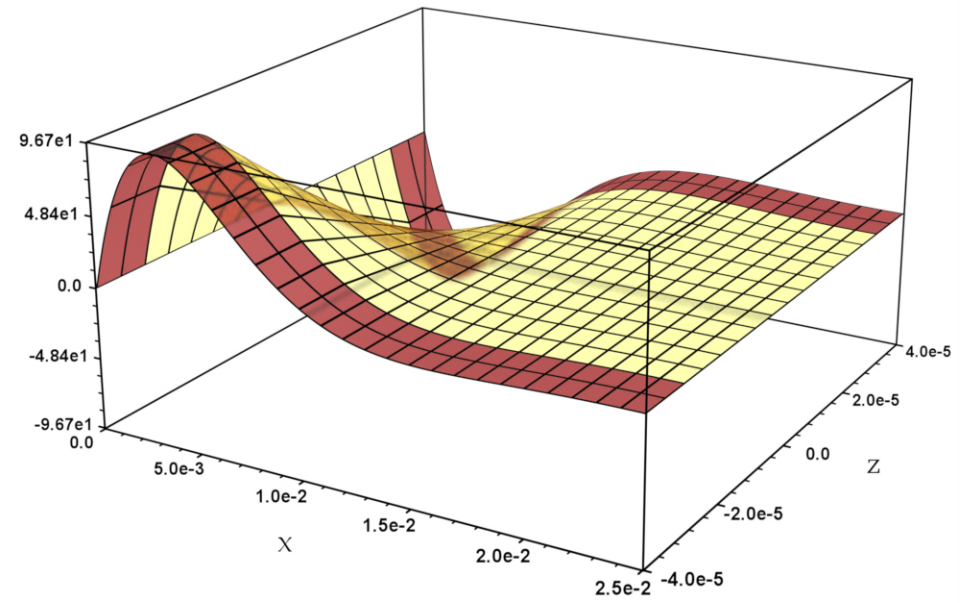

Figure 6.8: The cosine component, $\alpha_\phi(x,z)$. Very low conductivity.

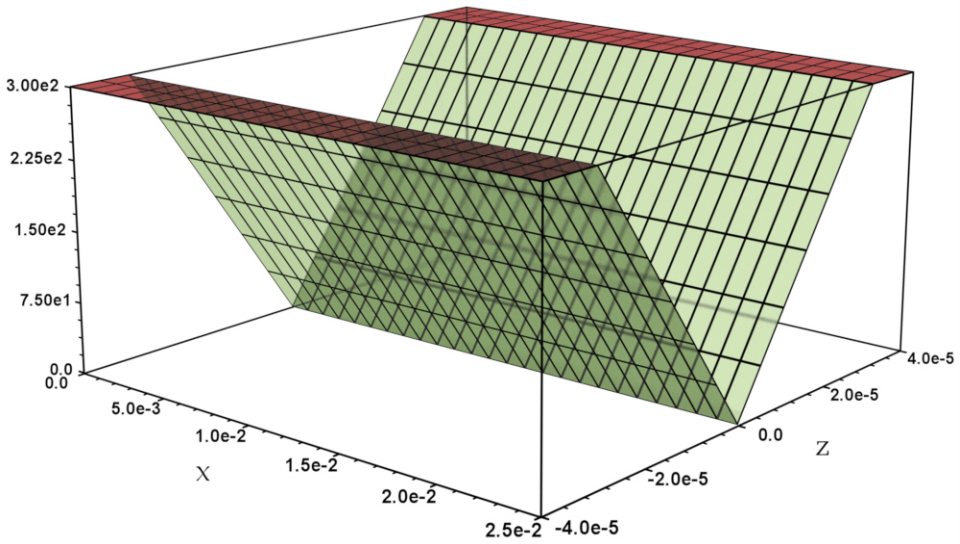

Figure 6.9: The amplitude, $\sqrt{\alpha_\phi^2 + \beta_\phi^2}$. High conductivity.

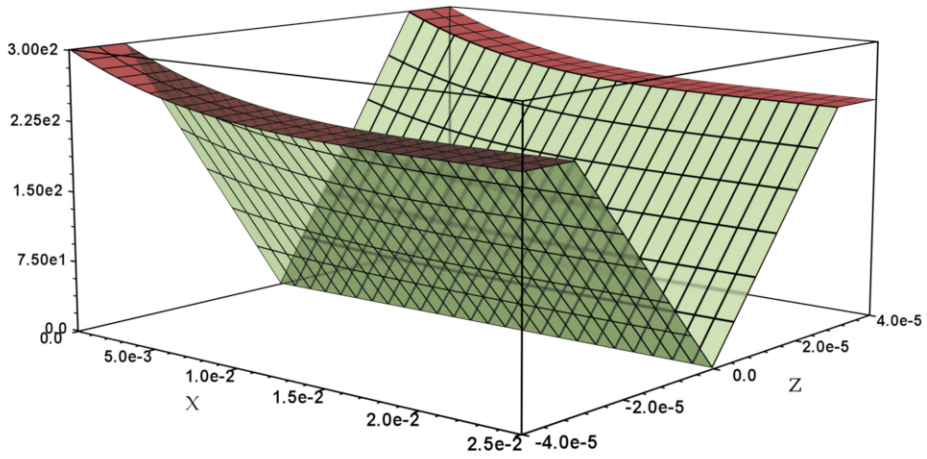

Figure 6.10: The amplitude, $\sqrt{\alpha_\phi^2 + \beta_\phi^2}$. Medium conductivity.

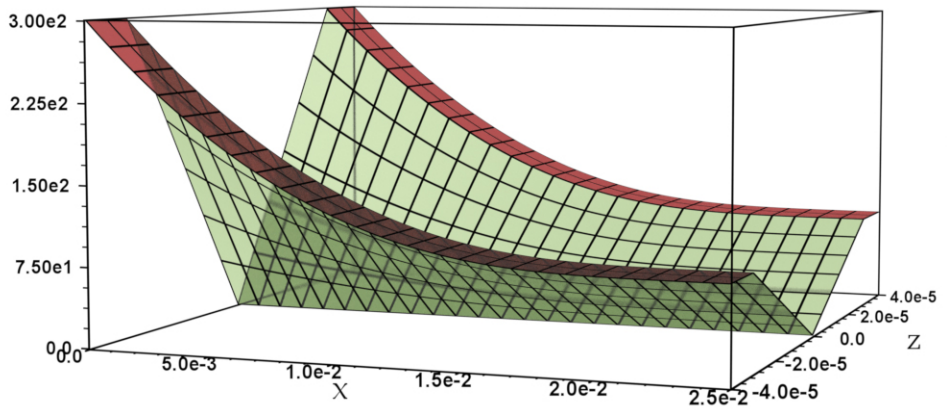

Figure 6.11: The amplitude, $\sqrt{\alpha_\phi^2 + \beta_\phi^2}$. Low conductivity.

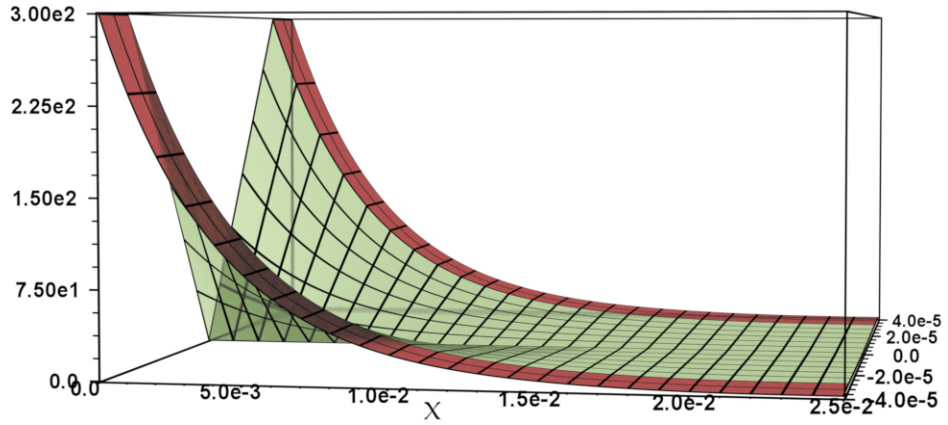

Figure 6.12: The amplitude, $\sqrt{\alpha_\phi^2 + \beta_\phi^2}$. Very low conductivity.

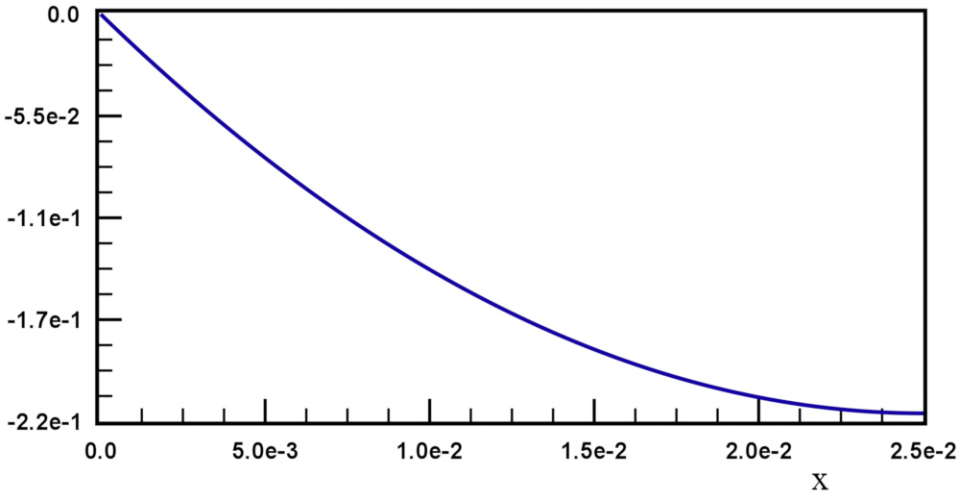

Figure 6.13: Phase, δ, in degrees. High conductivity.

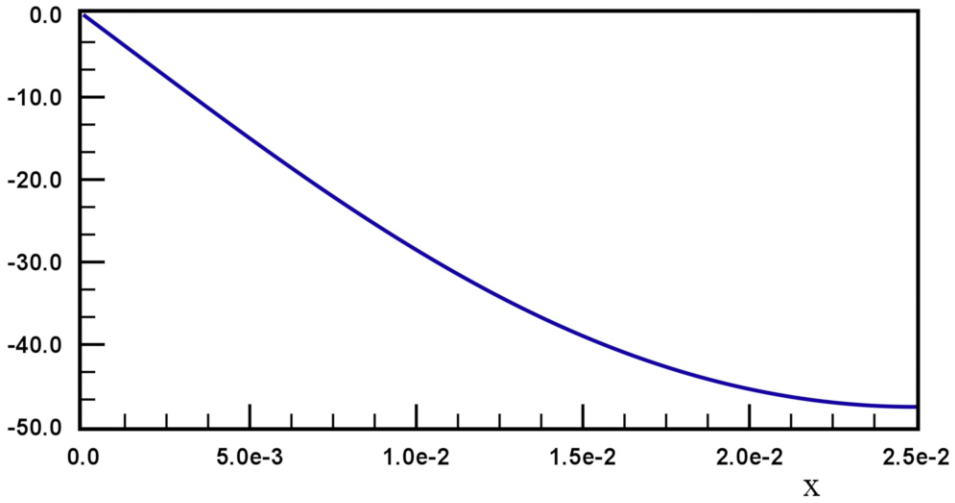

Figure 6.14: Phase, δ, in degrees. Medium conductivity.

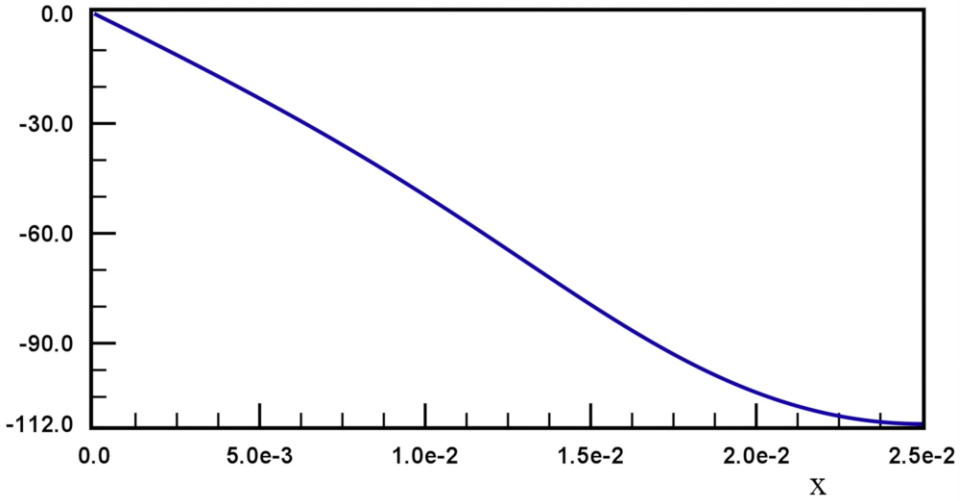

Figure 6.15: Phase, δ, in degrees. Low conductivity.

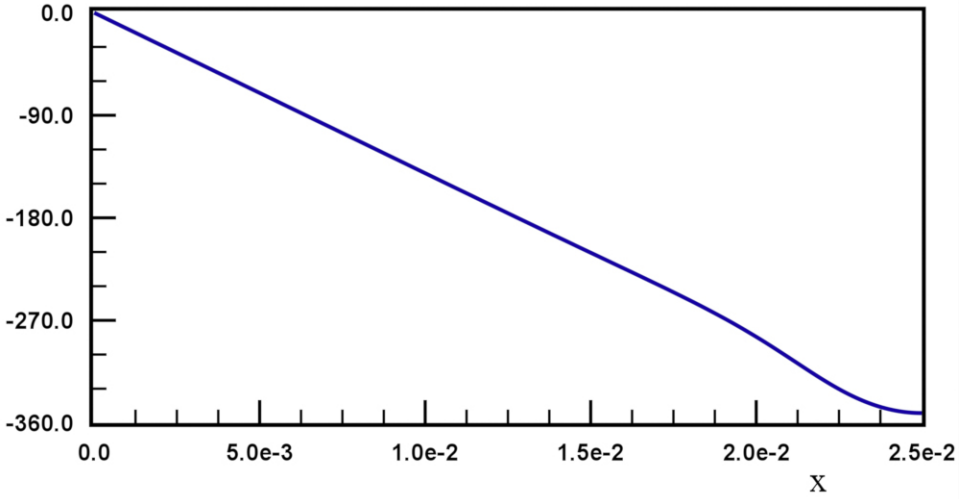

Figure 6.16: Phase, δ, in degrees. Very low conductivity.

Figures 6.17 to 6.28 show the results for w. The mechanical displacements will be affected by inertia. As the frequency of the applied voltage begins to increase from zero, inertia will cause the bimorph to bend more and more. The frequency at which the bending amplitude maximizes is called the resonance frequency. After the amplitude peaks, it will decrease to a minimum near zero, and then begin to increase again until it has a local maximum at the next resonance frequency. There is an infinite number of resonance frequencies. When the electrode conductivity is finite, the electric field across the bimorph will decrease with increasing frequency. There are two effects which are at odds. The inertia increases the amplitude, while the electric field strength loss decreases the amplitude.

For high conductivity, the sine components of the solutions will look almost identical to the static solution. The cosine components will be close to zero for high conductivity, but as the conductivity decreases, they will become comparable in amplitude to the sine components, or even surpass them. The greater the amplitude of the cosine component relative to the sine component, the greater the phase lag. As the conductivity is decreased, the curvature near the middle and end of the bimorph will become more flat, until it has zero curvature. At very low conductivity all the bending will be from a short region near $x = 0$, where the electric field is highest. As the conductivity begins to decrease, the cosine component will increase, until the conductivity becomes too small and the overall bending of the bimorph is greatly decreased.

Figures 6.29 to 6.40 show the results for u, which behaves similarly to w for varying conductivity. As the conductivity is decreased, the stretch and compression start out being distributed almost uniformly along x, but end up taking place at small x where the electric field is greatest. The amplitude of u is shown in figures 6.37 to 6.40. The crease with zero amplitude at $z = 0$ results from u being zero along $z = 0$.

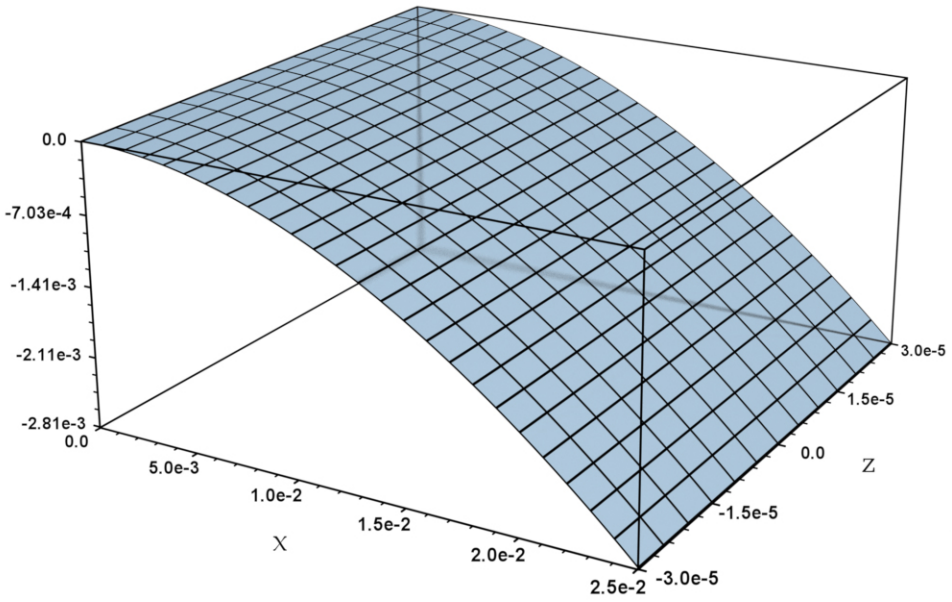

Figure 6.17: The sine component, $-\beta_w(x,z)$. High conductivity.

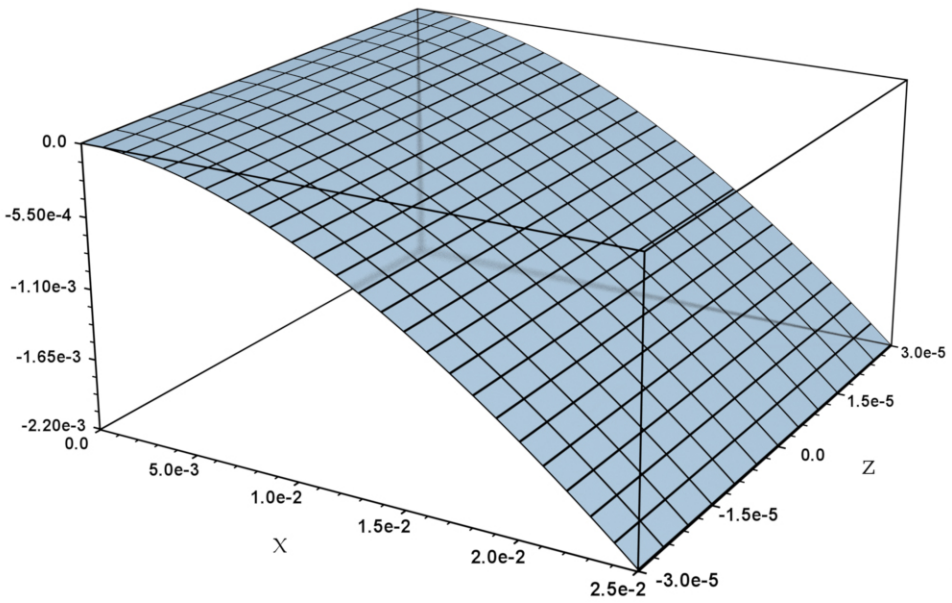

Figure 6.18: The sine component, $-\beta_w(x,z)$. Medium conductivity.

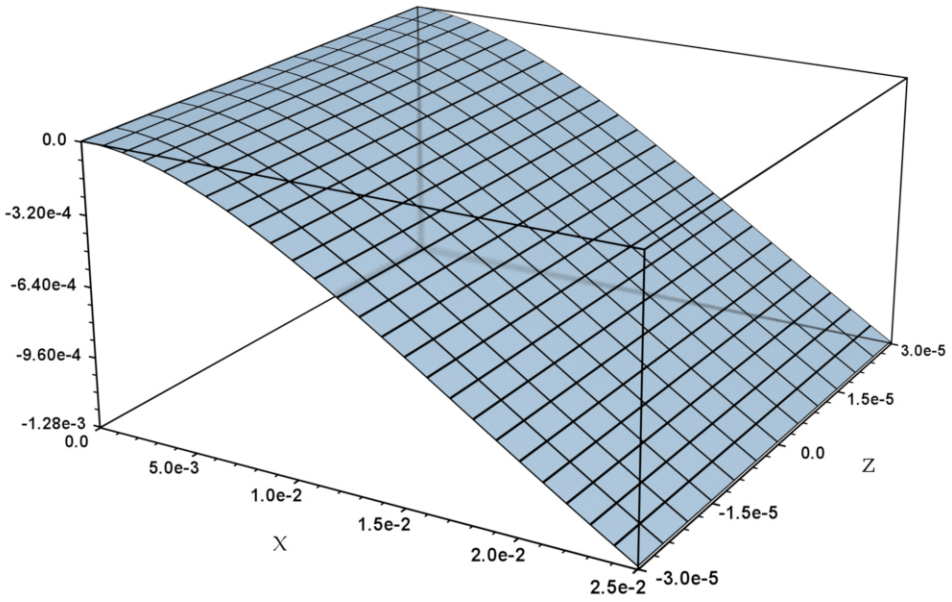

Figure 6.19: The sine component, $-\beta_w(x,z)$. Low conductivity.

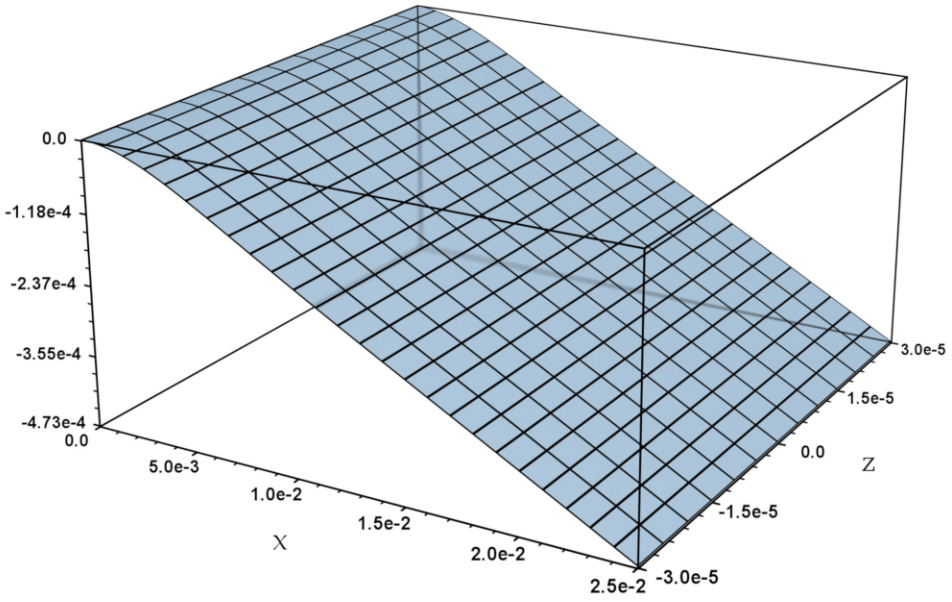

Figure 6.20: The sine component, $-\beta_w(x,z)$. Very low conductivity.

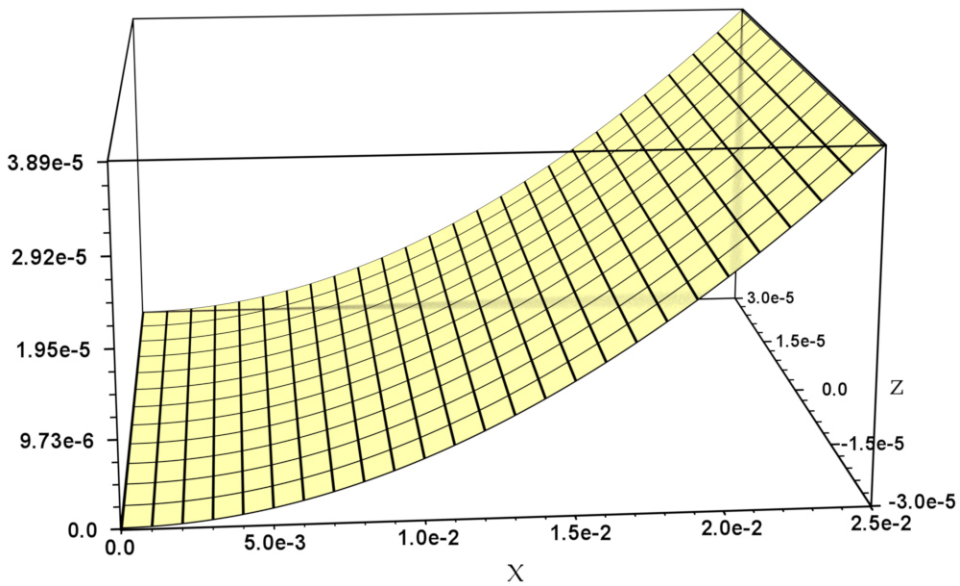

Figure 6.21: The cosine component, $\alpha_w(x,z)$. High conductivity.

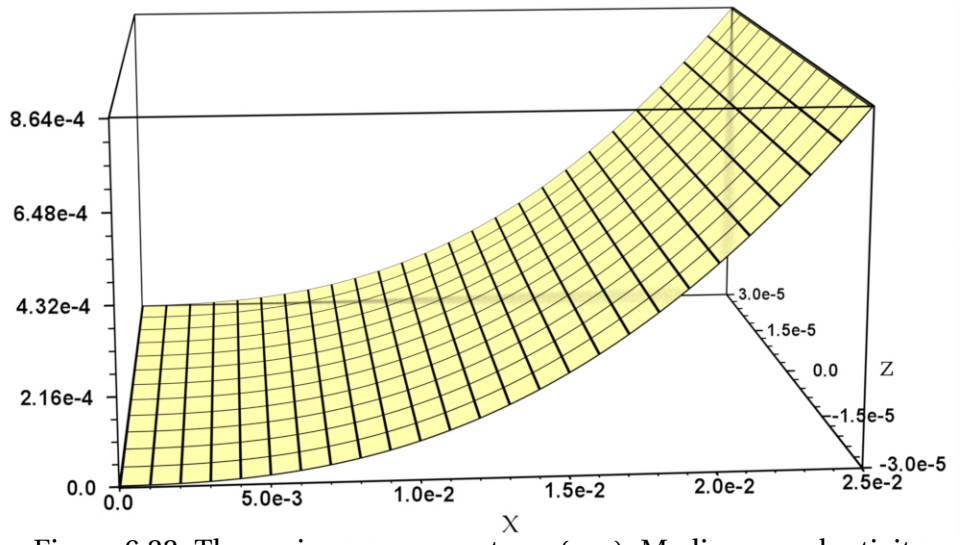

Figure 6.22: The cosine component, $\alpha_w(x,z)$. Medium conductivity.

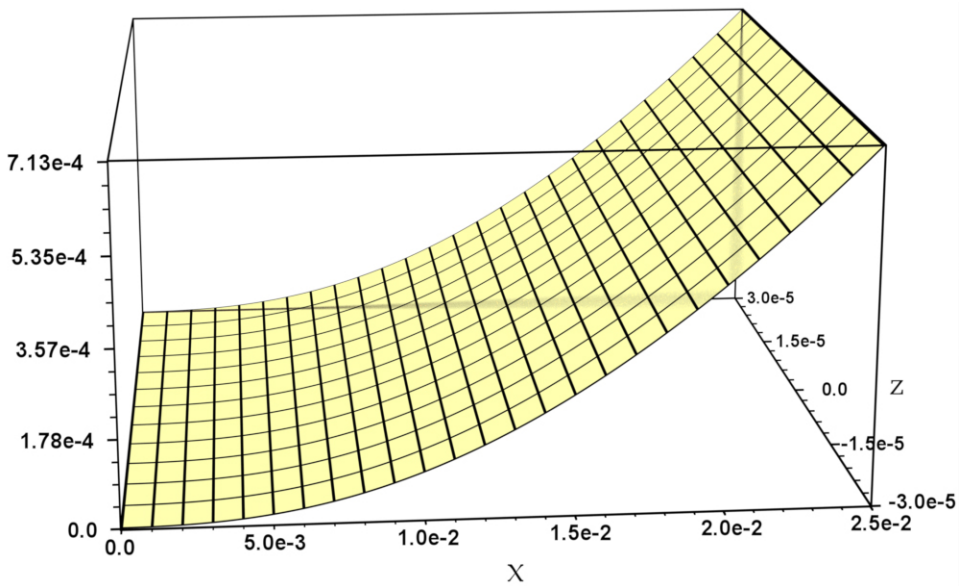

Figure 6.23: The cosine component, $\alpha_w(x,z)$. Low conductivity.

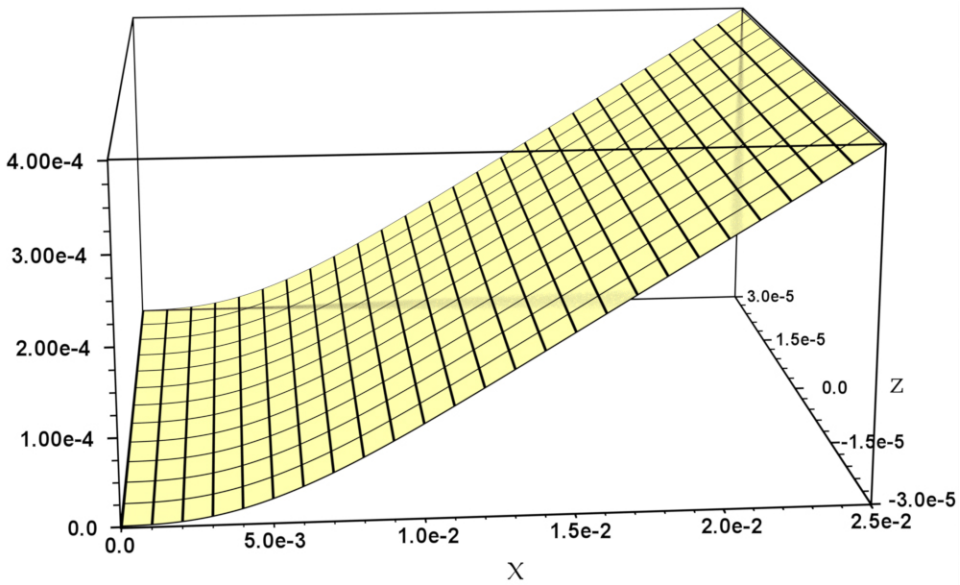

Figure 6.24: The cosine component, $\alpha_w(x,z)$. Very low conductivity.

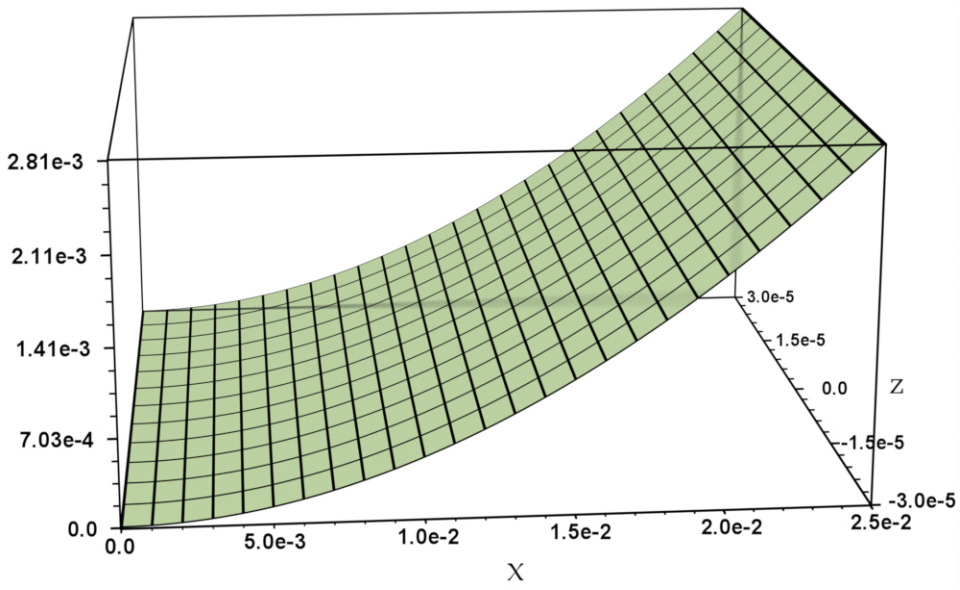

Figure 6.25: The amplitude, $\sqrt{\alpha_w^2 + \beta_w^2}$. High conductivity.

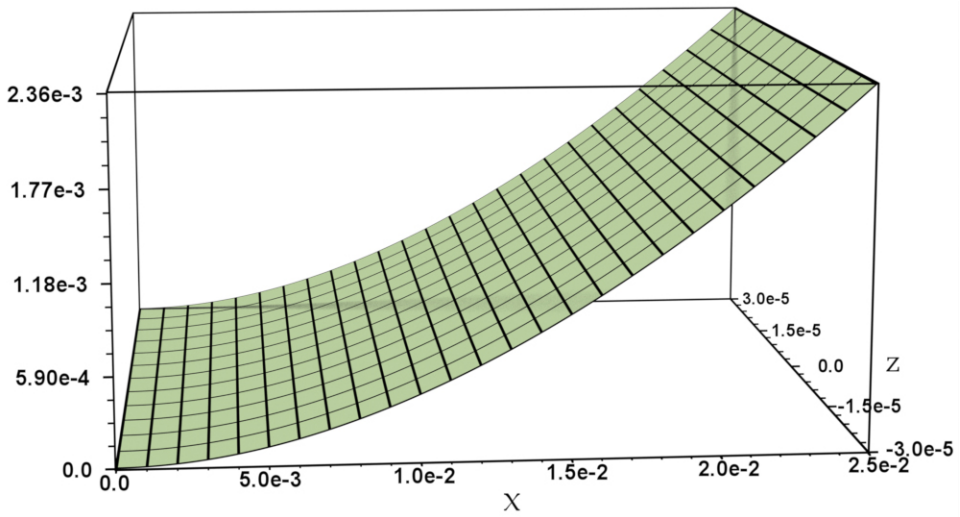

Figure 6.26: The amplitude, $\sqrt{\alpha_w^2 + \beta_w^2}$. Medium conductivity.

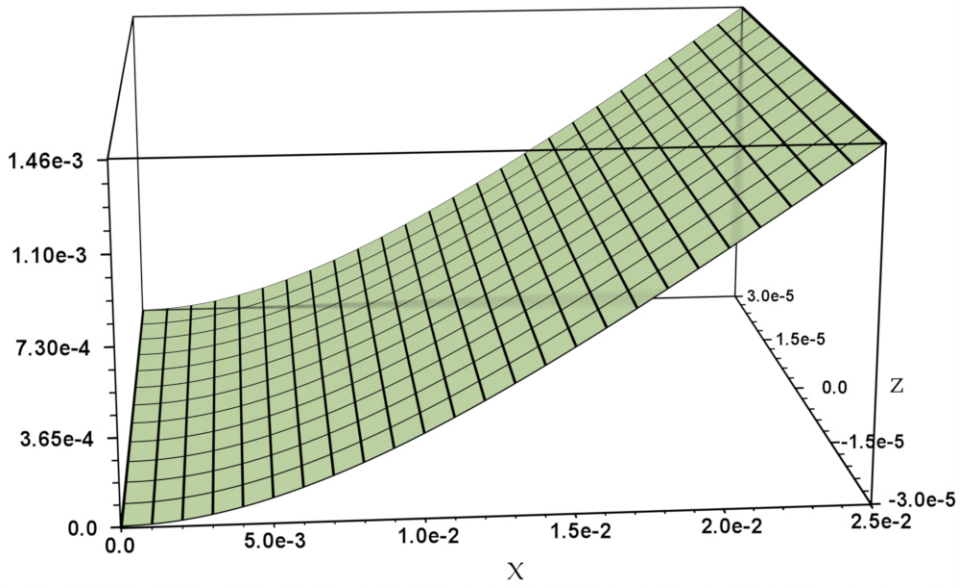

Figure 6.27: The amplitude, $\sqrt{\alpha_w^2 + \beta_w^2}$. Low conductivity.

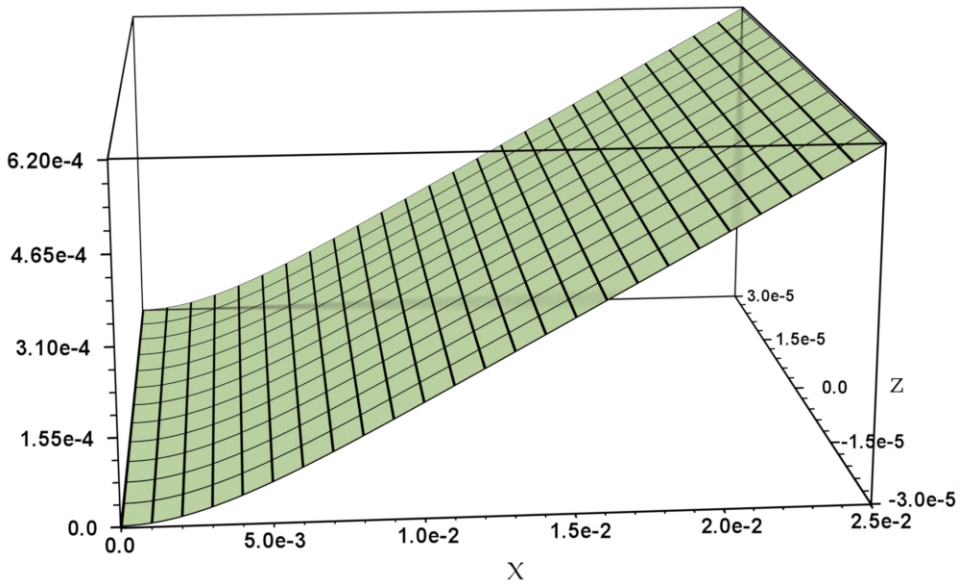

Figure 6.28: The amplitude, $\sqrt{\alpha_w^2 + \beta_w^2}$. Very low conductivity.

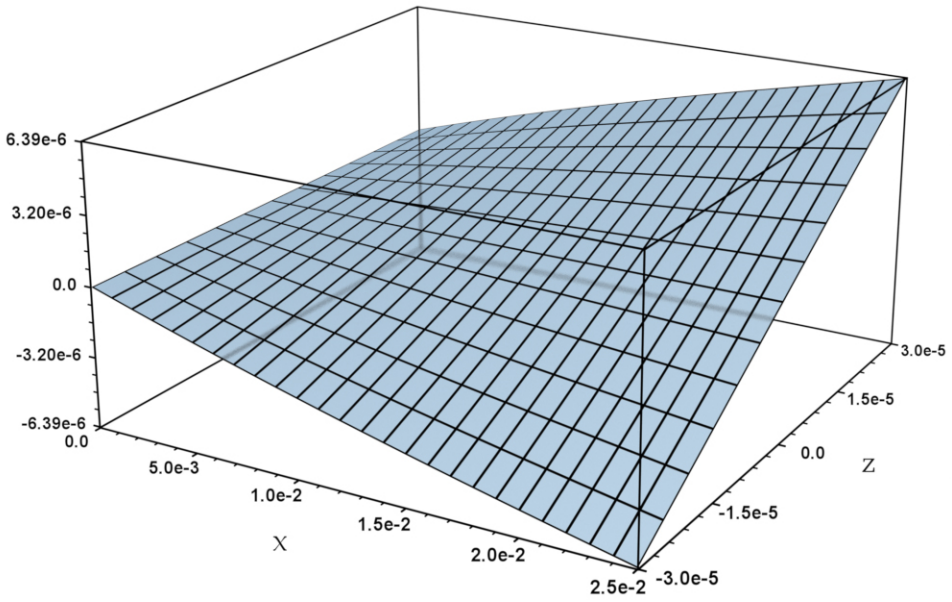

Figure 6.29: The sine component, $-\beta_u(x,z)$. High conductivity.

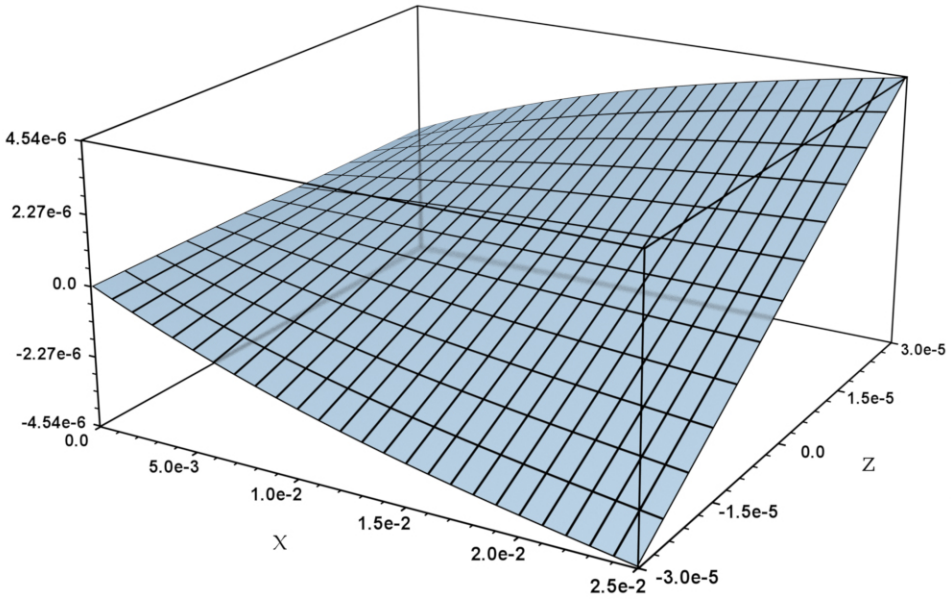

Figure 6.30: The sine component, $-\beta_u(x,z)$. Medium conductivity.

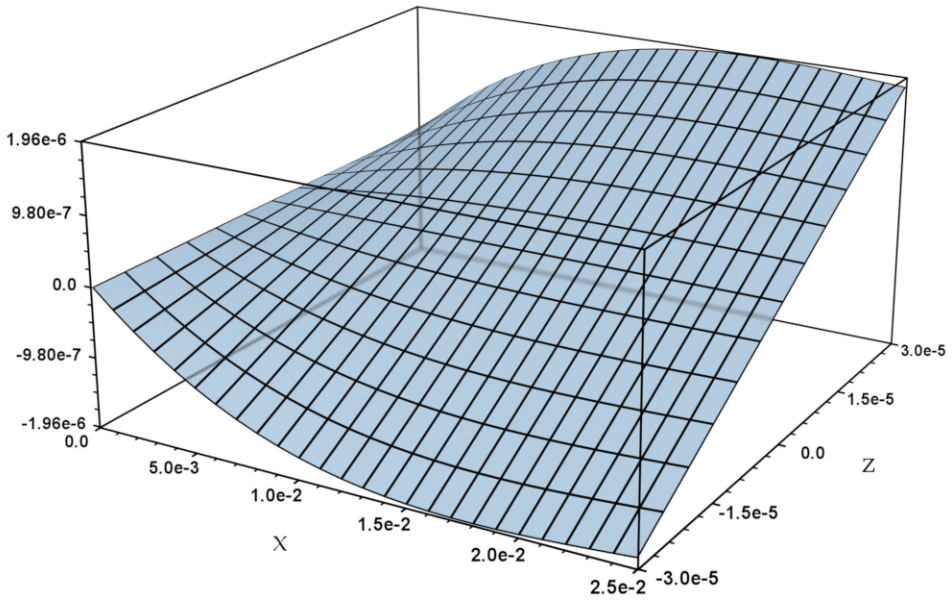

Figure 6.31: The sine component, $-\beta_u(x,z)$. Low conductivity.

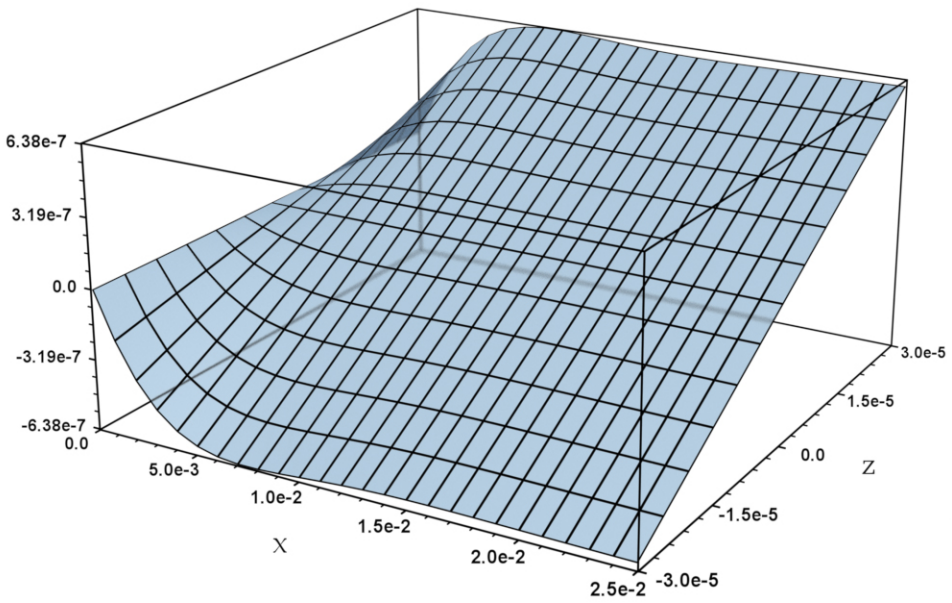

Figure 6.32: The sine component, $-\beta_u(x,z)$. Very low conductivity.

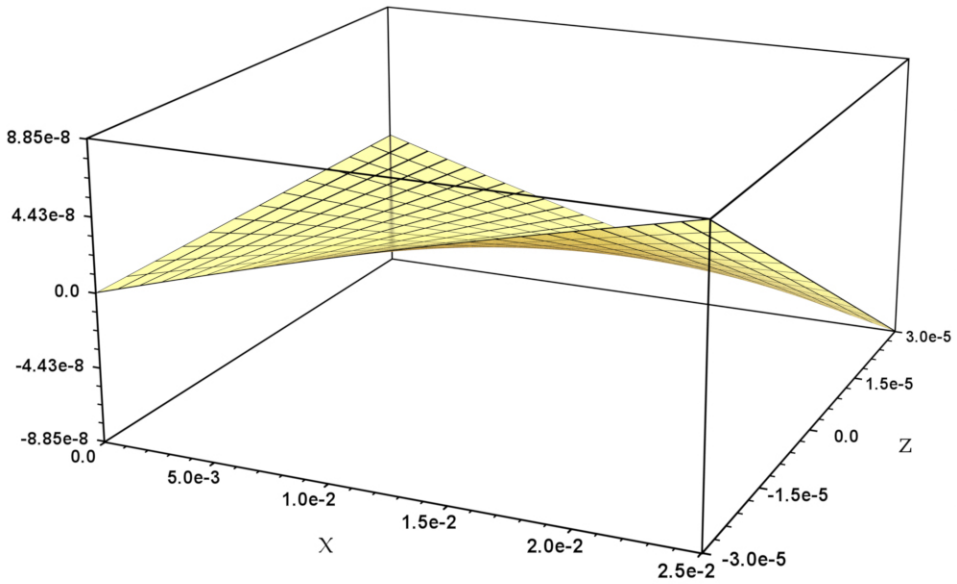

Figure 6.33: The cosine component, $\alpha_u(x,z)$. High conductivity.

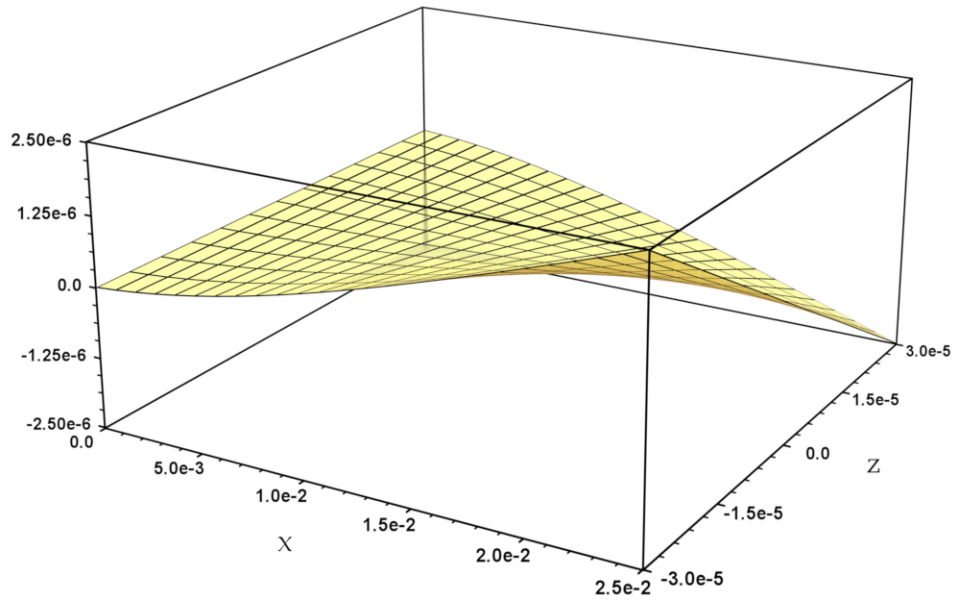

Figure 6.34: The cosine component, $\alpha_u(x,z)$. Medium conductivity.

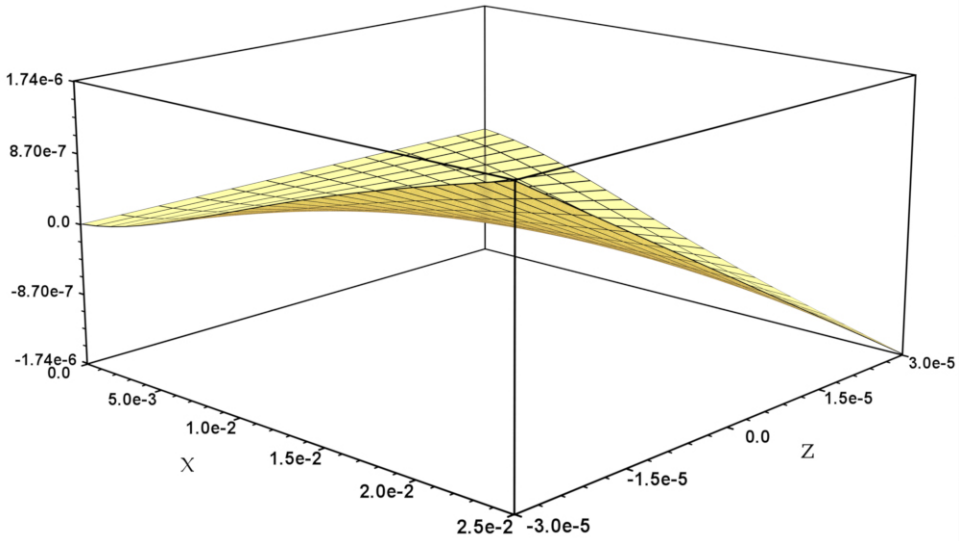

Figure 6.35: The cosine component, $\alpha_u(x,z)$. Low conductivity.

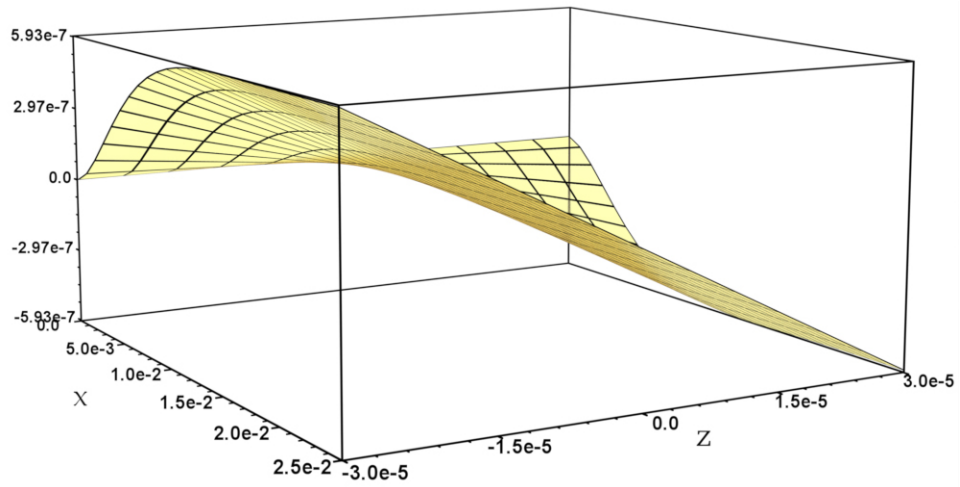

Figure 6.36: The cosine component, $\alpha_u(x,z)$. Very low conductivity.

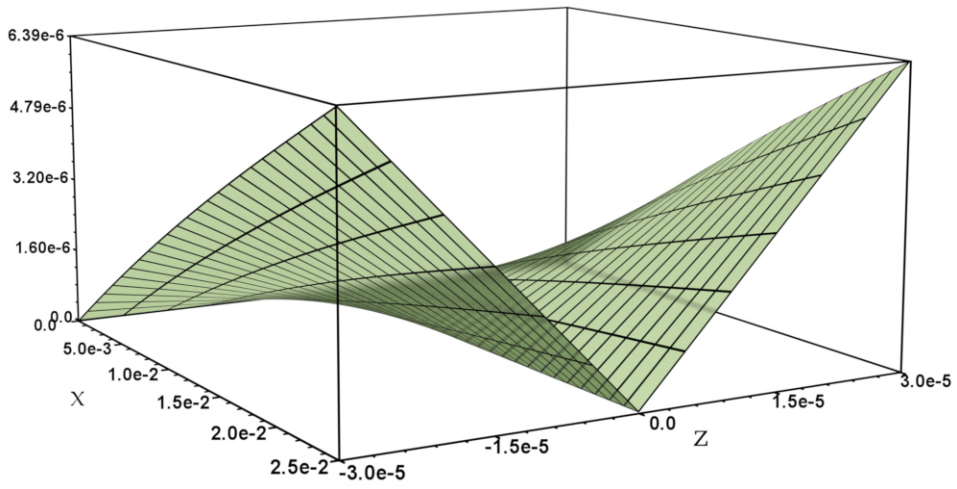

Figure 6.37: The amplitude, $\sqrt{\alpha_u^2 + \beta_u^2}$. High conductivity.

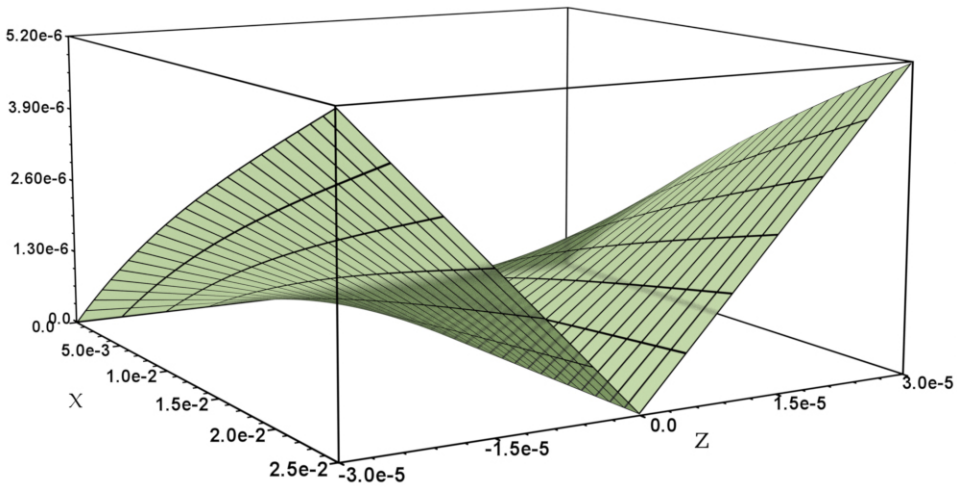

Figure 6.38: The amplitude, $\sqrt{\alpha_u^2 + \beta_u^2}$. Medium conductivity.

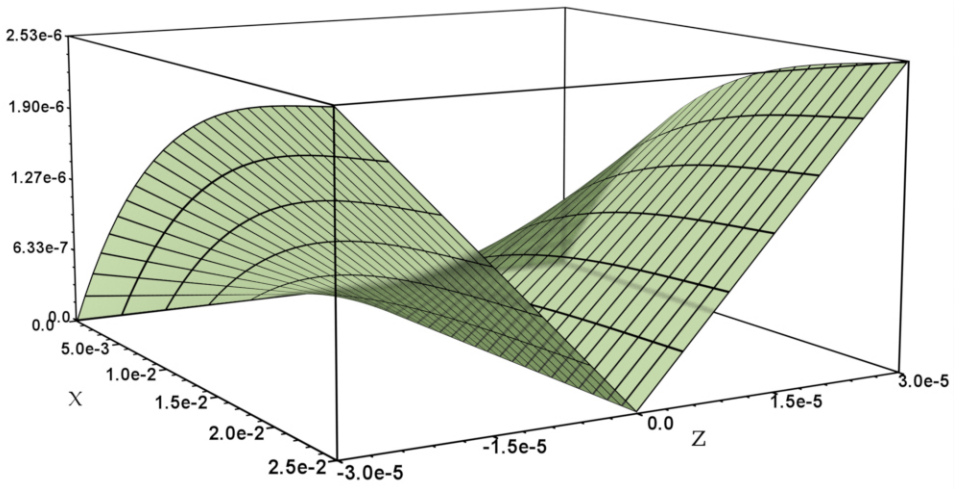

Figure 6.39: The amplitude, $\sqrt{\alpha_u^2 + \beta_u^2}$. Low conductivity.

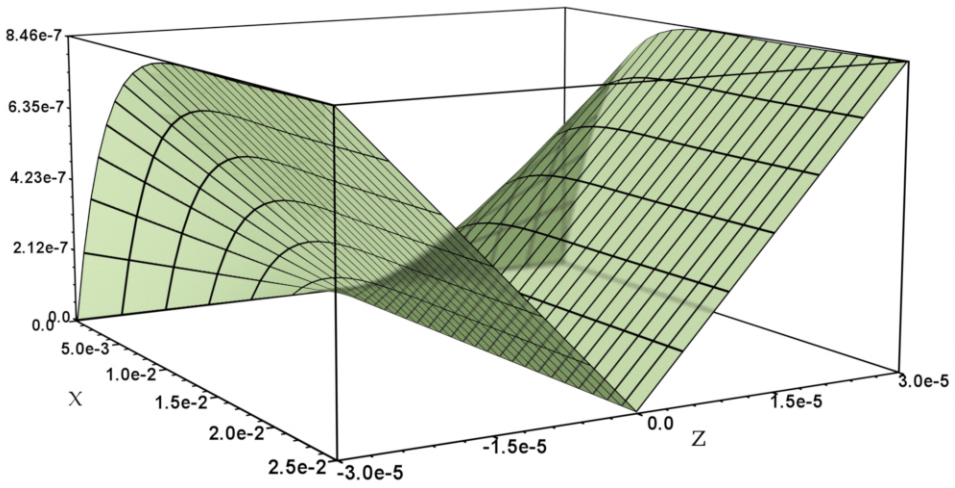

Figure 6.40: The amplitude, $\sqrt{\alpha_u^2 + \beta_u^2}$. Very low conductivity.

Resonance Frequencies

In the classical Bernoulli-Euler beam theory, the differential equation which governs the z-deflection w is [15]

$$\frac{\partial^2}{\partial x^2}\left[EI\frac{\partial^2 w}{\partial x^2}\right]+\rho A\frac{\partial^2 w}{\partial t^2}=0, \tag{6.34}$$

where E is the modulus of elasticity, I is the cross-sectional moment of inertia about the neutral ($z=0$) axis, A is the cross-sectional area, and ρ is the mass volume density.

The moment of inertia is

$$I=\int_{-h}^{h}\int_{y} z^2\,\mathrm{d}y\,\mathrm{d}z=\frac{2bh^3}{3}, \tag{6.35}$$

where b is the width of the bimorph, and h is the half-height $H/2$. The cross-sectional area is the width times the height, so $A=2bh$. The modulus of elasticity is

$$E=1/s_{11}, \tag{6.36}$$

which is the coefficient of S_1 in the stress-strain relation given in chapter 4.

$$T_1=(1/s_{11})\,S_1-(d_{31}/s_{11})\,E_3. \tag{6.37}$$

The assumption with the given form of the differential equation is that the resting shape of the beam is straight with no deflection. In the piezoelectric case, with an applied electric field, the equilibrium shape, as was derived earlier in the Analytical Solutions section of chapter 4, is given by the expression

$$w_{\mathrm{eq}}(x)=\frac{3d_{31}E_3}{4h}x^2. \tag{6.38}$$

Since the equilibrium deflection is not zero, the differential equation is modified so that w is substituted with the change in w from the equilibrium.

$$\frac{\partial^2}{\partial x^2}\left(w-w_{\mathrm{eq}}\right)=\frac{\partial^2}{\partial x^2}\left(w-\frac{3d_{31}E_3}{4h}x^2\right)=\frac{\partial^2 w}{\partial x^2}-\frac{3d_{31}E_3}{2h} \tag{6.39}$$

The differential equation now reads

$$\frac{\partial^2}{\partial x^2}\left[EI\left(\frac{\partial^2 w}{\partial x^2}-\frac{3d_{31}E_3}{2h}\right)\right]+\rho A\frac{\partial^2 w}{\partial t^2}=0. \tag{6.40}$$

When a uniform electric field is applied, the x derivative of E_3 is zero, and so we get back the original differential equation. There would only be a difference if $E_3 = E_3(x)$. Since the bimorph has a cross-sectional area which is constant, and the elasticity is also constant, the EI coefficient can be moved to the outside of the derivative. We now have a final form of the governing differential equation.

$$EI\frac{\partial^4 w}{\partial x^4}+\rho A\frac{\partial^2 w}{\partial t^2}=0. \tag{6.41}$$

In the harmonic case, when the electric field is changing sinusoidally, we have

$$w(x,t)=w(x)\mathrm{e}^{\mathrm{i}\omega t}, \tag{6.42}$$

and so the differential equation becomes

$$EI\frac{\partial^4 w}{\partial x^4}-\rho A\omega^2 w=0. \tag{6.43}$$

This can be written more compactly as

$$\frac{\partial^4 w}{\partial x^4}=k^4 w, \tag{6.44}$$

where

$$k^4=\frac{\rho A}{EI}\omega^2=\frac{3\rho s_{11}}{h^2}\omega^2. \tag{6.45}$$

The solution to the differential equation is given in terms of Krylov-Duncan functions [15].

$$w(kx)=C_1 S(kx)+C_2 T(kx)+C_3 U(kx)+C_4 V(kx) \tag{6.46}$$

$$S(kx)=\frac{1}{2}\left(\cosh(kx)+\cos(kx)\right) \tag{6.47}$$

$$T(kx) = \frac{1}{2}(\sinh(kx) + \sin(kx)) \tag{6.48}$$

$$U(kx) = \frac{1}{2}(\cosh(kx) - \cos(kx)) \tag{6.49}$$

$$V(kx) = \frac{1}{2}(\sinh(kx) - \sin(kx)) \tag{6.50}$$

Having the solution in this form is useful when applying boundary conditions. Also, the derivatives of the functions are transformed into each other. The list below show the values of the functions and their derivatives at $x = 0$.

$$\begin{array}{llll} S(0) = 1 & S'(0) = 0 & S''(0) = 0 & S'''(0) = 0 \\ T(0) = 0 & T'(0) = 1 & T''(0) = 0 & T'''(0) = 0 \\ U(0) = 0 & U'(0) = 0 & U''(0) = 1 & U'''(0) = 0 \\ V(0) = 0 & V'(0) = 0 & V''(0) = 0 & V'''(0) = 1 \end{array} \tag{6.51}$$

The boundary conditions are as follows.

$$w(0) = 0 \tag{6.52}$$

$$w'(0) = 0, \text{ The slope at the clamped end.} \tag{6.53}$$

$$w''(L) = 3d_{31}E_3, \text{ The curvature at the free end.} \tag{6.54}$$

$$w'''(L) = 0 \tag{6.55}$$

From the first two boundary conditions, we know that $C_1 = 0$ and $C_2 = 0$. From the third and fourth boundary conditions, we have

$$w''(L) = \frac{C_3 k^2}{2}(\cosh(kL) + \cos(kL)) + \frac{C_4 k^2}{2}(\sinh(kL) + \sin(kL)) = 3d_{31}E_3, \tag{6.56}$$

$$w'''(L) = \frac{C_3 k^3}{2}(\sinh(kL) - \sin(kL)) + \frac{C_4 k^3}{2}(\cosh(kL) + \cos(kL)) = 0. \tag{6.57}$$

After simplifying a bit, the coefficients are

$$C_3 = \frac{3d_{31}E_3}{k^2}\frac{\cos(kL) + \cosh(kL)}{1 + \cosh(kL)\cos(kL)}, \tag{6.58}$$

$$C_4 = \frac{3d_{31}E_3}{k^2}\frac{\sin(kL) - \sinh(kL)}{1 + \cosh(kL)\cos(kL)}. \tag{6.59}$$

To find the resonance frequencies, we find the frequencies which cause C_3 and C_4 to go to infinity. Besides the non-solution of $k = 0$, which is the static case and therefore not a resonance frequency, we have

$$1 + \cosh(kL)\cos(kL) = 0. \tag{6.60}$$

This is a transcendental equation, which has an infinite number of roots, the first six of which are

$$k_n L = 1.8751,\ 4.6941,\ 7.8548,\ 10.9955,\ 14.1372,\ 17.2788,\ \ldots \tag{6.61}$$

If we set $\lambda_n = k_n L$, then we have the expression for the resonance frequencies

$$\omega_n = \frac{\lambda_n^2}{L^2}\frac{h}{\sqrt{3\rho s_{11}}}, \tag{6.62}$$

where $h = 3\times10^{-5}$ m, $L = 2.5\times10^{-2}$ m, $\rho = 1.78\times10^{3}$ kg/m^3, and $s_{11} = 3.9544\times10^{-10}$ m s^2/kg, and so

$$\omega_n = \lambda_n^2\,(33.0315)\ \text{rad/s}. \tag{6.63}$$

The first six theoretical resonance frequencies are

$$\omega_n = 116.14,\ 727.83,\ 2037.97,\ 3993.54,\ 6601.68,\ 9861.73\ \text{rad/s}. \tag{6.64}$$

The theoretical values match up fairly well with the numerical results, listed below, with a difference of less than 2 percent. The numerical resonance frequencies were found by looking at which frequencies the amplitudes of the z deflection had a local maximum, which is plotted in figures 6.41 to 6.44. Neither damping, nor conductivity, affected the positions of the resonance frequencies. Damping only caused the peaks to broaden and decrease in amplitude, as shown in figure 6.42.

$$\omega_n = 116,\ 730,\ 2051,\ 4037,\ 6713,\ 10100\ \text{rad/s} \tag{6.65}$$

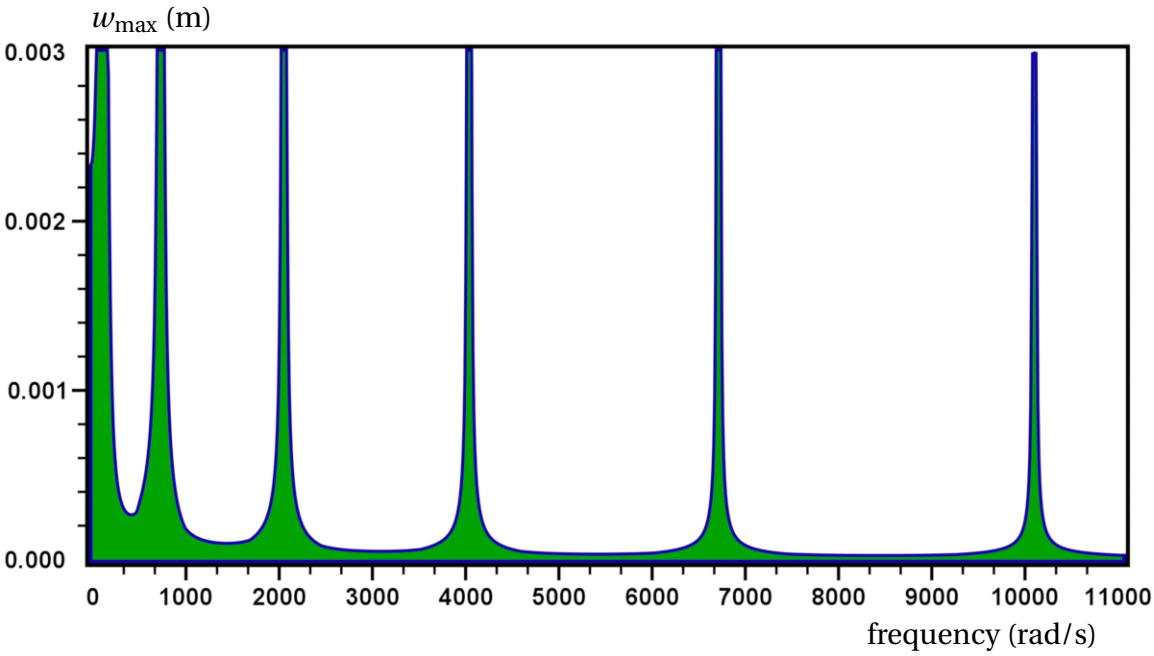

Figure 6.41: Maximum amplitude vs. frequency for high conductivity.

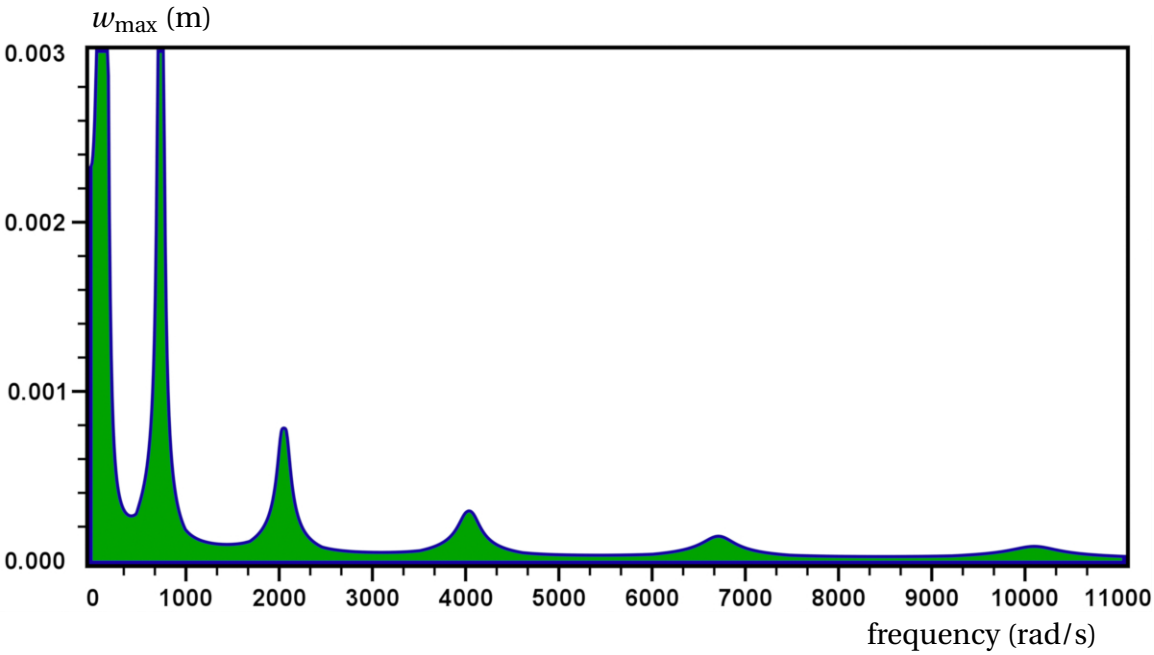

Figure 6.42: Maximum amplitude vs. frequency for high conductivity, with damping.

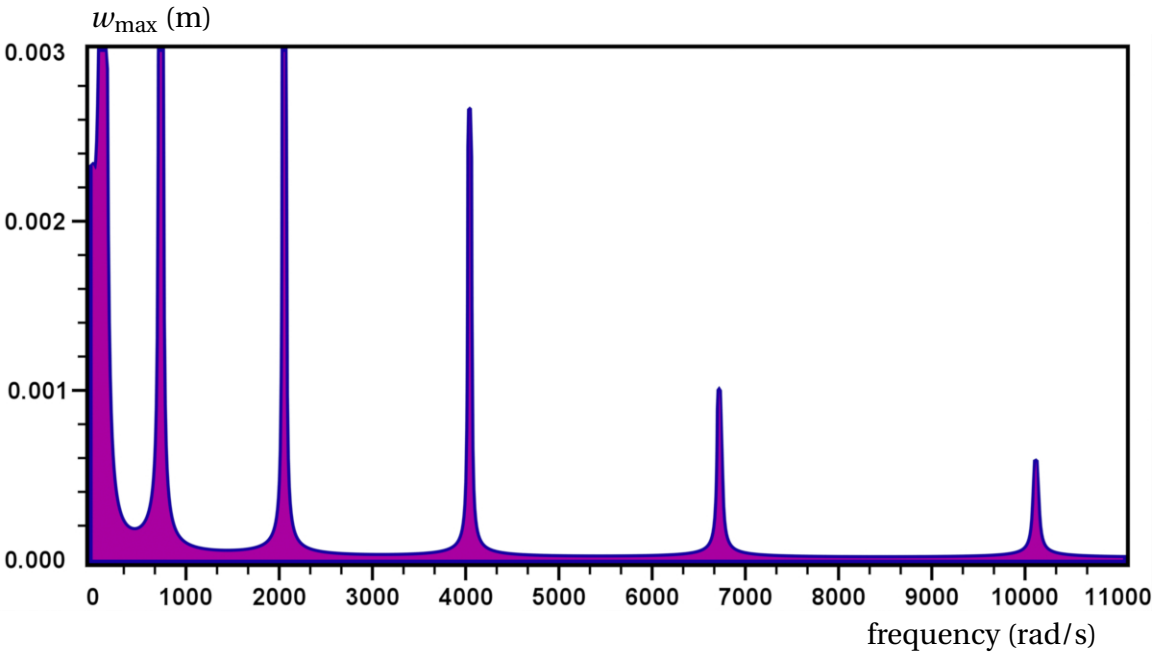

Figure 6.43: Maximum amplitude vs. frequency for medium conductivity.

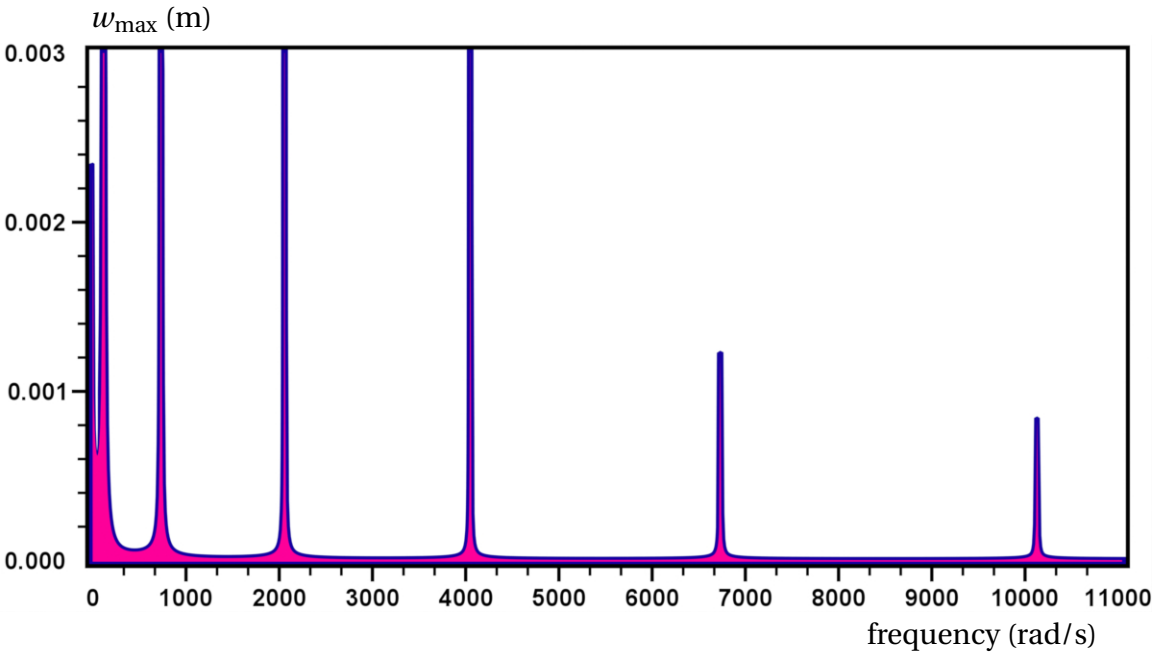

Figure 6.44: Maximum amplitude vs. frequency for very low conductivity.

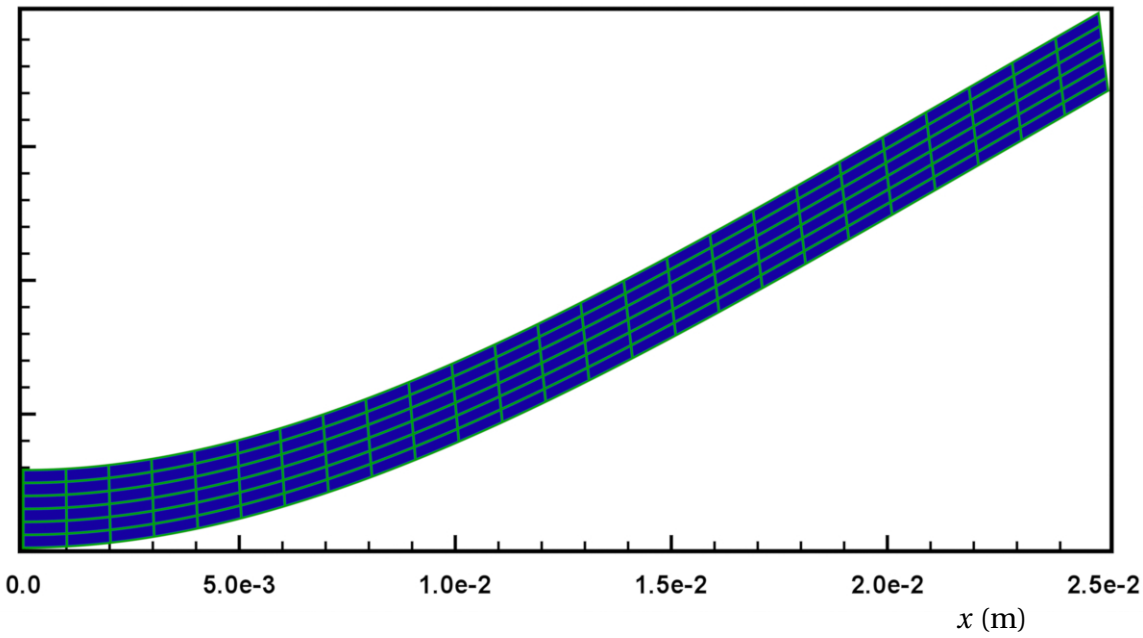

Figure 6.45: The 1st mode at $\omega = 116$ rad/s.

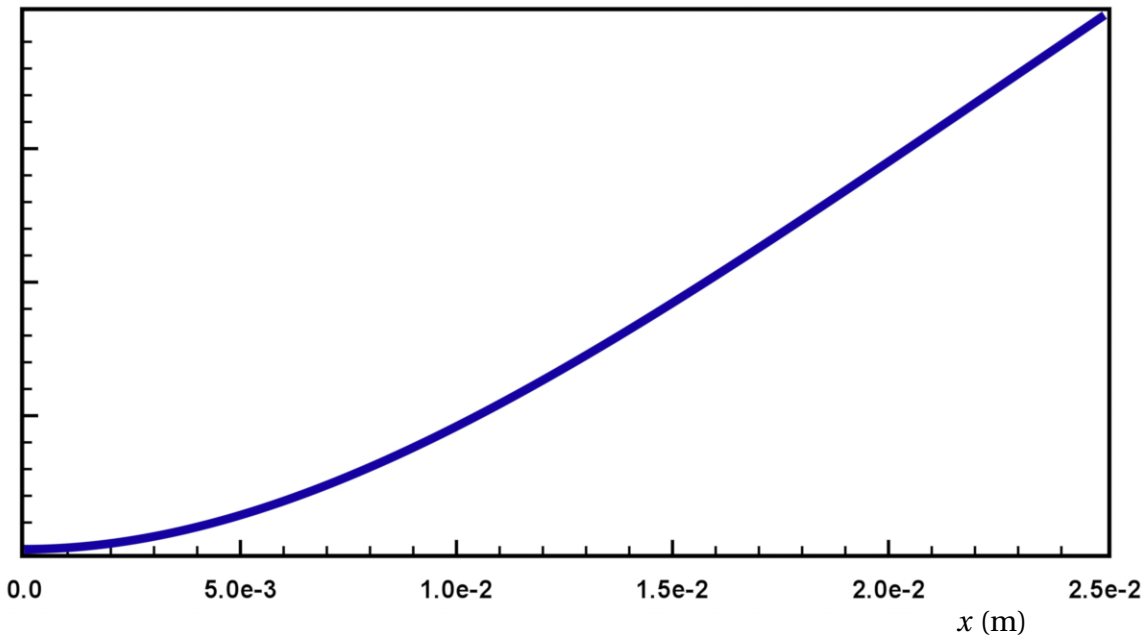

Figure 6.46: The analytical mode shape for the 1st mode.

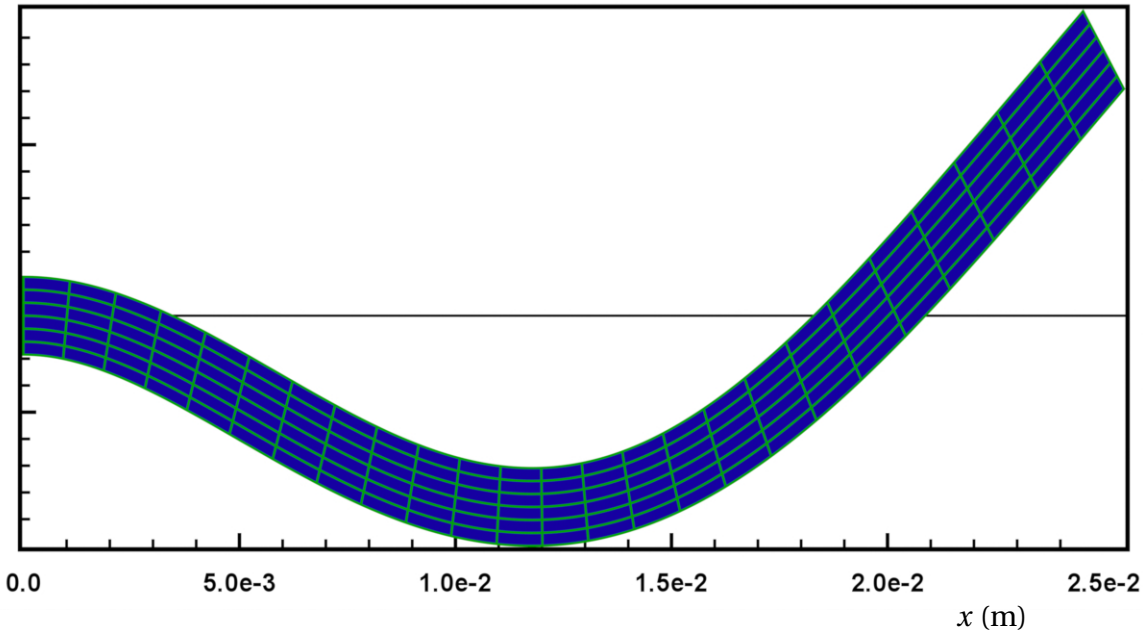

Figure 6.47: The 2nd mode at $\omega = 730$ rad/s.

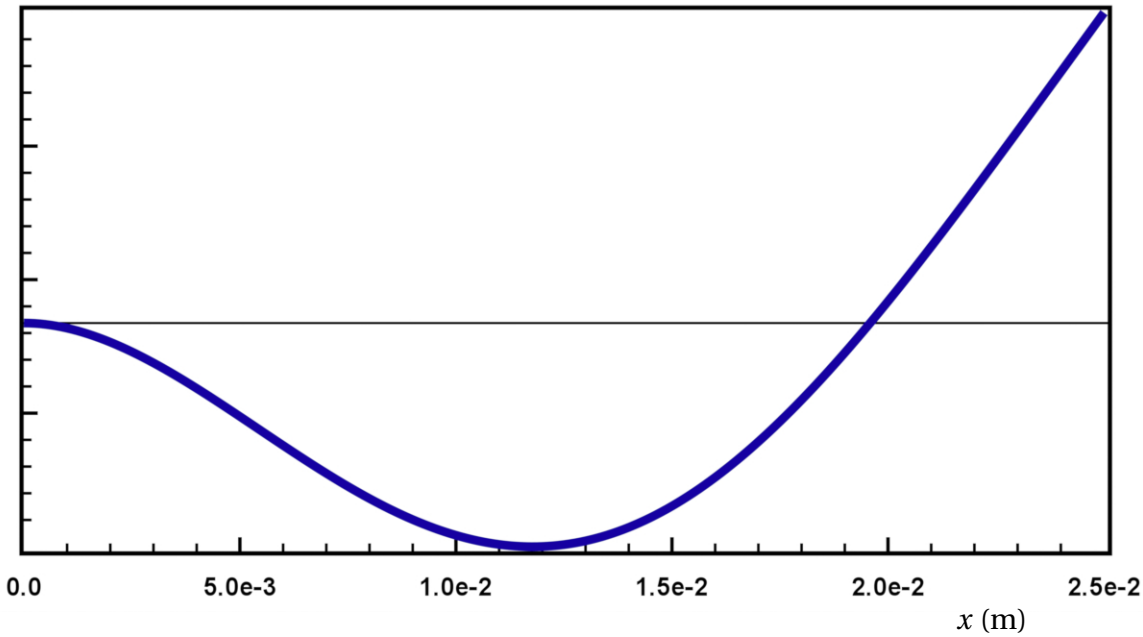

Figure 6.48: The analytical mode shape for the 2nd mode.

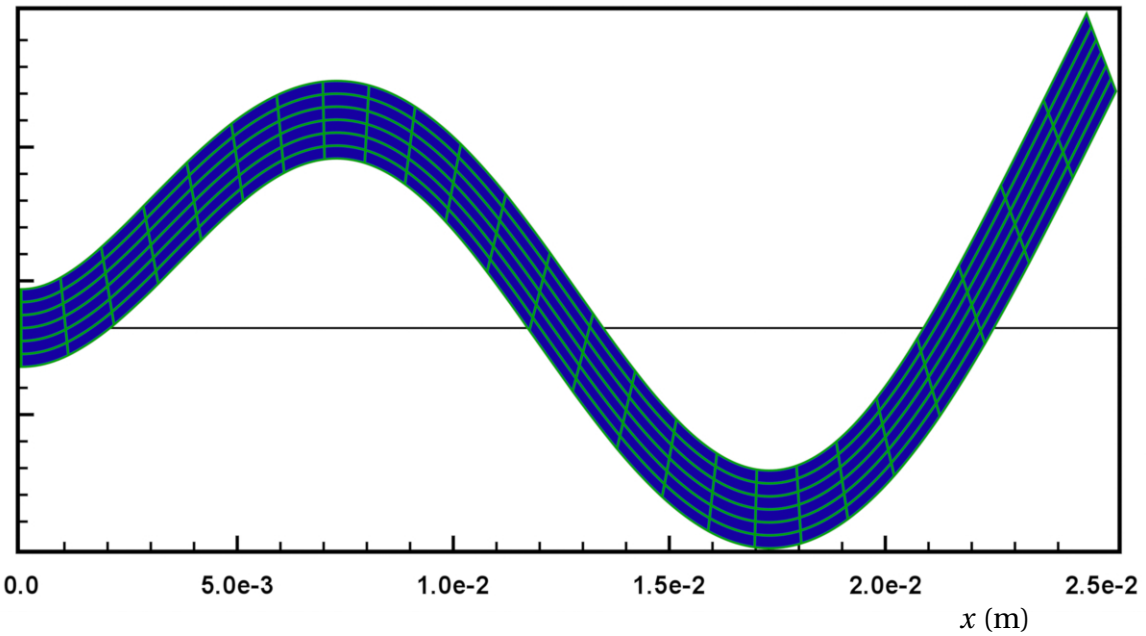

Figure 6.49: The 3rd mode at $\omega = 2051$ rad/s.

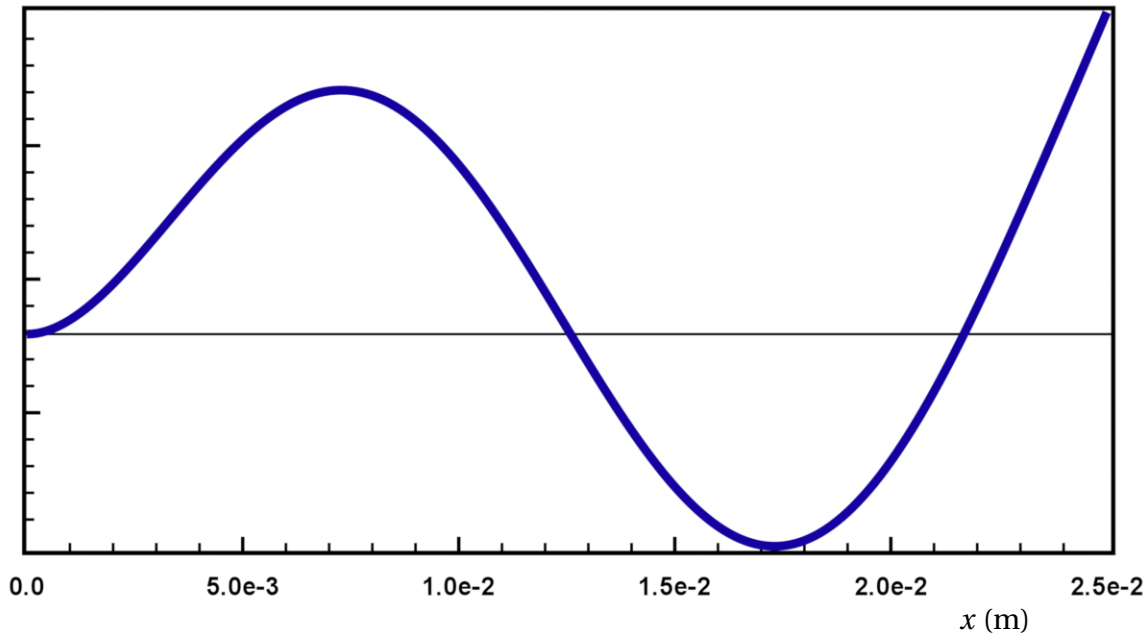

Figure 6.50: The analytical mode shape for the 3rd mode.

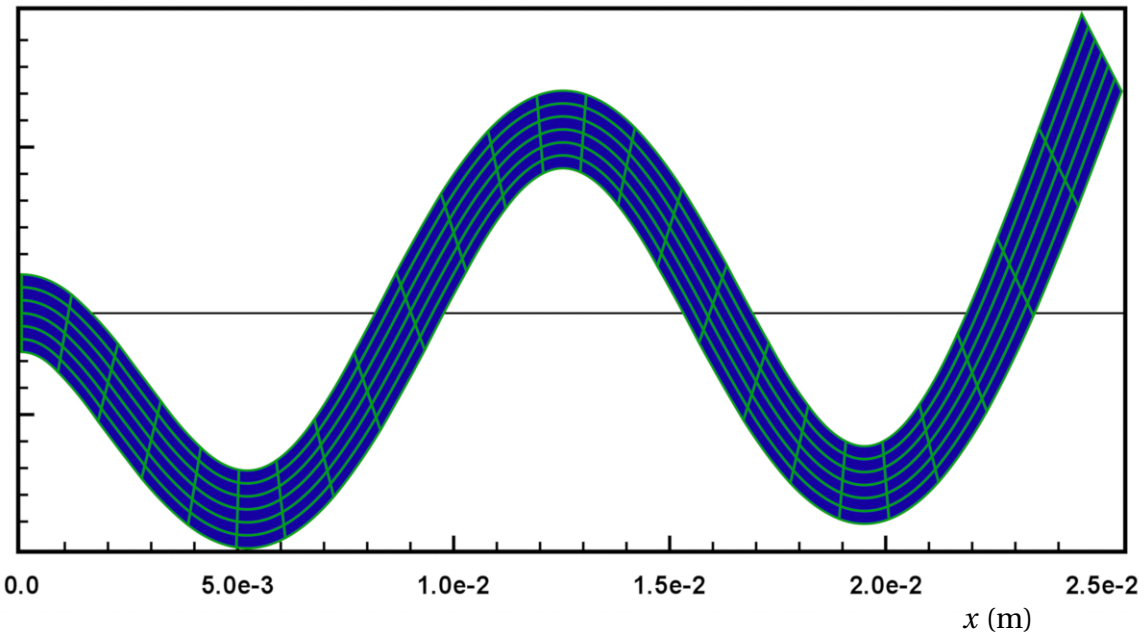

Figure 6.51: The 4$^{\text{th}}$ mode at $\omega = 4037$ rad/s.

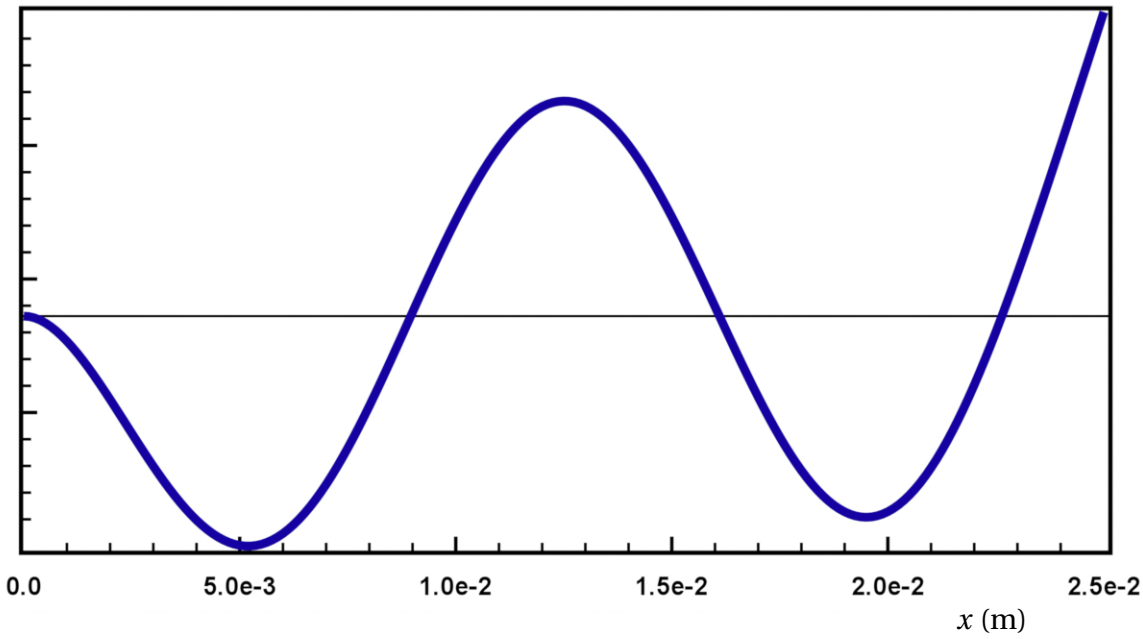

Figure 6.52: The analytical mode shape for the 4$^{\text{th}}$ mode.

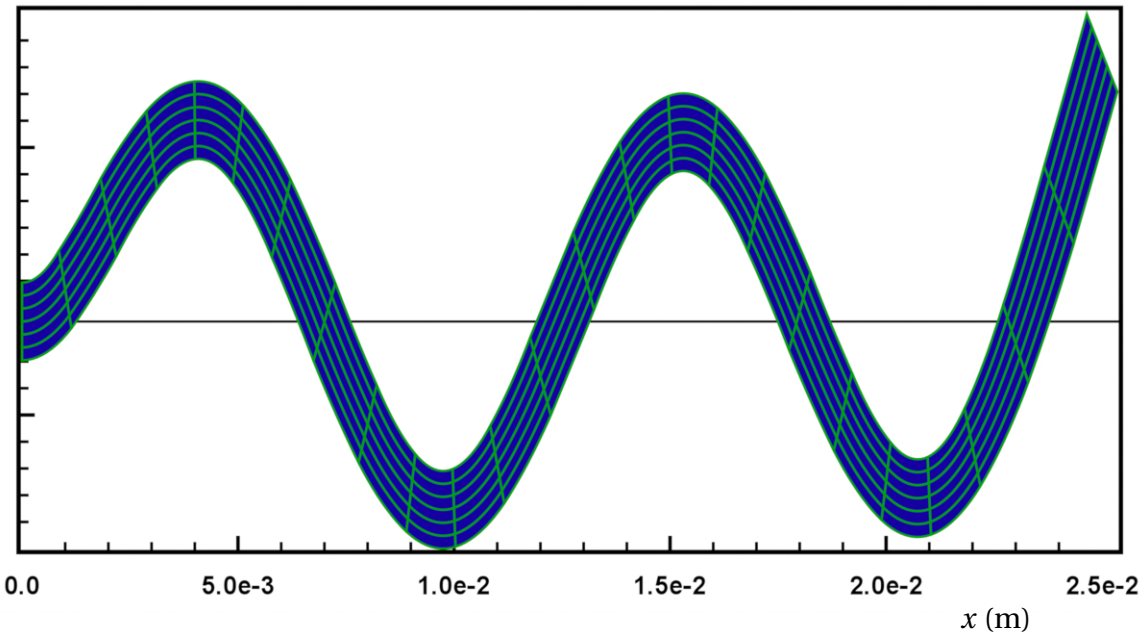

Figure 6.53: The 5th mode at $\omega = 6713$ rad/s.

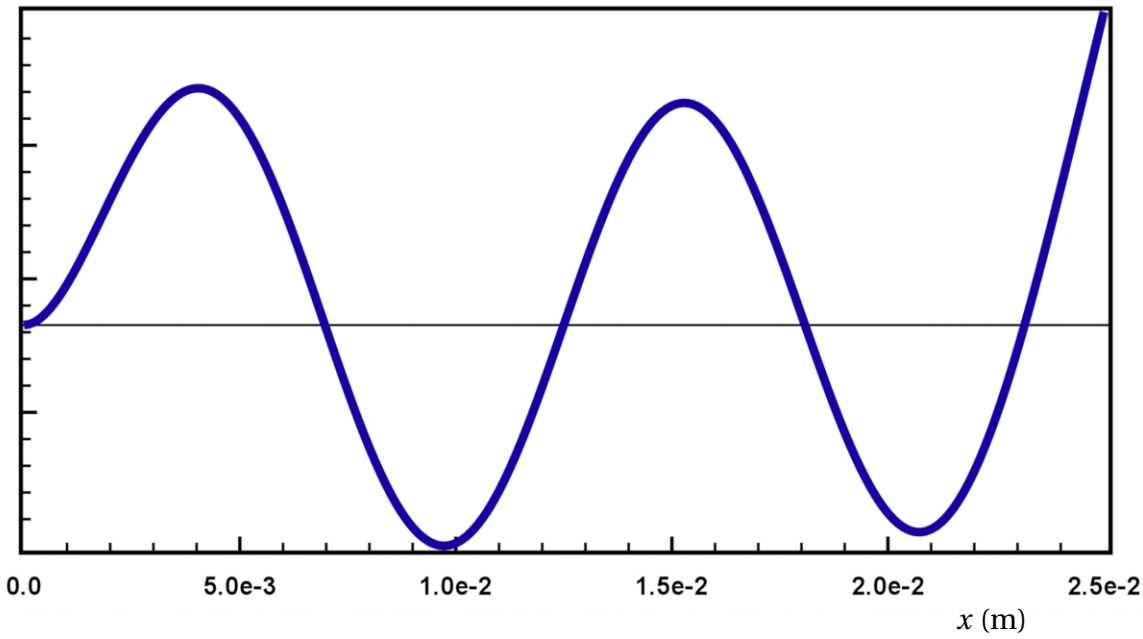

Figure 6.54: The analytical mode shape for the 5th mode.

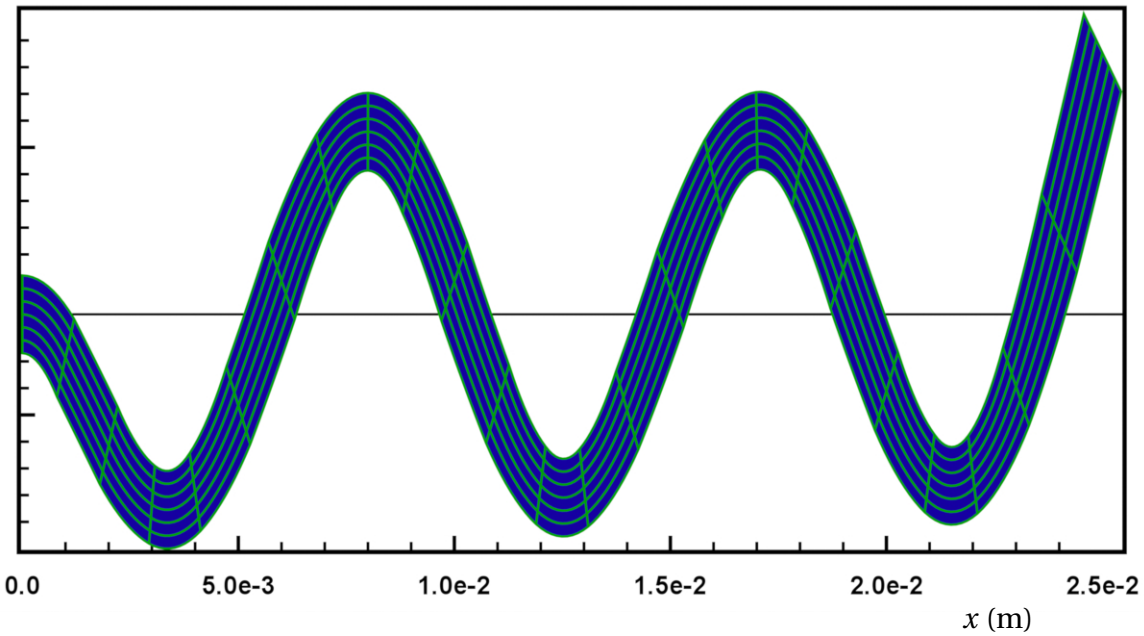

Figure 6.55: The 6th mode at $\omega = 10100$ rad/s.

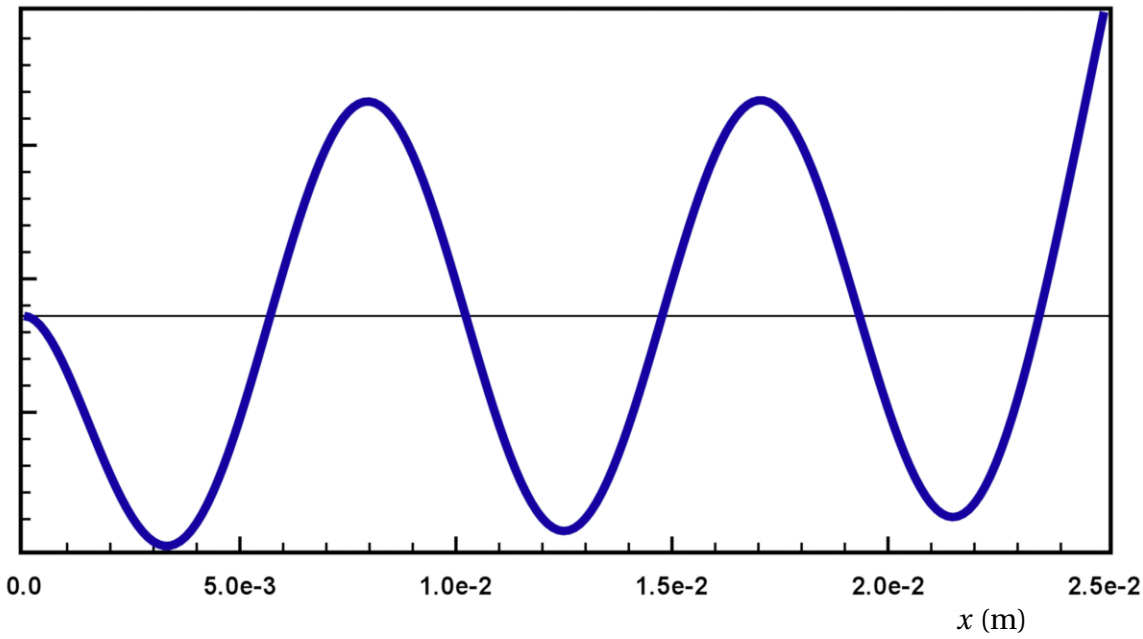

Figure 6.56: The analytical mode shape for the 6th mode.

CHAPTER 7

CONCLUSIONS

Traditionally, and for many applications, metal has been used as the electrode material for piezoelectric actuators. With the advent of intrinsically conductive polymers which can attain a moderately high conductivity with doping, it is now possible to use polymers instead of metal for electrodes.

A consideration when using finite-conductivity electrodes is what will be the electrical potential distribution within the electrodes for various frequency ranges. For very high conductivity electrodes, if a single voltage is applied anywhere on the electrode, the voltage will propagate nearly instantaneously throughout the electrode, and we can assume to have a uniform applied voltage. When this is the case, the electrodes do not need to be included when modeling the problem, except in the case where the electrodes contribute significantly to the stiffness of the device, in which case only the mechanical properties need to be modeled.

When the conductivity of the electrodes is not high enough for a particular applied voltage frequency, there will be two differences. First, there will be a significant decrease in the amplitude of the voltage as you get farther along the electrode away from the point of the applied voltage. Second, there will be a phase lag. In the case of harmonic time dependence, where all the variables respond to the applied voltage at the same frequency, the response will not be in phase. It is possible to have applications where this is a good thing. For the most part, having different parts of the bimorph respond at vastly different phases is problematic for predictability and control.

Independent of the conductivity, there is also the issue of frequency modes. Although for a given finite conductivity there will be a significant phase lag and a decreasing in voltage amplitude for high enough frequencies, for all but the lowest conductivities, the larger issue is that the bimorph will change shape depending on which mode it is in. For a bimorph, the resonance frequencies are low, and so the bimorph will enter into the higher modes quickly, before there might be issues with voltage and bending amplitude degradation.

The piezoelectric bimorph problem was modeled using coupled second order differential equations. It was straightforward to convert these equations into a finite element formulation. Although the resulting matrix was indefinite, and also problematic in that it had a very high condition number, it was still possible to solve the system of equations with a direct solver. The results show that for small bimorphs, the response will be very similar to metal electrodes as long as the conductivity is not very low. With the vast improvements over intrinsic conductivity by doping, it appears that PEDOT-PSS and similar polymers will be highly usable. There are other issues to consider though, such as the lifecycle of the polymer, and whether it is suitable for various environmental conditions, such as high moisture.

This work, being the first to show the effect of finite conductivity electrodes on the performance of a piezoelectric polymer actuator, can be extended to actuators of other designs and employing other materials. Such analysis will be a great aid in the design of higher performance actuators that employ the much more flexible conductive polymer electrodes. Since the Finite Element Method is suitable for any piece-wise polygonal geometry, it is possible to model a vast array of differently shaped actuators. Also, the voltage can be applied in any pattern. In this dissertation, the applied voltage was only applied along one edge of the bimorph. This is not a requirement, however. The voltage

can be applied in any pattern, in what is called a mask. For example, it is possible to have a very thin metal grid overlaying the polymer electrodes. This would minimize the reduction in the deflection from the stiffness of the metal, but also help ensure a more uniform applied voltage.

Results

There were three types of problems solved. There is the static case, where the conductivity of the electrodes does not affect the solution. This was solved for the full 3D case, and also the 2D case for the simple beam approximation of $T_2 = 0$. In addition to the FEM numerical solutions, an analytical solution was developed which involved most of the Bernoulli-Euler beam assumptions [11] along with the approximations $T_2 = 0$ and $T_3 = 0$. This analytical model, in the final form, involved the material constants s_{11} and d_{31}. The agreement between the theoretical and numerical results was astonishing. The first attempt at developing a model using pure Bernoulli-Euler beam assumptions used the material constants c_{11} and e_{31}. The amplitude of the results were highly inaccurate, although the form of the solution was correct.

The second problem solved was the case of harmonic time dependence. In the general time-dependent case, the applied voltage is an arbitrary function of time. The response of the bimorph would need to be calculated at each time step. An appropriate value for the time-step would need to be chosen, and most importantly, the correct method for stepping the solution forward in time would need to be chosen, possibly a Runge-Kutta scheme. If the applied voltage is sinusoidal, then the response of the bimorph will also be sinusoidal, since the governing equations for the bimorph are linear. If the input voltage is $V = V_0 \sin \omega t$, then the solution will have the form $\mathrm{Re}\left[u e^{i\omega t}\right] = \alpha \cos \omega t - \beta \sin \omega t$, where u is complex. The solution will only have a zero

cosine component if there is no phase lag of any kind, which is the case for infinite-conductivity electrodes and no damping. Electrode resistivity and mechanical damping will cause a cosine solution to develop. For a given frequency, the solutions for several different values of conductivity were found.

The third problem was finding the positions of the resonance frequencies and the mode shapes. This was an extension of the case of harmonic time dependence. A theoretical model was developed to find both the resonance frequencies, and the shape of w for any given frequency. Again the model was based on the Bernoulli-Euler beam assumptions. The analytical solution found for the static case was extended for the case of harmonic time dependence. The mode shapes appear identical to the FEM solutions, and the values of the resonance frequencies are very close, but not identical, being within 2% of each other for the first five resonance frequencies.

Future Direction

The results presented in this dissertation were found using Lagrange finite elements. These types of elements allow only one degree of freedom, which is the primary variable, such as u, v, w, or ϕ. Other degrees of freedom which we might want to know are the derivatives of the primary variables, or functions of the derivatives such as the strains S_{ij}, or the electric displacement $\boldsymbol{D}$. The formulas for calculating these quantities involve the first derivatives of all the primary variables, so that $\boldsymbol{D} = \boldsymbol{D}\left(\frac{\partial u}{\partial x}, \frac{\partial u}{\partial y}, \frac{\partial u}{\partial z}, \frac{\partial v}{\partial x}, \ldots\right)$. If we only want to know the strains and the electric displacement, then we could look at what are called mixed finite element methods [11]. These methods are known to be unstable, and so ensuring their correctness requires more advanced methods. The strains and electric displacement on the boundary are of interest because some of the boundary conditions for the bimorph problem include having surface traction values of zero,

and also a surface charge density of zero whenever the potential is not specified on the boundary. It would be nice to ensure that these boundary conditions are enforced in the solution.

If we are interested in the individual derivatives of the primary variables, then it may be possible to find the derivatives by taking the derivatives of the basis functions, since the solutions are just coefficients times basis functions. Problems could arise when using this approach, however, because although Lagrange basis functions are continuous across element boundaries, they are not smooth, and their derivatives are not necessarily continuous. Another approach is to use Hermite basis functions, which include the first derivatives, and the mixed second derivative in the finite element formulation. This method is a higher-order method, and although I have found it to be stable for certain problems, it seems to be unstable when solving the piezoelectric problem. One possible problem with my Hermite formulation, which was suggested to me, was that, in the Hermite approach, the derivatives on the boundary should not be included as unknowns in the formulation, that only interior derivatives should be included. The interior derivatives help to ensure smoothness of the solution. Also, Hermite elements are higher-order, and thus a coarser mesh can be used to achieve the same level of accuracy as Lagrange elements [17].

One problem that clearly arises when using Hermite elements is the problem of smoothness in the unknowns. When using Lagrange elements, only the primary variables need to be continuous. There are some advanced methods, such as the Discontinuous Galerkin Method, which can be used in solving problems which have jumps. They involve using extra terms in the finite element formulation, such as penalty (or stabilization) terms. If Hermite elements are used, then it is assumed that all the variables used in the formulation are continuous. In the case of the piezoelectric bimorph, there is a jump

in some of the derivatives across the boundary between the two piezoelectric sheet layers, since the polarization direction has a jump. The problem can be transformed into a continuous problem by adding a thin transition layer in which the polarization changes continuously. If the problem is not altered, then it is possible that the variables will simply be averaged across jumps, although serious oscillations can also occur which would render the solution useless.

The weak form of the equations of motion and the continuity equation with the boundary integrals are shown below. When using Hermite elements, some care is needed in dealing with the boundary integrals.

$$\int_\Omega \left[\rho\delta u\ddot{u} + \boldsymbol{\nabla}\delta u \cdot \boldsymbol{t}_u\right] \mathrm{d}\Omega - \oint_\Gamma \delta u\, \boldsymbol{t}_u \cdot \hat{\boldsymbol{n}}\, \mathrm{d}\Gamma = 0 \tag{7.1}$$

$$\int_\Omega \left[\rho\delta v\ddot{v} + \boldsymbol{\nabla}\delta v \cdot \boldsymbol{t}_v\right] \mathrm{d}\Omega - \oint_\Gamma \delta v\, \boldsymbol{t}_v \cdot \hat{\boldsymbol{n}}\, \mathrm{d}\Gamma = 0 \tag{7.2}$$

$$\int_\Omega \left[\rho\delta w\ddot{w} + \boldsymbol{\nabla}\delta w \cdot \boldsymbol{t}_w\right] \mathrm{d}\Omega - \oint_\Gamma \delta w\, \boldsymbol{t}_w \cdot \hat{\boldsymbol{n}}\, \mathrm{d}\Gamma = 0 \tag{7.3}$$

$$\int_\Omega \boldsymbol{\nabla}\delta\phi \cdot \left(\boldsymbol{J} + \frac{\partial \boldsymbol{D}}{\partial t}\right) \mathrm{d}\Omega - \oint_\Gamma \delta\phi \left(\boldsymbol{J} + \frac{\partial \boldsymbol{D}}{\partial t}\right) \cdot \hat{\boldsymbol{n}}\, \mathrm{d}\Gamma = 0 \tag{7.4}$$

where

$$\boldsymbol{t}_u = T_1\hat{\boldsymbol{x}} + T_6\hat{\boldsymbol{y}} + T_5\hat{\boldsymbol{z}}, \tag{7.5}$$

$$\boldsymbol{t}_v = T_6\hat{\boldsymbol{x}} + T_2\hat{\boldsymbol{y}} + T_4\hat{\boldsymbol{z}}, \tag{7.6}$$

$$\boldsymbol{t}_w = T_5\hat{\boldsymbol{x}} + T_4\hat{\boldsymbol{y}} + T_3\hat{\boldsymbol{z}}. \tag{7.7}$$

For a second-order differential equation (or system of equations), only one type of boundary condition can be specified simultaneously. Usually two types of boundary conditions can be specified for the problem (Dirichlet or Neumann), but they must be specified on different parts of the boundary. If the value of the primary variable is specified, then that is called a Dirichlet boundary condition. The weak form of the differential

equation reveals the form of the Neumann boundary condition. For the Poisson equation, the Neumann boundary condition is the normal derivative on the boundary. We can assume that either one type or the other is specified on the entirety of the boundary, for each primary variable. In a set of coupled differential equations, the positions of the Dirichlet and Neumann regions do not need to coincide for all the variables.

$$\Gamma = \Gamma_D + \Gamma_N \tag{7.8}$$

When the primary variables are not specified, the boundary condition is that all surface tractions are zero, and the surface charge density is zero. Therefore, the boundary integral is zero on all Neumann regions of the boundary, and we only have the Dirichlet regions to consider.

$$\begin{aligned}
&\int_\Omega \left[\frac{\partial \delta u}{\partial x}\left(c_{11}\frac{\partial u}{\partial x} + c_{12}\frac{\partial v}{\partial y} + c_{13}\frac{\partial w}{\partial z} + e_{31}\frac{\partial \phi}{\partial z}\right) + c_{66}\frac{\partial \delta u}{\partial y}\left(\frac{\partial u}{\partial y} + \frac{\partial v}{\partial x}\right) \right. \\
&\qquad \left. + \frac{\partial \delta u}{\partial z}\left(c_{55}\left(\frac{\partial u}{\partial z} + \frac{\partial w}{\partial x}\right) + e_{15}\frac{\partial \phi}{\partial x}\right)\right] \mathrm{d}\Omega \\
&- \oint_{\Gamma_{D_u}} \delta u \left[\left(c_{11}\frac{\partial u}{\partial x} + c_{12}\frac{\partial v}{\partial y} + c_{13}\frac{\partial w}{\partial z} + e_{31}\frac{\partial \phi}{\partial z}\right)\hat{\boldsymbol{x}} + c_{66}\left(\frac{\partial u}{\partial y} + \frac{\partial v}{\partial x}\right)\hat{\boldsymbol{y}} \right. \\
&\qquad \left. + \left(c_{55}\left(\frac{\partial u}{\partial z} + \frac{\partial w}{\partial x}\right) + e_{15}\frac{\partial \phi}{\partial x}\right)\hat{\boldsymbol{z}}\right] \cdot \hat{\boldsymbol{n}}\, \mathrm{d}\Gamma = -\int_\Omega \rho \delta u \ddot{u}\, \mathrm{d}\Omega
\end{aligned} \tag{7.9}$$

$$\begin{aligned}
&\int_\Omega \left[c_{66}\frac{\partial \delta v}{\partial x}\left(\frac{\partial u}{\partial y} + \frac{\partial v}{\partial x}\right) + \frac{\partial \delta v}{\partial y}\left(c_{12}\frac{\partial u}{\partial x} + c_{22}\frac{\partial v}{\partial y} + c_{23}\frac{\partial w}{\partial z} + e_{32}\frac{\partial \phi}{\partial z}\right) \right. \\
&\qquad \left. + \frac{\partial \delta v}{\partial z}\left(c_{44}\left(\frac{\partial v}{\partial z} + \frac{\partial w}{\partial y}\right) + e_{24}\frac{\partial \phi}{\partial y}\right)\right] \mathrm{d}\Omega \\
&- \oint_{\Gamma_{D_v}} \delta v \left[c_{66}\left(\frac{\partial u}{\partial y} + \frac{\partial v}{\partial x}\right)\hat{\boldsymbol{x}} + \left(c_{12}\frac{\partial u}{\partial x} + c_{22}\frac{\partial v}{\partial y} + c_{23}\frac{\partial w}{\partial z} + e_{32}\frac{\partial \phi}{\partial z}\right)\hat{\boldsymbol{y}} \right. \\
&\qquad \left. + \left(c_{44}\left(\frac{\partial v}{\partial z} + \frac{\partial w}{\partial y}\right) + e_{24}\frac{\partial \phi}{\partial y}\right)\hat{\boldsymbol{z}}\right] \cdot \hat{\boldsymbol{n}}\, \mathrm{d}\Gamma = -\int_\Omega \rho \delta v \ddot{v}\, \mathrm{d}\Omega
\end{aligned} \tag{7.10}$$

$$\begin{aligned}
&\int_\Omega \left[\frac{\partial \delta w}{\partial x}\left(c_{55}\left(\frac{\partial u}{\partial z}+\frac{\partial w}{\partial x}\right)+e_{15}\frac{\partial \phi}{\partial x}\right)+\frac{\partial \delta w}{\partial y}\left(c_{44}\left(\frac{\partial v}{\partial z}+\frac{\partial w}{\partial y}\right)+e_{24}\frac{\partial \phi}{\partial y}\right)\right. \\
&\left.+\frac{\partial \delta w}{\partial z}\left(c_{13}\frac{\partial u}{\partial x}+c_{23}\frac{\partial v}{\partial y}+c_{33}\frac{\partial w}{\partial z}+e_{33}\frac{\partial \phi}{\partial z}\right)\right] \mathrm{d}\Omega \\
&-\oint_{\Gamma_{Dw}} \delta w \left[\left(c_{55}\left(\frac{\partial u}{\partial z}+\frac{\partial w}{\partial x}\right)+e_{15}\frac{\partial \phi}{\partial x}\right)\hat{\boldsymbol{x}}+\left(c_{44}\left(\frac{\partial v}{\partial z}+\frac{\partial w}{\partial y}\right)+e_{24}\frac{\partial \phi}{\partial y}\right)\hat{\boldsymbol{y}}\right. \\
&\left.+\left(c_{13}\frac{\partial u}{\partial x}+c_{23}\frac{\partial v}{\partial y}+c_{33}\frac{\partial w}{\partial z}+e_{33}\frac{\partial \phi}{\partial z}\right)\hat{\boldsymbol{z}}\right]\cdot\hat{\boldsymbol{n}}\ \mathrm{d}\Gamma=-\int_\Omega \rho\delta w\ddot{w}\ \mathrm{d}\Omega
\end{aligned} \tag{7.11}$$

$$\begin{aligned}
&\int_\Omega \left[\frac{\partial \delta \phi}{\partial x}\left(e_{15}\left(\frac{\partial \dot{u}}{\partial z}+\frac{\partial \dot{w}}{\partial x}\right)-\varepsilon_1\frac{\partial \dot{\phi}}{\partial x}\right)+\frac{\partial \delta \phi}{\partial y}\left(e_{24}\left(\frac{\partial \dot{v}}{\partial z}+\frac{\partial \dot{w}}{\partial y}\right)-\varepsilon_2\frac{\partial \dot{\phi}}{\partial y}\right)\right. \\
&\left.\quad+\frac{\partial \delta \phi}{\partial z}\left(e_{31}\frac{\partial \dot{u}}{\partial x}+e_{32}\frac{\partial \dot{v}}{\partial y}+e_{33}\frac{\partial \dot{w}}{\partial z}-\varepsilon_3\frac{\partial \dot{\phi}}{\partial z}\right)\right] \mathrm{d}\Omega \\
&-\oint_{\Gamma_{D\phi}} \delta\phi \left[\left(e_{15}\left(\frac{\partial \dot{u}}{\partial z}+\frac{\partial \dot{w}}{\partial x}\right)-\varepsilon_1\frac{\partial \dot{\phi}}{\partial x}\right)\hat{\boldsymbol{x}}+\left(e_{24}\left(\frac{\partial \dot{v}}{\partial z}+\frac{\partial \dot{w}}{\partial y}\right)-\varepsilon_2\frac{\partial \dot{\phi}}{\partial y}\right)\hat{\boldsymbol{y}}\right. \\
&\left.\quad+\left(e_{31}\frac{\partial \dot{u}}{\partial x}+e_{32}\frac{\partial \dot{v}}{\partial y}+e_{33}\frac{\partial \dot{w}}{\partial z}-\varepsilon_3\frac{\partial \dot{\phi}}{\partial z}\right)\hat{\boldsymbol{z}}\right]\cdot\hat{\boldsymbol{n}}\ \mathrm{d}\Gamma=0
\end{aligned} \tag{7.12}$$

Figures 7.1 to 7.8 show the solution to the 2D bimorph problem when using Hermite elements. In this case the electric field was specified, and ϕ was not included as an unknown. There are some obvious problems, especially with ϕ. This may be caused by an incorrect implementation of Hermite elements.

There is a problem with the mixed second derivative. When the mesh is refined, the second derivative becomes worse, as shown if figures 7.9 and 7.10. There seems to be an instability which becomes worse with smaller mesh size. I do not think this is a numerical round-off problem. The same solution was found when the problem was solved in Mathematica with 60 decimal places of precision.

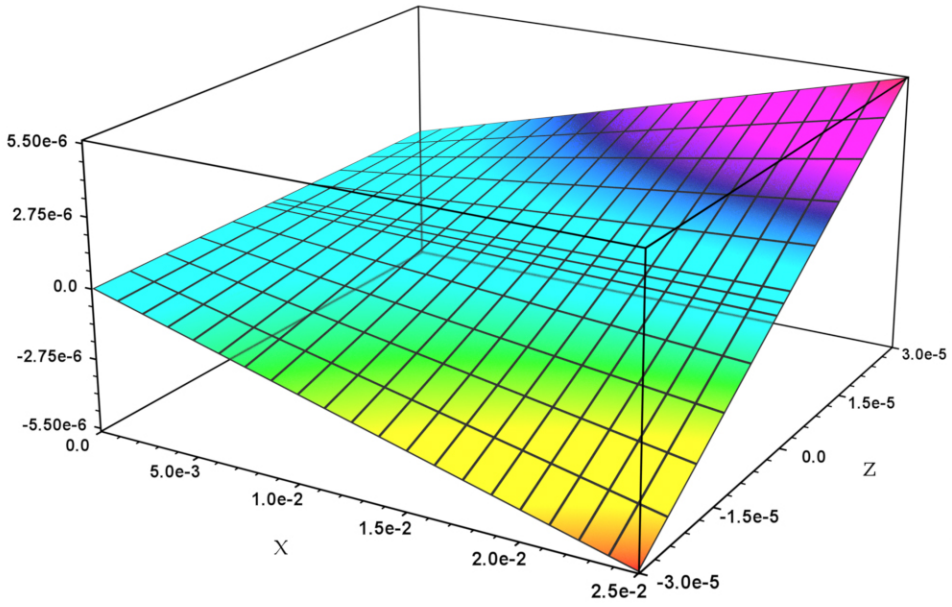

Figure 7.1: u

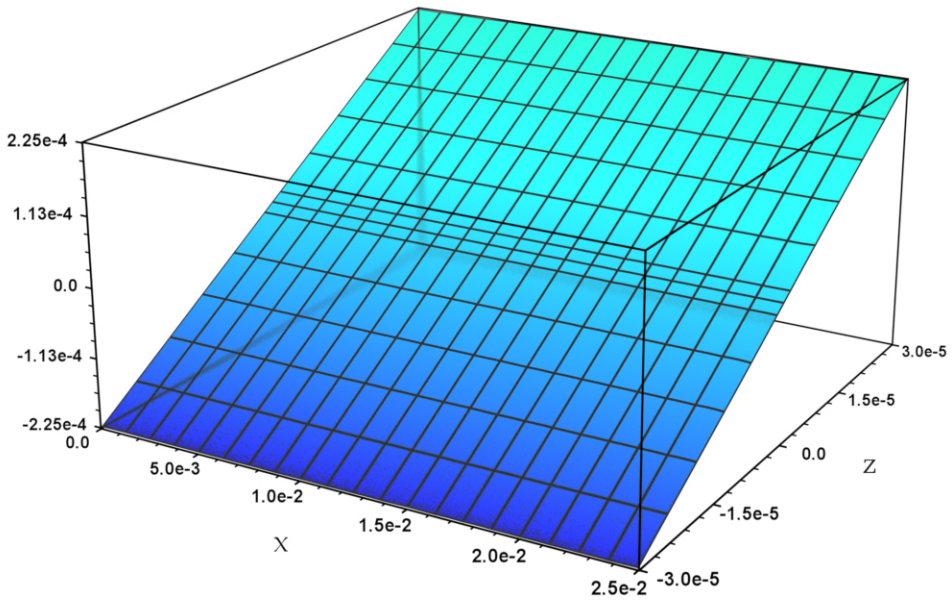

Figure 7.2: $\partial u/\partial x$

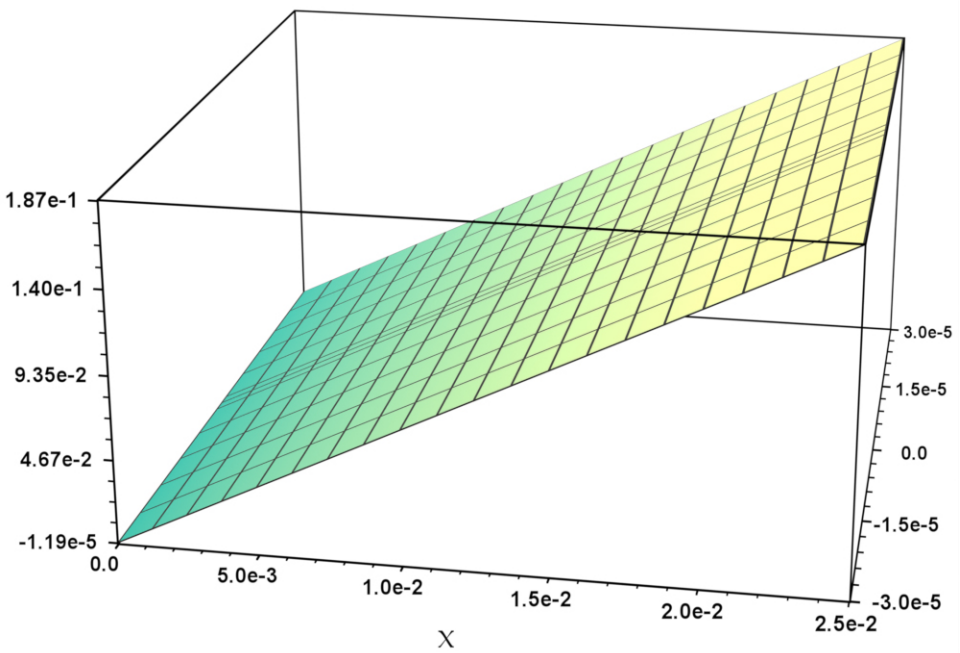

Figure 7.3: $\partial u/\partial z$

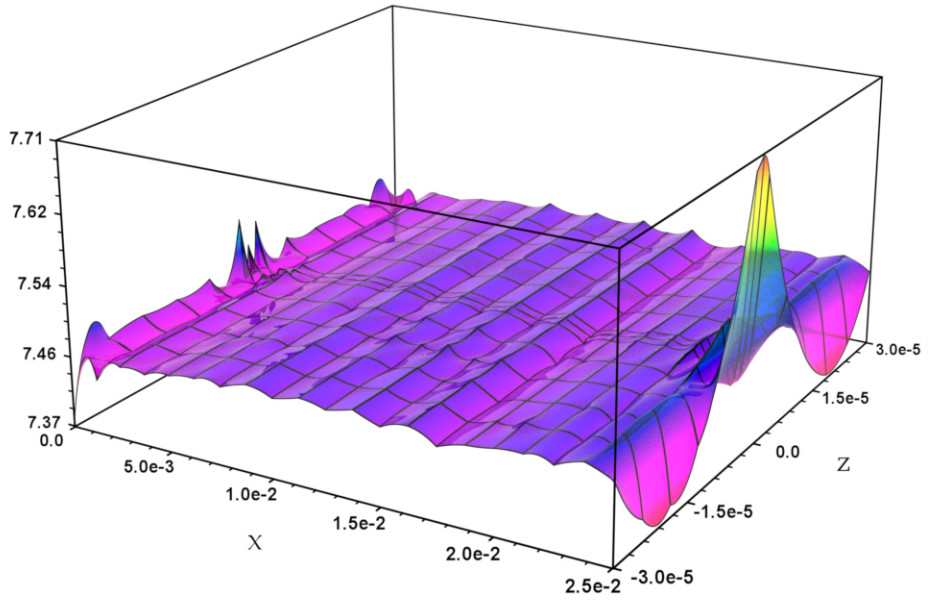

Figure 7.4: $\partial^2 u/\partial x \partial z$

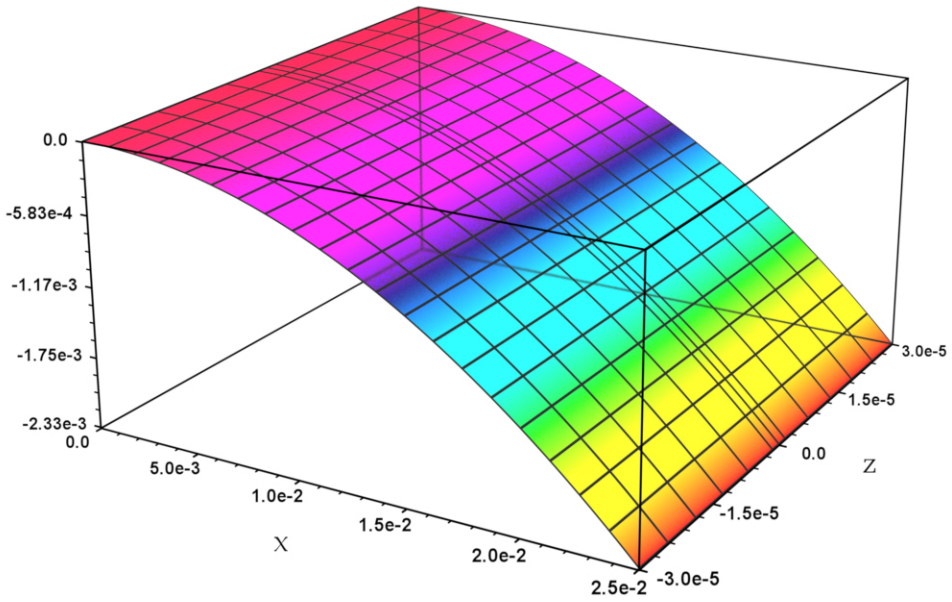

Figure 7.5: w

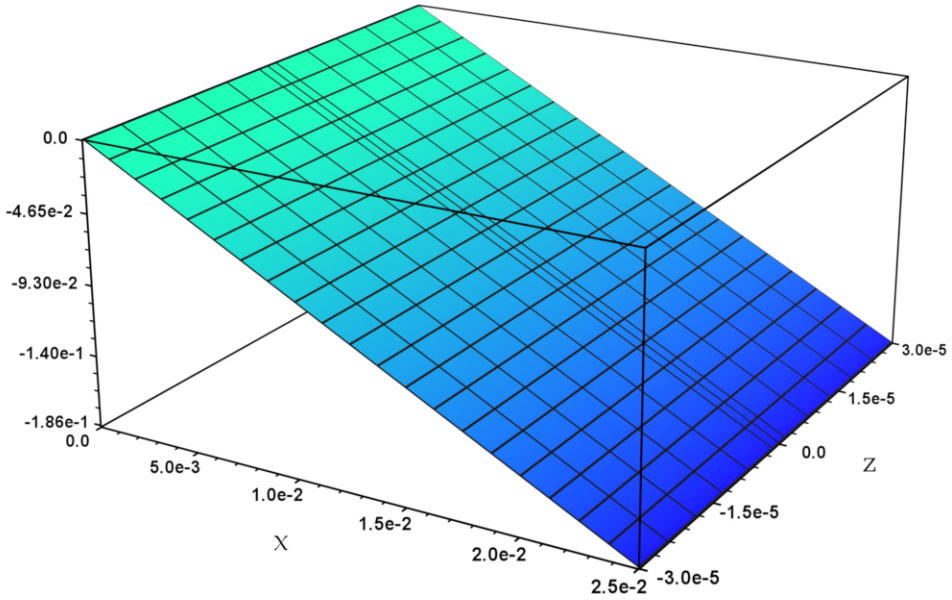

Figure 7.6: $\partial w/\partial x$

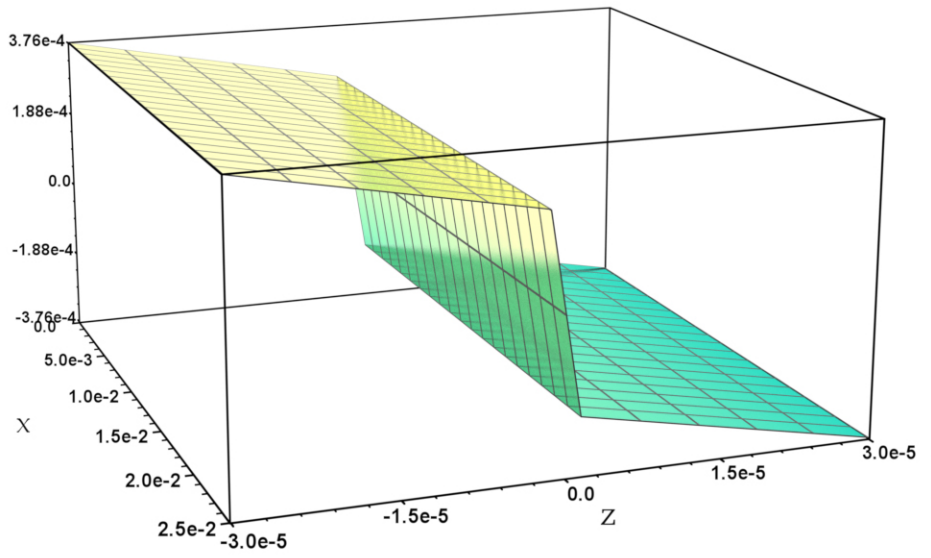

Figure 7.7: $\partial w/\partial z$

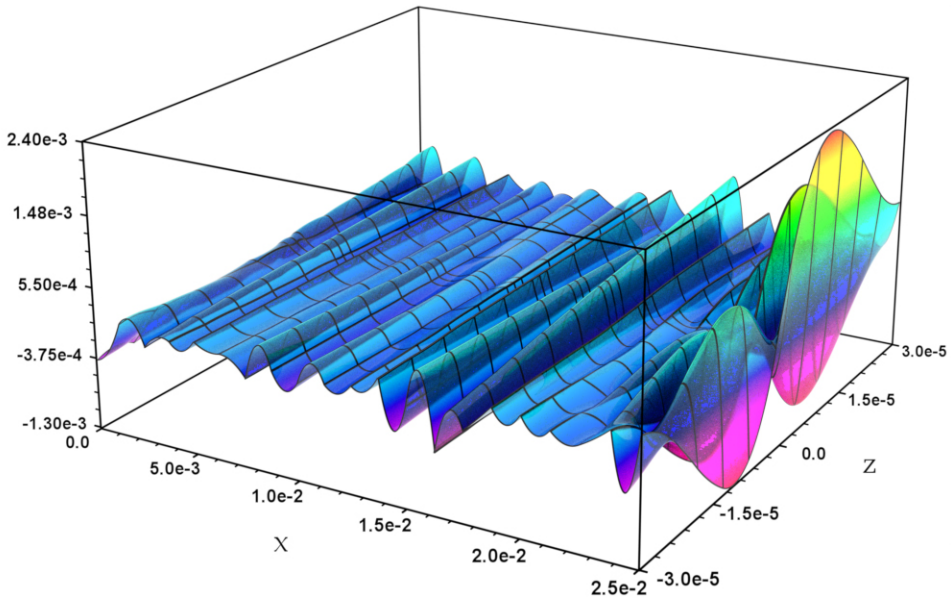

Figure 7.8: $\partial^2 w/\partial x \partial z$

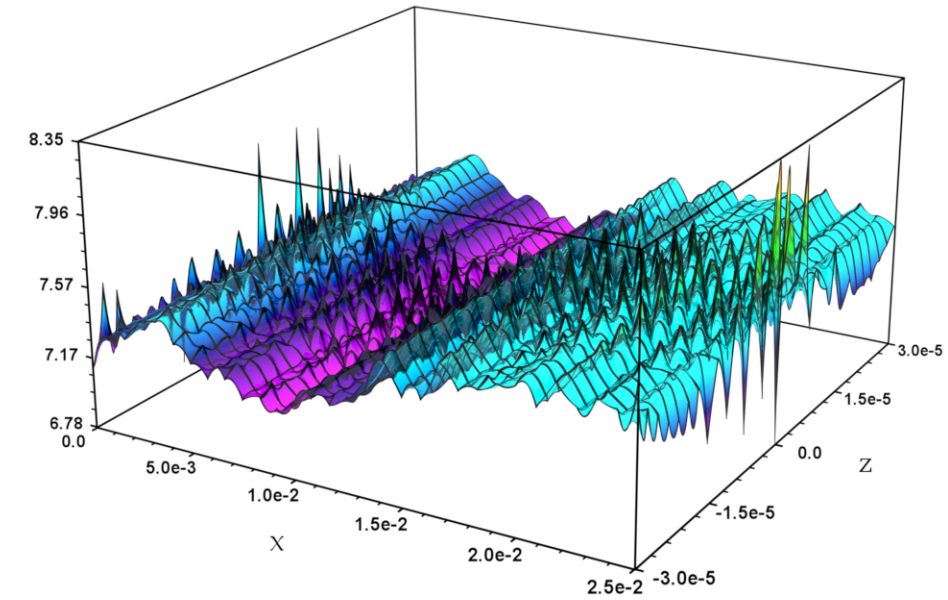

Figure 7.9: $\partial^2 u/\partial x \partial z$, with 30×30 elements.

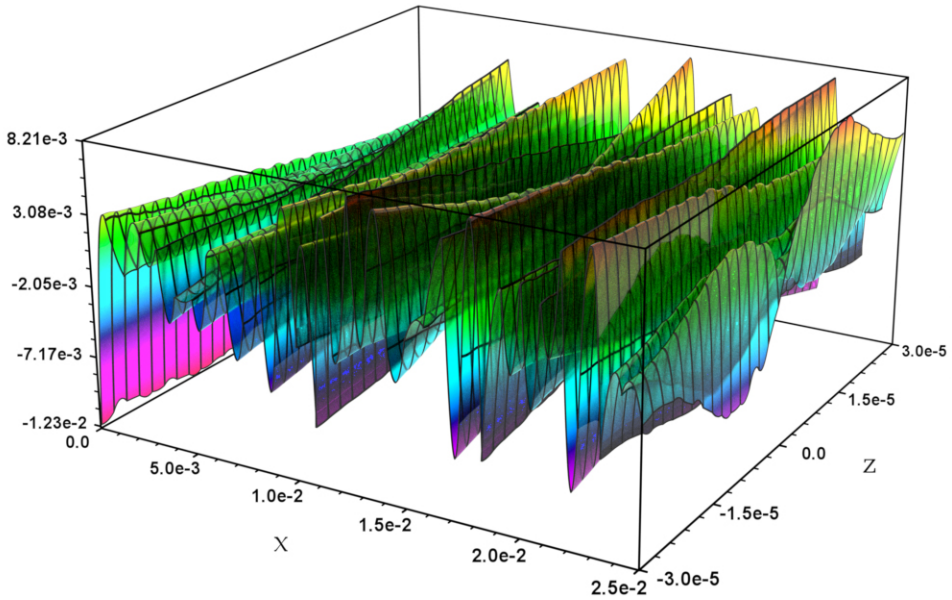

Figure 7.10: $\partial^2 w/\partial x \partial z$, with 30×30 elements.

APPENDICES

APPENDIX A

FINITE ELEMENT METHOD

The Finite Element Method (FEM) is a variational method [16]. The idea is that we have a situation where the best solution is the minimum of some function (or functional). This functional (a function of a function), for example, could be a measure of the energy of a system, where the function we are trying to find is the mechanical deformation of an elastic object. The idea of an energy can be applied very loosely, but in the end we are minimizing something to find the best approximate solution.

FEM is also a series solution. Instead of finding the exact analytical expression for a function, we can approximate it with a series of known (and simple) functions of our choosing. In the finite element method the known functions are almost always low-order polynomials of small support (meaning they are zero everywhere except in a small region which we call an element).

I will now show an example of a functional. Let's say we want to solve a very simple differential equation such as this second order equation in 1D, where the domain of interest is a line of length L, and f is a known function of x, called the source function.

$$\frac{\mathrm{d}^2 u}{\mathrm{d}x^2} + f = 0 \text{ for } x \in [0, L] \tag{A.1}$$

With the FEM, we need to specify boundary conditions to get any kind of solution. The simplest possible boundary condition is to have u equal zero everywhere on the boundary. In the one-dimensional case the boundary consists of the two points $x = 0$ and $x = L$.

If we have a functional, then to find the extremum(s) we set the first variation equal to zero. There are only certain kinds of differential equations and boundary conditions which will have an explicit functional. First of all, the orders of the derivatives must be

even, so you can have u, u'', u'''' and so on. For the FEM to work we don't need an explicit functional because there is an equivalence between the variational (or weak) formulation of the problem and the original differential (or strong) form. But, for the sake of getting a feel for the topology of the energy functional which we are trying to find the global minimum of, it is usually nice to get the functional in explicit form.

To get the functional, we start by multiplying our differential equation with the variation of our function, δu, and then integrating over the domain.

$$\int_0^L \delta u \left(\frac{\mathrm{d}^2 u}{\mathrm{d}x^2} + f \right) \mathrm{d}x = 0 \tag{A.2}$$

We can use the distributive property of derivatives to change the second order derivative into a first order derivative on u. This is called the weak form, since from a mathematical perspective, the required smoothness of the function u has been decreased. It is now alright for u to have a discontinuity, because there are no infinities. If you take the derivative of a discontinuity you get a delta function, which you can still integrate, but taking the derivative of a delta function is problematic.

$$\begin{aligned} &\int_0^L \left[\frac{\mathrm{d}}{\mathrm{d}x} \left(\delta u \frac{\mathrm{d}u}{\mathrm{d}x} \right) - \frac{\mathrm{d}\delta u}{\mathrm{d}x} \frac{\mathrm{d}u}{\mathrm{d}x} + (\delta u) f \right] \mathrm{d}x = 0 \\ &= \left[\delta u \frac{\mathrm{d}u}{\mathrm{d}x} \right]_0^L + \int_0^L \left[-\frac{\mathrm{d}\delta u}{\mathrm{d}x} \frac{\mathrm{d}u}{\mathrm{d}x} + (\delta u) f \right] \mathrm{d}x \end{aligned} \tag{A.3}$$

Here is where the boundary conditions come in. According to the term $\delta u \frac{\mathrm{d}u}{\mathrm{d}x}$, we should either specify u, so that $\delta u = 0$, or we should specify the derivative u'. In order to get a functional we need this term to equal zero. Therefore, if we don't say what u is at both endpoints, then its derivative needs to be zero at the endpoint where u is unspecified. This is only if we want an explicit functional.

$$\int_0^L \left[-\frac{\mathrm{d}\delta u}{\mathrm{d}x} \frac{\mathrm{d}u}{\mathrm{d}x} + (\delta u) f \right] \mathrm{d}x = 0 \tag{A.4}$$

Now we can "back out" the variation. We want to have the variation symbol out in front. Variations are like derivatives, except they only work on unknown functions. Since we know the function f, and it has no dependence on u, the variation of f is zero.

$$\delta \int_0^L \left[-\frac{1}{2}\left(\frac{\mathrm{d}u}{\mathrm{d}x}\right)^2 + uf \right] \mathrm{d}x = 0 \tag{A.5}$$

Now we have the functional, which is the integral

$$F = \int_0^L \left[-\frac{1}{2}\left(\frac{\mathrm{d}u}{\mathrm{d}x}\right)^2 + uf \right] \mathrm{d}x. \tag{A.6}$$

This kind of functional is called a quadratic functional, and its minimum is guaranteed to be equal to the solution of the original differential equation. Now we can move on to the finite element part of FEM. We want to represent our true solution u with a not-so-good series of simple functions. The simple functions are called basis functions, which I will represent with the letter ψ, where the i^{th} basis function is ψ_i.

$$u(x) \approx \sum_{i=1}^{N} c_j \psi_i(x) \tag{A.7}$$

We now substitute this expression into the functional, and we minimize it with respect to every unknown coefficient c_k.

$$\begin{aligned} F &= \int_0^L \left[-\frac{1}{2}\frac{\mathrm{d}}{\mathrm{d}x}\left(\sum_{i=1}^{N} c_i\psi_i\right)\frac{\mathrm{d}}{\mathrm{d}x}\left(\sum_{j=1}^{N} c_j\psi_j\right) + f\sum_{i=1}^{N} c_i\psi_i \right] \mathrm{d}x \\ &= \int_0^L \left[-\frac{1}{2}\left(\sum_{i=1}^{N} c_i\frac{\mathrm{d}\psi_i}{\mathrm{d}x}\right)\left(\sum_{j=1}^{N} c_j\frac{\mathrm{d}\psi_j}{\mathrm{d}x}\right) + f\sum_{i=1}^{N} c_i\psi_i \right] \mathrm{d}x \end{aligned} \tag{A.8}$$

In order to find an extremum of the functional with respect to the coefficients, we set the derivative with respect to each coefficient equal to zero. This gives a set a linear equations.

$$\frac{\partial F}{\partial c_k} = \int_0^L \left[-\frac{\mathrm{d}\psi_k}{\mathrm{d}x}\sum_{j=1}^{N} c_j\frac{\mathrm{d}\psi_j}{\mathrm{d}x} + f\psi_k \right] \mathrm{d}x = 0 \tag{A.9}$$

This can be written in terms of the matrix equation,

$$\sum_{j=1}^{N} c_j \int_0^L \frac{\mathrm{d}\psi_i}{\mathrm{d}x}\frac{\mathrm{d}\psi_j}{\mathrm{d}x}\,\mathrm{d}x = \int_0^L f\psi_i\,\mathrm{d}x, \tag{A.10}$$

or more compactly,

$$K \cdot \underset{\sim}{c} = \underset{\sim}{b}, \tag{A.11}$$

where

$$K_{ij} = \int_0^L \frac{\mathrm{d}\psi_i}{\mathrm{d}x}\frac{\mathrm{d}\psi_j}{\mathrm{d}x}\,\mathrm{d}x, \tag{A.12}$$

and

$$b_i = \int_0^L \psi_i f\,\mathrm{d}x. \tag{A.13}$$

To solve for the coefficients, we invert the matrix, which is often called the stiffness matrix in elasticity problems.

$$\underset{\sim}{c} = K^{-1} \cdot \underset{\sim}{b} \tag{A.14}$$

We can get this same set of equations from the step just before we got the functional, the second part of equation A.3. We just substitute in the series solution for u and δu, taking into account that δu is zero when u is specified on the boundary. Getting the functional and then minimizing it is not necessary in practice, but it is good for analysis. If the stiffness matrix is well behaved, then the coefficients can be solved using an iterative method, in which an initial guess is improved at each iteration until the solution converges. In this case, the matrix does not need to be explicitly inverted.

In one dimension, the boundary only consists of the two endpoints. In two dimensions, the boundary is a closed curve, and in three dimensions the boundary is a closed

surface. The boundary can be broken into different regions, where each region specifies a different type of boundary condition. For a second order differential equation, we would expect to have two types of boundary conditions, Dirichlet or Neumann. In the case of Poisson's equation, Dirichlet boundary conditions correspond with specifying the value of the primary variable on the boundary. Neumann boundary conditions correspond with specifying the value of the normal derivative on the boundary. If purely Neumann boundary conditions are used, then at least one nodal value of the primary variable should be specified, otherwise the solution could be shifted by an unknown amount. Figure A.1 shows an example of a two-dimensional domain with two types of boundary condition regions.

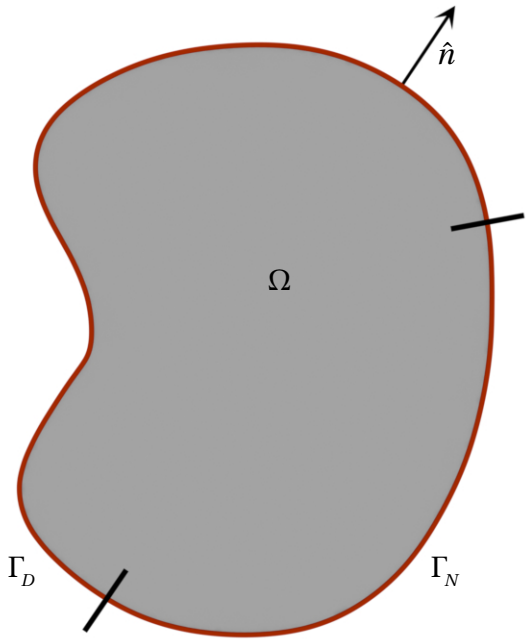

Figure A.1: An example domain Ω and boundary $\Gamma = \Gamma_D + \Gamma_N$.

Lagrange Finite Elements

Lagrange elements are some of the simplest elements. The most simple Lagrange element in one dimension is the hat function, which is composed of first order polynomials (lines). For each element, the basis function is equal to one at the node point, and equal to zero at its left and right neighbor nodes.

Figure A.2: A 1D mesh with six nodes.

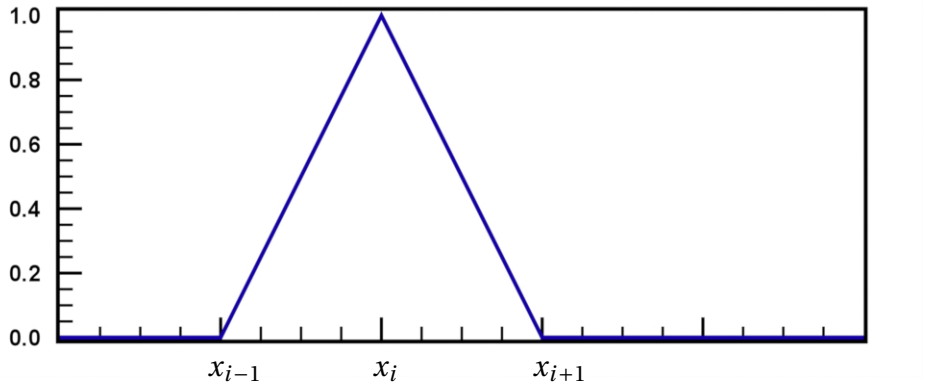

Figure A.3: A hat function, or first order Lagrange basis function.

A basic element is comprised of two nodes, and two basis functions. There is a distinction between a local element, and a global element. Strictly speaking, an element represents the support for a particular node. If I have a node at the point x_i, and if we are somewhere in the middle of our domain, then the element spans x_{i-1} to x_{i+1}. The basis function for the i^{th} node is the hat function that is equal to one at x_i, and zero at x_{i-1} and x_{i+1}. From the point of view of constructing the matrix equations, we would focus on the local element, with a partial basis function for the two nodes within the element. In one dimension, a global basis function ψ_i could at most be composed of two local

basis functions ψ_i^e. In two dimensions or higher, one node can belong to a lot of different neighboring elements. With a simple 2D grid, a non-boundary node will belong to 4 different elements.

$$\psi_i(\boldsymbol{x}) = \sum_e \psi_i^e(\boldsymbol{x}), \text{ where } e \text{ runs over all elements that node } i \text{ belongs to.} \tag{A.15}$$

The basis function must be smooth enough to represent the continuity requirement of the solution. In some cases, a first order basis is not adequate, and we must use second order (quadratic) polynomials. In this case, a local element would be comprised of three nodes, since we need three points to specify a quadratic function. A global element which is not on the edge of the domain would then have 5 nodes total.

A k^{th} order Lagrange element has $k+1$ nodes, with $k+1$ local basis functions. If the nodes within the element are located at positions x_j, then the basis functions have the following formula:

$$\psi_i(x) = \prod_{j=1, j\neq i}^{k+1} \frac{x - x_j}{x_i - x_j}. \tag{A.16}$$

For a linear Lagrange element that runs from 0 to h, the basis functions are as follows.

$$\psi_1(x) = \frac{h - x}{h} \tag{A.17}$$

$$\psi_2(x) = \frac{x}{h} \tag{A.18}$$

For a quadratic Lagrange element with node positions $\{0, h/2, h\}$ the basis functions are as follows.

$$\psi_1(x) = \frac{(h - 2x)(h - x)}{h^2} \tag{A.19}$$

$$\psi_2(x) = \frac{4x(h - x)}{h^2} \tag{A.20}$$

$$\psi_3(x) = \frac{x(2x-h)}{h^2} \tag{A.21}$$

The functions for interior nodes are called bubble functions. For quadratic elements, ψ_2 is a bubble function.

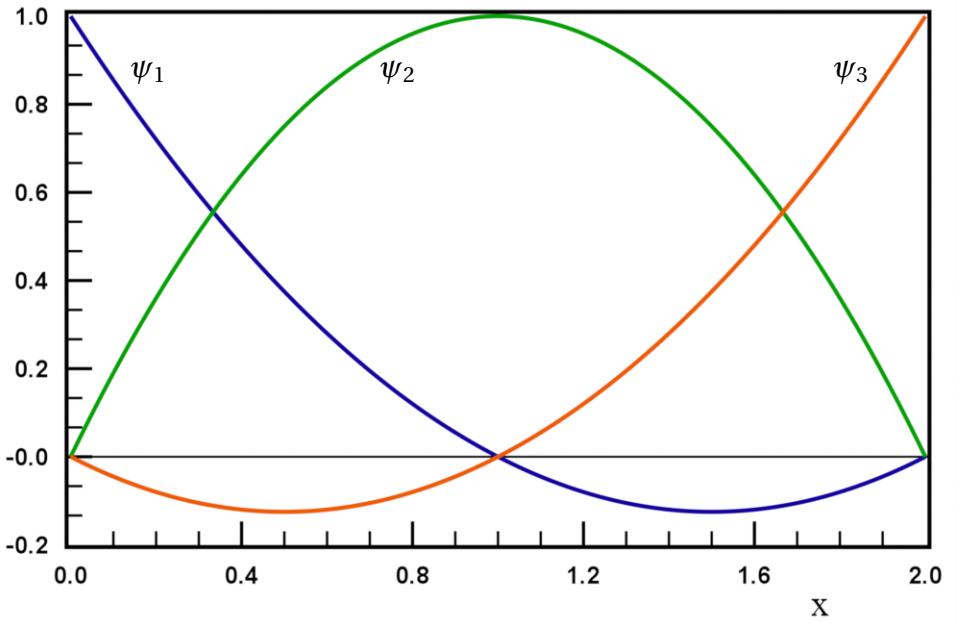

Figure A.4: Quadratic Lagrange basis functions.

When constructing basis functions for higher dimensions, the functions are simply the products of the one-dimensional functions.

Hermite Finite Elements

A characteristic of Lagrange elements is that they are used for interpolating a function $u(x)$ based on the values of u at all the node points r_i. There are other types of elements which use more information to interpolate $u(x)$, namely the values of the derivatives of u at each node. The Hermite element uses the value of the variable, and also its first derivative. In this section I will show how this type of element and other higher order elements (using higher derivatives) can be used to solve a second order equation

in one dimension. I will then give a more in-depth treatment for two-dimensional elements.

Let's say we want to solve the Poisson equation. The source function is the known function $f(x)$. If $f = 0$ then we get Laplace's equation.

$$-\frac{\partial^2 u}{\partial x^2} = f(x) \text{ for } x \in [0, L] \tag{A.22}$$

The weak form is

$$\int_0^L \left[-\frac{\partial \delta u}{\partial x}\frac{\partial u}{\partial x} + (\delta u) f \right] \mathrm{d}x + \left[\delta u \frac{\partial u}{\partial x} \right]_0^L = 0. \tag{A.23}$$

If we use the Hermite elements, then our interpolation will have two types of terms. The basis function for u_i is denoted by ψ_i, and the basis function for $u_i^x \equiv \frac{\partial u_i}{\partial x}$ is denoted by ψ_i^x.

$$u(x) \approx \sum_{j=1}^{N} \left[u_j \psi_j(x) + u_j^x \psi_j^x(x) \right] \tag{A.24}$$

$$\delta u(x) \approx \sum_{i=1}^{N} \left[\delta u_i \psi_i(x) + \delta u_i^x \psi_i^x(x) \right] \tag{A.25}$$

The Hermite interpolation is then substituted for u and δu in the weak form.

$$\begin{aligned} \sum_{i=1}^{N} \Bigg\{ \int_0^L \Bigg[& -\sum_{j=1}^{N} \left(\delta u_i \frac{\partial \psi_i}{\partial x} + \delta u_i^x \frac{\partial \psi_i^x}{\partial x} \right) \left(u_j \frac{\partial \psi_j}{\partial x} + u_j^x \frac{\partial \psi_j^x}{\partial x} \right) \\ & + \left(\delta u_i \psi_i + \delta u_i^x \psi_i^x \right) f \Bigg] \mathrm{d}x \\ & + \sum_{j=1}^{N} \left[\left(\delta u_i \psi_i + \delta u_i^x \psi_i^x \right) \left(u_j \frac{\partial \psi_j}{\partial x} + u_j^x \frac{\partial \psi_j^x}{\partial x} \right) \right]_0^L \Bigg\} = 0 \end{aligned} \tag{A.26}$$

All of the variations are independent from each other. For each value of i, we have a term which is multiplied by δu_i, and another term which is multiplied by δu_i^x. Both

terms are independently equal to zero.

$$\delta u_i \left\{ \int_0^L \left[-\sum_{j=1}^{N} \frac{\partial \psi_i}{\partial x} \left(u_j \frac{\partial \psi_j}{\partial x} + u_j^x \frac{\partial \psi_j^x}{\partial x} \right) + \psi_i f \right] \mathrm{d}x + \sum_{j=1}^{N} \left[\psi_i \left(u_j \frac{\partial \psi_j}{\partial x} + u_j^x \frac{\partial \psi_j^x}{\partial x} \right) \right]_0^L \right\} = 0 \tag{A.27}$$

$$\delta u_i^x \left\{ \int_0^L \left[-\sum_{j=1}^{N} \frac{\partial \psi_i^x}{\partial x} \left(u_j \frac{\partial \psi_j}{\partial x} + u_j^x \frac{\partial \psi_j^x}{\partial x} \right) + \psi_i^x f \right] \mathrm{d}x + \sum_{j=1}^{N} \left[\psi_i^x \left(u_j \frac{\partial \psi_j}{\partial x} + u_j^x \frac{\partial \psi_j^x}{\partial x} \right) \right]_0^L \right\} = 0 \tag{A.28}$$

A basic requirement of the finite element method is that in the interior of the domain, all variables are unknown. We can only specify the values of variables on the boundary. If we specify the value of the variable u at a certain node i, then δu_i will equal zero. If we specify u_i^x, then δu_i^x will equal zero. This is true for all degrees of freedom.

If u_i or u_i^x are unknown, then their respective variations will be an unknown value, not necessarily equal to zero. Since equations A.27 and A.28 are equal to zero regardless of the values of the variations, the terms themselves must equal zero when the variations are unknown (when the variables are unknown).

$$\int_0^L \left[-\sum_{j=1}^{N} \frac{\partial \psi_i}{\partial x} \left(u_j \frac{\partial \psi_j}{\partial x} + u_j^x \frac{\partial \psi_j^x}{\partial x} \right) + \psi_i f \right] \mathrm{d}x + \sum_{j=1}^{N} \left[\psi_i \left(u_j \frac{\partial \psi_j}{\partial x} + u_j^x \frac{\partial \psi_j^x}{\partial x} \right) \right]_0^L = 0 \tag{A.29}$$

$$\int_0^L \left[-\sum_{j=1}^{N} \frac{\partial \psi_i^x}{\partial x} \left(u_j \frac{\partial \psi_j}{\partial x} + u_j^x \frac{\partial \psi_j^x}{\partial x} \right) + \psi_i^x f \right] \mathrm{d}x + \sum_{j=1}^{N} \left[\psi_i^x \left(u_j \frac{\partial \psi_j}{\partial x} + u_j^x \frac{\partial \psi_j^x}{\partial x} \right) \right]_0^L = 0 \tag{A.30}$$

These are the general finite element equations for solving the one-dimensional the Poisson equation with Hermite elements. We can simplify the equations a little bit by taking a good look at the boundary terms. If i is an interior node, then ψ_i and ψ_i^x will equal zero on the boundary. Therefore, the boundary terms will be zero for all interior nodes. This is true because of a requirement on the basis functions themselves, which is explained in the section below on calculating the basis functions.

If i is a boundary node, then the situation is more interesting. ψ_i is equal to one at node i, but ψ_i^x is equal to zero. It just so happens that in one dimension, the boundary consists of node points alone, and the basis functions for the derivatives will always equal zero at node points. The only boundary term which is possibly non-zero is the boundary term in equation A.29 when u_i is unknown and on the boundary. It is also the case that the derivative of the basis functions for u are also zero at all node points, so that term can also be discarded. We therefore have the following possibilities.

For i an interior node,

$$\int_0^L \left[-\sum_{j=1}^{N} \frac{\partial \psi_i}{\partial x} \left(u_j \frac{\partial \psi_j}{\partial x} + u_j^x \frac{\partial \psi_j^x}{\partial x} \right) + \psi_i f \right] \mathrm{d}x = 0. \tag{A.31}$$

If i is a boundary node, and u_i is unknown,

$$\int_0^L \left[-\sum_{j=1}^{N} \frac{\partial \psi_i}{\partial x} \left(u_j \frac{\partial \psi_j}{\partial x} + u_j^x \frac{\partial \psi_j^x}{\partial x} \right) + \psi_i f \right] \mathrm{d}x + \sum_{j=1}^{N} u_j^x \left[\psi_i \frac{\partial \psi_j^x}{\partial x} \right]_0^L = 0. \tag{A.32}$$

For i either an interior or boundary node,

$$\int_0^L \left[-\sum_{j=1}^{N} \frac{\partial \psi_i^x}{\partial x} \left(u_j \frac{\partial \psi_j}{\partial x} + u_j^x \frac{\partial \psi_j^x}{\partial x} \right) + \psi_i^x f \right] \mathrm{d}x = 0. \tag{A.33}$$

Since we are solving a second order equation, we usually either specify u or its derivative on the boundary. For the sake of simplicity, I will assume that to be the case.

Therefore, if we don't specify u_i on the boundary, then we will specify u_i^x. With this in mind, I can write the previous equations in a matrix format, with unknown values on the left-hand side, and known values on the right.

For i an interior node,

$$\sum_{j=1}^{N} u_j \int_0^L \frac{\partial \psi_i}{\partial x}\frac{\partial \psi_j}{\partial x}\,\mathrm{d}x + \sum_{j=1}^{N} u_j^x \int_0^L \frac{\partial \psi_i}{\partial x}\frac{\partial \psi_j^x}{\partial x}\,\mathrm{d}x = \int_0^L \psi_i f\,\mathrm{d}x. \tag{A.34}$$

If i is a boundary node, and u_i is unknown,

$$\begin{aligned}&\sum_{j=1}^{N} u_j \int_0^L \frac{\partial \psi_i}{\partial x}\frac{\partial \psi_j}{\partial x}\,\mathrm{d}x + \sum_{j=1}^{N} u_j^x \int_0^L \frac{\partial \psi_i}{\partial x}\frac{\partial \psi_j^x}{\partial x}\,\mathrm{d}x \\ &= \int_0^L \psi_i f\,\mathrm{d}x + \left(u_i^x \text{ if } x = L, \text{ or } -u_i^x \text{ if } x = 0\right)\end{aligned} \tag{A.35}$$

For i either an interior or boundary node,

$$\sum_{j=1}^{N} u_j \int_0^L \frac{\partial \psi_i^x}{\partial x}\frac{\partial \psi_j}{\partial x}\,\mathrm{d}x + \sum_{j=1}^{N} u_j^x \int_0^L \frac{\partial \psi_i^x}{\partial x}\frac{\partial \psi_j^x}{\partial x}\,\mathrm{d}x = \int_0^L \psi_i^x f\,\mathrm{d}x. \tag{A.36}$$

As far as implementation is concerned, there is no reason to treat the various types of degrees of freedom differently from each other. Instead of having a set of u_i and another set of u_i^x, we can have one large set of degrees of freedom a_i. We would have one big set of basis functions ψ_i corresponding to a_i, and each degree of freedom would get a unique node number. When assembling the stiffness matrix and load vector, we would start with the following construction:

$$\sum_{j=1}^{N_{\mathrm{DOF}}} a_j \left[\int_0^L \frac{\partial \psi_i}{\partial x}\frac{\partial \psi_j}{\partial x}\,\mathrm{d}x - \left[\psi_i \frac{\partial \psi_j}{\partial x}\right]_0^L\right] = \int_0^L \psi_i f\,\mathrm{d}x, \tag{A.37}$$

or

$$\sum_{j=1}^{N_{\mathrm{DOF}}} K_{ij} a_j = b_i, \tag{A.38}$$

where

$$K_{ij} = \int_0^L \frac{\partial \psi_i}{\partial x} \frac{\partial \psi_j}{\partial x} \, \mathrm{d}x - \left[\psi_i \frac{\partial \psi_j}{\partial x} \right]_0^L, \tag{A.39}$$

and

$$b_i = \int_0^L \psi_i f \, \mathrm{d}x. \tag{A.40}$$

In this case $N_{\mathrm{DOF}} = 2N$. After constructing K_{ij} and b_i, we would loop through the set of known boundary values and take the corresponding columns in the stiffness matrix, multiply them by the known values, and subtract that from the load vector. If we specify a specific value u_i, then the i^{th} column from K times u_i is subtracted from $\underset{\sim}{b}$. Since u_i is not an unknown, it does not need to be solved for, and its corresponding row and column are removed from the stiffness matrix, as is b_i. If we know N_b values, then the dimension of K is reduced from $N_{\mathrm{DOF}} \times N_{\mathrm{DOF}}$ to $(N_{\mathrm{DOF}} - N_b) \times (N_{\mathrm{DOF}} - N_b)$, and the length of $\underset{\sim}{b}$ is reduced to $N_{\mathrm{DOF}} - N_b$. This method automatically takes care of the boundary integrals. Most of the boundary integrals will be zero, but we don't need to know which ones. For two-dimensional elements, the boundary integrals become more complicated, and it becomes essential that the assembly algorithm takes care of all the boundary terms automatically.

As an example, let's say we have four nodes ($N = 4$), and we have eight degrees of freedom ($N_{\mathrm{DOF}} = 8$). We would start with the following construction:

$$\begin{bmatrix} k_{11} & k_{12} & k_{13} & k_{14} & k_{15} & k_{16} & k_{17} & k_{18} \\ k_{21} & k_{22} & k_{23} & k_{24} & k_{25} & k_{26} & k_{27} & k_{28} \\ k_{31} & k_{32} & k_{33} & k_{34} & k_{35} & k_{36} & k_{37} & k_{38} \\ k_{41} & k_{42} & k_{43} & k_{44} & k_{45} & k_{46} & k_{47} & k_{48} \\ k_{51} & k_{52} & k_{53} & k_{54} & k_{55} & k_{56} & k_{57} & k_{58} \\ k_{61} & k_{62} & k_{63} & k_{64} & k_{65} & k_{66} & k_{67} & k_{68} \\ k_{71} & k_{72} & k_{73} & k_{74} & k_{75} & k_{76} & k_{77} & k_{78} \\ k_{81} & k_{82} & k_{83} & k_{84} & k_{85} & k_{86} & k_{87} & k_{88} \end{bmatrix} \cdot \begin{bmatrix} a_1 \\ a_2 \\ a_3 \\ a_4 \\ a_5 \\ a_6 \\ a_7 \\ a_8 \end{bmatrix} = \begin{bmatrix} b_1 \\ b_2 \\ b_3 \\ b_4 \\ b_5 \\ b_6 \\ b_7 \\ b_8 \end{bmatrix}. \tag{A.41}$$

If we have Dirichlet boundary conditions, where u_1 and u_4 are specified, then we would end up with the following final matrix equation:

$$\begin{bmatrix} k_{22} & k_{23} & k_{25} & k_{26} & k_{27} & k_{28} \\ k_{32} & k_{33} & k_{35} & k_{36} & k_{37} & k_{38} \\ k_{52} & k_{53} & k_{55} & k_{56} & k_{57} & k_{58} \\ k_{62} & k_{63} & k_{65} & k_{66} & k_{67} & k_{68} \\ k_{72} & k_{73} & k_{75} & k_{76} & k_{77} & k_{78} \\ k_{82} & k_{83} & k_{85} & k_{86} & k_{87} & k_{88} \end{bmatrix} \cdot \begin{bmatrix} a_2 \\ a_3 \\ a_5 \\ a_6 \\ a_7 \\ a_8 \end{bmatrix} = \begin{bmatrix} b_2 - k_{21}a_1 - k_{24}a_4 \\ b_3 - k_{31}a_1 - k_{34}a_4 \\ b_5 - k_{51}a_1 - k_{54}a_4 \\ b_6 - k_{61}a_1 - k_{64}a_4 \\ b_7 - k_{71}a_1 - k_{74}a_4 \\ b_8 - k_{81}a_1 - k_{84}a_4 \end{bmatrix}. \tag{A.42}$$

In order to determine our unknown values ($\{a_2, a_3, a_5, a_6, a_7, a_8\}$ which correspond to $\{u_2, u_3, u_1', u_2', u_3', u_4'\}$), we would only have to invert the final K matrix, and multiply that by our final $\underset{\sim}{b}$ vector.

Calculating the 1D Hermite Basis Functions

The Hermite basis functions are cubic polynomials in x in one dimension. The set of polynomials (the space) which will make up the basis functions is

$$Q = \{1, x, x^2, x^3\}. \tag{A.43}$$

Each basis function ψ_i is equal to Q times a coefficient vector C_i.

$$\psi_i(x) = Q \cdot C_i = c_{i1} + c_{i2}x + c_{i3}x^2 + c_{i4}x^3 \tag{A.44}$$

In order to determine these coefficients, we need four equations. A Hermite element consists of two nodes with two degrees of freedom each, for a total of four degrees of freedom. Although there are two nodes as far as position is concerned, in terms of degrees of freedom, we can treat the element as having four separate nodes. A node, then, will be defined by both position and the degree of freedom it represents.

We have two types of degrees of freedom, the Lagrange DOF, which is just the value of our function u, and also the first derivative $\partial u/\partial x$. As with all Lagrange degrees of freedom, the basis function is required to equal one at its respective node, and equal zero at all the other nodes within the element. For the Hermite type degrees of freedom (the derivatives), the respective derivative of the basis function has the same requirements as the Lagrange basis functions. For a basis function ψ_i which represents a particular derivative, which we can represent as an operator L_i, the requirement on the basis function is that $L_i\psi_i$ equal one at the node r_i, and equal zero at all other nodes r_j. This can be represented compactly as

$$\left(L_j\psi_i\right)\left(r_j\right) = \delta_{ij}, \tag{A.45}$$

where δ_{ij} is equal to one if i equals j, and is equal to zero otherwise.

Since $\psi_i = Q \cdot C_i$, we have

$$\left[\left(L_j Q\right)\left(r_j\right)\right] \cdot C_i = \delta_{ij}. \tag{A.46}$$

Each value of i gives a row in a matrix, which when inverted gives us all the coefficients, since the right hand side becomes the identity matrix. If we order the degrees of freedom as $\left\{u(0), u(h), u'(0), u'(h)\right\}$ so that the node positions are $\{0, h, 0, h\}$ and the operators are $\{1, 1, \partial/\partial x, \partial/\partial x\}$, then for the one-dimensional Hermite element we have

$$Q(0) = \{1, 0, 0, 0\} \tag{A.47}$$

$$Q(h) = \left\{1, h, h^2, h^3\right\} \tag{A.48}$$

$$\frac{\partial Q}{\partial x}(0) = \{0, 1, 0, 0\} \tag{A.49}$$

$$\frac{\partial Q}{\partial x}(h) = \left\{0, 1, 2h, 3h^2\right\}. \tag{A.50}$$

The final matrix equation reads

$$\begin{bmatrix} 1 & 0 & 0 & 0 \\ 1 & h & h^2 & h^3 \\ 0 & 1 & 0 & 0 \\ 0 & 1 & 2h & 3h^2 \end{bmatrix} \cdot \begin{bmatrix} c_{11} & c_{21} & c_{31} & c_{41} \\ c_{12} & c_{22} & c_{32} & c_{42} \\ c_{13} & c_{23} & c_{33} & c_{43} \\ c_{14} & c_{24} & c_{34} & c_{44} \end{bmatrix} = \begin{bmatrix} 1 & 0 & 0 & 0 \\ 0 & 1 & 0 & 0 \\ 0 & 0 & 1 & 0 \\ 0 & 0 & 0 & 1 \end{bmatrix}, \tag{A.51}$$

and the solution is

$$\begin{bmatrix} c_{11} & c_{21} & c_{31} & c_{41} \\ c_{12} & c_{22} & c_{32} & c_{42} \\ c_{13} & c_{23} & c_{33} & c_{43} \\ c_{14} & c_{24} & c_{34} & c_{44} \end{bmatrix} = \frac{1}{h^3} \begin{bmatrix} h^3 & 0 & 0 & 0 \\ 0 & 0 & h^3 & 0 \\ -3h & 3h & -2h^2 & -h^2 \\ 2 & -2 & h & h \end{bmatrix}. \tag{A.52}$$

We now know the four basis functions.

$$\psi_1 = 1 - \frac{3x^2}{h^2} + \frac{2x^3}{h^3} \tag{A.53}$$

$$\psi_2 = \frac{3x^2}{h^2} - \frac{2x^3}{h^3} \tag{A.54}$$

$$\psi_3 = x - \frac{2x^2}{h} + \frac{x^3}{h^2} \tag{A.55}$$

$$\psi_4 = -\frac{x^2}{h} + \frac{x^3}{h^2} \tag{A.56}$$

The basis functions and their derivatives are shown below for $h = 2$.

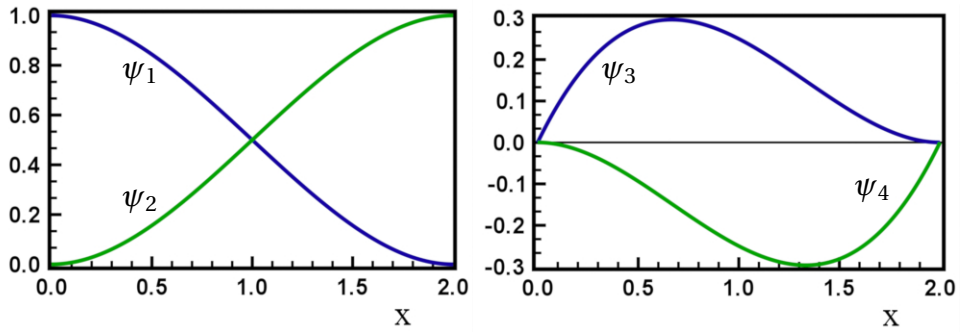

Figure A.5: The local 1D Hermite basis functions.

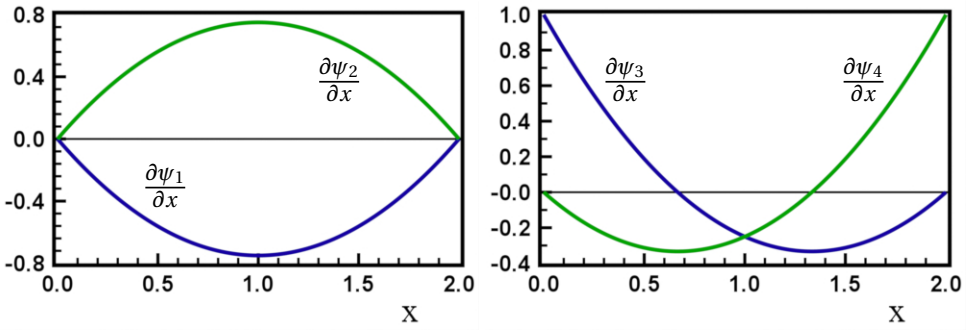

Figure A.6: Derivatives of the local 1D Hermite basis functions.

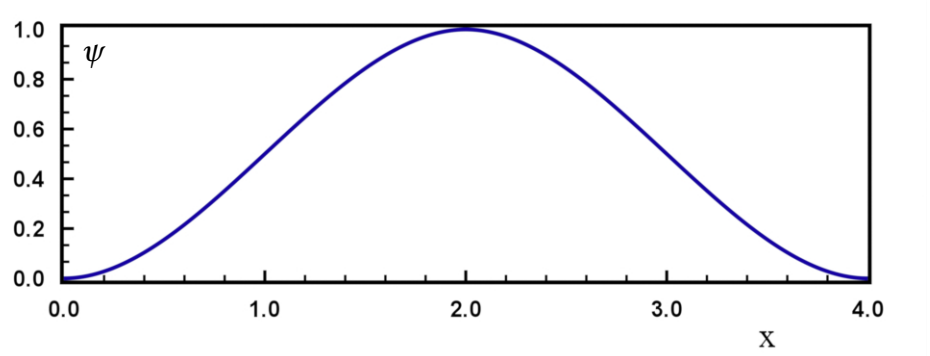

Figure A.7: The global 1D Hermite basis function for u.

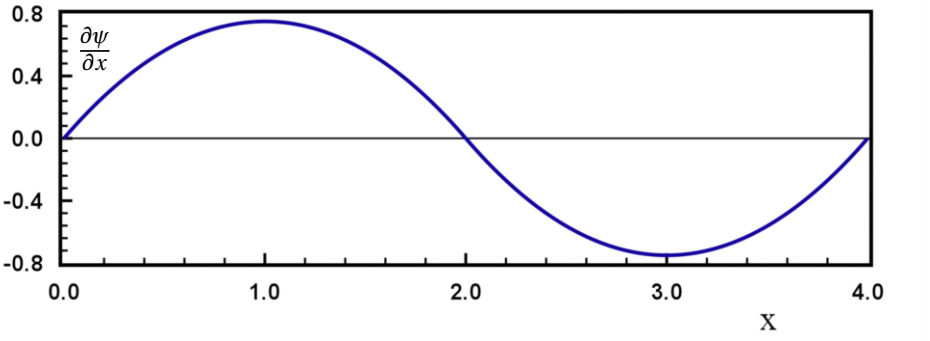

Figure A.8: The derivative of the global 1D Hermite basis function for u.

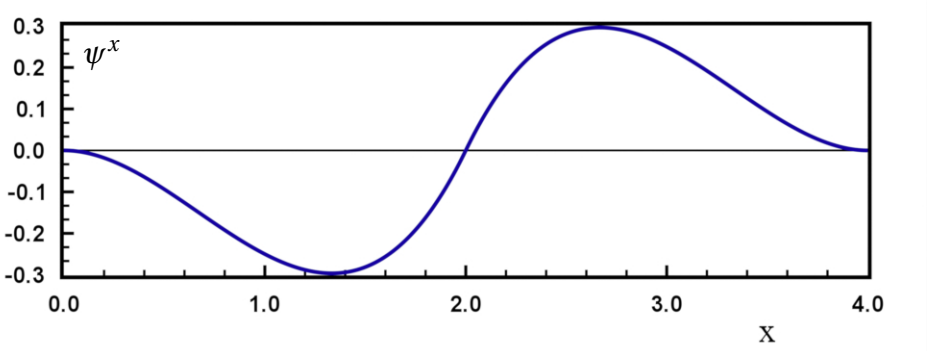

Figure A.9: The global 1D Hermite basis function for $\partial u/\partial x$.

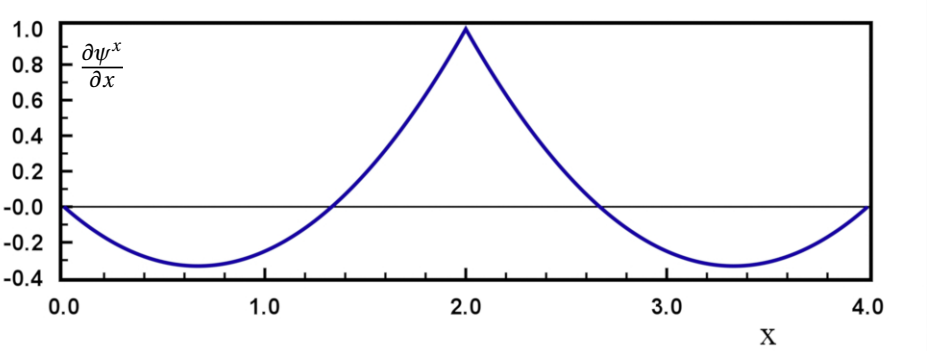

Figure A.10: The derivative of the global 1D Hermite basis function for $\partial u/\partial x$.

Example

Solve the Poisson equation for the test function $u(x) = \sin(2\pi x + \pi/5)$ with a Dirichlet boundary condition at $x = 0$ and a Neumann boundary condition at $x = 1$.

$$-\frac{\partial^2 u}{\partial x^2} = 4\pi^2 \sin(2\pi x + \pi/5) \text{ for } x \in [0,1] \tag{A.57}$$

$$u(0) = \sin(\pi/5) \tag{A.58}$$

$$\frac{\partial u}{\partial x}(1) = 2\pi \cos(\pi/5) \tag{A.59}$$

Since this is a one-dimensional problem, the domain will be a line, and the mesh will be a series of segments with two nodes each. Each node will represent two degrees

of freedom, u and $\frac{\partial u}{\partial x}$. The boundary will be the two end points. In the diagram below, a Lagrange degree of freedom is represented by a dot, and the first derivative is represented by a ring.

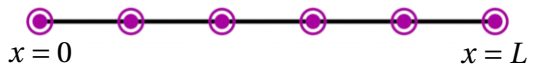

Figure A.11: A 1D Hermite mesh with six nodes.

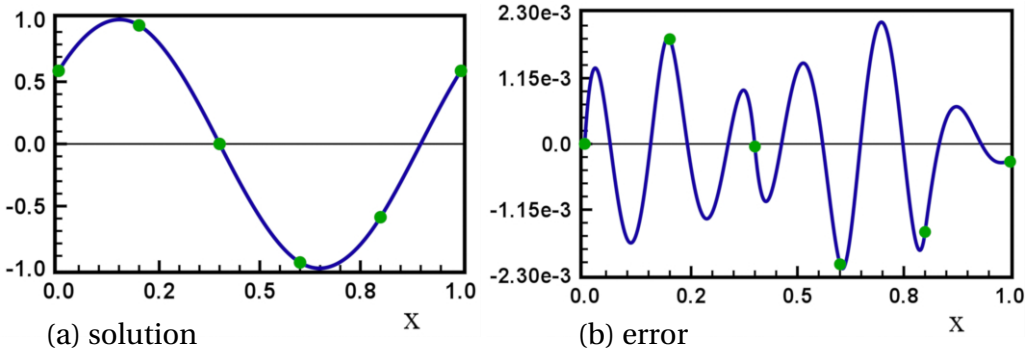

(a) solution (b) error

Figure A.12: The solution for u. The dots are the nodal values.

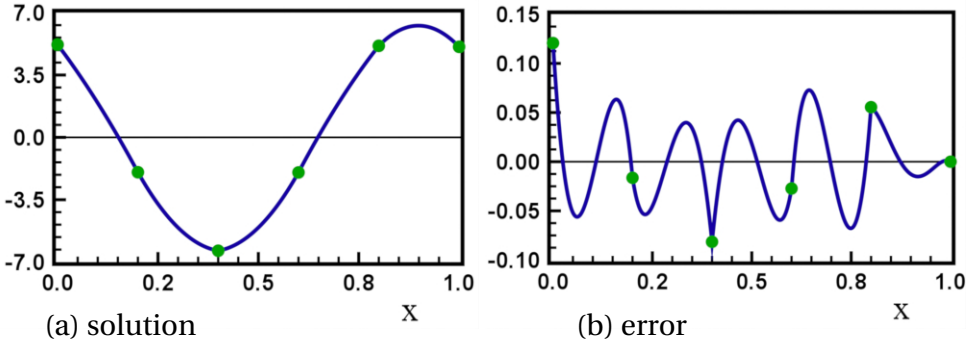

(a) solution (b) error

Figure A.13: The solution for $\partial u/\partial x$. The dots are the nodal values.

2D Hermite Element

The two-dimensional Hermite element is a four-node rectangular element with 16 degrees of freedom. It is also known as the Bogner-Fox-Schmidt rectangle [11]. It has C^1 continuity, meaning it is continuous and smooth across neighboring elements. The degrees of freedom at each node are

$$\Sigma = \left\{ u, \frac{\partial u}{\partial x}, \frac{\partial u}{\partial y}, \frac{\partial^2 u}{\partial x \partial y} \right\}. \tag{A.60}$$

In this section I will go into detail about the use of these type of elements for solving second order equations. It is generally ill advised to use higher order basis functions to solve lower order problems. This is for the simple reason that without a priori knowledge of the smoothness of the solution, it is possible that the solution will have a lower smoothness than the basis functions. For example, a second order equation admits a C^0 solution which is continuous but not smooth everywhere, such as a piecewise linear function, or a function which has two regions where there is a discontinuity in the first derivative across the boundary between the two regions. That being said, there are ways around these situations, and there are plenty of problems where it is known that the solution is smooth. In the worst case scenario, there is going to be an error at the discontinuity, such as a large oscillation, and a very fine mesh will be needed to converge to the correct solution in the rest of the domain.

As an example second order equation, I will solve the Poisson equation:

$$-\nabla^2 u + f(x, y) = 0, \tag{A.61}$$

where the weak form is

$$\int_\Omega \left[-\boldsymbol{\nabla} \delta u \cdot \boldsymbol{\nabla} u + (\delta u) f \right] \mathrm{d}x + \oint_\Gamma \delta u \frac{\partial u}{\partial n} \mathrm{d}\Gamma = 0. \tag{A.62}$$

The exact nature of the boundary integral needs to be clarified. When converting the differential equation into the weak form, we got the term which was destined to become the boundary integral,

$$\int_\Omega \boldsymbol{\nabla} \cdot (\delta u \boldsymbol{\nabla} u)\, \mathrm{d}\Omega. \tag{A.63}$$

This is the flux through the surface. It can be converted into a line integral using Green's theorem in the plane, which is a special case of the generalized Stokes' theorem, which states that

$$\int_\Omega \left(\frac{\partial Q}{\partial x} - \frac{\partial P}{\partial y} \right) \mathrm{d}x\, \mathrm{d}y = \oint_\Gamma \left(P\, \mathrm{d}x + Q\, \mathrm{d}y \right). \tag{A.64}$$

For our boundary term,

$$Q = \delta u \frac{\partial u}{\partial x}, \tag{A.65}$$

and

$$P = -\delta u \frac{\partial u}{\partial y}. \tag{A.66}$$

We therefore have

$$\int_\Omega \boldsymbol{\nabla} \cdot (\delta u \boldsymbol{\nabla} u)\, \mathrm{d}\Omega = \oint_\Gamma \delta u \left(-\frac{\partial u}{\partial y}\, \mathrm{d}x + \frac{\partial u}{\partial x}\, \mathrm{d}y \right). \tag{A.67}$$

This integral can be represented as

$$\int_\Gamma \delta u \frac{\partial u}{\partial n} \mathrm{d}\Gamma, \tag{A.68}$$

where $\mathrm{d}\Gamma$ is the path-length element counterclockwise around the outside of the domain.

The finite element equations are

$$\sum_{j=1}^{N_{\mathrm{DOF}}} a_j \left[\int_\Omega \boldsymbol{\nabla}\psi_i \cdot \boldsymbol{\nabla}\psi_j\, \mathrm{d}\Omega - \oint_\Gamma \psi_i \left(-\frac{\partial \psi_j}{\partial y}\, \mathrm{d}x + \frac{\partial \psi_j}{\partial x}\, \mathrm{d}y \right) \right] = \int_\Omega \psi_i f\, \mathrm{d}\Omega. \tag{A.69}$$

In the one-dimensional case, when we had Dirichlet boundary conditions and u was specified everywhere on the boundary, the boundary integrals could be neglected. That was because the boundary consisted of nodes and all the derivative basis functions are equal to zero at nodes. In higher dimensions, however, the boundary will consist of curves, and now there will be non-zero boundary integrals. It is essential that these terms are not neglected.

When solving a second order equation, we usually supply u, or a combination of first derivatives on the boundary. With the Hermite square elements we have a mixed second derivative as a degree of freedom, which will remain unspecified on the boundary. Even if we were solving a fourth order equation, the second derivative would still be free on the boundary. This situation is more extreme with higher order elements, such as the Argyris triangle. Since a certain number of unknowns will be free on the boundary, they will be treated similarly to unknown nodal values in the interior. The only difference is that the stiffness matrix will be modified by the boundary integrals for those elements which reside along the boundary. As far as the formulation is concerned, the extra degrees of freedom on the boundary are no different than any other type of unknown nodal value.

Calculating the 2D Hermite Basis Functions

The basis functions are bicubic. They are equal to products of the one-dimensional basis functions.

$$\psi(x,y) = \psi(x)\psi(y) \tag{A.70}$$

$$\psi^x(x,y) = \psi^x(x)\psi(y) \tag{A.71}$$

$$\psi^y(x,y) = \psi(x)\psi^y(y) \tag{A.72}$$

$$\psi^{xy}(x,y) = \psi^x(x)\psi^y(y) \tag{A.73}$$

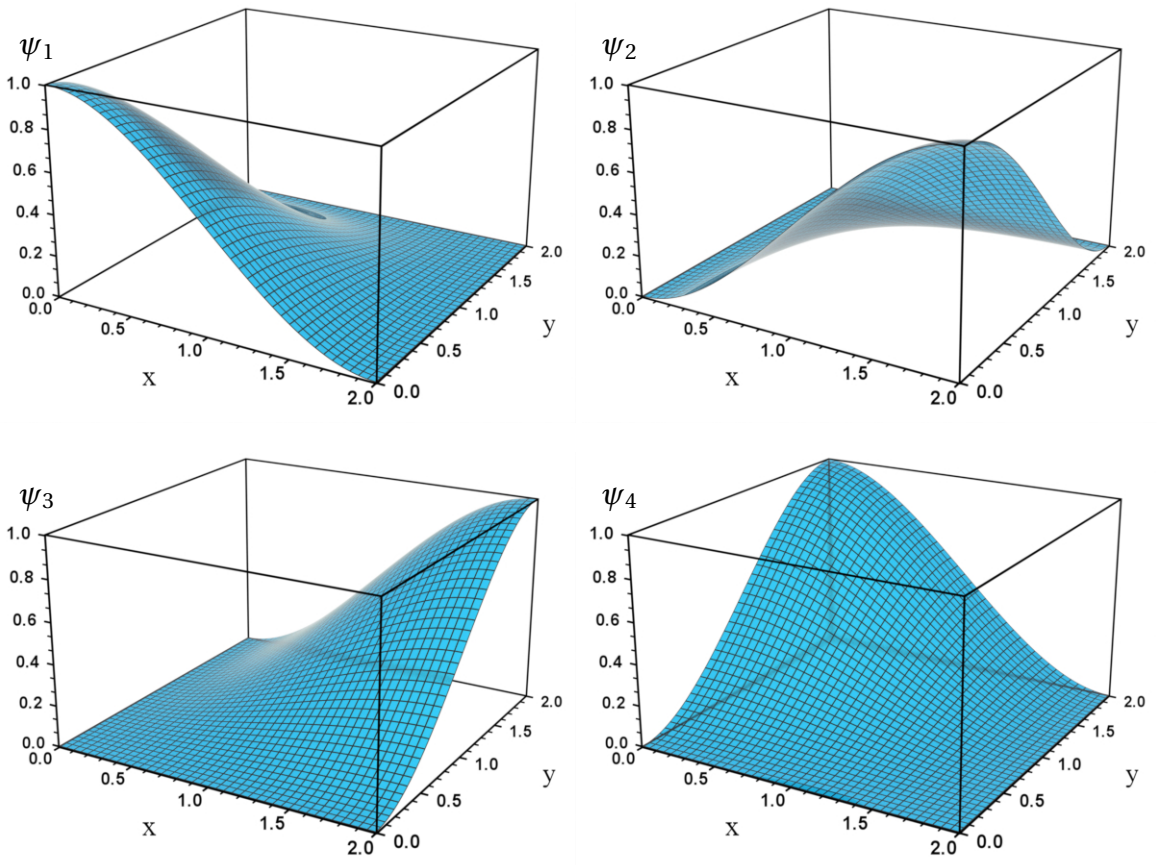

Figure A.14: The local 2D Hermite basis functions for u.

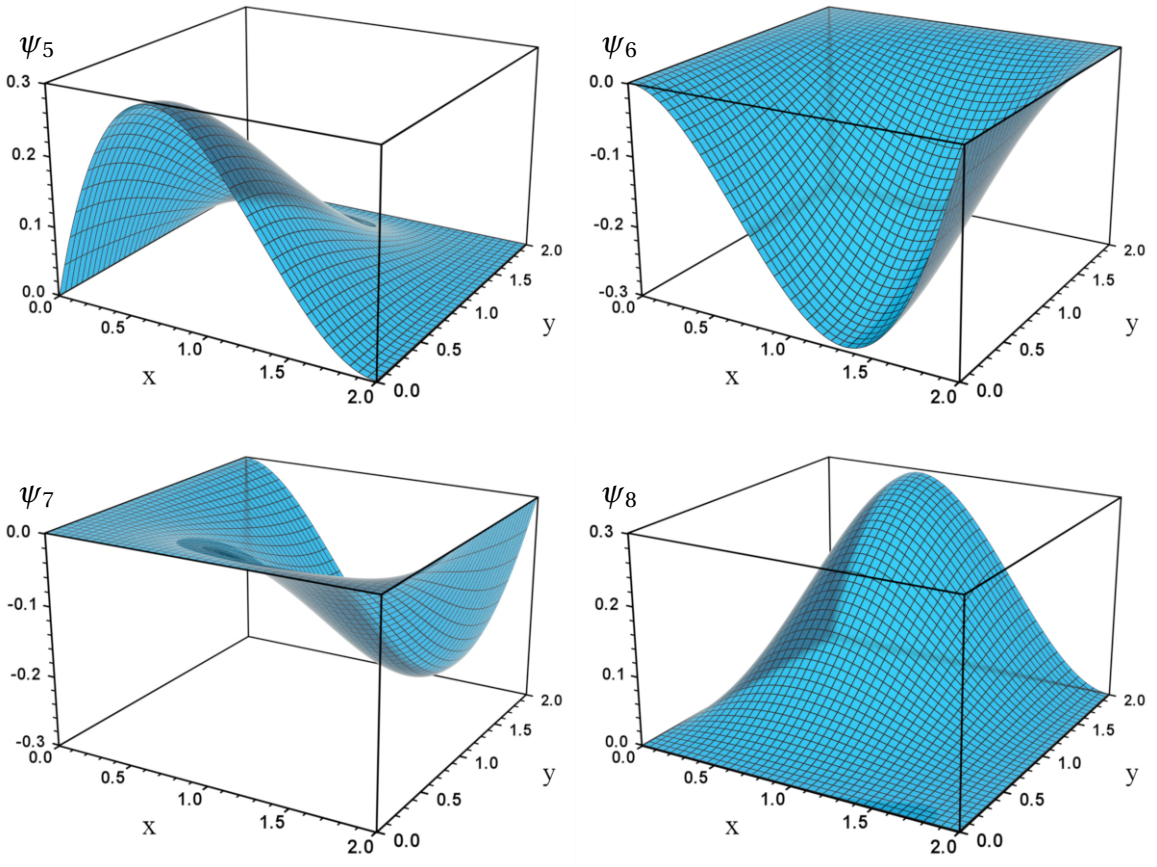

Figure A.15: The local 2D Hermite basis functions for $\partial u/\partial x$.

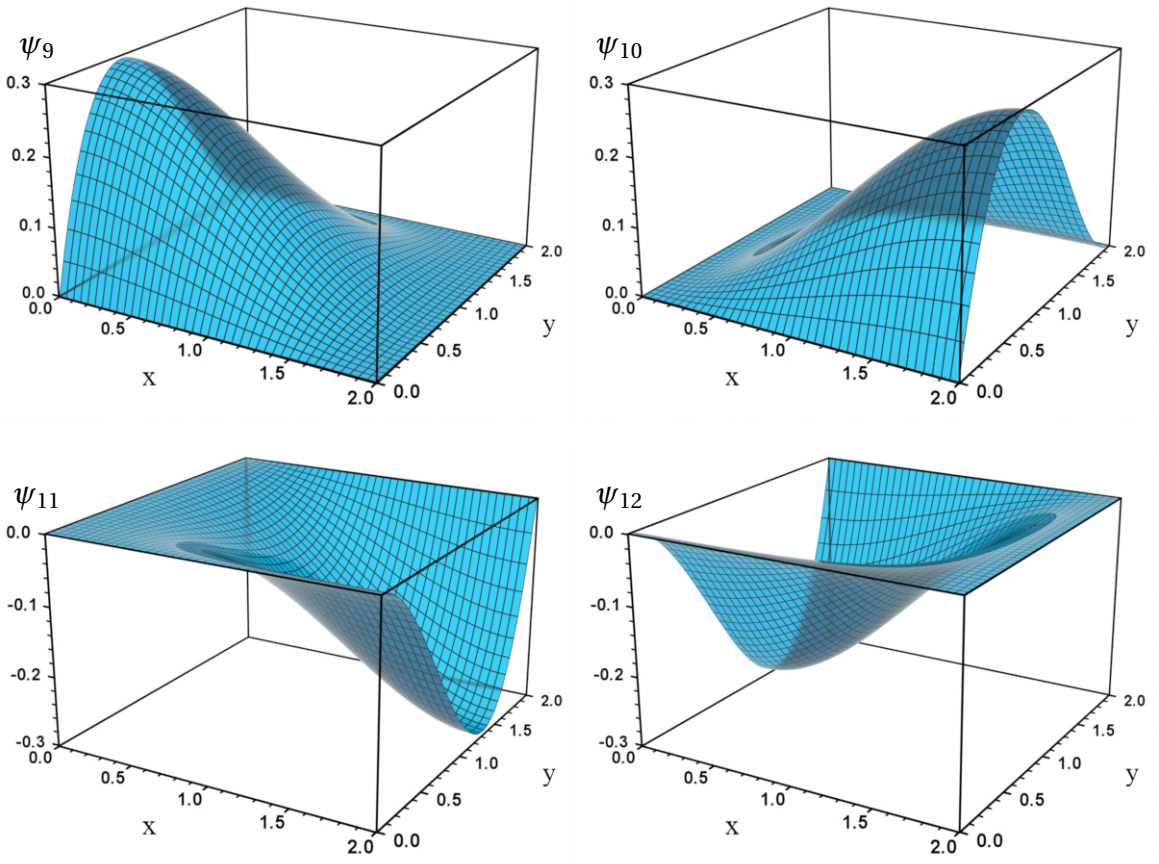

Figure A.16: The local 2D Hermite basis functions for $\partial u/\partial y$.

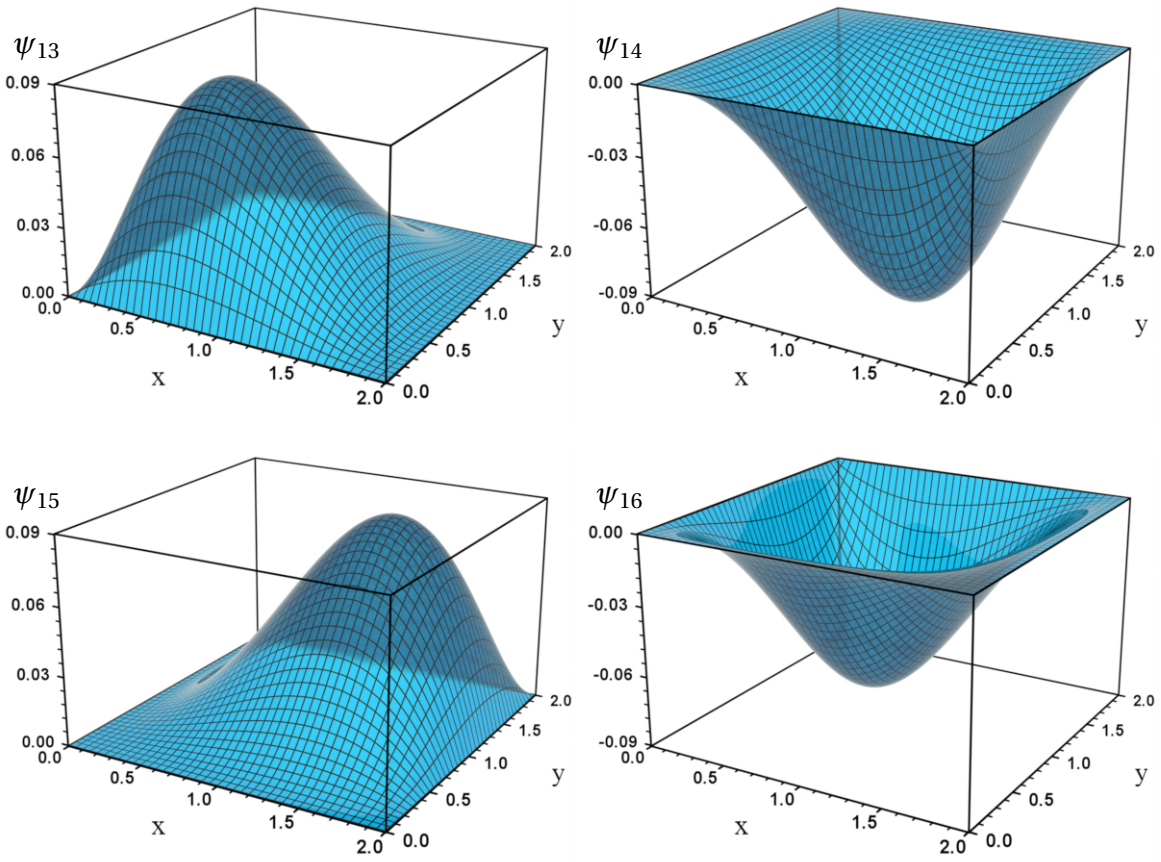

Figure A.17: The local 2D Hermite basis functions for $\partial^2 u/\partial x \partial y$.

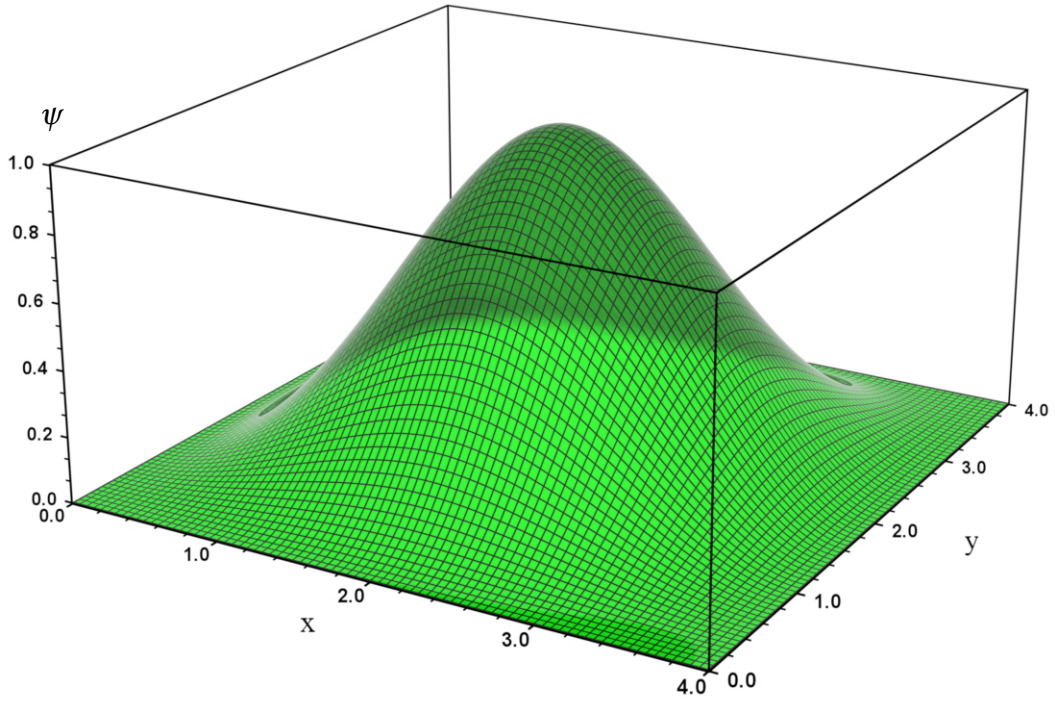

Figure A.18: The global 2D Hermite basis function for u.

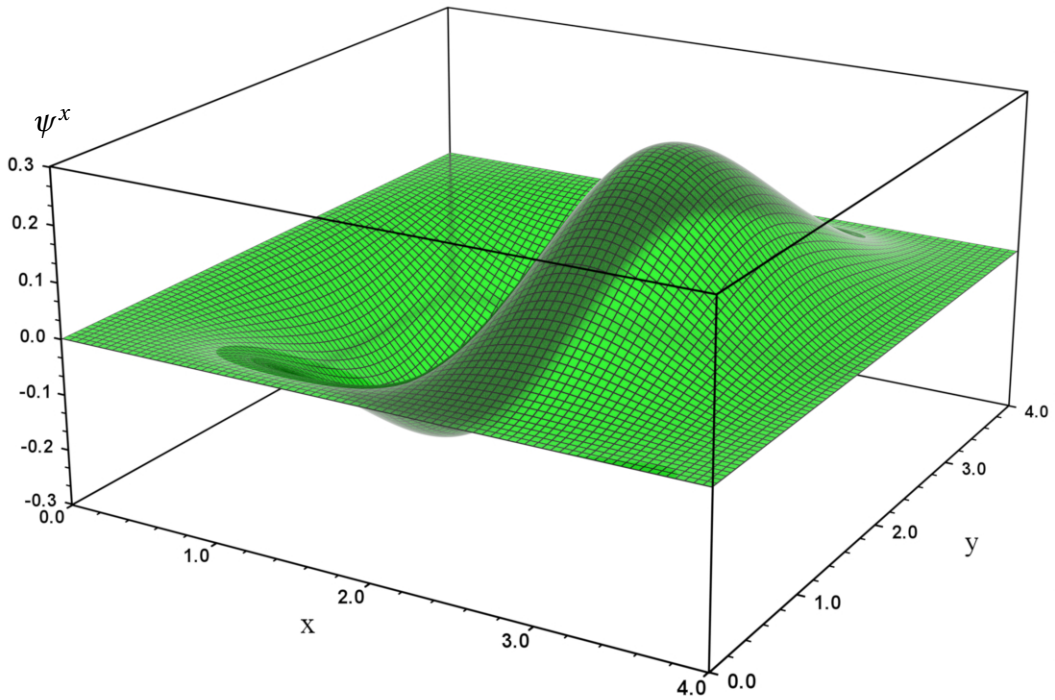

Figure A.19: The global 2D Hermite basis function for $\partial u/\partial x$.

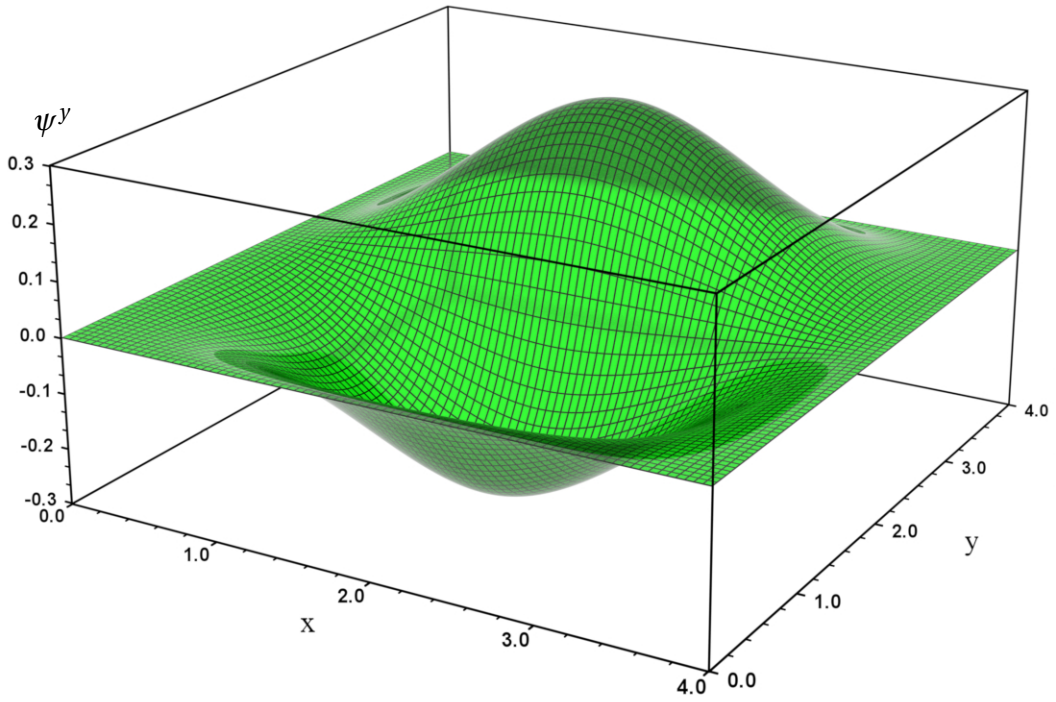

Figure A.20: The global 2D Hermite basis function for $\partial u/\partial y$.

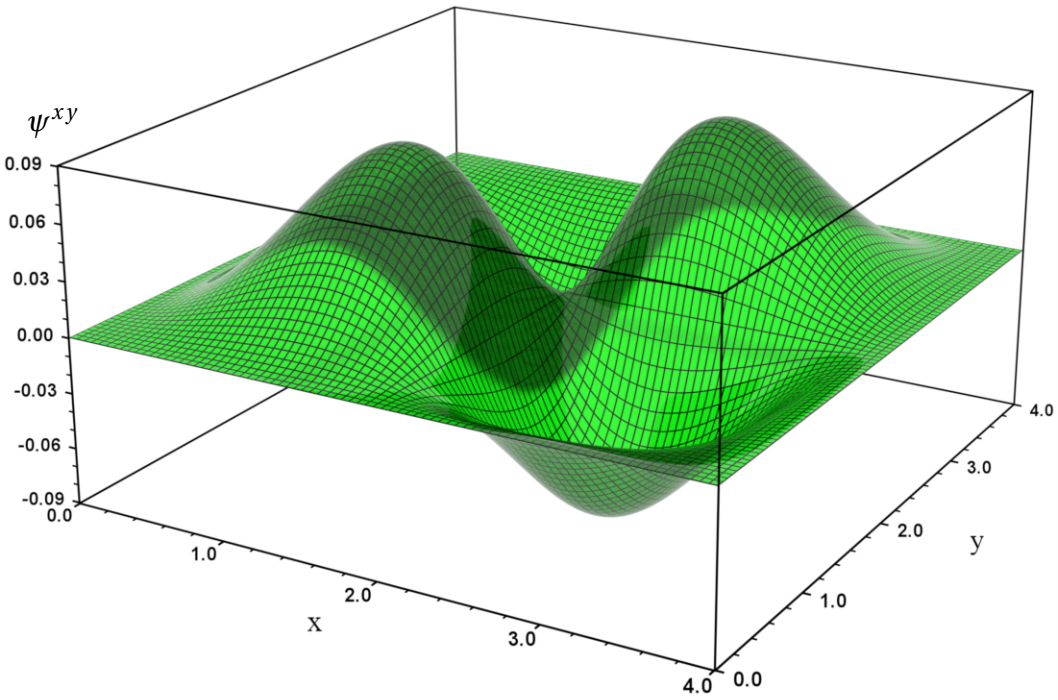

Figure A.21: The global 2D Hermite basis function for $\partial^2 u/\partial x \partial y$.

Example

Solve the Poisson equation for the test function $u(x,y) = \frac{\sin(r)}{r}$ with Dirichlet boundary conditions.

$$-\nabla^2 u = \frac{\left(r^2-1\right)\sin(r) + r\cos(r)}{r^3} \text{ for } x, y \in [-12, 12]\,,\ r = \sqrt{x^2+y^2} \tag{A.74}$$

The domain is square, with a total of 400 elements (20×20).

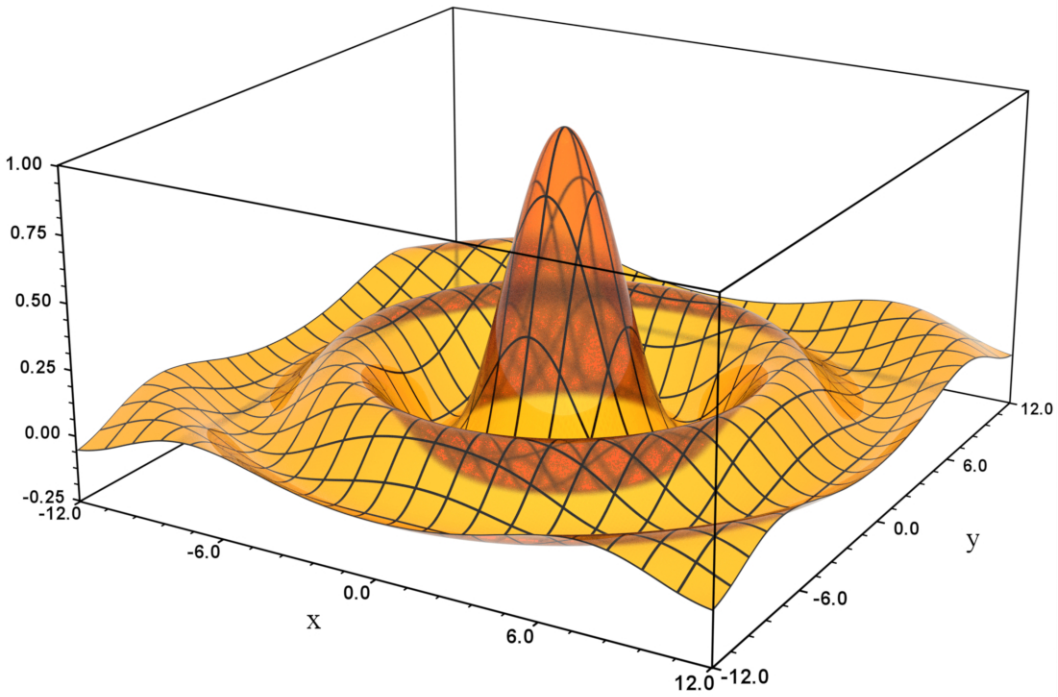

Figure A.22: The solution for u.

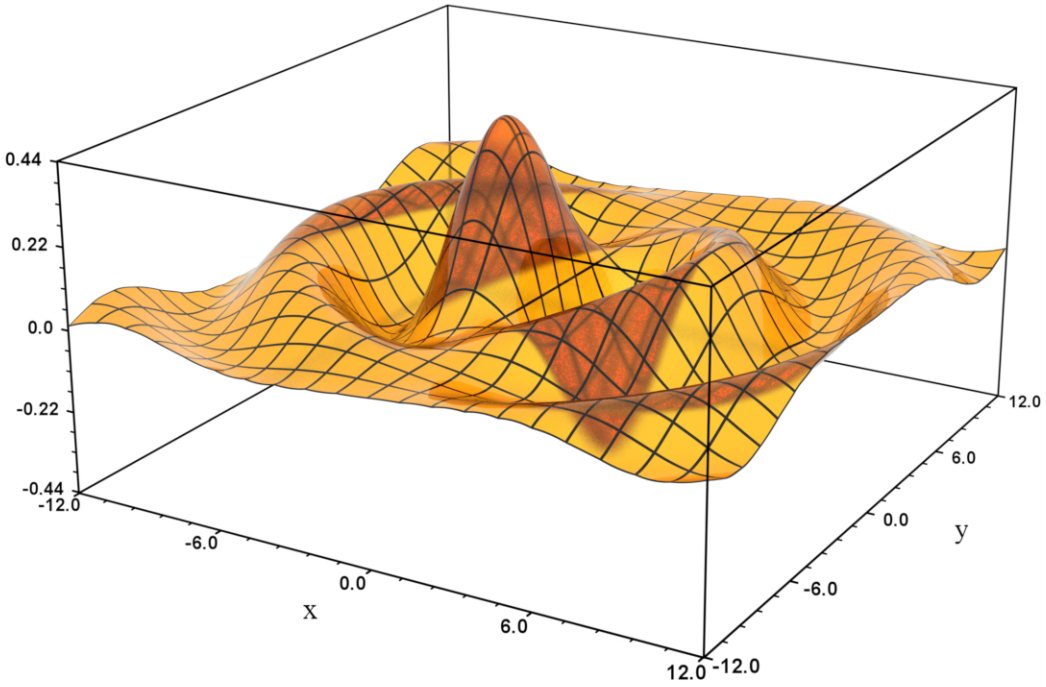

Figure A.23: The solution for $\partial u/\partial x$.

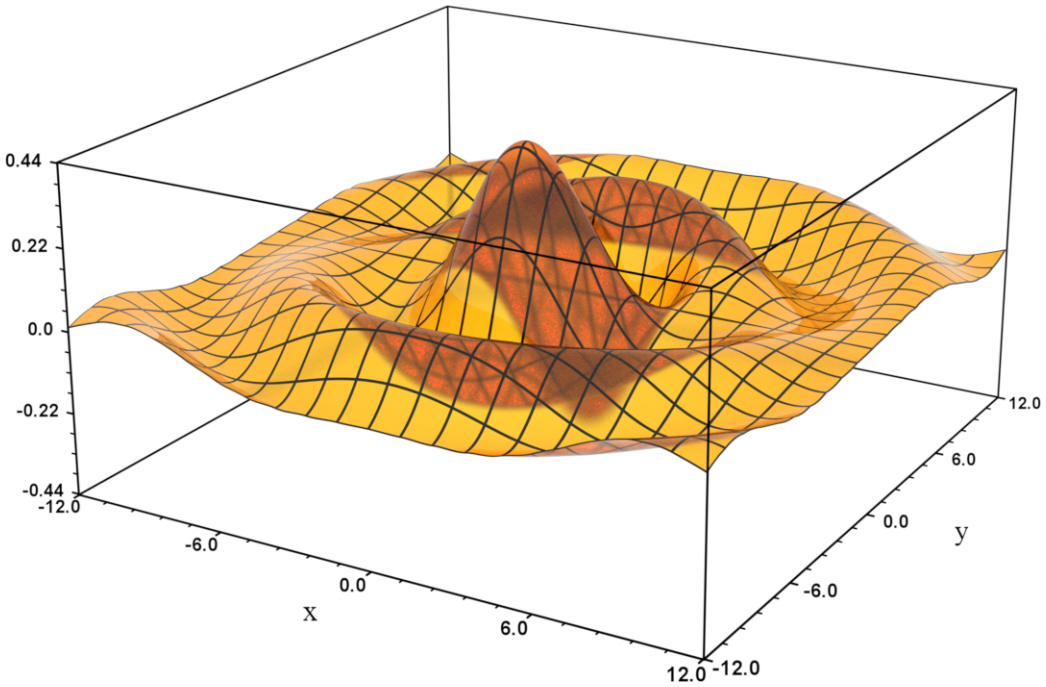

Figure A.24: The solution for $\partial u/\partial y$.

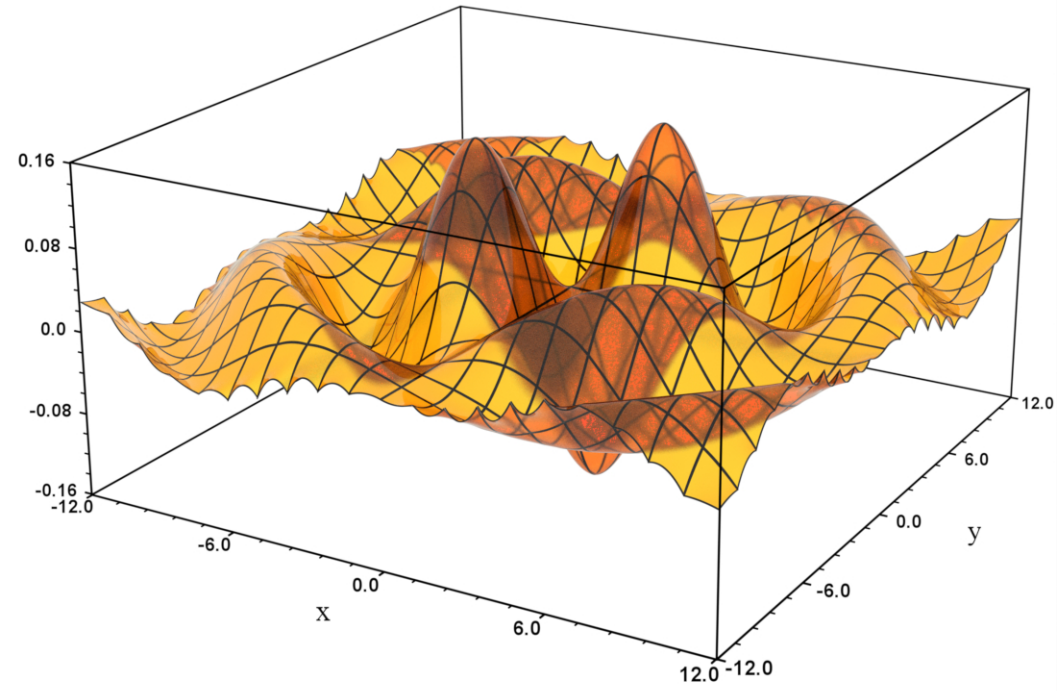

Figure A.25: The solution for $\partial^2 u/\partial x \partial y$.

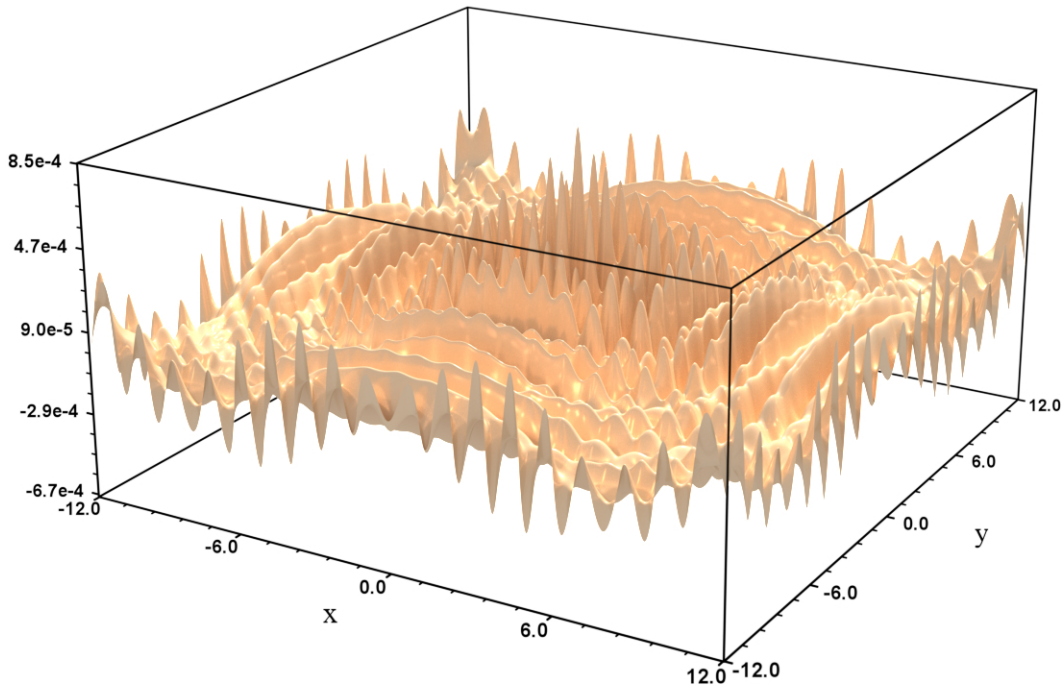

Figure A.26: The solution error for u.

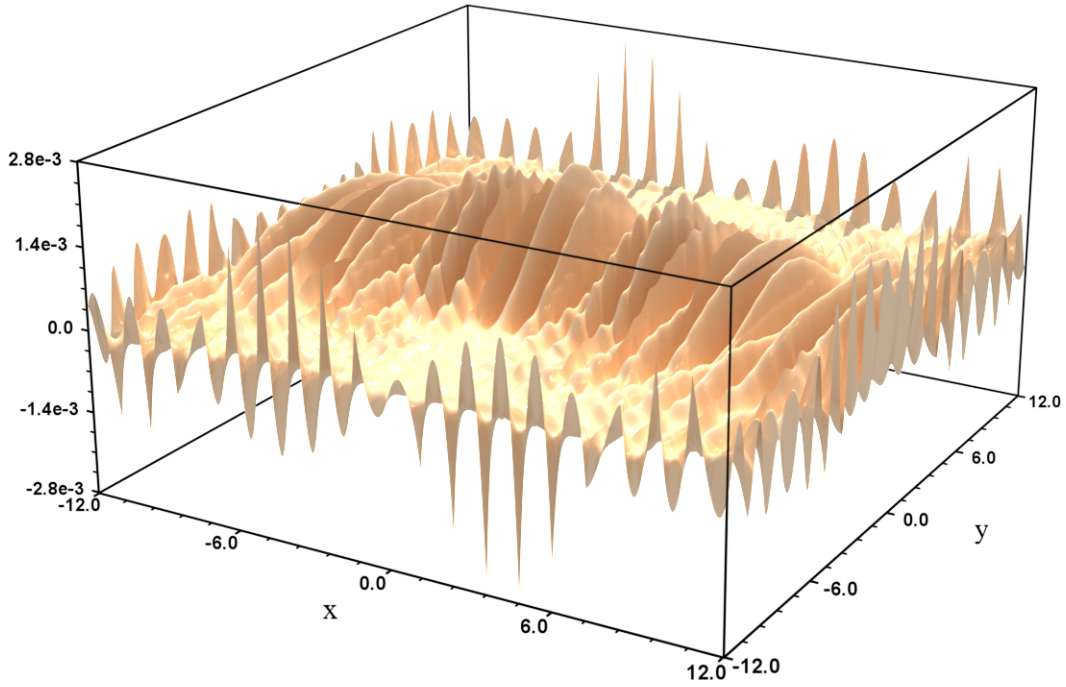

Figure A.27: The solution error for $\partial u/\partial x$.

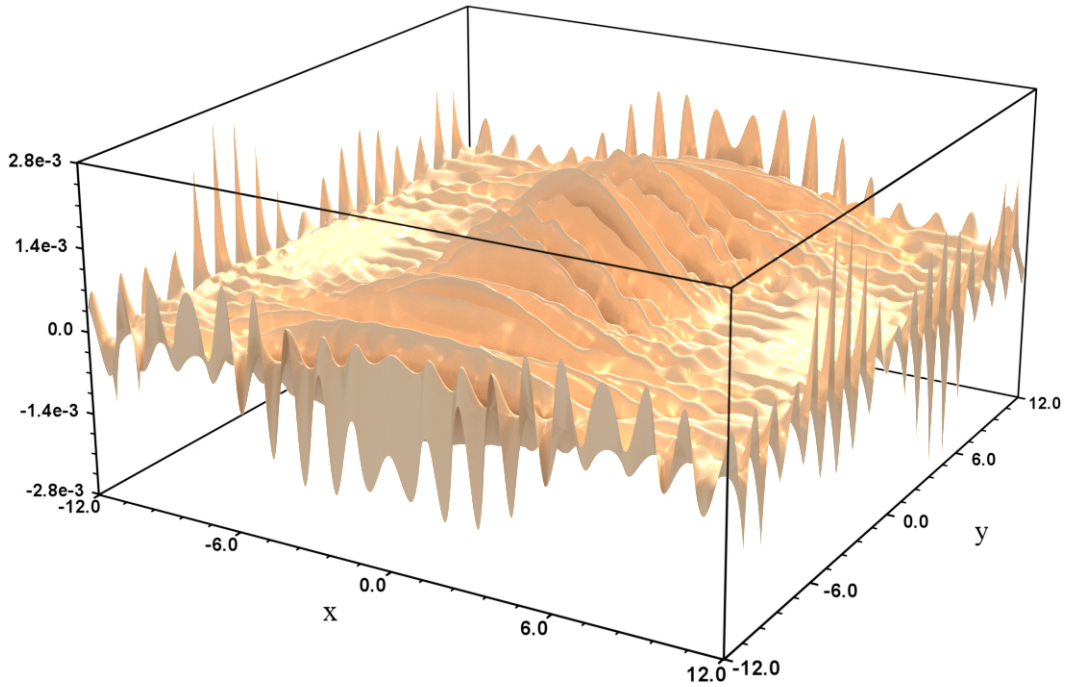

Figure A.28: The solution error for $\partial u/\partial y$.

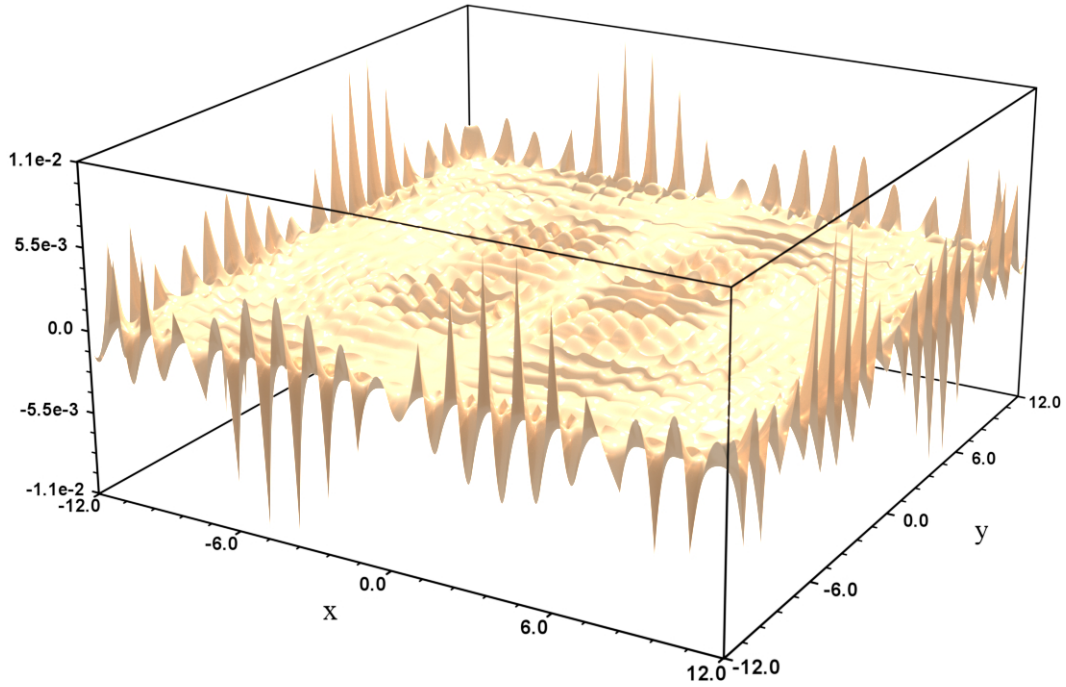

Figure A.29: The solution error for $\partial^2 u/\partial x \partial y$.

Let's go back to the weak form of the Poisson equation.

$$\int_\Omega \left[-\boldsymbol{\nabla}\delta u \cdot \boldsymbol{\nabla} u + (\delta u)\, f\right] \mathrm{d}x + \oint_\Gamma \delta u \frac{\partial u}{\partial n} \mathrm{d}\Gamma = 0 \tag{A.75}$$

If we have Dirichlet boundary conditions, where we specify u on the boundary Γ, we might be tempted to say $\delta u = 0$ everywhere on Γ and say that the boundary integral is equal to zero. This, however, would produce incorrect results, because in actuality we are not specifying u everywhere on Γ. We are only specifying u at the node points, so only $\delta u_i = 0$ on Γ. If our interpolation only involved u_i, then the boundary integral would be zero. The Hermite interpolation includes terms other than u_i, namely the x and y derivatives, and the second order x, y mixed derivative. Since we are not specifying these values on the boundary, their respective variations are not identically equal to zero. We therefore cannot dismiss the boundary integral, even with pure Dirichlet

boundary conditions.

If the boundary integral is discarded for the previous example, we get the solution shown below. The error along the boundary is significant. This example shows that the boundary terms must be treated very carefully, even when they would normally equal zero when using Lagrange elements.

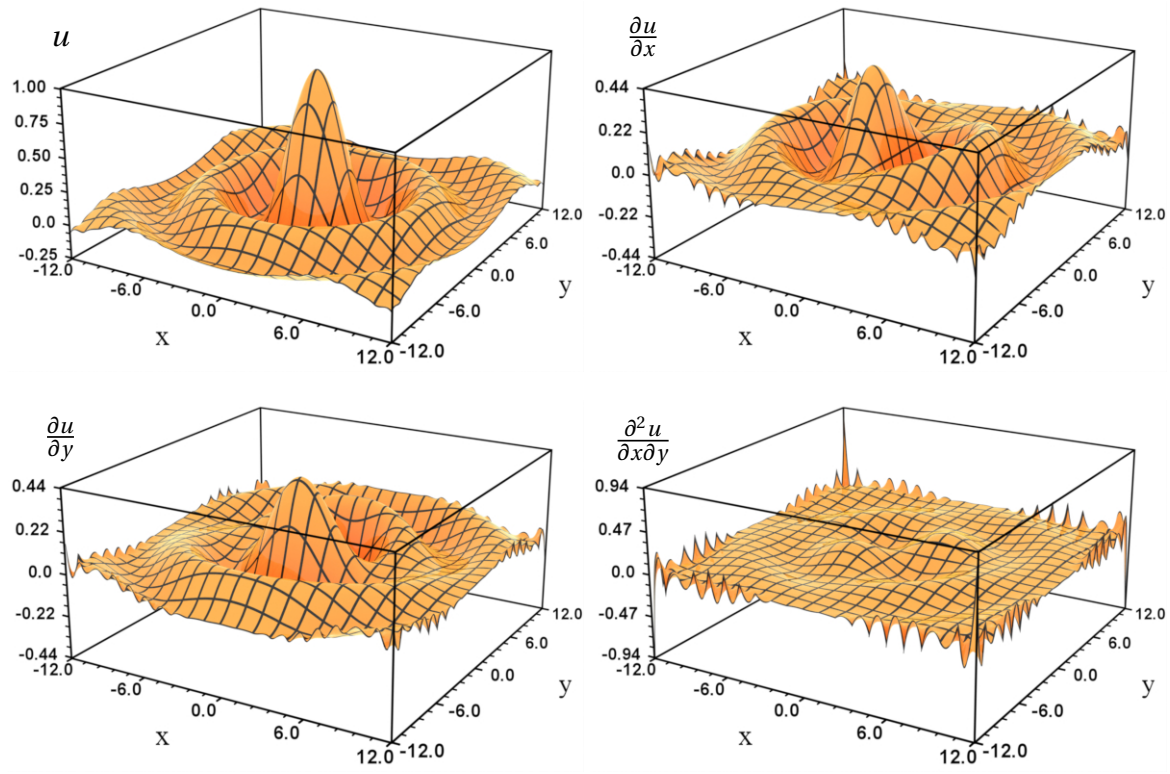

Figure A.30: An incorrect solution.

APPENDIX B

C PROGRAMS

harmonic_3D_phi.cpp

The C programs are chiefly responsible for generating the results found in this dissertation. The C-Lapack library was used for solving the linear system which resulted from the Finite Element formulation. The version of the C-Lapack library used was the version found in veclib, which is a framework optimized for the dual-processor Intel Mac, 64-bit. The solver ran very fast compared to comparable Mathematica code.

```
// Solve for u,v,w,phi, 3D harmonic case using quadratic Lagrange elements.

#include <vecLib/vecLib.h>
#include <iostream>
#include <stdio.h>
#include <time.h>
#include <math.h>
#include "../stuff.h"
#include "../PVDF.h"

const bool VFREE = true;
const bool WFREE = true;
const bool DAMPED = true;

const double dens = 1.78e3; // PVDF mass density, kg/m^3
double freq = 50; // angular frequency, rad/s
double cond = 0.1;  // electrode conductivity, S/m

// lengths in meters. 2.54 cm = 1.0 in
const double LZ = 60e-6;  // thickness
const double LY = 1.25e-2; // width
const double LX = 2.5e-2; // length
const double LE = 10e-6; // electrode thickness
const double phiTop = 300; // in V
const double phiBottom = -300;
const long int Ne = 3; // Nodes per electrode.
const long int Nx = 8;
const long int Ny = 5; // must be odd
const long int Nz = 5; // must be odd
const long int nZE = Nz+2*Ne-2; // total Z-nodes
const long int midY = (Ny-1)/2;
const long int midZ = (Nz-1)/2 + Ne-1;
const double hx = LX/(double)(Nx-1);
const double hy = LY/(double)(Ny-1);
const double hz = LZ/(double)(Nz-1);
const double he = LE/(double)(Ne-1);
const long int LagrangeN = 3; // order + 1 = # of 1D node points
const long int NPE = LagrangeN*LagrangeN*LagrangeN; // nodes per element
const long int Nx2 = Nx*(LagrangeN-1)+2-LagrangeN;
const long int Ny2 = Ny*(LagrangeN-1)+2-LagrangeN;
const long int Nz2 = Nz*(LagrangeN-1)+2-LagrangeN;
const long int Ne2 = Ne*(LagrangeN-1)+2-LagrangeN;
const long int Nz3 = Nz2+2*Ne2-2;
const long int nNodes = Nx2*Ny2*Nz2;
const long int nNodes2 = Nx2*Ny2*Nz3;
long int nBNodes;
const long int nElements = (Nx-1)*(Ny-1)*(nZE-1);
const long int nVar = 4;
const long int nVar2 = 2*nVar;
const long int nDOF = 3*nNodes+nNodes2;
const long int nDOF2 = 2*nDOF;
```

```
const long int n_shift = (1-Ne2)*Nx2*Ny2;
const long int NN1 = n_shift; //Shift u,w nodes to the left.
const long int NN2 = nNodes+n_shift;
const long int NN3 = 2*nNodes+n_shift;
const long int NN4 = 3*nNodes;
const long int NNa = 0;
const long int NNb = nDOF;

int main (int argc, char * const argv[]) {
   long int elNodes[nElements][NPE],*neighbors,nNeighbors;
   long int i,j,k,m,n,s,m1,m2,n1,n2,n3,p,p1,p2;
   long int m1a,m2a,m3a,m4a,m1b,m2b,m3b,m4b,n1a,n2a,n3a,n4a,n1b,n2b,n3b,n4b;
   double F[nDOF2],Z[nDOF2],x,tau,beta,delta0;
   bool *piezoLower = new bool[nElements],*electrode = new bool[nElements];
   row_sp *A_sp = new row_sp[nDOF2],bNodes;

   // Specify the global node numbers for each element. This is the mesh.
   for (i=0; i<Nx-1; i++) {
      for (j=0; j<Ny-1; j++) {
         for (k=0; k<nZE-1; k++) {
            n = i + j*(Nx-1) + k*(Nx-1)*(Ny-1); // element #
            piezoLower[n] = (k < midZ);
            electrode[n] = (k<(Ne-1) || k>=(Ne+Nz-2));
            // global node # of bottom-left corner
            m = (LagrangeN-1)*(i + j*Nx2 + k*Nx2*Ny2);
            for (n1=0; n1<LagrangeN; n1++) {
               for (n2=0; n2<LagrangeN; n2++) {
                  for (n3=0; n3<LagrangeN; n3++) {
                     // local node #
                     m1 = n1 + LagrangeN*n2 + LagrangeN*LagrangeN*n3;
                     s = m + n1 + Nx2*n2 + Nx2*Ny2*n3; // global node #
                     elNodes[n][m1] = s;

                     // Specify the boundary nodes.
                     // NNa =  Cos component
                     // NNb = -Sin component

                     // u
                     if (n1==0 && i==0 && k>=Ne-1 && k<Ne+Nz-2) {
                        m1a = bNodes.n;
                        bNodes.add_index(s+NN1+NNa,0.0);
                        bNodes.add_index(s+NN1+NNb,0.0);
                     }

                     // v
                     if ((n1==0 && i==0 && k>=Ne-1 && k<Ne+Nz-2) &&
                           ((VFREE && (n2==0 && j==midY)) || !VFREE)) {
                        m1a = bNodes.n;
                        bNodes.add_index(s+NN2+NNa,0.0);
                        bNodes.add_index(s+NN2+NNb,0.0);
                     }
```

```
                    // w
                    if ((n1==0 && i==0 && k>=Ne-1 && k<Ne+Nz-2) &&
                          ((WFREE && (n2==0 && j==midY) && (n3==0 && k==midZ))
                             || !WFREE)) {
                       m1a = bNodes.n;
                       bNodes.add_index(s+NN3+NNa,0.0);
                       bNodes.add_index(s+NN3+NNb,0.0);
                    }

                    // phi - ground
                    if (n3==0 && k==0) {
                       m1a = bNodes.n;
                       bNodes.add_index(s+NN4+NNa,0.0);
                       bNodes.add_index(s+NN4+NNb,-phiBottom);
                    }

                    // phi - applied
                    if (n3==(LagrangeN-1) && k==(nZE-2)) {
                       m1a = bNodes.n;
                       bNodes.add_index(s+NN4+NNa,0.0);
                       bNodes.add_index(s+NN4+NNb,-phiTop);
                    }
                 }}}}}}
   nBNodes = bNodes.n;

   // The inverse of the 3X3 Jacobian matrix, for an affine transformation.
   double JD = hx*hy*hz/8; // determinant
   double j11 = 2.0/hx;
   double j22 = 2.0/hy;
   double j33 = 2.0/hz;
   double JDe = hx*hy*he/8;
   double j33e = 2.0/he;

   long int shifts[8] =
{NN1+NNa,NN2+NNa,NN3+NNa,NN4+NNa,NN1+NNb,NN2+NNb,NN3+NNb,NN4+NNb};

   // The neighbor list. All the nodes in a particular element are neighbors
   // of each other. A node is its own neighbor.
   for (i=0; i<nElements; i++) {
     for (j=0; j<NPE; j++) {
        m = elNodes[i][j]; // global node #
        for (k=0; k<NPE; k++) {
           n = elNodes[i][k]; // global node #

           if (electrode[i]) {
              A_sp[m+NN4+NNa].add_index(n+NN4+NNa);
              A_sp[m+NN4+NNa].add_index(n+NN4+NNb);
              A_sp[m+NN4+NNb].add_index(n+NN4+NNa);
              A_sp[m+NN4+NNb].add_index(n+NN4+NNb);
           } else {
```

```
            for (m1=0; m1<nVar2; m1++)
               for (n1=0; n1<nVar2; n1++)
                  A_sp[m + shifts[m1]].add_index(n + shifts[n1]);
         }
      }
   }
}

for (i=0; i<nDOF2; i++) {
   n = A_sp[i].n;
   A_sp[i].x = new double[n];
}

// Remove the boundary nodes from the matrix. Calculate the row/column
// shifts for the remaining stiffness matrix entries.
long int rcount[nDOF2];
bool bcheck[nDOF2];
for (i=0; i<nDOF2; i++) {
   rcount[i] = i;
   bcheck[i] = true;
}
for (i=0; i<nBNodes; i++) {
   m = bNodes.j[i];
   bcheck[m] = false;
   for (j=m; j<nDOF2; j++)
      rcount[j]--;
}
long int a_N = nDOF2 - nBNodes;
long int global_dof_number[a_N];
for (i=0; i<nDOF2; i++) {
   if (bcheck[i]) {
      m = rcount[i];
      global_dof_number[m] = i;
   }
}

// stiffness matrix ++++++++++++++++++++++++++++++++++++++++++++++++++++++++

polynomial bases1D[LagrangeN],bases1D_der[LagrangeN];
double M1D[NPE][4];
for (i=0; i<LagrangeN; i++) {
   bases1D[i] = Lagrange1D(i,0,1);
   bases1D_der[i] = derivative(bases1D[i],0);
}

for (i=0; i<LagrangeN; i++) {
   for (j=0; j<LagrangeN; j++) {
      n = i + j*LagrangeN;
      M1D[n][0] = integral(bases1D[i]*bases1D[j]); // psi*psi
      M1D[n][1] = integral(derivative(bases1D[i],0)*bases1D[j]); // psi'*psi
      M1D[n][2] = integral(bases1D[i]*derivative(bases1D[j],0)); // psi*psi'
```

```
      M1D[n][3] = integral(derivative(bases1D[i],0)*
                                    derivative(bases1D[j],0)); // psi'*psi'
    }
}

// All the integrals for a single element.
double **MMxx,**MMxy,**MMxz,**MMyy,**MMyz,**MMzz,**MM;
double **MMxxe,**MMyye,**MMzze;
initSqrMat(MMxx,NPE);
initSqrMat(MMxy,NPE);
initSqrMat(MMxz,NPE);
initSqrMat(MMyy,NPE);
initSqrMat(MMyz,NPE);
initSqrMat(MMzz,NPE);
initSqrMat(MM,NPE);
initSqrMat(MMxxe,NPE);
initSqrMat(MMyye,NPE);
initSqrMat(MMzze,NPE);
for (m1=0; m1<LagrangeN; m1++) {
  for (n1=0; n1<LagrangeN; n1++) {
     for (p1=0; p1<LagrangeN; p1++) {
       j = m1 + n1*LagrangeN + p1*LagrangeN*LagrangeN;
       for (m2=0; m2<LagrangeN; m2++) {
          m = m1 + m2*LagrangeN;
         for (n2=0; n2<LagrangeN; n2++) {
            n = n1 + n2*LagrangeN;
            for (p2=0; p2<LagrangeN; p2++) {
              k = m2 + n2*LagrangeN + p2*LagrangeN*LagrangeN;
                p = p1 + p2*LagrangeN;
                MMxx[j][k] = JD*j11*j11*M1D[m][3]*M1D[n][0]*M1D[p][0];
                MMyy[j][k] = JD*j22*j22*M1D[m][0]*M1D[n][3]*M1D[p][0];
                MMzz[j][k] = JD*j33*j33*M1D[m][0]*M1D[n][0]*M1D[p][3];
                MMxy[j][k] = JD*j11*j22*M1D[m][1]*M1D[n][2]*M1D[p][0];
                MMxz[j][k] = JD*j11*j33*M1D[m][1]*M1D[n][0]*M1D[p][2];
                MMyz[j][k] = JD*j22*j33*M1D[m][0]*M1D[n][1]*M1D[p][2];
                MM[j][k] = JD*M1D[m][0]*M1D[n][0]*M1D[n][0];

                MMxxe[j][k] = JDe*j11*j11*M1D[m][3]*M1D[n][0]*M1D[p][0];
                MMyye[j][k] = JDe*j22*j22*M1D[m][0]*M1D[n][3]*M1D[p][0];
                MMzze[j][k] = JDe*j33e*j33e*M1D[m][0]*M1D[n][0]*M1D[p][3];
            }}}}}}

__CLPK_integer N = (__CLPK_integer)(a_N); // order of the matrix (N by N)
__CLPK_integer NRHS = (__CLPK_integer)(1); // number of columns in the RHS
__CLPK_doublereal *AMat = new __CLPK_doublereal[a_N*a_N];
__CLPK_integer LDA = N; // leading dimension of the matrix
__CLPK_integer *IPIV = new __CLPK_integer[a_N]; // output
__CLPK_doublereal *loadVec = new __CLPK_doublereal[a_N];
__CLPK_integer LDB = N; // leading dimension of the RHS (=N)
__CLPK_integer INFO; // output
```

```
//+++++++++++++++++++++++++++++++++++++++++++++++++++++++++++++++++++++++++++++
// LOOP ++++++++++++++++++++++++++++++++++++++++++++++++++++++++++++++++++++++
//+++++++++++++++++++++++++++++++++++++++++++++++++++++++++++++++++++++++++++++
int imax,loopcount,loopN = 1;
freq = 1.0;

FILE *output_Z,*output_Z2;
if (loopN > 1)
  output_Z = fopen("../../ZScan.dat","w");
else
  output_Z2 = fopen("../../Z.dat","w");

for (loopcount=0; loopcount<loopN; loopcount++) {
  if (loopN > 1) {
    // near a known resonance frequency.
    if (loopcount==0)
      freq = 0.001;
    else if ((freq>100 && freq<130) ||
             (freq>720 && freq<740) ||
             (freq>2040 && freq<2060) ||
             (freq>4030 && freq<4050) ||
             (freq>6700 && freq<6720))
      freq += 2.0;
    else
      freq += 10.0;
  }

  // solving ++++++++++++++++++++++++++++++++++++++++++++++++++++++++++++++++++
  for (i=0; i<nDOF2; i++) {
    n = A_sp[i].n;
    for (k=0; k<n; k++)
      A_sp[i].x[k] = 0;
  }

  for (i=0; i<nElements; i++) {
    s = (piezoLower[i] ? 1 : -1);
    for (j=0; j<NPE; j++) { // local node #
      m = elNodes[i][j]; // global node #
      m1a = m + NN1;
      m2a = m + NN2;
      m3a = m + NN3;
      m4a = m + NN4;
      m1b = m1a + nDOF;
      m2b = m2a + nDOF;
      m3b = m3a + nDOF;
      m4b = m4a + nDOF;
      for (k=0; k<NPE; k++) { // local node #
        n = elNodes[i][k]; // global node #
        n1a = n + NN1;
        n2a = n + NN2;
        n3a = n + NN3;
```

```
n4a = n + NN4;
n1b = n1a + nDOF;
n2b = n2a + nDOF;
n3b = n3a + nDOF;
n4b = n4a + nDOF;

if (electrode[i]) {
   x = MMxxe[j][k] + MMyye[j][k] + MMzze[j][k];
   A_sp[m4a].add(n4a,-cond*x);
   A_sp[m4a].add(n4b,freq*eps3*x);
   A_sp[m4b].add(n4a,-freq*eps3*x);
   A_sp[m4b].add(n4b,-cond*x);
} else {
   //+++++++++++++++++++++++++++++++++++++++++++++++++++++++++++++
   A_sp[m1a].add(n1a,c11*MMxx[j][k] + c66*MMyy[j][k]
                  + c55*MMzz[j][k] - freq*freq*dens*MM[j][k]);
   A_sp[m1a].add(n2a,c12*MMxy[j][k] + c66*MMxy[k][j]);
   A_sp[m1a].add(n3a,c13*MMxz[j][k] + c55*MMxz[k][j]);
   A_sp[m1a].add(n4a,s*(e31*MMxz[j][k] + e15*MMxz[k][j]));

   A_sp[m1b].add(n1b,c11*MMxx[j][k] + c66*MMyy[j][k]
                  + c55*MMzz[j][k] - freq*freq*dens*MM[j][k]);
   A_sp[m1b].add(n2b,c12*MMxy[j][k] + c66*MMxy[k][j]);
   A_sp[m1b].add(n3b,c13*MMxz[j][k] + c55*MMxz[k][j]);
   A_sp[m1b].add(n4b,s*(e31*MMxz[j][k] + e15*MMxz[k][j]));

   if (DAMPED) {
      A_sp[m1a].add(n1b,-(c11_i*MMxx[j][k] + c66_i*MMyy[j][k]
                                    + c55_i*MMzz[j][k]));
      A_sp[m1a].add(n2b,-(c12_i*MMxy[j][k] + c66_i*MMxy[k][j]));
      A_sp[m1a].add(n3b,-(c13_i*MMxz[j][k] + c55_i*MMxz[k][j]));

      A_sp[m1b].add(n1a,c11_i*MMxx[j][k] + c66_i*MMyy[j][k]
                                    + c55_i*MMzz[j][k]);
      A_sp[m1b].add(n2a,c12_i*MMxy[j][k] + c66_i*MMxy[k][j]);
      A_sp[m1b].add(n3a,c13_i*MMxz[j][k] + c55_i*MMxz[k][j]);
   }
   //+++++++++++++++++++++++++++++++++++++++++++++++++++++++++++++
   A_sp[m2a].add(n1a,c12*MMxy[k][j] + c66*MMxy[j][k]);
   A_sp[m2a].add(n2a,c66*MMxx[j][k] + c22*MMyy[j][k]
                  + c44*MMzz[j][k] - freq*freq*dens*MM[j][k]);
   A_sp[m2a].add(n3a,c23*MMyz[j][k] + c44*MMyz[k][j]);
   A_sp[m2a].add(n4a,s*(e32*MMyz[j][k] + e24*MMyz[k][j]));

   A_sp[m2b].add(n1b,c12*MMxy[k][j] + c66*MMxy[j][k]);
   A_sp[m2b].add(n2b,c66*MMxx[j][k] + c22*MMyy[j][k]
                  + c44*MMzz[j][k] - freq*freq*dens*MM[j][k]);
   A_sp[m2b].add(n3b,c23*MMyz[j][k] + c44*MMyz[k][j]);
   A_sp[m2b].add(n4b,s*(e32*MMyz[j][k] + e24*MMyz[k][j]));

   if (DAMPED) {
```

```
   A_sp[m2a].add(n1b,-(c12_i*MMxy[k][j] + c66_i*MMxy[j][k]));
   A_sp[m2a].add(n2b,-(c66_i*MMxx[j][k] + c22_i*MMyy[j][k]
                                        + c44_i*MMzz[j][k]));
   A_sp[m2a].add(n3b,-(c23_i*MMyz[j][k] + c44_i*MMyz[k][j]));

   A_sp[m2b].add(n1a,c12_i*MMxy[k][j] + c66_i*MMxy[j][k]);
   A_sp[m2b].add(n2a,c66_i*MMxx[j][k] + c22_i*MMyy[j][k]
                                       + c44_i*MMzz[j][k]);
   A_sp[m2b].add(n3a,c23_i*MMyz[j][k] + c44_i*MMyz[k][j]);
}
//+++++++++++++++++++++++++++++++++++++++++++++++++++++++++++++
A_sp[m3a].add(n1a,c13*MMxz[k][j] + c55*MMxz[j][k]);
A_sp[m3a].add(n2a,c23*MMyz[k][j] + c44*MMyz[j][k]);
A_sp[m3a].add(n3a,c55*MMxx[j][k] + c44*MMyy[j][k]
               + c33*MMzz[j][k] - freq*freq*dens*MM[j][k]);
A_sp[m3a].add(n4a,s*(e15*MMxx[j][k] + e24*MMyy[j][k]
               + e33*MMzz[j][k]));

A_sp[m3b].add(n1b,c13*MMxz[k][j] + c55*MMxz[j][k]);
A_sp[m3b].add(n2b,c23*MMyz[k][j] + c44*MMyz[j][k]);
A_sp[m3b].add(n3b,c55*MMxx[j][k] + c44*MMyy[j][k]
               + c33*MMzz[j][k] - freq*freq*dens*MM[j][k]);
A_sp[m3b].add(n4b,s*(e15*MMxx[j][k] + e24*MMyy[j][k]
               + e33*MMzz[j][k]));

if (DAMPED) {
   A_sp[m3a].add(n1b,-(c13_i*MMxz[k][j] + c55_i*MMxz[j][k]));
   A_sp[m3a].add(n2b,-(c23_i*MMyz[k][j] + c44_i*MMyz[j][k]));
   A_sp[m3a].add(n3b,-(c55_i*MMxx[j][k] + c44_i*MMyy[j][k]
                               + c33_i*MMzz[j][k]));

   A_sp[m3b].add(n1a,c13_i*MMxz[k][j] + c55_i*MMxz[j][k]);
   A_sp[m3b].add(n2a,c23_i*MMyz[k][j] + c44_i*MMyz[j][k]);
   A_sp[m3b].add(n3a,c55_i*MMxx[j][k] + c44_i*MMyy[j][k]
                               + c33_i*MMzz[j][k]);
}
//+++++++++++++++++++++++++++++++++++++++++++++++++++++++++++++
A_sp[m4a].add(n1b,s*(e31*MMxz[k][j] + e15*MMxz[j][k]));
A_sp[m4a].add(n2b,s*(e32*MMyz[k][j] + e24*MMyz[j][k]));
A_sp[m4a].add(n3b,s*(e15*MMxx[j][k] + e24*MMyy[j][k]
                               + e33*MMzz[j][k]));
A_sp[m4a].sub(n4b,eps1*MMxx[j][k] + eps2*MMyy[j][k]
                               + eps3*MMzz[j][k]);

A_sp[m4b].add(n1a,s*(e31*MMxz[k][j] + e15*MMxz[j][k]));
A_sp[m4b].add(n2a,s*(e32*MMyz[k][j] + e24*MMyz[j][k]));
A_sp[m4b].add(n3a,s*(e15*MMxx[j][k] + e24*MMyy[j][k]
                               + e33*MMzz[j][k]));
A_sp[m4b].sub(n4a,eps1*MMxx[j][k] + eps2*MMyy[j][k]
                               + eps3*MMzz[j][k]);
//+++++++++++++++++++++++++++++++++++++++++++++++++++++++++++++
```

```
         }
      }
   }
}

// load vector ++++++++++++++++++++++++++++++++++++++++++++++++++++++++++++
for (i=0; i<nDOF2; i++)
   F[i] = 0.0;

for (i=0; i<nBNodes; i++) {
   n = bNodes.j[i]; // column
   x = bNodes.x[i];

   if (x != 0) {
      neighbors = A_sp[n].j;
      nNeighbors = A_sp[n].n;

      for (j=0; j<nNeighbors; j++) {
         m = neighbors[j]; // row
         F[m] -= x*A_sp[m].x_at(n);
      }
   }
}

for (i=0; i<nDOF2; i++) {
   if (bcheck[i]) {
      m = rcount[i];
      loadVec[m] = F[i];
   }
}

j = a_N*a_N;
for (i=0; i<j; i++)
   AMat[i] = 0.0;

for (m=0; m<nDOF2; m++) {
   neighbors = A_sp[m].j;
   nNeighbors = A_sp[m].n;
   for (k=0; k<nNeighbors; k++) {
      n = neighbors[k];
      m1 = rcount[m];
      n1 = rcount[n];
      if (bcheck[m] && bcheck[n]) {
         AMat[m1 + a_N*n1] = A_sp[m].x[k];
      }
   }
}

// Solves a general square matrix with LU decomposition.
dgesv_(&N,&NRHS,AMat,&LDA,IPIV,loadVec,&LDB,&INFO);
```

```
      for (i=0; i<a_N; i++)
         Z[global_dof_number[i]] = loadVec[i];

      // add in the boundary node values
      for (i=0; i<nBNodes; i++) {
         m = bNodes.j[i];
         x = bNodes.x[i];
         Z[m] = x;
      }

      if (loopN == 1)
         fprintf(output_Z2,"%ld %ld %ld %ld %ld %e %e %e %e %e
                     \n",LagrangeN,Nx,Ny,Nz,Ne,LX,LY,LZ,LE,freq);

      delta0 = 0.0;
      for (i=0; i<nDOF2; i++) {
         if (loopN == 1) {
            if (i<nDOF)
               fprintf(output_Z2,"%1.30e ",Z[i]);
            else
               fprintf(output_Z2,"%1.30e ",-Z[i]);
         }
         if (i >= NN3-n_shift && i < NN4) {
            tau = ((delta0 < 0) ? -delta0 : delta0);
            //beta = ((Z[i] < 0) ? -Z[i] : Z[i]);
            beta = sqrt(Z[i]*Z[i]+Z[i+nDOF]*Z[i+nDOF]);
            if (beta > tau) {
               delta0 = beta;//Z[i];
               imax = i;
            }
         }
      }

      if (loopN > 1)
         fprintf(output_Z,"%1.30e %1.30e %1.30e %1.30e\n",freq,delta0,
                                                   Z[imax],-Z[imax+nDOF]);

      printf("%e %e (%e,%e)\n",freq,delta0,Z[imax],-Z[imax+nDOF]);
   }

   if (loopN > 1)
      fclose(output_Z);
   else
      fclose(output_Z2);

   delSqrMat(MMxx,NPE);
   delSqrMat(MMxz,NPE);
   delSqrMat(MMzz,NPE);

   return 0;
}
```

PVDF.h

This “include” file contains all of the material constants for PVDF.

```
#ifndef _PVDF_H
#define _PVDF_H

// in N/m^2
const double c11 = 3.70e9;
const double c22 = 3.20e9;
const double c33 = 1.51e9;
const double c44 = 0.55e9;
const double c55 = 0.59e9;
const double c66 = 0.70e9;
const double c12 = 1.47e9;
const double c13 = 1.23e9;
const double c23 = 1.00e9;

// imaginary parts, for testing
const double c11_i = 0.01*c11;
const double c22_i = 0.01*c22;
const double c33_i = 0.01*c33;
const double c44_i = 0.01*c44;
const double c55_i = 0.01*c55;
const double c66_i = 0.01*c66;
const double c12_i = 0.01*c12;
const double c13_i = 0.01*c13;
const double c23_i = 0.01*c23;

// in C^2/N*m^2
const double eps1 = 7.35*8.85e-12;
const double eps2 = 9.27*8.85e-12;
const double eps3 = 8.05*8.85e-12;

// in V*m/N
const double g31 = 0.21;
const double g32 = 0.03;
const double g33 = -0.46;
const double g15 = -0.32;
const double g24 = -0.27;

// in N/V*m
const double e31 = eps3*(g31*c11+g32*c12+g33*c13); /* 1.807524e-02 */
const double e32 = eps3*(g31*c12+g32*c22+g33*c23); /* -3.915240e-03 */
const double e33 = eps3*(g31*c13+g32*c23+g33*c33); /* -2.876604e-02 */
const double e15 = eps1*g15*c55; /* -1.336704e-02 */
const double e24 = eps2*g24*c44; /* -1.051380e-02 */

// for T2=0 2D approximation
const double c11_2 = c11-c12*c12/c22;
const double c13_2 = c13-c12*c23/c22;
const double c33_2 = c33-c23*c23/c22;
const double e31_2 = e31-c12*e32/c22;
const double e33_2 = e33-c23*e32/c22;
const double eps3_2 = eps3-e32*e32/c22;
```

```
// imaginary parts, for testing
const double c11_2i = 0.01*c11_2;
const double c13_2i = 0.01*c13_2;
const double c33_2i = 0.01*c33_2;

#endif
```

stuff.h

This “include” file contains all of the auxiliary functions and data structures used in implementing the finite element method with Lagrange elements.

```
#ifndef _Stuff_H
#define _Stuff_H

#include <stdio.h>
#include <stdlib.h>
#include <string.h>
#include <math.h>
#include <iostream>

extern const long int LagrangeN;
#define PI M_PI /* From <math.h>. */
#define EPSILON 1.0e-15
#define APPROX(A1,A2) (((A1)>=((A2)-EPSILON)) && ((A1)<=((A2)+EPSILON)))

#define initSqrMat(M,NM)                    \
M = (double **)malloc(NM*sizeof(double *)); \
for (i=0; i<NM; i++)                        \
M[i] = (double *)malloc(NM*sizeof(double)); \
for (i=0; i<NM; i++)                        \
for (j=0; j<NM; j++)                        \
M[i][j] = 0;

#define delSqrMat(M,NM) \
for (i=0; i<NM; i++)    \
delete[] M[i];          \
delete[] M;

class polynomial;
polynomial operator+(polynomial L,polynomial R);
polynomial power(polynomial base,int t);
polynomial operator-(polynomial L,polynomial R);
polynomial operator*(polynomial L,polynomial R);
polynomial operator*(double v,polynomial R);
polynomial operator*(polynomial R,double v);
polynomial operator*(int v,polynomial R);
polynomial operator*(polynomial R,int v);
std::ostream& operator<<(std::ostream &s,polynomial &L);

class polynomial {
public:
   double *coefficient;
   int **exponent;
   int N; // number of non-zero coefficients
   int n_dim; // dimensions

   ~polynomial() {}//destroy();}

  void destroy() {
     if (coefficient != NULL)
        delete[] coefficient;
```

```
   if (exponent != NULL) {
      int i;
      for (i=0; i<N; i++)
         delete[] exponent[i];
      delete[] exponent;
   }

   coefficient = NULL;
   exponent = NULL;
}

double* alloc_coeff(int d1) {
   return (double *)malloc(d1*sizeof(double));
}

int** alloc_exp(int d1,int d2) {
   int i,**r;
   r = (int **)malloc(d1*sizeof(int *));
   for (i=0; i<d1; i++)
      r[i] = (int *)malloc(d2*sizeof(int));
   return r;
}

void resize(int n) {
   destroy();
   N = n;
   if (N > 0) {
      coefficient = alloc_coeff(N);
      exponent = alloc_exp(N,n_dim);
   }
}

 polynomial() {
   N = 0;
   n_dim = 1;
   coefficient = NULL;
   exponent = NULL;
 }

 polynomial(int n,int d=1) {
   n_dim = d;
   coefficient = NULL;
   exponent = NULL;
   if (n == 0)
      N = 0;
   else
      resize(n);
 }

 void minimize(bool use_approx=false) { // remove zero-valued entries.
   int i,j,count=0;
```

```
   for (i=0; i<N; i++) {
      if (use_approx) {
         if (!APPROX(coefficient[i],0))
            count++;
      } else {
        if (coefficient[i] != 0)
            count++;
      }
   }
   if (count < N) {
      double *c2 = alloc_coeff(count);
      int **e2 = alloc_exp(count,n_dim);
      count = 0;
      for (i=0; i<N; i++) {
         if (use_approx) {
            if (!APPROX(coefficient[i],0)) {
               c2[count] = coefficient[i];
               for (j=0; j<n_dim; j++)
                  e2[count][j] = exponent[i][j];
               count++;
            }
         } else {
            if (coefficient[i] != 0) {
               c2[count] = coefficient[i];
               for (j=0; j<n_dim; j++)
                  e2[count][j] = exponent[i][j];
               count++;
            }
         }
      }
      destroy();
      N = count;
      coefficient = c2;
      exponent = e2;
   }
}

void add(int *p,double v) {
   if (v == 0.0) return;
   int i,j,count;
   bool found = false, remove = false;
   for (i=0; i<N && !found; i++) {
      found = true;
      for (j=0; j<n_dim; j++) {
         if (exponent[i][j] != p[j])
            found = false;
      }
      if (found) {
         coefficient[i] += v;
         if (coefficient[i] == 0) {
            remove = true;
```

```
            count = i;
          }
        }
      }
      if (remove) {
        double *c2 = alloc_coeff(N-1);
        int **e2 = alloc_exp(N-1,n_dim);
        for (i=0; i<count; i++) {
          c2[i] = coefficient[i];
          for (j=0; j<n_dim; j++)
            e2[i][j] = exponent[i][j];
        }
        for (i=count+1; i<N; i++) {
          c2[i-1] = coefficient[i];
          for (j=0; j<n_dim; j++)
            e2[i-1][j] = exponent[i][j];
        }
        destroy();
        N--;
        coefficient = c2;
        exponent = e2;
      }
      if (!found) {
        double *c2 = alloc_coeff(N+1);
        int **e2 = alloc_exp(N+1,n_dim);
        count = 0;
        for (i=0; i<N; i++) {
          c2[i] = coefficient[i];
          for (j=0; j<n_dim; j++)
            e2[i][j] = exponent[i][j];
        }
        c2[N] = v;
        for (j=0; j<n_dim; j++)
          e2[N][j] = p[j];
        destroy();
        N++;
        coefficient = c2;
        exponent = e2;
      }
    }

    polynomial& operator=(polynomial R) {
      if (N != R.N || n_dim != R.n_dim) {
        n_dim = R.n_dim;
        resize(R.N);
      }
      int i,j;
      for (i=0; i<N; i++) {
        coefficient[i] = R.coefficient[i];
        for (j=0; j<n_dim; j++)
          exponent[i][j] = R.exponent[i][j];
```

```
  }
  return *this;
}

polynomial& operator+=(polynomial R) {
  int i;
  n_dim = R.n_dim;
  for (i=0; i<R.N; i++) {
     add(R.exponent[i],R.coefficient[i]);
  }
  return *this;
}

polynomial& operator-=(polynomial R) {
  int i;
  n_dim = R.n_dim;
  for (i=0; i<R.N; i++) {
     add(R.exponent[i],-1*R.coefficient[i]);
  }
  return *this;
}

polynomial& operator*=(double v) {
  int i;
  for (i=0; i<N; i++) {
     coefficient[i] *= v;
  }
  return *this;
}

polynomial translate(double x0) {
  int i;
  polynomial R,base(2);
  base.exponent[0][0] = 0;
  base.exponent[1][0] = 1;
  base.coefficient[0] = -x0;
  base.coefficient[1] = 1;

  for (i=0; i<N; i++) {
       R += coefficient[i]*power(base,exponent[i][0]);
  }

  return R;
}

double evaluate(double *x) {
  double r = 0.0, d;
  int i,j,k,p;
  for (i=0; i<N; i++) {
     d = 1.0;
     for (j=0; j<n_dim; j++) {
```

```
            p = exponent[i][j];
            for (k=0; k<p; k++)
               d *= x[j];
         }
         r += coefficient[i]*d;
      }
      return r;
   }

   polynomial evaluate(double x,int n) {
      polynomial S(0,n_dim);
      double d;
      int i,j,k,p,e2[n_dim];
      for (i=0; i<N; i++) {
         p = exponent[i][n];
         for (j=0; j<n_dim; j++)
            e2[j] = exponent[i][j];
         e2[n] = 0;
         d = 1.0;
         for (k=0; k<p; k++)
            d *= x;
         S.add(e2,coefficient[i]*d);
      }
      return S;
   }

   double evaluate(double x) {
      polynomial S(0,n_dim);
      double d;
      int i,j,k,p,e2[n_dim];
      for (i=0; i<N; i++) {
         p = exponent[i][0];
         for (j=0; j<n_dim; j++)
            e2[j] = exponent[i][j];
         e2[0] = 0;
         d = 1.0;
         for (k=0; k<p; k++)
            d *= x;
         S.add(e2,coefficient[i]*d);
      }
      if (S.N == 0)
         return 0;
      else
         return S.coefficient[0];
   }

   double operator()(double x) {
      return evaluate(x);
   }
};
```

```
polynomial power(polynomial base,int t) {
   int i;
   polynomial R(1);
   R.exponent[0][0] = 0;
   R.coefficient[0] = 1;

   for (i=0; i<t; i++) {
     R = R*base;
   }

   return R;
}

polynomial operator+(polynomial L,polynomial R) {
   polynomial S;
   S = L;
   return (S += R);
}

polynomial operator-(polynomial L,polynomial R) {
   polynomial S;
   S = L;
   return (S -= R);
}

polynomial operator*(polynomial L,polynomial R) {
   polynomial S;
   S.n_dim = L.n_dim;
   int *p = new int[S.n_dim];
   int i,j,k;
   for (i=0; i<L.N; i++) {
     for (j=0; j<R.N; j++) {
        for (k=0; k<S.n_dim; k++)
           p[k] = L.exponent[i][k]+R.exponent[j][k];
       S.add(p,L.coefficient[i]*R.coefficient[j]);
     }
   }
   return S;
}

polynomial operator*(double v,polynomial R) {
   polynomial S;
   if (v == 0) return S;
   S = R;
   int i;
   for (i=0; i<S.N; i++)
     S.coefficient[i] *= v;
   return S;
}

polynomial operator*(polynomial R,double v) {
```

```
   polynomial S;
   if (v == 0) return S;
   S = R;
   int i;
   for (i=0; i<S.N; i++)
     S.coefficient[i] *= v;
   return S;
}

polynomial operator*(int v,polynomial R) {
   polynomial S;
   if (v == 0) return S;
   S = R;
   int i;
   for (i=0; i<S.N; i++)
     S.coefficient[i] *= v;
   return S;
}

polynomial operator*(polynomial R,int v) {
   polynomial S;
   if (v == 0) return S;
   S = R;
   int i;
   for (i=0; i<S.N; i++)
     S.coefficient[i] *= v;
   return S;
}

std::ostream& operator<<(std::ostream &s,polynomial &L)
{
   int i,j,N = L.N;

   for (i=0; i<(N-1); i++) {
     s << '(' ;
     for (j=0; j<L.n_dim; j++)
       s << L.exponent[i][j] << ',';
     s << L.coefficient[i] << ") ";
   }
   if (N > 0) {
     s << '(' ;
     for (j=0; j<L.n_dim; j++)
       s << L.exponent[i][j] << ',';
     s << L.coefficient[i] << ")";
   }

   if (N==0) s << "0";

   return s;
}
```

```
// integral along all directions
double integral(polynomial P) {
   polynomial S;
   S = P;
   int i,j;
   for (i=0; i<S.N; i++)
     for (j=0; j<S.n_dim; j++)
        S.coefficient[i] /= ++S.exponent[i][j];

   for (i=0; i<P.n_dim; i++)
     S = S.evaluate(1,i) - S.evaluate(-1,i);
   if (S.N == 0)
     return 0;
   else
     return S.coefficient[0];
}

double integral(polynomial P,double limits[]) {
   // limits[2*i] = x_i start, limits[2*i+1] = x_i end
   polynomial S;
   S = P;
   int i,j;
   for (i=0; i<S.N; i++)
     for (j=0; j<S.n_dim; j++)
        S.coefficient[i] /= ++S.exponent[i][j];

   for (i=0; i<P.n_dim; i++)
     S = S.evaluate(limits[2*i+1],i) - S.evaluate(limits[2*i],i);
   if (S.N == 0)
     return 0;
   else
     return S.coefficient[0];
}

// derivative along one direction (the J-direction)
polynomial derivative(polynomial P,int J=0) {
   polynomial S;
   S = P;
   int i;
   for (i=0; i<S.N; i++)
     S.coefficient[i] *= S.exponent[i][J]--;
   S.minimize();
   return S;
}

// Lagrange basis fuction (order = LagrangeN-1).
polynomial Lagrange1D(long int type,long int d,long int ndim) {
   // type = node position (0 to LagrangeN-1)
   // d = coordinate index (0 to ndim-1)
   long int i;
   polynomial P(2,ndim),L(1,ndim);
```

```
   for (i=0; i<ndim; i++) {
     L.exponent[0][i] = 0;
     P.exponent[0][i] = 0;
     P.exponent[1][i] = 0;
   }
   L.coefficient[0] = 1; // L = 1 initially
   P.exponent[1][d] = 1;

   double x[LagrangeN];
   for (i=0; i<LagrangeN; i++)
     x[LagrangeN-1-i] = cos(PI*i/(LagrangeN-1));

   for (i=0; i<LagrangeN; i++)
     if (i != type) {
        P.coefficient[1] = 1.0/(x[type]-x[i]);
        P.coefficient[0] = -x[i]/(x[type]-x[i]);
        L = L*P;
     }

   return L;
}

// sparse row
class row_sp {
public:
   long int *j,n;
   double *x;

   row_sp() {
     n = 0;
     x = NULL;
     j = NULL;
   }

   void push_back(long int p) {
     long int i;
     if (n > 0) {
       long int *old_j = new long int[n];
       for (i=0; i<n; i++)
         old_j[i] = j[i];
       delete[] j;
       j = new long int[n+1];
       for (i=0; i<n; i++)
          j[i] = old_j[i];
       delete[] old_j;
     } else
        j = new long int[1];
     j[n++] = p;
   }

   void add_index(long int p) {
```

```
  long int i;
  bool found = false;
  for (i=0; i<n; i++) {
     if (j[i] == p) found = true;
  }
  if (!found)
    push_back(p);
}

void push_back(long int p,double val) {
  long int i;
  if (n > 0) {
    long int *old_j = new long int[n];
     double *old_x = new double[n];
    for (i=0; i<n; i++) {
       old_j[i] = j[i];
        old_x[i] = x[i];
     }
     delete[] j;
     delete[] x;
     j = new long int[n+1];
     x = new double[n+1];
     for (i=0; i<n; i++) {
        j[i] = old_j[i];
        x[i] = old_x[i];
     }
     delete[] old_j;
     delete[] old_x;
  } else {
     j = new long int[1];
     x = new double[1];
  }
  j[n] = p;
  x[n] = val;
  n++;
}

void add_index(long int p,double val) {
  long int i;
  bool found = false;
  for (i=0; i<n; i++) {
     if (j[i] == p) found = true;
  }
  if (!found)
    push_back(p,val);
}

long int find_index(long int p) {
  long int i=0;
  for (;;) {
     if (i >= n) {
```

```
            printf("find_index: not found (%ld)\n",p);
            return -99;
          }
          if (p == j[i])
            return i;
          i++;
        }
      }

      double x_at(long int p) {
        return x[find_index(p)];
      }

      void add(long int p,double val) {
        x[find_index(p)] += val;
      }

      void sub(long int p,double val) {
        x[find_index(p)] -= val;
      }
};

#endif
```

APPENDIX C

MATHEMATICA PROGRAMS

2Dphi_wfree.nd

This Mathematica program solves the two-dimensional bimorph in the static case. The approximation that $T_2 = 0$ was made in order to simplify the full 3D equations. The y-deflection, v, is neglected since it is small in the beam approximation. The designation "wfree" means that the z-deflection is mostly free everywhere on the boundary, and is only specified to be zero at a single point on the left edge ($x = 0, z = 0$) in order to have a unique solution. In contrast, the x-deflection, u, is specified to be zero everywhere along the left edge ($x = 0$), so that we have clamped-free boundary conditions (clamped at the left end, and free at the right end).

What makes the Mathematica program of interest is that I have a routine called Exact[] which can turn all numerical values, such as given material constants, into integer fractions, and thus have infinite precision. I can then choose how much numerical precision I want to have in the solution. For the most part, I have chosen to have 30 decimal places of precision, although I have also used as much as 60 when I wanted to test whether the solution is affected by round-off error. I have found that double precision (16 digits of precision) gives the same solution to within 3 decimal places as the higher precision. This indicates that no drastic errors are occurring because of round-off. Also, any plots of results or the derivatives have looked the same at all amounts of precision. Any problems that may occur in the solutions are therefore from the discretization properties of the model itself. This is important to know, because sometimes round-off error can cause serious errors in the solution.

```
(* This program solves the 2D bimorph problem for u,w and electric
 potential by using quadratic Lagrange elements. *)

Clear[hx, hz, x, z];
LagrangeN = 2; (* Order of the lagrange basis functions. *)
NPE = (LagrangeN + 1) ^ 2;
Kron[u_, v_] := Outer[Times, u, v];
Lag[n_, i_, x_, h_] := Module[{j, k, y},
  y = Function[{k}, (1 + Cos[Pi * (1 + n - k) / n]) * h / 2];
  Product[If[j == i, 1, (x - y[j]) / (y[i] - y[j])], {j, n + 1}]]

basisX = Table[Lag[LagrangeN, i, x, hx], {i, LagrangeN + 1}];
basisXDer = Simplify[D[basisX, x]];
basisZ = Table[Lag[LagrangeN, i, z, hz], {i, LagrangeN + 1}];
basisZDer = Simplify[D[basisZ, z]];
Mx = Table[Null, {i, (LagrangeN + 1) ^ 2}];
For[i = 0, i ≤ LagrangeN, i++,
  For[j = 0, j ≤ LagrangeN, j++,
    n = 1 + i + j * (LagrangeN + 1);
    Mx[[n]] = Simplify[Integrate[{basisX[[1 + i]] * basisX[[1 + j]],
        basisXDer[[1 + i]] * basisX[[1 + j]],
        basisX[[1 + i]] * basisXDer[[1 + j]],
        basisXDer[[1 + i]] * basisXDer[[1 + j]]}, {x, 0, hx}]];
   ];];
Mz = Mx /. hx → hz;

MMxx = Table[Table[Null, {i, NPE}], {j, NPE}];
MMxz = MMxx;
MMzx = MMxx;
MMzz = MMxx;
For[i1 = 0, i1 ≤ LagrangeN, i1++,
  For[j1 = 0, j1 ≤ LagrangeN, j1++,
    j = 1 + i1 + j1 * (LagrangeN + 1);
    For[i2 = 0, i2 ≤ LagrangeN, i2++,
     For[j2 = 0, j2 ≤ LagrangeN, j2++,
       k = 1 + i2 + j2 * (LagrangeN + 1);
       m = 1 + i1 + i2 * (LagrangeN + 1);
       n = 1 + j1 + j2 * (LagrangeN + 1);
       MMxx[[j, k]] = Mx[[m, 4]] * Mz[[n, 1]];
       MMzz[[j, k]] = Mx[[m, 1]] * Mz[[n, 4]];
       MMxz[[j, k]] = Mx[[m, 2]] * Mz[[n, 3]];
       MMzx[[j, k]] = Mx[[m, 3]] * Mz[[n, 2]];
      ];];];];

GPrec = 30; (* global precision *)
$MaxExtraPrecision = 40;
```

```
Exact[n_] := Module[{p, q, c, d},
   q = MantissaExponent[n];
   c = q[[1]];
   p = q[[2]];
   d = 1;
   While[FractionalPart[c * d] ≠ 0, d *= 10;];
   (IntegerPart[c * d] / d) * 10^p
  ];

(* constants and boundary values *)
c11 = Exact[3.70 * 10^9]; (* in N/m^2 *)
c22 = Exact[3.20 * 10^9];
c33 = Exact[1.51 * 10^9];
c44 = Exact[0.55 * 10^9];
c55 = Exact[0.59 * 10^9];
c66 = Exact[0.70 * 10^9];
c12 = Exact[1.47 * 10^9];
c13 = Exact[1.23 * 10^9];
c23 = Exact[1.00 * 10^9];

(* in C^2/N*m^2 *)
eps1 = Exact[7.35 * 8.85 * 10^-12];
eps2 = Exact[9.27 * 8.85 * 10^-12];
eps3 = Exact[8.05 * 8.85 * 10^-12];

(* in V*m/N *)
g31 = Exact[0.21];
g32 = Exact[0.03];
g33 = Exact[-0.46];
g15 = Exact[-0.32];
g24 = Exact[-0.27];

(* in N/V*m *)
e31 = eps3 * (g31 * c11 + g32 * c12 + g33 * c13); (* 1.807524e-02 *)
e32 = eps3 * (g31 * c12 + g32 * c22 + g33 * c23); (* -3.915240e-03 *)
e33 = eps3 * (g31 * c13 + g32 * c23 + g33 * c33); (* -2.876604e-02 *)
e15 = eps1 * g15 * c55; (* -1.336704e-02 *)
e24 = eps2 * g24 * c44; (* -1.051380e-02 *)

c11s = c11 - c12 * c12 / c22;
c13s = c13 - c12 * c23 / c22;
c33s = c33 - c23 * c23 / c22;
e31s = e31 - c12 * e32 / c22;
e33s = e33 - c23 * e32 / c22;
eps3s = eps3 - e32 * e32 / c22;
```

```
(* Piezo sheet dimensions, in meters. *)
Lz = Exact[60 * 10^-6];
Lx = Exact[2.5 * 10^-2];

(* Electrical boundary values. *)
phiTop = Exact[600];
phiBottom = Exact[0];

Nx = 11;
Nz = 7; (* must be odd, ≥3 *)
midZ = (Nz - 1) / 2;
hx = Lx / (Nx - 1);
hz = Lz / (Nz - 1);

NDIM = 2; (* spacial dimensions *)
Nx2 = Nx * LagrangeN + 1 - LagrangeN;
Nz2 = Nz * LagrangeN + 1 - LagrangeN;

nNodes = Nx2 * Nz2;
nBNodesU = Nz2;
nBNodesW = 1;
nBNodesPhi = Nx2;
nElements = (Nx - 1) * (Nz - 1);

nVar = 3; (* Number of variables per node. *)
nDOF = nVar * nNodes; (* Total number of degrees of freedom. *)
nn1 = 0;
nn2 = nNodes;
nn3 = 2 * nNodes;

MMxx = N[MMxx, GPrec];
MMxz = N[MMxz, GPrec];
MMzx = N[MMzx, GPrec];
MMzz = N[MMzz, GPrec];

bnodes = Table[Null, {i, nBNodesU}];
bnodesW = Table[Null, {i, nBNodesW}];
phiLower = Table[Null, {i, nBNodesPhi}];
phiUpper = phiLower;
elnodes = Table[Table[Null, {i, NPE}], {j, nElements}];

(* Specify the global node numbers for each element.
  This is the mesh. *)
piezoLower = Table[Null, {i, nElements}];
count = 0;
p1 = 0;
p2 = 0;
```

```
For[i = 0, i < (Nx - 1), i++,
 For[k = 0, k < (Nz - 1), k++,
  n = i + k * (Nx - 1);
  piezoLower[[1 + n]] = (k < midZ);
  m = LagrangeN * (i + k * Nx2);
  For[n1 = 0, n1 <= LagrangeN, n1 ++,
   For[n3 = 0, n3 <= LagrangeN, n3 ++,
    m1 = n1 + n3 * (LagrangeN + 1);
    node = m + n1 + n3 * Nx2;
    elnodes[[n + 1, m1 + 1]] = node;

    If[(n1 == 0) && (i == 0), If[(n3 > 0) || (k == 0),
      bnodes[[1 + count ++]] = node;
     ]];
    If[(i == 0) && (k == midZ) && (n1 == 0) && (n3 == 0),
     bnodesW[[1]] = node;
    ];
    If[(n3 == 0) && (k == 0), If[(n1 > 0) || (i == 0),
      phiLower[[1 + p1 ++]] = node;
     ]];
    If[(n3 == LagrangeN) && (k == (Nz - 2)),
     If[(n1 > 0) || (i == 0),
      phiUpper[[1 + p2 ++]] = node;
     ]];
   ]]]]

nMat = nDOF;
AMat = Table[Table[0, {i, nMat}], {j, nMat}];
loadVec = Table[0, {i, nMat}];
For[i = 1, i <= nElements, i++,
  If[piezoLower[[i]], s = 1, s = -1;];
  For[j = 1, j <= NPE, j ++,
   m = 1 + elnodes[[i, j]];
   m1 = m + nn1;
   m2 = m + nn2;
   m3 = m + nn3;
   For[k = 1, k <= NPE, k++,
    n = 1 + elnodes[[i, k]];
    n1 = n + nn1;
    n2 = n + nn2;
    n3 = n + nn3;
    AMat[[m1, n1]] += c11s * MMxx[[j, k]] + c55 * MMzz[[j, k]];
    AMat[[m1, n2]] += c13s * MMxz[[j, k]] + c55 * MMzx[[j, k]];
    AMat[[m1, n3]] += s * (e31s * MMxz[[j, k]] + e15 * MMzx[[j, k]]);
    AMat[[m2, n1]] += c13s * MMzx[[j, k]] + c55 * MMxz[[j, k]];
    AMat[[m2, n2]] += c55 * MMxx[[j, k]] + c33s * MMzz[[j, k]];
    AMat[[m2, n3]] += s * (e15 * MMxx[[j, k]] + e33s * MMzz[[j, k]]);
```

```
    AMat[[m3, n1]] += s * (e31s * MMzx[[j, k]] + e15 * MMxz[[j, k]]);
    AMat[[m3, n2]] += s * (e15 * MMxx[[j, k]] + e33s * MMzz[[j, k]]);
    AMat[[m3, n3]] -= eps1 * MMxx[[j, k]] + eps3s * MMzz[[j, k]];
   ];];];

For[j = 1, j <= nBNodesPhi, j++,
  m = 1 + phiLower[[j]];
  loadVec -= phiBottom * AMat[[All, m + nn3]];
  m = 1 + phiUpper[[j]];
  loadVec -= phiTop * AMat[[All, m + nn3]];
 ];

zero = Table[0, {i, nMat}];
For[j = 1, j <= nBNodesU, j++,
  m = 1 + bnodes[[j]];
  m1 = m + nn1;
  loadVec[[m1]] = 0;
  AMat[[m1]] = zero;
  AMat[[All, m1]] = zero;
  AMat[[m1, m1]] = 1;
 ];

For[j = 1, j <= nBNodesW, j++,
  m = 1 + bnodesW[[j]];
  m2 = m + nn2;
  loadVec[[m2]] = 0;
  AMat[[m2]] = zero;
  AMat[[All, m2]] = zero;
  AMat[[m2, m2]] = 1;
 ];

For[j = 1, j <= nBNodesPhi, j++,
 m = 1 + phiLower[[j]];
 m3 = m + nn3;
 loadVec[[m3]] = phiBottom;
 AMat[[m3]] = zero;
 AMat[[All, m3]] = zero;
 AMat[[m3, m3]] = 1;
 m = 1 + phiUpper[[j]];
 m3 = m + nn3;
 loadVec[[m3]] = phiTop;
 AMat[[m3]] = zero;
 AMat[[All, m3]] = zero;
 AMat[[m3, m3]] = 1;
]

AMat = N[AMat, GPrec];
```

```
loadVec = N[loadVec, GPrec];
Print["solving"];
sol = LinearSolve[AMat, loadVec];
(* maximum z deflection *)
Print[ScientificForm[Max[Abs[sol[[1 ;; 1 + nn3]]]]]];

(* plot results *)
r1 = 1;
r2 = 1;
r3 = 0.5;
nx2 = 5;
nz2 = 5;
nx3 = (Nx - 1) * (nx2 - 1) + 1;
nz3 = (Nz - 1) * (nz2 - 1) + 1;
nNodes3 = nx3 * nz3;
Clear[plist, r, count];
plist = Table[Null, {i, (nx3 - 1) * (nz3 - 1)}];
r = Table[Null, {i, 12}];
For[c2 = 0, c2 < 3, c2++,
  For[c1 = 0, c1 < 4, c1++,
    count = 1;
    For[i = 0, i < (Nx - 1), i++,
     For[k = 0, k < (Nz - 1), k++,
       n = i + k * (Nx - 1);
       x0 = i * hx;
       z0 = k * hz;
       hx3 = hx / (nx2 - 1);
       hz3 = hz / (nz2 - 1);
       m = LagrangeN * (i + k * Nx2);
       t = 0;
       For[n1 = 0, n1 <= LagrangeN, n1++,
        For[n3 = 0, n3 <= LagrangeN, n3++,
          node = 1 + m + n1 + n3 * Nx2;
          If[c1 == 0,
           tx = basisX[[n1 + 1]];
           tz = basisZ[[n3 + 1]];
          ];
          If[c1 == 1,
           tx = basisXDer[[n1 + 1]];
           tz = basisZ[[n3 + 1]];
          ];
          If[c1 == 2,
           tx = basisX[[n1 + 1]];
           tz = basisZDer[[n3 + 1]];
          ];
          If[c1 == 3,
           tx = basisXDer[[n1 + 1]];
```

```
            tz = basisZDer[[n3 + 1]];
           ];
           t += tx * tz * sol[[node + nNodes * c2]];
          ];];

        t = (t /. {x → x - x0, z → z - z0});
        For[n1 = 0, n1 < nx2 - 1, n1++,
         For[n3 = 0, n3 < nz2 - 1, n3++,
           x1 = x0 + n1 * hx3;
           z1 = z0 + n3 * hz3;
           x2 = x1 + hx3;
           z2 = z1 + hz3;
           plist[[count++]] = {EdgeForm[{Black}], Polygon[N[{
                 {x1, z1, t /. {x -> x1, z -> z1}},
                 {x2, z1, t /. {x -> x2, z -> z1}},
                 {x2, z2, t /. {x -> x2, z -> z2}},
                 {x1, z2, t /. {x -> x1, z -> z2}}
                }, GPrec]]};
          ];];
       ];];
     r[[1 + c1 + c2 * 4]] = Graphics3D[plist, Axes → True,
       BoxRatios → {r1, r2, r3}, AxesLabel → {x, z, ""}];
    ];];

Show[r[[1]]](*u*)
Show[r[[2]]](*du/dx*)
Show[r[[3]]](*du/dz*)
Show[r[[4]]](*d^2 u/dx dz*)
Show[r[[5]]](*w*)
Show[r[[6]]](*dw/dx*)
Show[r[[7]]](*dw/dz*)
Show[r[[8]]](*d^2 w/dx dz*)
Show[r[[9]]](*phi*)
Show[r[[10]]](*d phi/dx*)
Show[r[[11]]](*d phi/dz*)
Show[r[[12]]](*d^2 phi/dx dz*)
```

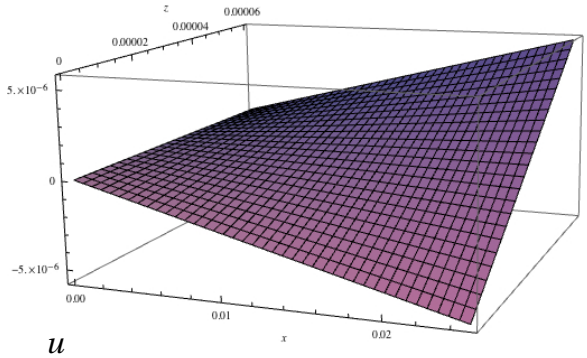

u

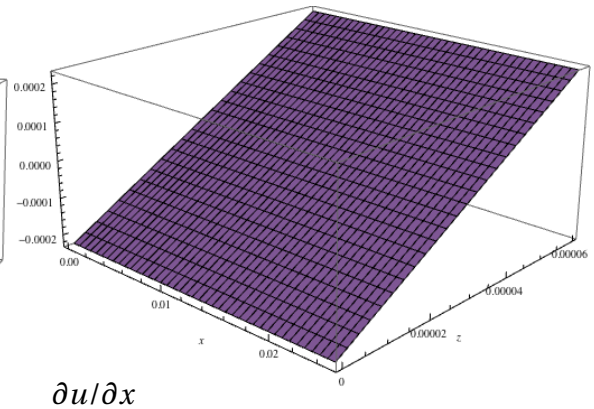

$\partial u/\partial x$

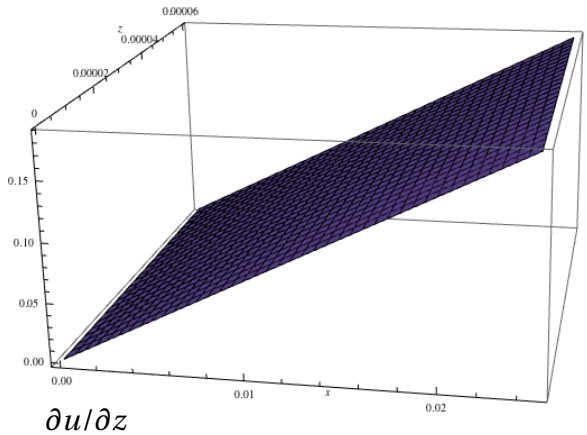

$\partial u/\partial z$

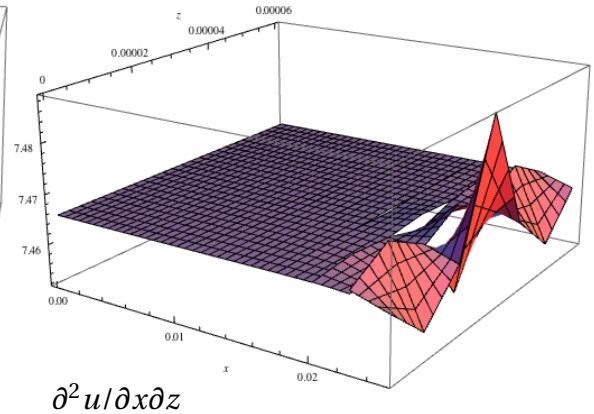

$\partial^2 u/\partial x \partial z$

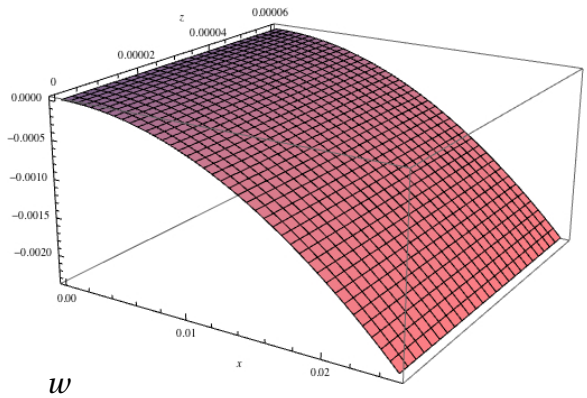

w

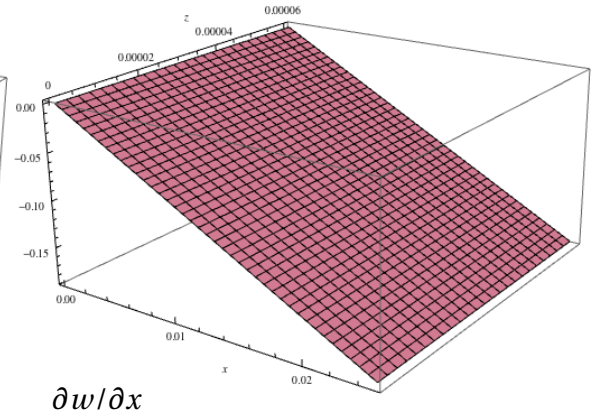

$\partial w/\partial x$

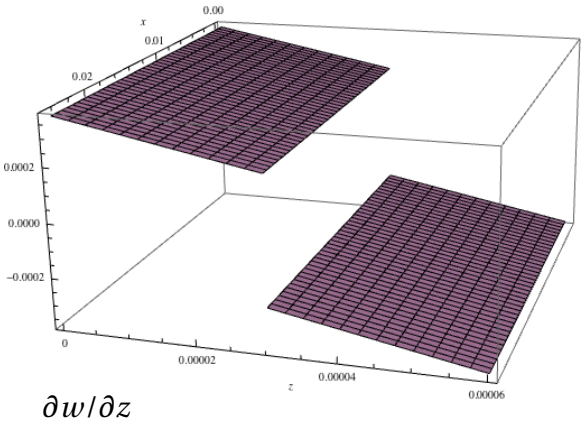

$\partial w/\partial z$

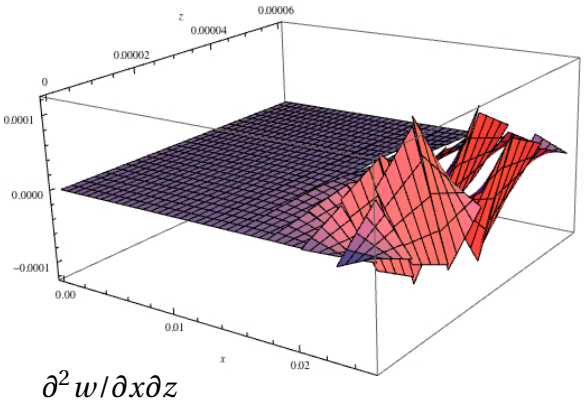

$\partial^2 w/\partial x \partial z$

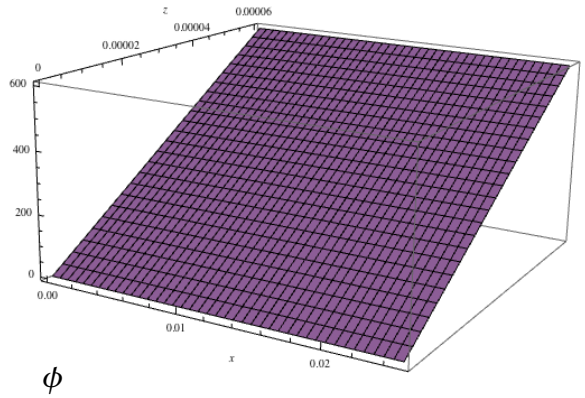

ϕ

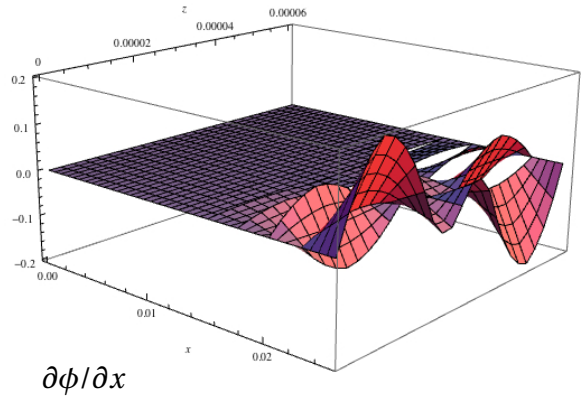

$\partial\phi/\partial x$

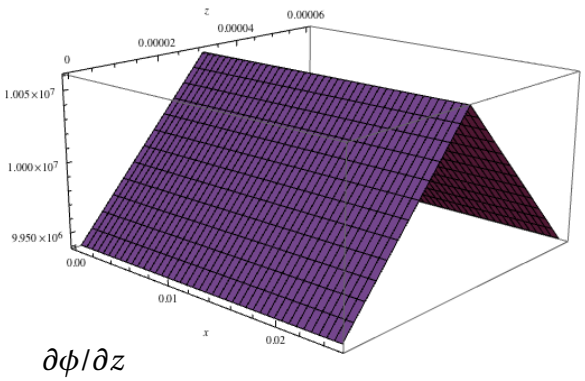

$\partial\phi/\partial z$

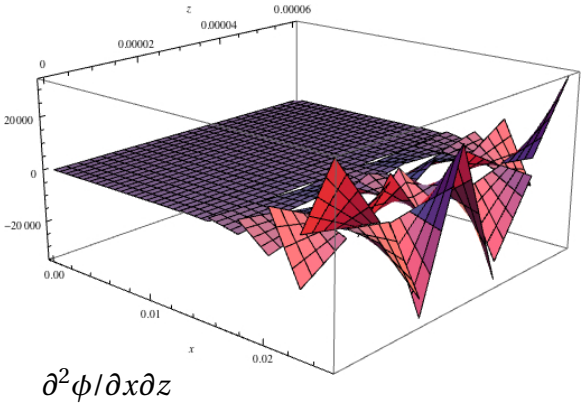

$\partial^2\phi/\partial x \partial z$

REFERENCES CITED

[1] T. Ikeda, *Fundamentals of Piezoelectricity*, Oxford University Press, New York, 1996.

[2] *Kynar Piezo Film Technical Manual*, Pennwalt Corporation, 1983.

[3] A. J. Lovinger, *Poly(Vinylidene Fluoride)*, Bell Laboratories, New Jersey.

[4] W. Heywang, K. Lubitz, and W. Wersing, *Piezoelectricity: Evolution and Future of a Technology*, Springer-Verlag, Berlin, 2008.

[5] A. G. MacDiarmid, "Synthetic Metals: A Novel Role for Organic Polymers," Nobel Lecture, 2000.

[6] A. J. Heeger, "Semiconducting and Metallic Polymers: The Fourth Generation of Polymeric Materials," Nobel Lecture, 2000.

[7] E. U. Condon and H. Odishaw, *Handbook of Physics*, McGraw-Hill Companies Inc., New York, 1958.

[8] J. R. Sambles, K. C. Elsom, and D. J. Jarvis, "The Electrical Resistivity of Gold Films," *Philosophical Transactions of the Royal Society of London. Series A, Mathematical and Physical Sciences* 304 [1486] 365-396 (1982).

[9] Y. Roh, V. V. Varadan, and V. K. Varadan, "Characterizations of All the Elastic, Dielectric, and Piezoelectric Constants of Uniaxially Oriented Poled PVDF Films," *IEEE Transactions on Ultrasonics, Ferroelectrics, and Frequency Control* 49 [6] 836-847 (2002).

[10] S. Timoshenko, *Vibration Problems in Engineering*, D. Van Nostrand Company, New York, 1928.

[11] D. Braess, *Finite Elements: Theory, Fast Solvers, and Applications in Solid Mechanics*, Cambridge University Press, New York, 2001.

[12] A. Benjeddou, "Advances in Piezoelectric Finite Element Modeling of Adaptive Structural Elements: A Survey," *Computers and Structures* 76 347-363 (2000).

[13] J. G. Smits and S. I. Dalke, "The Constituent Equations of Piezoelectric Bimorphs," *IEEE Ultrasonics Symposium* 781-784 (1989).

[14] C. Poizat and A. Benjeddou, "On Analytical and Finite Element Modelling of Piezoelectric Extension and Shear Bimorphs," *Computers and Structures*, 84 1426-1437 (2006).

[15] I. A. Karnovsky and O. I. Lebed, *Free Vibrations of Beams and Frames: Eigenvalues and Eigenfunctions*, McGraw Hill Companies Inc., 2004.

[16] J. N. Reddy, *An Introduction to the Finite Element Method*, 2nd edition, McGraw Hill Companies Inc., New York, 1993.

[17] P. Solin, *Partial Differential Equations and the Finite Element Method*, John Wiley & Sons, Hoboken, 2006.

[18] S. T. McGovern, G. M. Spinks, B. Xi, G. Alici, V. Truong, and G. G. Wallace, "Fast Bender Actuators for Fish-like Aquatic Robots," Proceedings of the SPIE: Electroactive Polymer Actuators and Devices (EAPAD), ed., Y. Bar-Cohen, 6927 69271L (2008).

[19] S. Cygan and J. R. Laghari, "Visual Damage to Polypropylene and Polyvinylidene Fluoride Films from High-Voltage Discharges," *Journal of Materials Science Letters* 8 [7] 835-837 (1989).

[20] J. I. Lorenz-Hallenberg, *Application of poly(3,4-ethylenedioxytheophene)-poly(styrenesulfonate) to poly(vinylidene fluoride) as a Replacement for Traditional Electrodes*, M.S. Thesis, Montana State University, August 2003.

[21] J. Polasik and V. H. Schmidt, "Conductive Polymer PEDOT/PSS Electrodes on the Piezoelectric Polymer PVDF," Proceedings of the SPIE: Electroactive Polymer Actuators and Devices (EAPAD), ed., Y. Bar-Cohen, 5759 114-120 (2005).

[22] L. Lediaev and V. H. Schmidt, "Modeling PVDF Actuators with Conducting Polymer Electrodes," Proceedings of the SPIE: Electroactive Polymer Actuators and Devices (EAPAD), ed., Y. Bar-Cohen, 5759 470-478 (2005).

[23] L. Lediaev, *Modeling Piezoelectric PVDF Sheets with Conductive Polymer Electrodes*, M.S. Thesis, Montana State University, April 2006.